AD-A216 242

Effects of Elevated Temperatures
and Thermal Cycling on
Ceramic Composite Materials

THESIS

Michael A. Hoobler
Captain, USAF

AFIT/GAE/ENY/89D-14

DEPARTMENT OF THE AIR FORCE
AIR UNIVERSITY
AIR FORCE INSTITUTE OF TECHNOLOGY

Wright-Patterson Air Force Base, Ohio

89 12 29 047

AFIT/GAE/ENY/89D-14

Effects of Elevated Temperatures
and Thermal Cycling on
Ceramic Composite Materials

THESIS

Michael A. Hoobler
Captain, USAF

AFIT/GAE/ENY/89D-14

Approved for public release; distribution unlimited

AFIT/GAE/ENY/89D-14

Effects of Elevated Temperatures

and Thermal Cycling on

Ceramic Composite Materials

THESIS

Presented to the Faculty of the School of Engineering

of the Air Force Institute of Technology

Air University

In Partial Fulfillment if the

Requirements for the Degree of

Master of Science in Aeronautical Engineering

Michael A. Hoobler

Captain, USAF

December 1989

Acknowledgements

Several people have been instrumental in enabling me to accomplish this project. I would first like to thank my thesis advisor, Dr. S. Mall, whose knowledge and guidance made this thesis possible. I would also like to thank my sponsor, Dr. Ted Nicholas, whose sponsorship enabled me to use the facilities of the materials laboratory at will. Larry Zawada provided the plates for me to use and gave me much information on the processing and mechanical properties of the materials. George Hartman designed the thermal cycling lamps and provided much needed technical assistance on numerous occasions. I appreciate the test fixture construction and advice given by Major John Mol, who began this work the year before me. Thanks go to Jay Anderson, Andy Pitts, and Mark Derriso who helped me construct the thermal fixture stand and reinstrument the load fixture.

To my children, Harmony, Christopher, and Nathan, thank you for the inspiration you always provided.

Final thanks go to Karla, my wife. Without her help and patience this project would not have been possible.

ii

Table of Contents

iv

List of Figures

xiii

List of Tables

AFIT/GAE/ENY/89D-14

Abstract

The need to determine the effects of elevated
temperature and thermal cycling on the mode II fracture
toughness of fiber reinforced ceramic composites was
identified. The two materials chosen for this purpose were
CGW 1723 and CGW 7740. In addition to mode II fracture
toughness, preliminary mode I fracture toughness values were
determined in order to evaluate similarities or dissimi-
larities in fracture toughness trends with increasing
temperature. A pre-cracking fixture was designed and built
to allow for precise pre-cracking of the specimens. A test
stand for subjecting specimens to thermal cycling was
designed and constructed. CGW 1723 Mode II specimens were
tested at room temperature, 600 F, 1000 F, after being cycled
from 130 F to 600 F for 25 cycles, and after exposure to 600
F for 125 minutes. CGW 7740 mode II specimens were tested at
room temperature. Compliance data was plotted as a function
of non-dimensional crack length. 2nd and 3rd order
polynomial curves were fitted to the data. These curve fits
were compared to a theoretical compliance to crack length
relationship. Critical loads were determined from the load-
displacement curves by identifying the load at which the
specimens compliance changed. Mode II critical strain energy

release rate was then calculated. The three methods of determining the compliance to crack length relationship were compared to find the one that produced the narrowest band of fracture toughness values. The theoretical solution was found to be the best method and fracture toughness values were computed from this method. The fracture toughness value, G_{IIc}, at 600 F decreased by 50% in comparison to its value at room temperature and the G_{IIc} value at 1000 F decreased by another 30%. The specimens subjected to thermal cycling showed a decrease in fracture toughness from that of the 600 F specimens. The specimen exposed to a constant 600 F for 125 minutes had almost the same fracture toughness value as that of the 600 F specimen. CGW 1723 mode I specimens were tested at room temperature and 1000 F. They displayed the same trend of decreasing fracture toughness, G_{Ic}, at elevated temperatures as did the mode II specimens. Post mortem examination for both modes revealed an embrittlement of the matrix that increased with increasing temperatures. Fiber pullout was decreased in the elevated temperature tests, showing a degradation in the fiber matrix interface. These mechanisms were the primary cause for the decrease in G_{IIc} and G_{Ic} with increasing temperature.

I. Introduction

Problem

"Ceramic materials in general have a very attractive package of properties: high strength and high stiffness at very high temperatures, chemical inertness, low density, and so on. This attractive package is marred by one deadly flaw, namely, an utter lack of toughness. It is therefore understandable that an overriding consideration in ceramic matrix composites (CMCs) has been to toughen the ceramic matrices by incorporating fibers in them and thus exploit the attractive high temperature strength and environmental resistance of ceramic materials without risking catastrophic failures" (5:134). These attractive properties provide CMCs with the potential of meeting future needs in high temperature applications such as engines and engine components.

Numerous catastrophic engine component failures in the aerospace industry, directly attributable to fracture mechanics type failures, have demonstrated the need for accurately predicting crack growth behavior in these components. With CMCs showing great promise for being used in these areas, the accurate characterization of their fracture toughness properties has become an area of

1

heightened interest. Several complications arise in this area. The first is that a standard, valid procedure needs to be developed to determine the fracture toughness of these CMCs. Additionally, due to the proposed applications for these materials, the testing needs to be accomplished at high temperatures as well as room temperature. This significantly increases the difficulties associated with the testing procedures. Due to the limited availability of these materials, the specimens need to be of the smallest size. This dictates the need for very sensitive measuring techniques to determine the instant of crack propagation and the critical loads.

In unidirectional composite layups, fracture parallel to the fibers is potentially more significant than that perpendicular to them. This is due to the crack growth arrest mechanism provided by the fibers to crack growth perpendicular to them. This will, in general, involve mixed Mode I & II or Mode II conditions under general loading. This study is focussed towards the investigation of Mode II fracture behavior in ceramic composites. Vazzola (18) studied this behavior at room temperature. Mol (16) furthered that work by testing at room and elevated temperatures. This study is a continuation of these two previous studies.

Objective

The objectives of this study were fourfold. First was to continue the previous study by Mol (16) on Corning Glass Works (CGW) 1723 CMC material. In this portion of the present study, the Mode II fracture behavior of CGW 1723 CMC material was investigated. This study was done with thinner specimens, .1" instead of .2" as used by Mol, at room temperature, 600 F, and 1000 F. Second, to investigate the effect of thermal cycling of this material on its fracture toughness. Third, to investigate the Mode I fracture behavior of CGW 1723 material at room temperature and 1000 F. Fourth, to use the same methods to determine the fracture toughness of another CMC, CGW 7740, at room and elevated temperatures.

Approach

The basic approach to this study was the same as that used by Mol (16) with several modifications to the test setup to improve the accuracy in determining the displacements and critical loads as the specimens used in this study were one half the thickness used in the previous studies by Vozolla (18) and Mol (16). A new pre-cracking jig was designed and constructed to allow for precise growth of the initial flaw. A test stand was designed and constructed for the thermal cycling portion of the study.

3

For the calculation of the Mode II fracture toughness of the specimens, first the compliance to crack length relationship had to be determined. Next, the critical loads at various crack lengths were found. From this data the Mode II fracture toughness could be calculated. For Mode I fracture toughness calculations, only the critical loads were required.

The composite specimens used were CGW 1723, an aluminosilicate glass matrix material with silicon carbide reinforcing fibers and CGW 7740, a borosilicate glass matrix material with the same reinforcing fibers. Both of these materials are being developed and tested by the Air Force Materials Laboratories at Wright-Patterson AFB, OH.

II. Background

One of the basic theories on fracture was proposed by Griffith (9,10) in the 1920's. He did extensive work with brittle glasses and developed what is known as the Griffith Criterion. Simply put, it states that crack propagation will occur if the energy released upon crack growth is sufficient to provide all the energy that is required for crack growth (4:22). From this comes the concept of a critical strain energy release rate criterion for characterizing the fracture toughness of a material.

With the extensive use of high strength materials in the 1940's and 1950's came the problem of failure of components under low stress conditions. It was during this time that it was discovered that material deficiencies in the form of pre-existing flaws could initiate cracks and fractures (4:4). It was this realization that led to the development of fracture mechanics. Irwin (11) did extensive work during this time with metals and postulated the effect of crack tip plasticity and hence crack tip plastic zone size on crack propagation.

Although much of the early work done by Griffith, Irwin, and others was on brittle glasses and metals, isotropic homogenous materials, an attempt has been made to extend these basic theories to composite materials which are non-

homogenous and anisotropic. Glass and glass ceramic matrix composites have the same fundamental problem associated with this anisotropic nature, low transverse and interlaminar shear strengths (6:99). It is these weaknesses that make Mode II fracture of unidirectional composites potentially more critical than Mode I.

Atkins and Mai (2) give a good background discussion of the mechanics of elastic fracture in composite materials. They state that a peculiarity of fracture in filamentary composites is that the fracture surfaces are rarely simply planar, that they have bits of fiber sticking out of the matrix and this feature contributes to the additional toughness of composites (2:47). The concept of fiber pullout increasing the toughness of the these ceramic composite materials has become of increased interest in the last 10 years. Much research has been conducted on the effects of fiber pullout on Mode I fracture toughness, however very little work has been done on Mode II loading.

Much of the study of the toughening mechanism in fibrous ceramic composites has focussed on the increased toughening effects of debonding, crack deflection, and fiber pullout. All of these mechanisms depend on a weak bond at the fiber-matrix interface (14:253). However, as stated before, work in this area has been almost exclusively Mode I behavior. Lewis states "Unfortunately, the low interfacial shear (or

tensile) strength of the fiber-matrix interface which gives
high toughness for one crack propagation direction may also
yield low strength <u>and</u> toughness in other directions"
(13:269). Agarwal and Broutman propose that in Mode II
loading, failure will occur by matrix shear failure,
constituent debonding, or a combination of two the (1:57).

Lowden, Stinton, and Besmann examined the mechanical
behavior of SiC fibers and the influence of interfacial
frictional stress on matrix fracture stress and ultimate
strength (14). Lewis also looked at the effects of the
properties of the fiber-matrix interface on the properties of
the composite and on the importance of this interface on
preserving the composite properties through long term high
temperature exposure and cyclical loading of various
types (13).

Giare (8) studied the Mode II failure in unidirectional
fiber reinforced composites. He determined that linear
elastic fracture mechanics apply to these materials in
Mode II.

Briggs and Davidge have investigated the properties and
applications of borosilicate glass reinforced with continuous
silicon fibers (3). In their work they describe the
fabrication process, mechanical properties including an
energy balance approach to matrix cracking, and propose some
possible applications for this material.

Mall (15) investigated the effects of overhang of ENF specimens on the Mode II strain energy release rate.

Vozzola (18) studied the fabrication of glass-ceramic composites and developed a test for Mode II fracture toughness at room temperature. He used ENF specimens on a three point bend fixture to calculate G_{IIc}. Mol (16) carried this work further and tested the specimens at elevated temperatures. Mol used specimens that were .2" thick for his tests.

This study applied Mol's techniques to thinner, .1", specimens of CGW 1723 CMC material to calculate the Mode II fracture toughness at room temperature, 600 F, and 1000 F. In addition, thermal cycling effects were studied, and the effects of elevated temperatures on the Mode I fracture toughness were examined. The Mode II fracture toughness of another CMC, CGW 7740, was determined at room temperature.

8

III. TEST SETUP AND VALIDATION

This work utilized the basic setup designed and constructed by Mol (16) for the actual testing of the specimens as shown in Figure 1. Modifications to this setup were made primarily to increase the sensitivity of the displacement measurements and to decrease the effects of the load fixture compliance. See Figures 1 and 2. A test setup with the capability to provide thermal cycling of the specimens, along with new lamps for this setup, had to be designed and constructed.

Test Equipment Specifications

The test fixture comprised of four main parts; the load cell, the Linear Voltage Displacement Transducer (LVDT) support frame, the three point bend fixture, and the Instron TTD Tension/Compression Tester. See Figure 3.

__ Load Cell. An Interface 1000 lb load cell was used to measure the applied load on the specimen for the Mode II tests. For the Mode I tests, this was replaced by an Interface 25 lb load cell. For both tests the load cell was placed at the very bottom of the test fixture. Calibration factors were provided by Interface and validated periodically by dead weight testing. The signal from this was supplied to
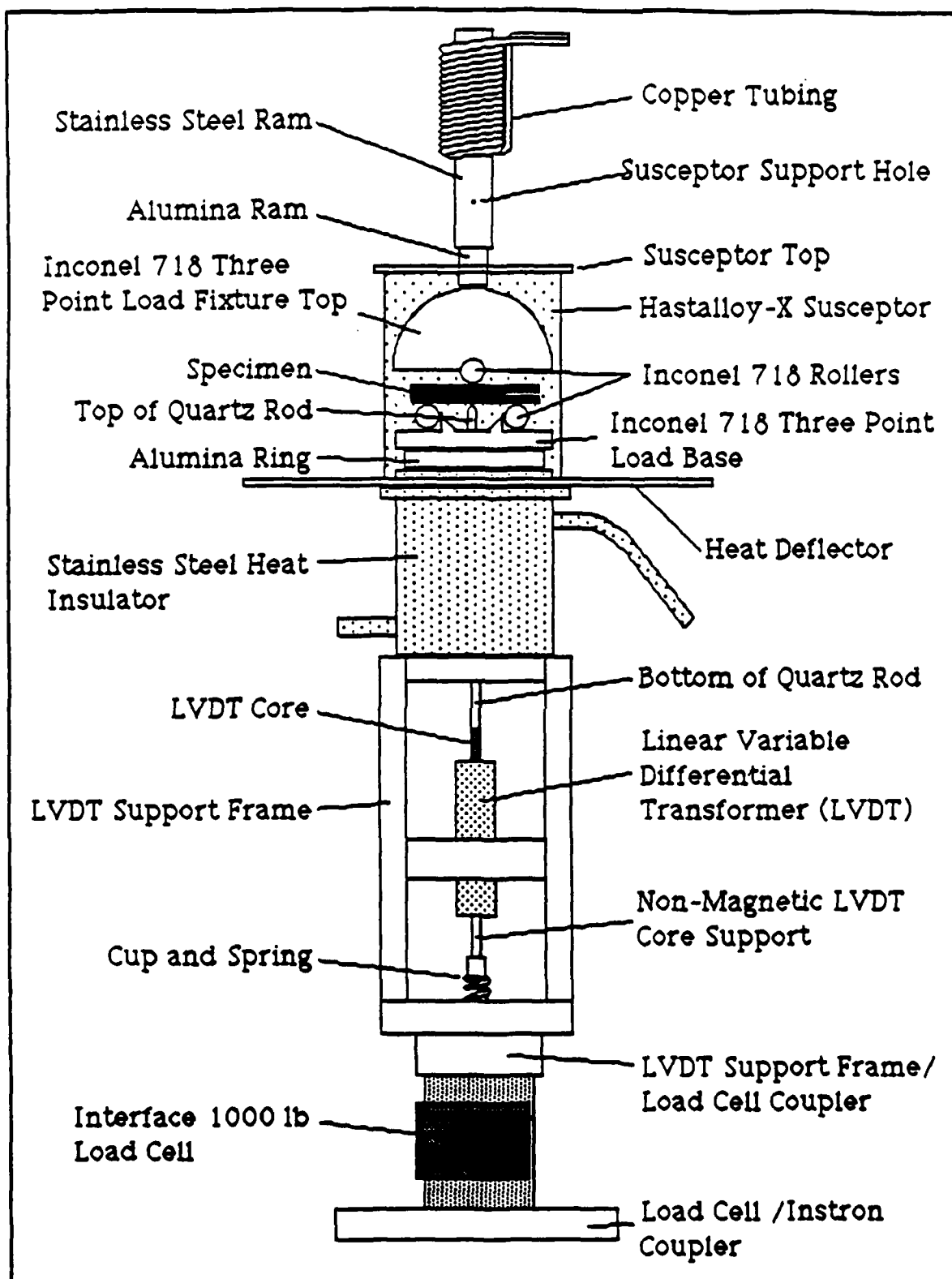
Fig. 1. Test Fixture Designed by Mol (16)

10

Stainless Steel Ram

Copper Tubing

Susceptor Support Hole

Alumina Ram

Inconel 718 Three
Point Load Fixture Top

Susceptor Top

Hastalloy-X Susceptor

Specimen

Inconel 718 Rollers

Top of Quartz Rod

Alumina Ring

Inconel 718 Three Point
Load Base

Stainless Steel Heat
Insulator

Heat Deflector

Bottom of Quartz Rod

Linear Variable
Differential
Transformer (LVDT)

LVDT Support Frame

LVDT Support Frame/
Load Cell Coupler

Interface 1000 lb
Load Cell

Load Cell /Instron
Coupler

Fig.2.   Modified Test Fixture

11
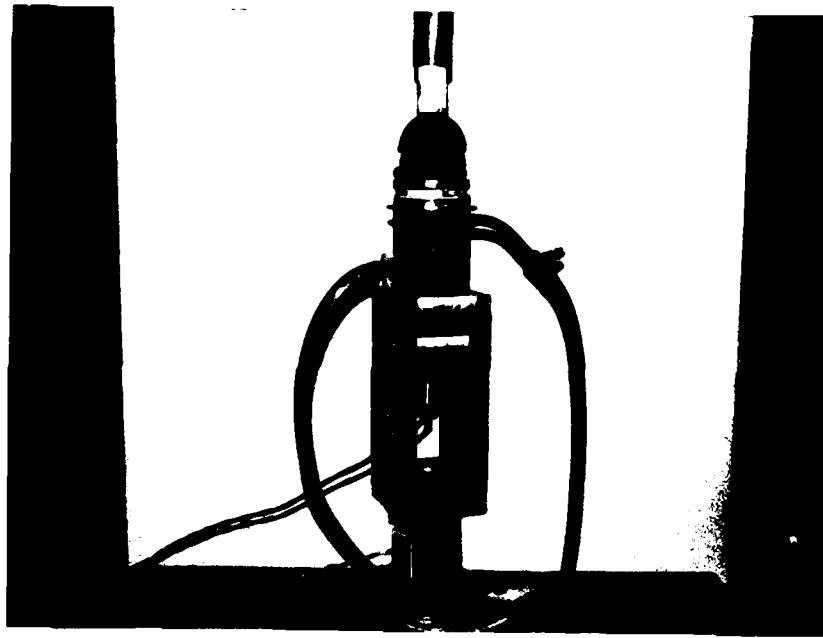
Fig. 3.   Test Fixture Mounted On Instron
TTD Tension/Compression Tester

an Endevco 4225 Power Supply and Signal Conditioner. The
calibration factor between the load input to voltage output
was a constant value of 0.622978 lb/mv for the 1000 lb load
cell and 0.078125 lb/mv for the 25 lb load cell throughout
the study.

LVDT Support Frame. The LVDT support frame was made of
aluminum and sits directly on top of the load cell. It
serves as both a support for the LVDT itself as well as a
support for the rest of the test fixture.

A Daytronic Model DS200A LVDT and a Daytronic Model 3130
LVDT Signal Conditioner with a Model 3200 Digital Indicator

were acquired from Mr. George Hartman of the University of Dayton Research Institute. This was to increase the sensitivity of the displacement measuring capability and the signal to noise ratio. The LVDT signal could then be amplified to a point where a 0.025 inch deflection of the LVDT resulted in a 15 volt signal change and still have no appreciable degradation of the signal quality. The calibration factor between displacement input to voltage output was a constant $6.59E-06$ in/mv throughout the testing. This was a major change in the instrumentation setup than used by Mol (16). Also, in response to recommendations made by Mol the LVDT support frame itself was changed. The compactness of the new LVDT, and the fact that it incorporated an internal return spring, allowed it to move much closer to the top of the support frame. This drastically reduced the effects of the load fixture compliance as compared to the specimen compliance. See Figure 2.

Three Point Bend Fixture. The same three point bend fixture as designed and used by Mol (16) was employed in this study except for one modification. See Figure 2. The fixture contained a stainless steel heat insulator. This heat insulator was used to protect the lower portion of the test fixture, and particularly the LVDT, from heat during the elevated temperature tests. The insulator was hollow except for a tube running top to bottom through the center. This

13

allowed a quartz rod to pass through and reach the specimen from the LVDT. A dedicated Neslab HX-75 refrigerated recirculating heat exchanger was used to pass water through the hollow portion of the heat insulator to carry away the heat. Water was passed at approximately 90 degrees F. This provided enough cooling to keep the LVDT within its operating temperature limits, while not creating an unacceptably large heat sink. The heat insulator also provided a platform for a heat deflector used to contain the heat radiated from the lights. The heat insulator was connected directly to the top of the LVDT support frame by two machine bolts.

On top of the heat insulator was a 0.5" thick alumina insulating ring. This was cemented to the heat insulator with high temperature ceramic adhesive. To this was cemented the actual three point bend load base.

The three point bend load base was constructed of Inconel 718 to withstand temperatures up to 1500 F. The rollers were also constructed of Inconel 718. The span at the top of the rollers was 1.5 inches, +/- 0.001 inches. The half-moon top was also made of Inconel 718 and was constructed to allow for slight variations in position without affecting the test or creating sideloads on the specimen. Provisions were made for the insertion of alignment pins during setup and preload to insure consistent alignment of the top.

14

A modification to the setup used by Mol (16) was made here. A one piece quartz rod that would extend the entire distance from the specimen to the LVDT was fabricated. The rod diameter was chosen to be very close to the inside diameter of the tube running through the heat insulator and the hole in the load base. The top of the rod was ground to a point and the bottom of the rod was glued to the top of the LVDT displacement rod. This modification was made to eliminate any extraneous motion or "giving" of the displacement train.

To insure even heating of the specimen in the high temperature tests, a "heat oven" was used. This was a cylinder of super steel alloy that fit over the entire load base and rested on the heat insulator. A small slit in the bottom allowed the wires for the thermocouples to be run inside. Once the ram was in place, two U-shaped pieces were placed on top to act as a lid that fit around the ram.

Instron TTD Tension/Compression Tester. An Instron TTD Tension/Compression Tester was used to apply loads to the specimens. A ram was connected to the crosshead for this purpose. Mol (16) had attached an 1 inch diameter alumina rod to the stainless steel portion of the ram. This was to protect the stainless steel portion from the heat at high temperatures as well as to prevent heat loss to the machine. The same setup was used in the current study. See Figure 2.

15

Thermal Cycling Fixture. A fixture for exposing
specimens to controlled thermal cycling was designed and
constructed. The design of the lamps was done by Mr. George
Hartman. They consisted of an aluminum body and 4 quartz
bulbs. The design provided for air cooling of the bulbs and
water cooling of the lamp body itself. Detailed drawings and
specifications for these lamps are given in Appendix D. Two
of these lamps were used for the thermal cycling portion of
this study. They were mounted on a test stand as shown in
Figure 4, one on each side of the specimen mounted on movable
arms. The design of the test stand allowed the specimen to

Fig. 4. Thermal Cycling Fixture

16

be instrumented with thermocouples in position with the upper
lamp arm out of the way. The upper lamp arm could then be
swung into its proper position without disturbing the
specimen. Keepers on the swinging arms of the stand
prevented any movement of the arms in the vertical, insuring
proper spacing of the lamps on subsequent tests. A stainless
steel grip was fabricated to hold the specimens between the
lamps. No insulation was found necessary for the grip as the
heat from the lamps was focused directly on the specimen.

Instrumentation. The test fixture as described above
was combined with necessary instrumentation to complete the
test setup shown in Figure 5.

Fig. 5. Test Setup Showing Test Fixture and
Instrumentation, Elevated Temperature Test in Progress

17

The overall setup consisted of: the Instron TTD Tension/
Compression Tester with 3 point bend fixture, load cell, and
LVDT mounted on it; the Daytronics Model 3130 LVDT Signal
Conditioner and Digital Indicator; the Endevco 4225 Power
Supply and Signal Conditioner; the Hewlett Packard 7045B X-Y
plotter; Hewlett Packard 3466A Digital Multimeter (DVM); the
Research Inc. Microcon 823 Digital controller; Research Inc.
Model 5193 Line Heaters (2); Research Inc. Model 5305
Parabolic Strip Heaters (2); and the Neslab HX-75
Refrigerated Recirculating Heat Exchanger.

Room Temperature Tests

Mode II. For these tests the heat shield, heat oven
parts, Microcon controller, and heat exchanger were not used.
The output from the load cell and LVDT went to their
respective signal conditioners and were plotted by the
Hewlett Packard plotter. The load cell signal was also sent
to the DVM so the test could be closely monitored to prevent
damage to the specimen or fixture.

Mode I. For Mode I tests with the crack growth parallel
to the fibers, the quartz rod was removed and the LVDT was
not used. Only the load cell signal was plotted. The rest
of the test setup was the same as Mode II.

For the Mode I tests with the crack growth perpendicular
to the fibers, the same set up as used in Mode II tests was

18

used with one modification. The quartz rod was placed in contact with the top roller instead of the bottom of the specimen. Displacements and loads were plotted as in Mode II tests.

Elevated Temperature Tests

Mode II. The same instrumentation setup was used for these tests as for the room temperature tests, the differences being that the heat shields, heat oven, and heat exchanger cooling water were used. Mol (16:35) elected to use only 2 lamps for the 600 F tests and 4 lamps for the 1000 F tests. This study used 4 lamps for both tests. A total of four thermocouples were placed against the surface of the specimen. These were not attached with ceramic cement. Instead, a thin nichrome wire was very loosely wound around the end of the specimen, outside of the point of contact with the roller. Then two thermocouples were routed through this loop, one on each side of the specimen, and the tips of these thermocouples were bent to put a spring tension against the side faces of the specimen. The third thermocouple was laid in the machined notch and the fourth was placed in such a way that it held a spring tension against the other end of the specimen. See Figure 6. It was felt that the long soak times and the use of the heat oven would allow for stabilization of the temperature in the region of the

19
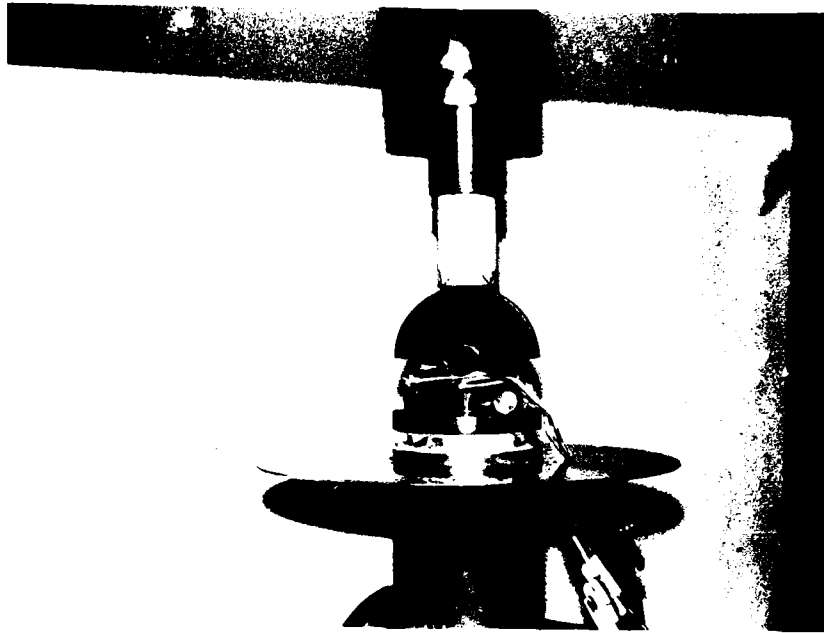
Fig. 6. Specimen Ready for Elevated Temperature
Test With Thermocouples in Place

specimen and that the thermocouples would provide accurate

temperature information in this configuration. In addition,

it was desirable to have no foreign substances on the

specimen during the measurement of the critical load.

Figure 7 shows the setup ready for a test with the heat oven,

heat shield, and lamps in place.

Mode I. The same test fixture setup was used in the

Mode I tests as in the Mode II tests with the exceptions

already discussed concerning the removal or modified

placement of the quartz rod based on the fiber orientation in

the Mode I tests.
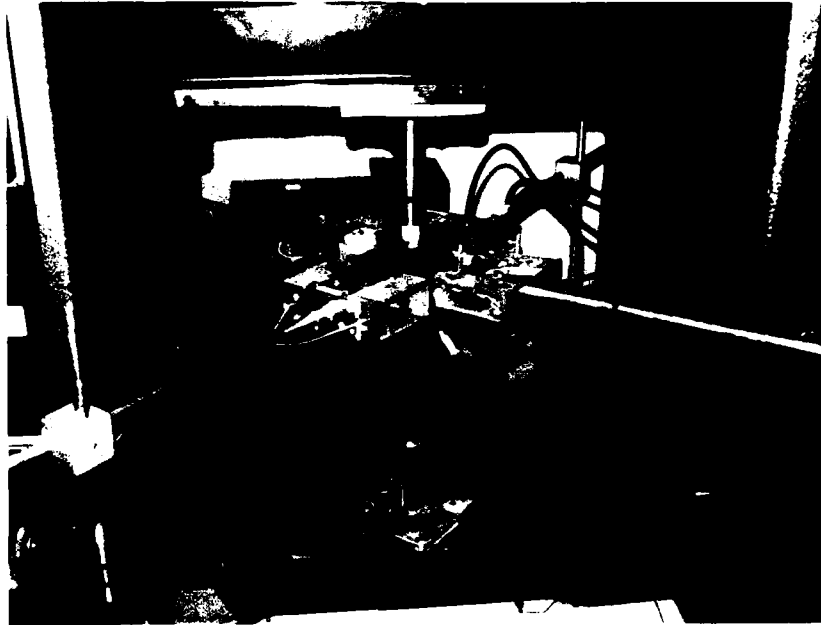
Fig. 7. Test Setup for Elevated Temperature Tests
Showing Placement of Heating Lamps

Validation

The same procedure used by Mol (16) was employed to
validate the test stand and instrumentation. The procedure
was to determine within acceptable accuracy the modulus of
elasticity of aluminum by using a three point bend specimen
and beam theory including shear deformation. A beam of 6061-
T6 aluminum was machined and tested. Table 1 summarizes the
physical and material properties of the specimen. Prior to
testing the aluminum bar, the compliance of the test fixture
was tested. After the new LVDT was installed in the new
location the load fixture deflection was decreased

21

Table 1. Properties of aluminum specimen

height	0.495	in
width	0.262	in
length between rollers	1.500	in
Young's Modulus (E)	10,000	ksi
Shear Modulus (G)	3,300	ksi

significantly and became almost perfectly linear in the range
of loads anticipated. The deflection of the fixture showed
no significant change at the three temperatures tested: room
tempe_ature; 600 F; and 1000 F. This was expected as the
fixture itself was cooled and the temperature of the LVDT
support frame and the heat exchanger is the same at all three
testing temperatures. The deflection attributed to the
specimen was then taken to be the difference between the
total measured deflection at a given load and the deflection
of the test fixture at that load. This same procedure was
used later when determining the deflection of the composite
specimens.

From beam theory that includes the shear deformation of
the specimen, the following equation for Young's Modulus can
be obtained for the three point bend specimen:

$$E = (PL^3/48I)/(\delta_c - (PL\alpha_s/4GA)) \qquad (1)$$

where I is the moment of inertia of the beam, P is the load, L is the distance between the beam supports, G is the shear modulus, δ_c is the deflection of the midpoint of the beam and α_s is 1.5 for rectangular cross-sections (1:412). The value for Young's Modulus was found to be consistently within 10% and most often within 5% of its standard quoted value.

IV. Experimental Procedure

This chapter will describe the procedures used in this study for determining the Mode II fracture toughness (G_{IIc}) of two ceramic matrix composites, CGW 1723 and CGW 7740. Testing was conducted at room and elevated temperatures. In addition, thermal cycling effects on G_{IIc} of CGW 1723 were studied. Mode I fracture toughness, G_{Ic}, and Mode I apparent fracture toughness, G_{Ic}^{*}, of CGW 1723 were also investigated at room temperature and 1000 F. This chapter will begin with the fabrication of the composite plates from which the specimens were cut and go through the post mortem examination. Differences in the procedures for each phase of testing; room temperature, elevated temperature, thermal cycling, and Mode II vs Mode I will be elaborated on.

Plate Fabrication

All plates were manufactured at the Air Force Materials Laboratory under the supervision of Mr. Larry Zawada. The following processing information comes from conversations with him, actual observation of the process, and from details furnished by him in a recent paper (20,19).

CGW 1723. This material is a Nicalon fiber/alumino-silicate glass matrix composite. Fibers were from the Nippon Carbon Company, of 12.5 micron average diameter. Organic

24

handling binder was burned off prior to infiltration in the glass slurry. The fiber tow was pulled through a mixture of glass frit in distilled water. The fibers were then wound onto a mandrel, lamp dried, and cut into 10 cm by 10 cm squares. These were then stacked in a unidirectional orientation in a graphite die, and hot pressed. The processing temperature and pressures were in excess of 1100 C and 1500 psi respectively. Processing time was in excess of 10 minutes at stabilized pressure and temperature. The plates were designated 89C0403, 87C12, and 87C17.

CGW 7740. This material is a Nicalon fiber/borosilicate glass matrix composite. The process for infiltrating, winding and drying the tow is the same as for the CGW 1723. The processing temperature for this material was slightly higher than for the CGW 1723. The processing pressure and time were the same. This plate was designated 89E08.

General Procedures

The following information applies to all specimens and all tests. Separate sections will detail how the room temperature, elevated temperature, and thermal cycling portions of this study were conducted.

Specimen preparation. Mr. Larry Zawada provided both plates from which the specimens were cut. The plates were

25

approximately 4" x 4" in size. Fiber orientation and layup of the CGW 1723 was $[0_9]_T$ and the CGW 7740 was $[0_{10}]_T$. An oil lubricated diamond wafering blade at low speed was used to cut the specimens to approximately 2" long and 0.3" wide. Final dimensions were achieved by grinding on a 40 micron diamond wheel. The specimens were machined so as the largest variation in height or thickness did not exceed 0.002" on a single specimen. This occasionally required grinding to a slightly smaller size than the desired 0.1" width and 0.3" height. Maximum overhang beyond the rollers on the testing setup was desired; therefore, specimen length was not altered. All dimensions used in calculations were averaged from three measurements taken on the specimen, one at each end and one in the middle. Appendix A gives the dimensions of all specimens after machining. Mode II and Mode I specimen orientations and notations are shown in Figures 8 and 9 respectively.

Pre-cracking of specimens.

Mode II. The specimens were notched on the midplane, parallel to the fibers, with the same diamond saw as used to cut the specimens. The notch was 0.015" wide, and approximately 0.1" deep. Prior to pre-cracking, each specimen was tested with no crack to measure compliance and determine Young's modulus. Then, a Mode I pre-crack was grown from the machined notch to provide a "natural" starter

26
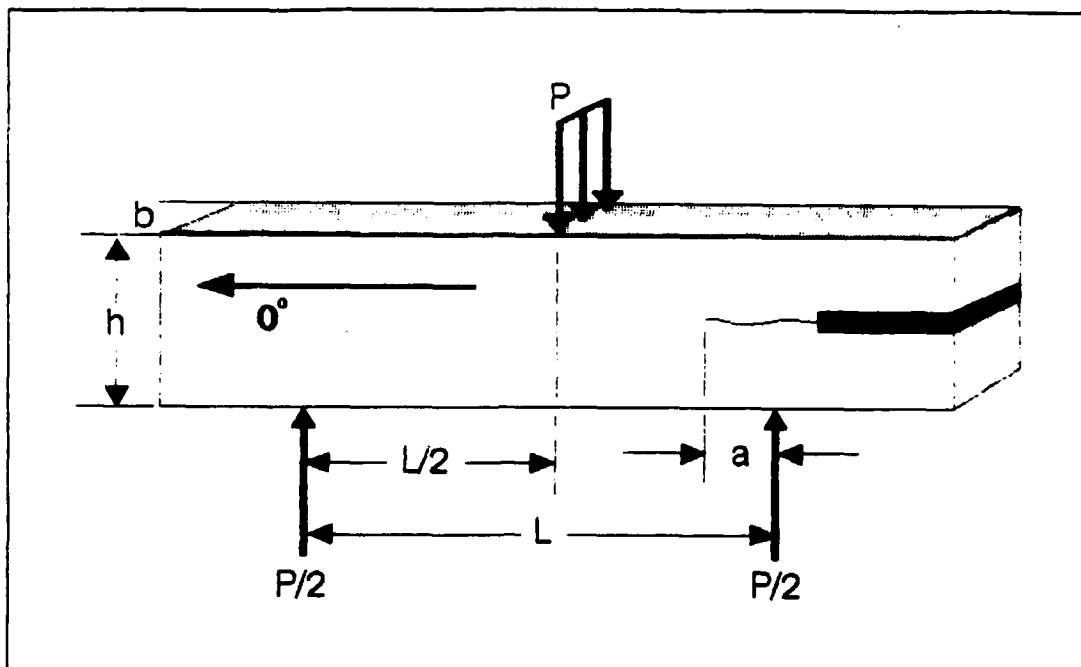
Fig. 8. Mode II Specimen Orientation and Notation
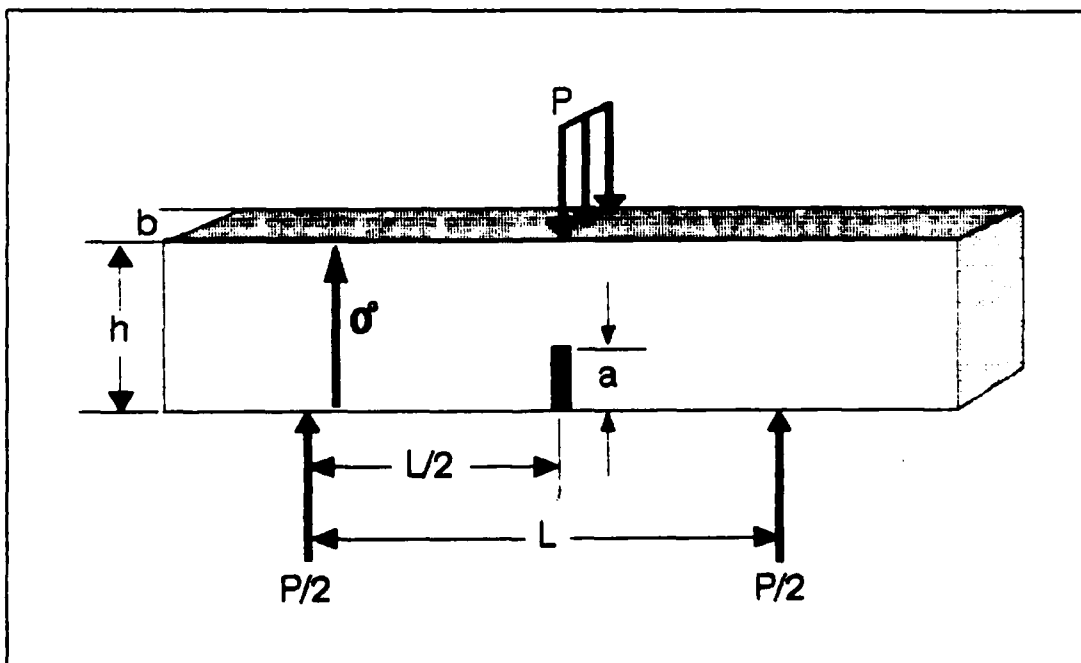
Fig. 9A. Mode I Specimen Orientation and Notation
For Tests With Crack Parallel to Fibers

27
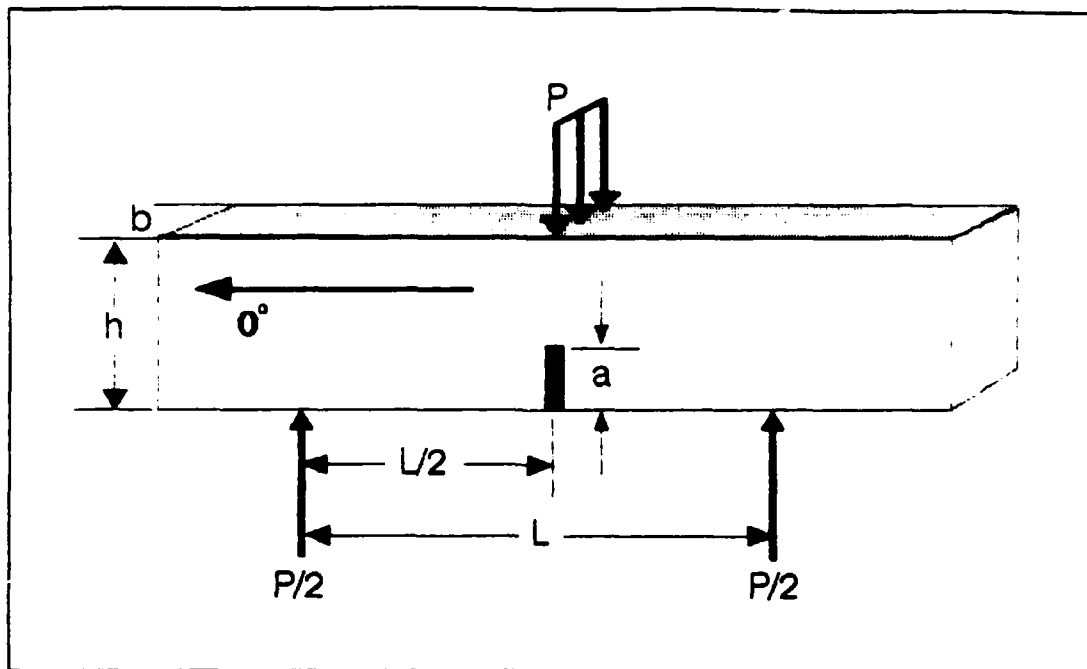
Fig. 9B. Mode I Specimen Orientation and Notation
For Tests With Crack Perpendicular to Fibers

crack for testing. A pre-cracking jig was designed by the

author and fabricated at the AFIT fabrication shop. The jig

consisted of a double sided clamp to hold the specimen, a

modified jewelers screwdriver to act as a wedge in the

machined notch, and an extending micrometer to drive the

wedge into the notch. This setup allowed the specimen to be

clamped flat and the crack to be grown very precisely. The

specimen was clamped at the location of the maximum desired

crack length and the wedge very slowly driven into the notch

with the micrometer. The growth of the crack was observed

through a traveling microscope. No attempt to achieve an

exact pre-crack length was made. Rather, a range of

acceptable lengths was determined based on test needs and the amount of adjustment that could be made on the test fixture by moving the specimen on the rollers. The pre-crack lengths were chosen to preclude having less than 0.1" overhang beyond a roller, to have the notch over a roller, or to have the crack tip under the top load application point. The pre-crack lengths varied from 0.0" to 0.7". The specimen was clamped at the end of the desired range and the specimen pre-cracked until the crack was within this range and the crack tip was well defined. A pencil mark was made at the crack tip for later reference to insure the crack had grown after the determination of the critical load. A traveling microscope was instrumented to measure up to 0.0001". From the crack tip, the desired crack length was measured back towards the notched end and a pencil mark was placed on the edge of the specimen that would be in contact with the roller. Later, this mark would be used to place the specimen in the proper location on the test fixture, with this mark directly over the apex of the roller. Figure 10 shows the pre-cracking jig and microscope with a specimen in place.

Mode I. A 0.008" wide starter notch was cut at the midpoint of the specimen approximately 0.12" deep. Originally, it was planned to grow a Mode I pre-crack at the center of the notch to a depth of 0.13". However, due to the small size, five specimens were damaged during the
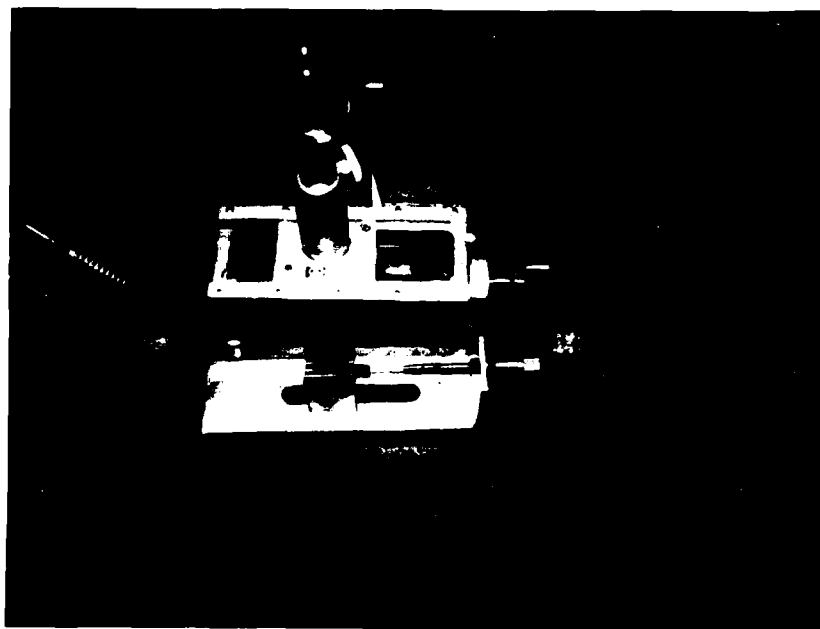
Fig. 10. Pre-cracking Setup Showing Pre-Cracking Jig
and Travelling Microscope, With
Specimen in Place

machining of the starter notch and pre-cracking procedure and
were unsuitable for testing. Because of the limited
availability of this material only four tests, two at room
temperature and two at 1000 F, were conducted with each fiber
orientation (fibers parallel and fibers perpendicular to
crack). Additionally, the specimens were not pre-cracked
beyond the starter notch.

Test fixture preparation. The test fixture was prepared
for testing in the same manner for each test. All

30

instrumentation was warmed up for a minimum of 30 minutes to allow all readings to stabilize. The load cell was then loaded slowly 3 times to a load greater than was anticipated during testing. The LVDT signal conditioner provided a calibration feature for the LVDT to confirm no changes in the calibration factor had occurred. This was used and the reading was checked against the baseline value that was established at installation.

Specimen alignment.

Mode II. The small size of the specimens and hence the small loads and displacements to be measured required consistent placement and alignment of the specimen. Eight pins were inserted in holes in the load base, four to hold the rollers in place and four to act as alignment guides for the top piece. The specimen was then placed in position with the roller position pencil mark at the apex of the roller. A spacer was used that when placed between the roller alignment pins and the specimen would line the specimen up directly over the quartz rod connected to the LVDT. This was very effective in assuring consistent alignment of the specimen. The half moon top piece was then put in place. Once all of the equipment that would be on the test fixture for a given test was in place (there were additional pieces during the elevated temperature tests that will be described later) the load cell was zeroed. A slight

pre-load was placed on the specimen (approximately 15 lb)
See Figure 11. The roller mark was rechecked and the LVDT
was checked for freedom of movement. The spacer and
alignment pins were then removed. See Figure 12.
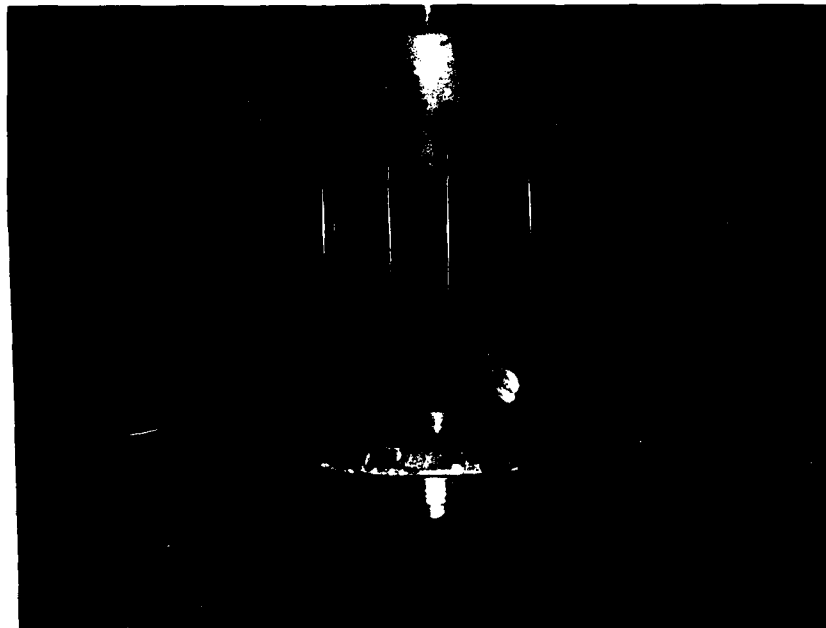
Fig. 11.   Specimen on Test Fixture, Alignment Pins
and Spacer in Place

Mode I. The same procedure was followed in the
Mode I tests with two minor differences. No preload was put
on the specimen. Instead the alignment pins were left in
place and the ram was lowered only enough to prevent the half
moon top from slipping. This procedure was adopted due to
the very small critical loads anticipated. The other change
from Mode II procedures was in the placement of the alignment
marks on the specimen. Instead of using a bottom roller

32
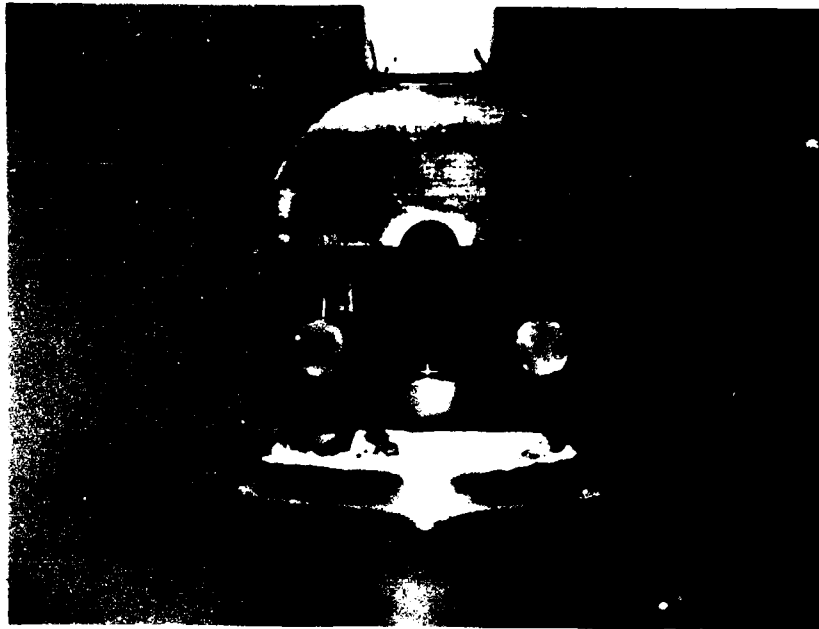
Fig. 12. Specimen on Test Fixture, Ready For Test,
Alignment Pins and Spacer Removed

position mark as in Mode II tests, a pencil mark was placed

directly above the starter notch and this was aligned with

the load application point of the half moon top. This

insured the load was applied directly over the starter notch.

Room Temperature Tests

Mode II. For the Mode II room temperature tests, the

setup just described was used. The Instron was then unloaded

to 15 mv load cell output (approximately 10 lb) and then

loaded to 20 mv (approximately 15 lb) to take any slack out

of the load train. The X-Y plotter was then zeroed to the

appropriate starting point. The load was plotted on the Y

33

axis with scales ranging from 0.01 v/in to 0.05 v/in depending on the crack length and anticipated critical load. The displacement was plotted on the X axis, with scales ranging from 0.1 v/in to 0.5 v/in, once again depending on the critical load anticipated. It was found from experience that keeping the X scale a multiple of 10 of the Y scale was a good starting point. The specimen was then loaded at a crosshead speed of .005 in/min. Typically three runs were made with each crack length. The first and second would load the specimen to about one-half of its anticipated critical load. This provided the compliance data only. On the final run, the specimen was loaded until a definite change in the compliance curve could be seen. The specimen was then removed from the load fixture and examined under the microscope to insure crack growth had occurred. This was done without putting the wedge in the notch so as to not inadvertently grow the crack. On several occasions the cracked specimen was loaded to about one-fourth of the critical load to see if the compliance had changed after crack growth. This change in compliance showed no consistent pattern, which can be attributed to varied amounts of fiber entanglement and interlocking.

After crack growth was confirmed by visual examination, the specimen was again pre-cracked in Mode I to a desired length. This was to prevent any effect on the compliance due

34

to fiber locking or other phenomena. This insured that all Mode II crack growth began under the same conditions.

Mode I. The only data needed for calculation of G_{ic} was the critical load. In the tests with the crack growth parallel to the fibers it was anticipated that the failure mode would be a rapid decrease in the measured applied load at failure and the maximum measured load would be P_{crit}. This is what was observed during the tests. In order to prevent any interference with the crack growth, the quartz rod was removed during these tests and displacement data was not recorded. Crack growth in these specimens could be observed without magnification as all specimens failed catastrophically.

In the Mode I tests with the crack growth perpendicular to the fibers, it was anticipated that the failure Mode would be a change in the compliance of the specimen similar to the Mode II case. Therefore, displacement information was required in these tests. In order to prevent any interference from the quartz rod in the starter notch, the rod was run up to the top roller and displacements were measured at this point. This was accurate in determining the load at which the compliance changed and this was determined to be P_{crit}.

Elevated Temperature Tests

Mode II. The tests conducted at elevated temperatures used exactly the same instrumentation and specimen testing procedures as the room temperature tests. The only differences were in the fixture arrangement, the specimen instrumentation with thermocouples, and the heating itself. The fixture arrangement and specimen instrumentation are described in Chapter 3. The heating of the specimen was controlled with a Microcon Proportional, Integral, Differential (P.I.D.) controller. The Microcon was programmed to raise the temperature of the specimen linearly to 600 F in 15 minutes or 1000 F in 25 minutes, depending on the desired final temperature. These long times were used to prevent any thermal shock and to enable the Microcon to better balance the temperature zones. During the heating process, the specimen had to be continually unloaded to prevent overloads due to the thermal expansion of the fixture. Once the temperature had stabilized at the desired level, it was left to soak for 20 minutes. It was found that this was ample time for all thermal expansion of the fixture to stop. Once this time expired, the tests were conducted in the same manner as the room temperature tests as far as loading procedures and rates are concerned.

Mode I. Elevated temperature Mode I tests were only conducted at 1000 F due to limited specimen availability.

The same testing procedures used in the Mode I room temperature tests for both fiber orientations were used. The heating procedures and test fixture arrangement were the same as used in elevated temperature Mode II tests. The effects of thermal expansion of the fixture were minimized by the lack of pre-load on the specimen. The maximum load observed on the specimen due fixture expansion was less than 0.5 lb.

Thermal Cycling Tests

The compliance and critical load tests of the specimens exposed to thermal cycling were conducted in exactly the same manner as the room temperature tests. The only difference in the procedure was the cycling itself. The specimens were cycled in a no crack condition, with only the machined pre-notch present. The fixture for cycling is described in Chapter 2. The tests were all conducted in air under a true no-load condition. The eight quartz bulbs were divided into four temperature zones, 2 bulbs in each, and each zone was controlled independently by a Microcon channel, which were in turn independently controlled by a thermocouple in that zone. Bulbs 4 and 8 were controlled by channel 1, 1 and 5 by channel 2. 2 and 3 by channel 3, and 6 and 7 by channel 4. It took several attempts with dummy specimens to achieve good temperature balance of the four zones as this was very sensitive to thermocouple placement. The locations of the

temperature zones and thermocouples are shown in Figure 13.
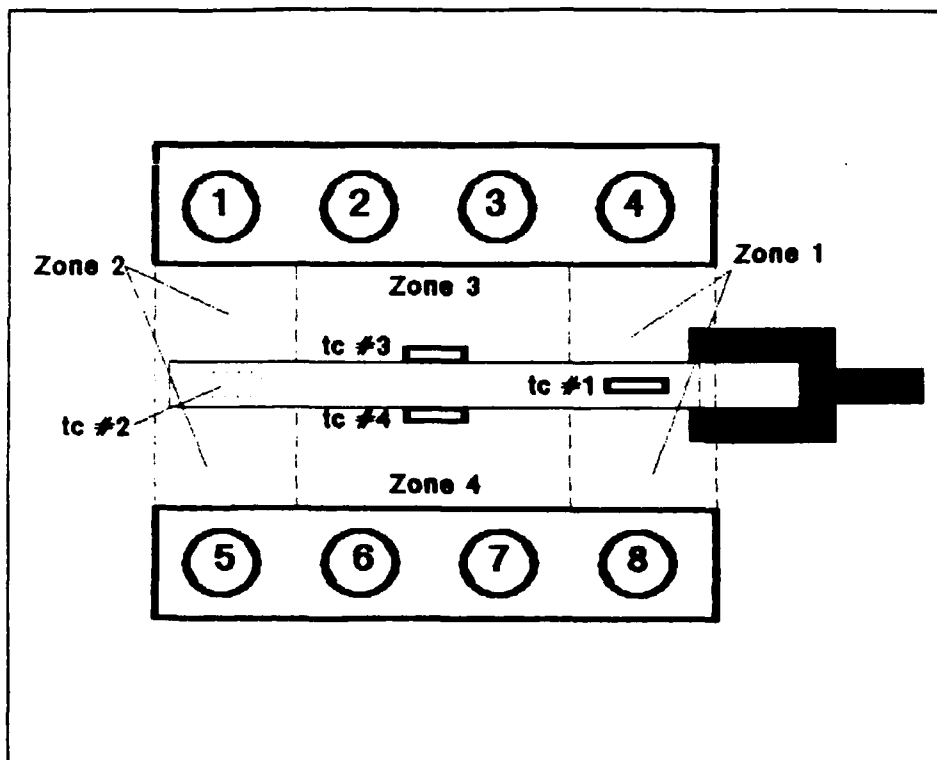
Fig. 13.   Temperature Zones on Specimens for
Control of Thermal Cycling

The specimens were heated on a linear ramp profile from 130 F

to 600 F in 3.5 minutes, held at 600 F for 5 minutes, and

then allowed to air cool for 3.5 minutes. The time of 3.5

minutes was chosen after several trials to determine how long

it took to cool the specimen by ambient air from 600 F to a

temperature at which the cooling rate decreased signifi-

cantly. This temperature was determined to be 130 F and the

time to cool from 600 F to 130 F was on average 3.5 minutes.

It was desired to use the same heating and cooling rates,

38

therefore 130 F was used as the base temperature. The
measured and programmed temperature profiles are shown in
Figure 14. After the desired number of cycles had occurred,
the specimen was removed and tested at room temperature.
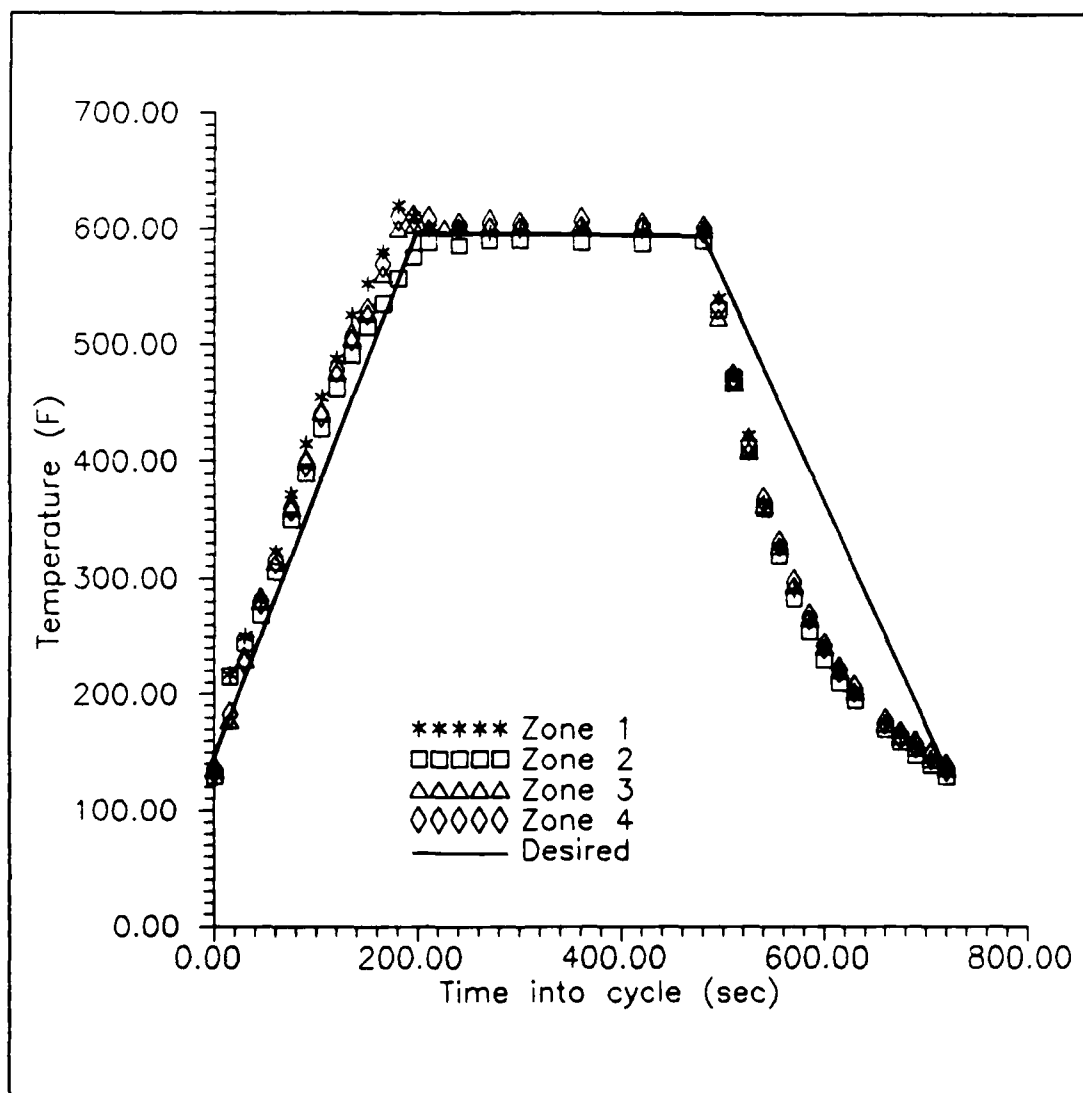
Fig. 14. Thermal Cycling Profile, 130 F to 600 F
Measured and Programmed

Post Test Analysis

Mode II. After the specimens had been tested at a crack length greater than .7 inches, they were no longer usable for further testing. Specimens were examined for crack surface, fracture surface, and microstructure characteristics. Microphotographs of the crack surface were made using a Nikon Epiphot M400 at magnifications ranging from 50x to 400x. After this was done, the specimens were opened in the plane of the crack in Mode I by pulling apart the two halves of the specimen. The fracture surface was then microphotographed with a Wild Photomakroskop at magnifications of 6.3X to 32X. If warranted they were reexamined on the Nikon. The fracture surfaces of selected specimens were then coated with carbon for viewing in an Etec Corp. Autoscan scanning electron microscope (SEM). Mr. Robert Brodecki operated the SEM, took the pictures, and developed the negatives. The micro-structure of the fracture surface was examined for evidence of any change in crack growth behavior (Mode I pre-crack versus Mode II growth) and for changes in its chemical or mechanical nature between room and elevated temperatures.

Mode I. The specimens could be used only one time in the Mode I tests. After testing was completed, the micro-structure of the fracture surface was examined on the SEM in the same manner as in the Mode II tests.

40

V. Results and Discussion

To calculate the Mode II fracture toughness (G_{IIc}) of the
tested CMC materials, it was first necessary to determine the
compliance vs crack length relationships. This was accompl-
ished by plotting the load vs displacement curve for dif-
ferent crack lengths and computing the compliance of the
specimen. The compliance values obtained were plotted
against non-dimensional crack length. Experimental data was
fitted with second and third order polynomial curve fits.
The experimental data was also compared to theoretical values
predicted by a closed form solution, Russell's equation (17).
The critical loads were measured at various crack lengths.
These values were found at room temperature, 600 F, 1000 F,
after thermal cycling, and after thermal exposure for a
predetermined period for the CGW 1723. These values were
also determined for CGW 7740 at room temperature. This data
was used to compute the experimental fracture toughness
values for the different temperature conditions and
materials. The three methods used to determine the
compliance vs crack length relationships were compared.

The Mode I fracture toughness (G_{Ic}) of the CGW 1723 was
measured with crack growth parallel to the fibers. This data
was collected at room temperature and 1000 F to compare any

41

trends found to that of G_{IIc}. K_{Ic} values were determined from the standard solution using the geometry of the specimen and the critical loads. K_{Ic} was then converted to G_{Ic} using a relationship for orthotropic materials.

The apparent fracture toughness, G_{Ic}^*, of CGW 1723 was measured with crack growth in this case perpendicular to the fibers. Data was collected for this fiber orientation at room temperature and 1000 F also. K_{Ic}^* and G_{Ic}^* values were determined using the same relationships as K_{Ic} and G_{Ic}.

Mode II

Compliance Calculations. A total of 22 specimens of CGW 1723 were tested for compliance data, 18 came from a plate designated as 89C0403 and 4 from another plate designated 87C12. Room temperature tests were conducted with 6 specimens, 600 F tests with 6, 1000 F tests with 4, and thermal cycling tests with 2 from plate 89C0403. Specimens from plate 87C12 were used in 2 tests at room temperature and 2 at 1000 F to confirm the results obtained from plate 89C0403. Room temperature tests were performed on 4 specimens of CGW 7740 from plate 89E08. Each Mode II specimen was tested at differing crack lengths. Appendix A lists the details of specimens which were used in the various tests. Compliance was calculated from the equation

$$C = \delta / P \qquad (2)$$

where C is the compliance, δ the midpoint displacement, and P is the applied load. The compliance was determined from the change in displacement and the change in load between two points on the linear portion of the load vs displacement curve. This was necessary as the slope of the load vs displacement curve was not linear at very low loads due to settling of the test fixture and its components. This curve would become linear after approximately 15 lbs applied load. Two data points were chosen in this linear region and calculations were made from these. The displacement of the load fixture at the chosen loads was subtracted from the measured displacement to obtain the actual displacement of the specimen. For this purpose the displacement to load relationship of the test fixture was established in the same manner as done by Mol (16:22-23). A sample of an X-Y plot used to calculate compliance data is shown in Appendix B.

To account for variations in height and width of individual specimens, the compliance values calculated were normalized to the nominal dimensions of 0.1" thickness and 0.3" height with an equation developed and used by Mol (2),

$$C_{Normalized} = C_{Experimental}(b/.1)(h/.3)^3 \qquad (3)$$

The lengths of the specimens were not included in this normalization equation as the distance between the rollers was fixed at 1.5" for all tests.

43

As stated in Chapter 4, multiple compliance curves were obtained from each test at the differing crack lengths. The compliance value obtained from each of these curves was normalized and plotted against non-dimensional crack length (2a/L) for each test. After all data was collected, second and third order curve fits were used to represent the normalized compliance vs non-dimensional crack length relationships. Russell (17) developed a theoretical relationship for the compliance

$$C = [1+1.5(2a/L)^3]/[4Eb(h/L)^3]) \qquad (4)$$

where a is the crack length, b the thickness, h the height, L the length, and E the value of Young's Modulus of the material. This equation is based on linear beam theory. This relationship was plotted against non-dimensional crack length to determine how well it fit the experimental data. This equation requires the value of Young' Modulus for the specimen. This was calculated at each temperature by determining the compliance of a specimen with a = 0.0" and then solving Equation 4 for E. This is the same procedure used by Mol (16:40). For the room temperature, 600 F, and thermal cycling tests, no change in Young's Modulus was seen in the CGW 1723. A slight decrease in this value was noticed at 1000 F in the CGW 1723. Elevated temperature tests were not conducted on the CGW 7740. Table 2 shows the calculated

values of Young's Modulus for the various materials and temperature conditions. The average room temperature value for E of CGW 1723, 1.71E+07, is within 10% of the value of 1.878E+07 found by Zawada (19) in tensile tests at room temperature and within 4% of the value of 1.6622E+07 found by Mol (16:40) in 3 point bend tests at room temperature. From these values of E the curves for Russell's equation at the different temperatures were constructed.

Table 2. Calculated Young's Modulus
of Specimens

CGW code	Plate number	Temperature	E (lbs/in^2)
CGW 1723	89C0403	Room temperature, 600 F, and post thermal cycling	1.72E+07
CGW 1723	89C0403	1000 F	1.68E+07
CGW 1723	87C12	Room temperature	1.70E+07
CGW 1723	87C12	1000 F	1.65E+07
CGW 7740	89E08	Room temperature	1.20E+07

Room Temperature Compliance, CGW 1723. Figure 15 shows experimental compliance values from room temperature tests and the theoretical compliance from Russell's equation with its +/- 10% variation as a function of non-dimensional crack length. It can be seen that the majority of the data falls within this range. Figures 16, 17, and 18 show the

room temperature compliance data plotted against non-dimensional crack length with Russell's equation, and 2nd and 3rd order polynomial curve fits of the data, respectively. The following equations for the 2nd and 3rd order polynomial fits were computed:

$$C = 3.65(2a/L)^2 - 1.56(2a/L) + 1.86 \tag{5}$$
$$C = 3.44(2a/L)^3 - 1.28(2a/L)^2 + .27(2a/L) + 1.84 \tag{6}$$

As can be seen from Figure 16, Russell's equation is a good representation of the data throughout the entire range of crack lengths. The second order polynomial curve fit, shown in Figure 17, is a fairly good representation of the data at midrange crack lengths (.3 < 2a/L < .6), but at shorter non-dimensionalized crack lengths the curve has a negative slope. This is not the case in reality. Also, for 2a/L > .6, the slope of the curve does not increase fast enough to accurately represent the data. The third order curve fit in Figure 18 is also a good representation of the data, with the exception of very short crack lengths (2a/L < .1) where the curve deflects oddly. Of the three curves, Russell's equation appears to best represent the data over the complete range of crack lengths and to have the smoothest change in slope.
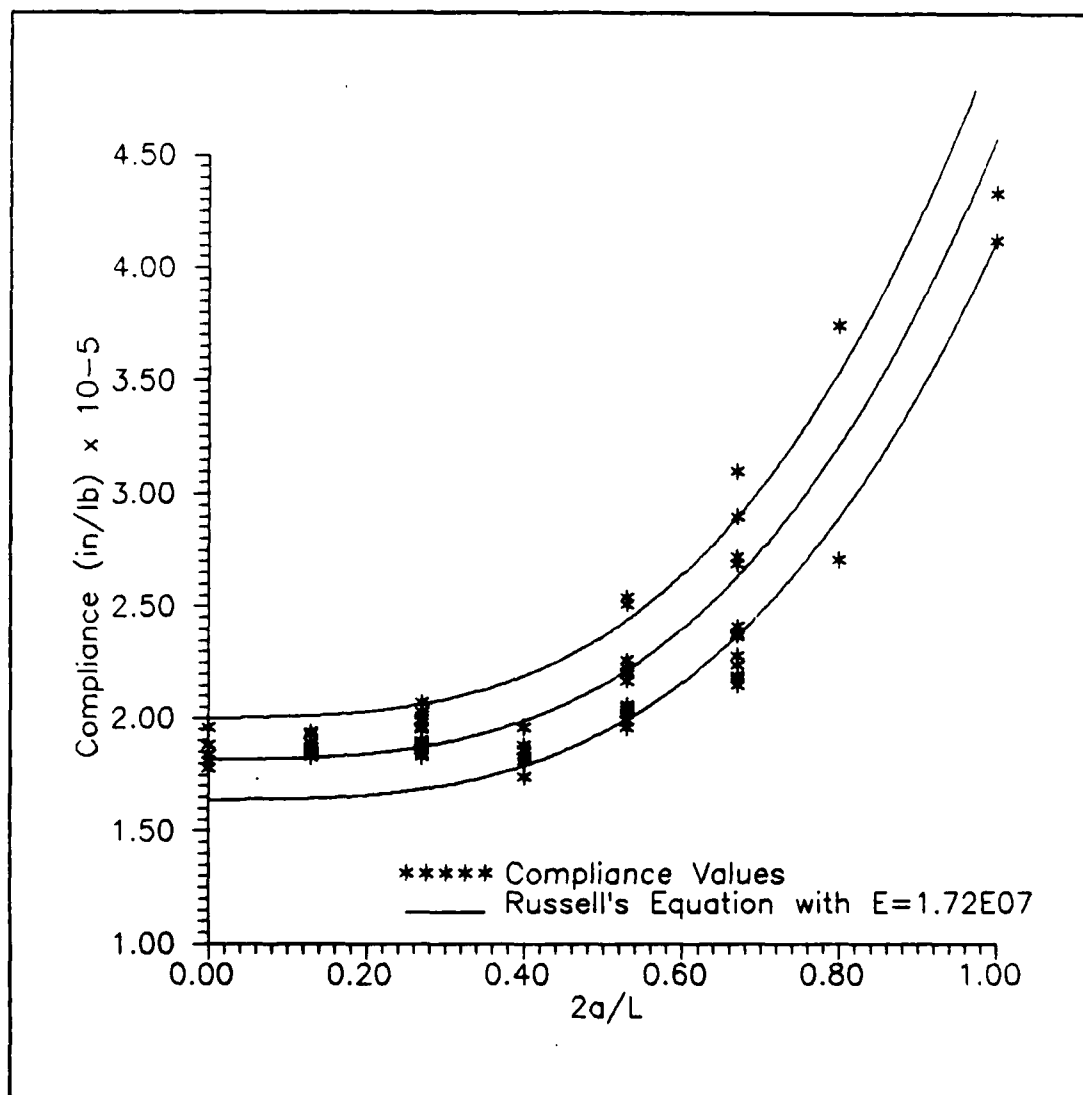
Fig. 15. Room Temperature Compliance vs Non-dimensional
Crack Length with +/- 10% Russell's Equation Shown
CGW 1723

47
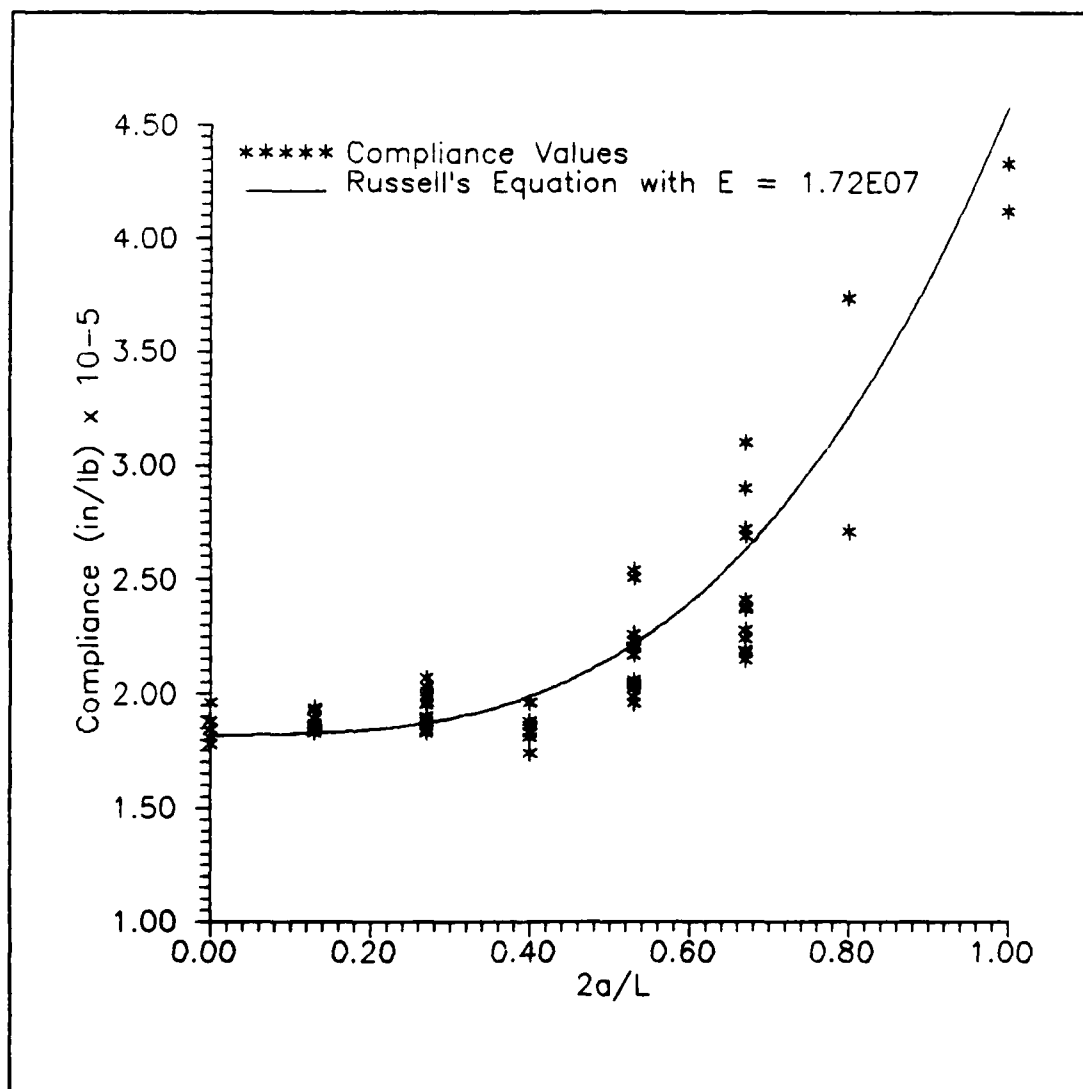
Fig. 16. Room Temperature Compliance vs Non-dimensional
Crack Length with Russell's Equation Shown
CGW 1723

48
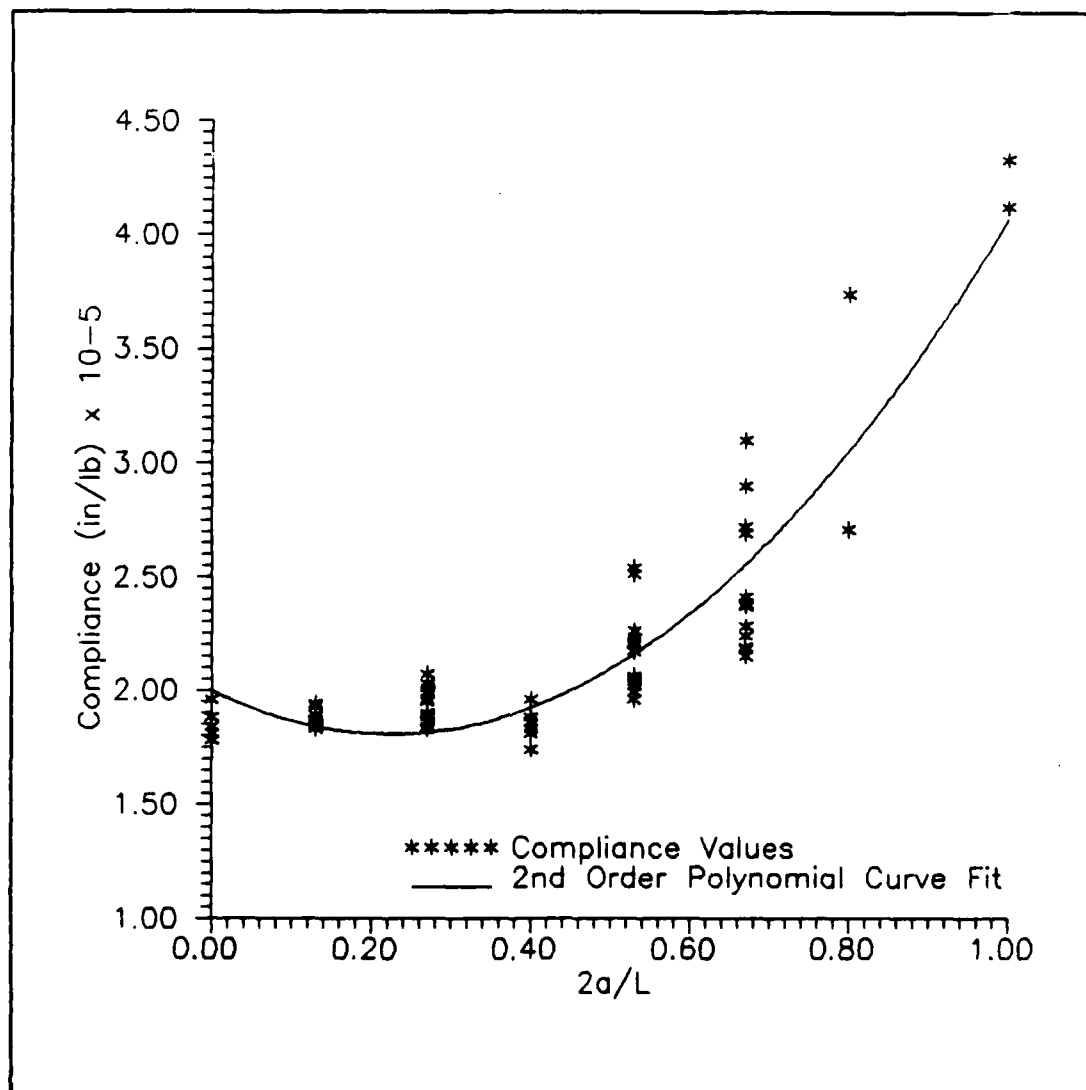
Fig. 17. Room Temperature Compliance vs Non-dimensional
Crack Length with 2nd Order Polynomial Curve Fit Shown
CGW 1723

49
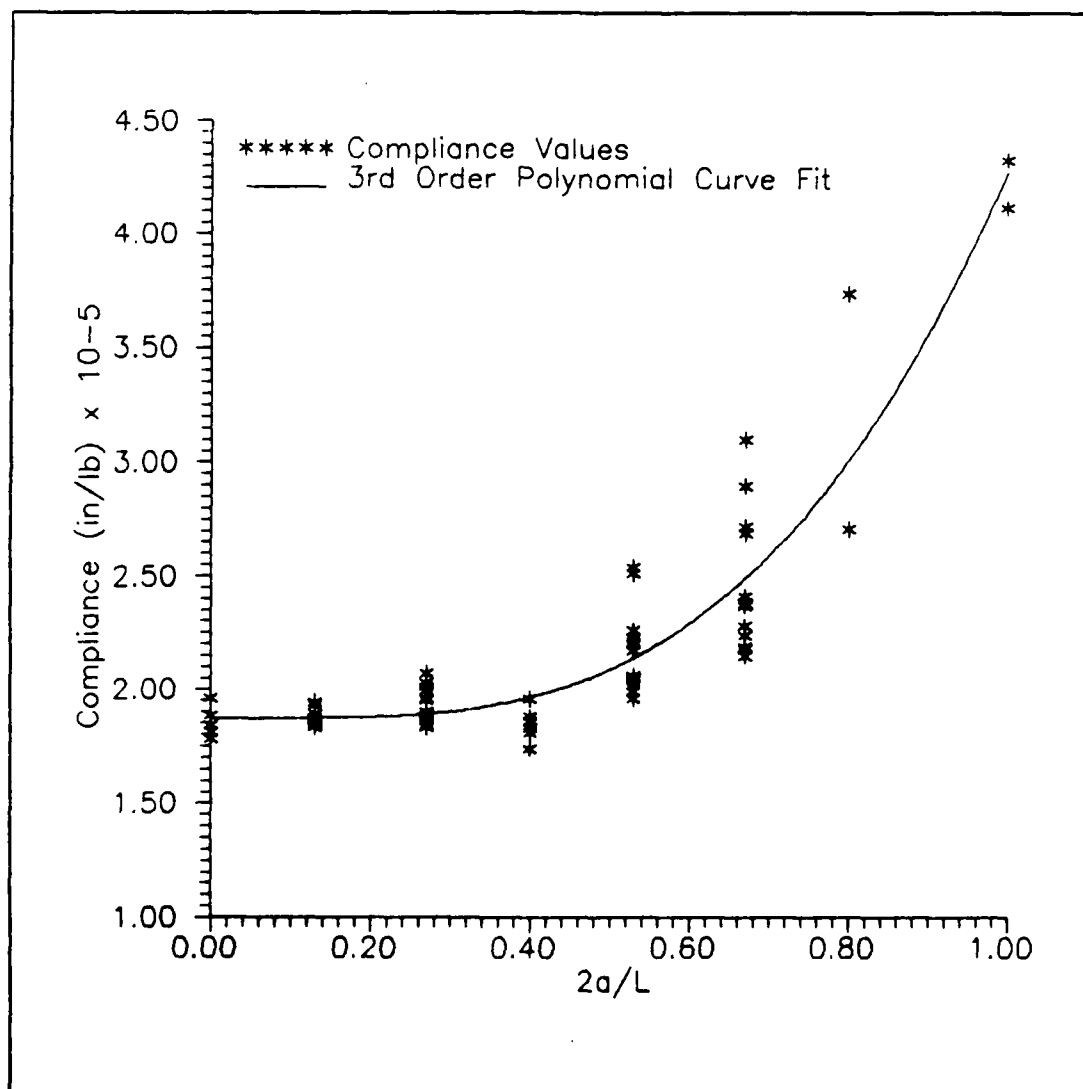
Fig. 18. Room Temperature Compliance vs Non-dimensional
Crack Length with 3rd Order Polynomial Curve Fit Shown
CGW 1723

600 F Compliance, CGW1723. Figure 19 shows the
values of experimental compliance from 600 F tests and the
theoretical compliance from Russell's equation along with its
+/- 10% variation as a function of non-dimensional crack
length. It can be seen that the majority of the data falls
within this range. Figures 20, 21, and 22 show the 600 F
compliance data plotted against non-dimensional crack length
with Russell's equation, 2nd order, and 3rd order polynomial
curve fits of the data displayed. The following equations
for the 2nd and 3rd order polynomial fits were computed:

$$C = 2.42(2a/L)^2 - 0.72(2a/L) + 1.88 \qquad (7)$$

$$C = 4.14(2a/L)^3 - 2.58(2a/L)^2 + 0.82(2a/L) + 1.82 \qquad (8)$$

The same trends can be observed in these curves as was seen
in the room temperature curves. As can be seen from Figure
20, Russell's equation is a good representation of the data
throughout the entire range of crack lengths although at
crack lengths of $2a/L > .6$ the curve predicts about 10%
greater values of compliance than were observed. The second
order polynomial curve fit is a fairly good representation of
the data at midrange crack lengths ($.3 < 2a/L < .6$), but at
shorter non dimensionalized crack lengths the curve has a
negative slope. For $2a/L > .6$ the slope of the curve does

51

Fig. 19.   600 F Compliance vs Non-dimensional
Crack Length with +/- 10% Russell's Equation Shown
CGW 1723

52

Fig. 20. 600 F Compliance vs Non-dimensional
Crack Length with Russell's Equation Shown
CGW 1723

53

Fig. 21.   600 F Compliance vs Non-dimensional
Crack Length with 2nd Order Polynomial Curve Fit Shown
CGW 1723

54

Fig. 22.   600 F Compliance vs Non-dimensional
Crack Length with 3rd Order Polynomial Curve Fit Shown
CGW 1723

55

not increase fast enough to accurately model the data as was the case in the room temperature curve. See Figure 21. The third order curve fit in Figure 22 is also a good representation of the data, but for short crack lengths (2a/L < .4) the curve deflects oddly. The third order curve is not able to capture the initial flat portion of the curve that occurs. This can be attributed to having fewer data points at the short crack lengths and they are therefore not weighted as much in the curve fit. Russell's equation represents the data, in general, over the complete range of crack lengths and has the smoothest change in slope of the three curves.

Combined Room Temperature and 600 F Compliance, CGW 1723. From looking at the compliance values at room temperature and 600 F, it was noted that the majority of the compliance values calculate! at both temperatures fell within the +/- 10% band of values predicted by Russell's equation. See Figure 23. The measured value of E did not change between these two temperatures and therefore the Russell's equation curve is the same for both temperatures. When plotted together, the data points for 600 F fall within the experimental scatter band of the room temperature tests. It was therefore considered appropriate that the two sets of data points could be combined and 2nd and 3rd order poly- nomials would be fit to the combined data. This allowed a

56

better compliance to crack length relationship to be established because of the increase in the number of data points available. Figure 24 shows the combined experimental compliance values vs non-dimensional crack length along with the compliance curve predicted by Russell's equation plotted for comparison. Figures 25 and 26 show the same data with 2nd and 3rd order polynomial curve fits. The equations for the 2nd and 3rd order polynomial curve fits of this combined compliance data are

$$C = 3.41(2a/L)^2 - 1.44(2a/L) + 1.97 \qquad (9)$$

$$C = 3.92(2a/L)^3 - 2.06(2a/L)^2 + 0.56(2a/L) + 1.83 \qquad (10)$$

Russell's equation is a good representation for this data as expected. Also as expected, the 2nd order curve fit does not represent the data well at the short crack lengths, $2a/L <$ .3. The 2nd order curve fit did become a better representation of the data at the longer crack lengths. See Figure 25. Figure 26 shows that the third order curve fit has improved at the shorter crack lengths and shows no odd changes in slope. Figures 27, 28, 29, and 30 show the 2nd and 3rd order curve fits obtained at room temperature and 600 F data and those from the combined data. The assumption that the compliance of CGW is unaffected by a temperature increase from room temperature to 600 F appears valid.
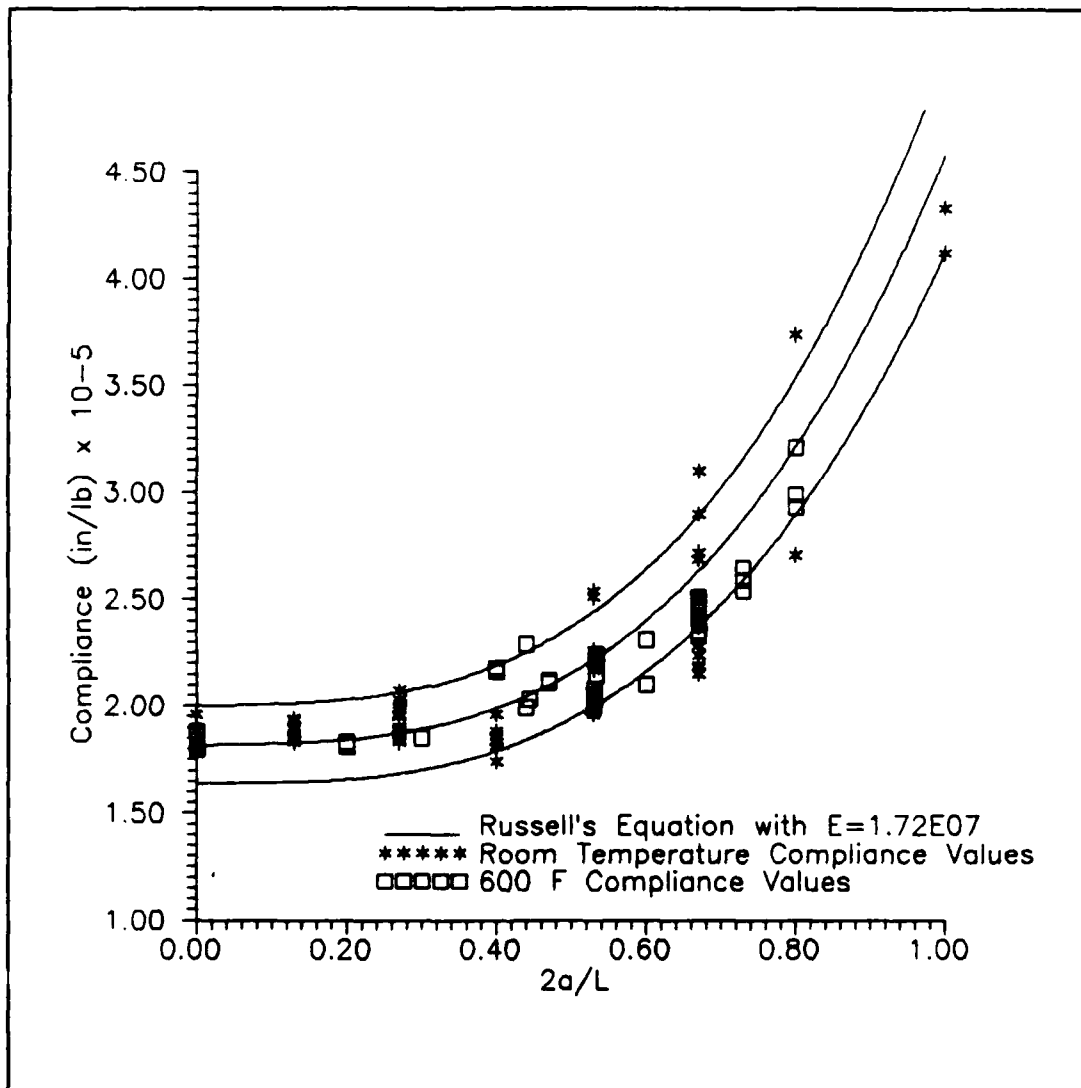
Fig. 23. Combined Room Temperature and 600 F Compliance Data vs Non-dimensional Crack Length with +/- 10% Russell's Equation Shown CGW 1723

58
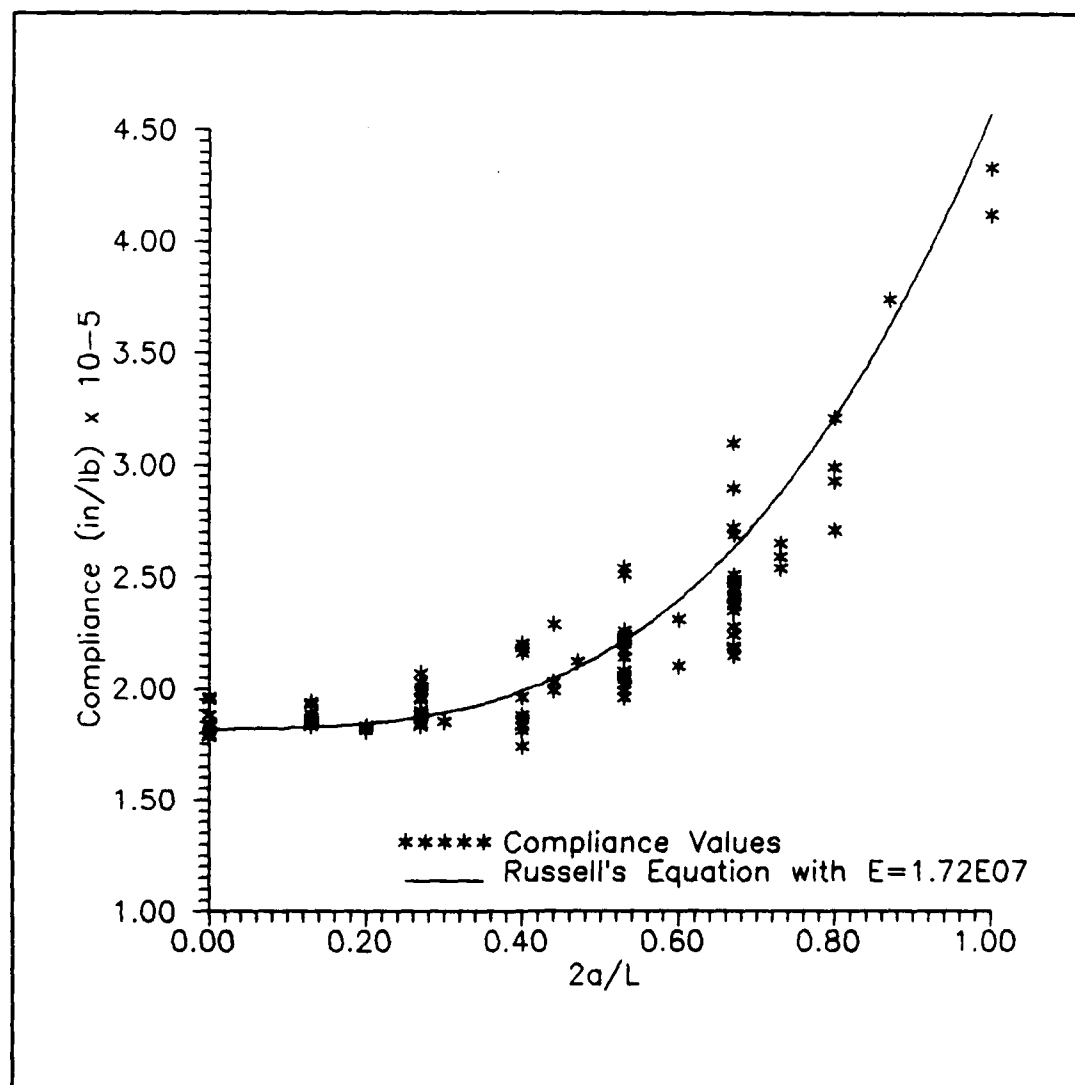
Fig. 24. Combined Room Temperature and 600 F Compliance Data
vs Non-dimensional Crack Length
with Russell's Equation Shown
CGW 1723

59
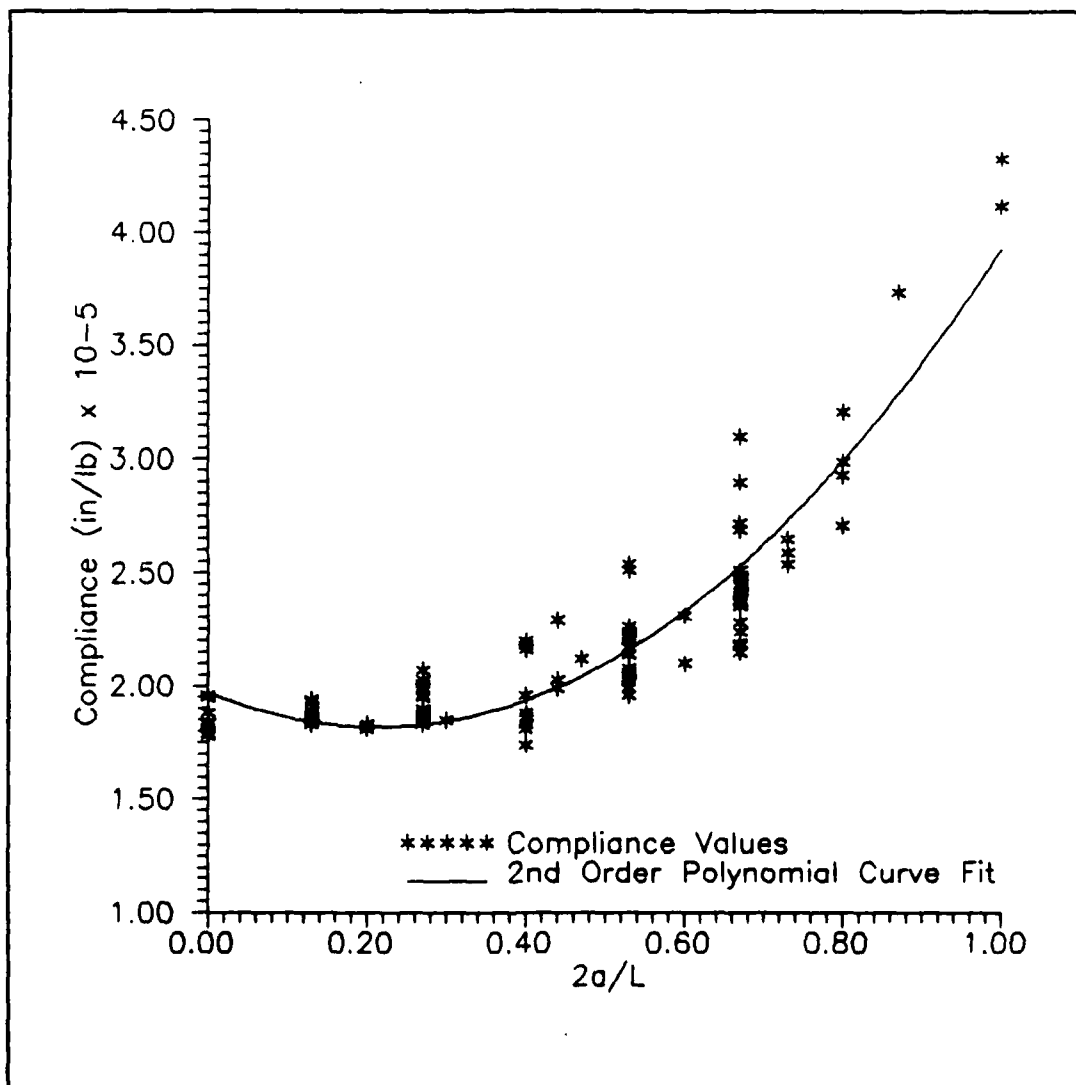
Fig. 25. Combined Room Temperature and 600 F Compliance Data
vs Non-dimensional Crack Length
with 2nd Order Polynomial Curve Fit Shown
CGW 1723

60
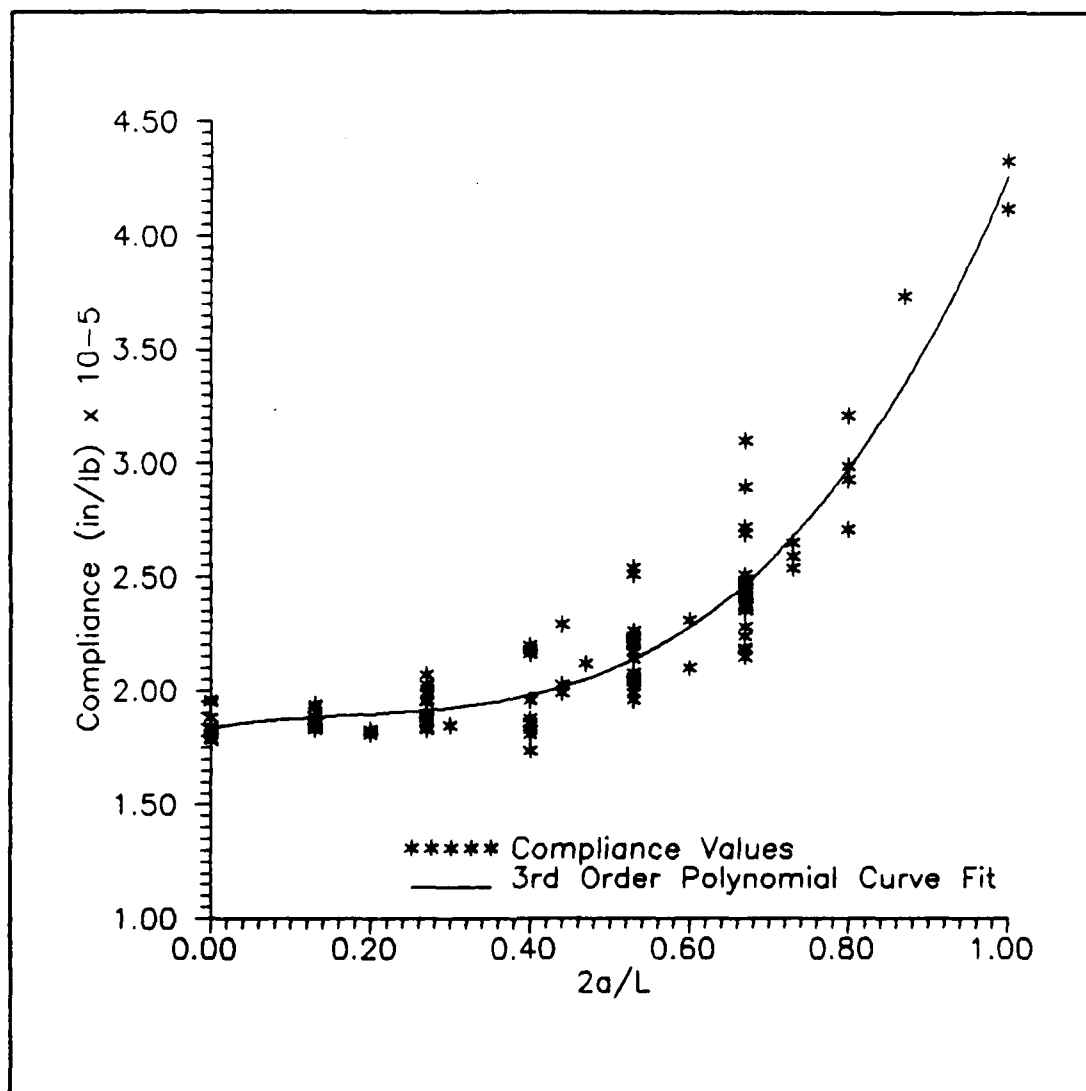
Fig. 26.   Combined Room Temperature and 600 F Compliance Data
vs Non-dimensional Crack Length
with 3rd Order Polynomial Curve Fit Shown
CGW 1723

61
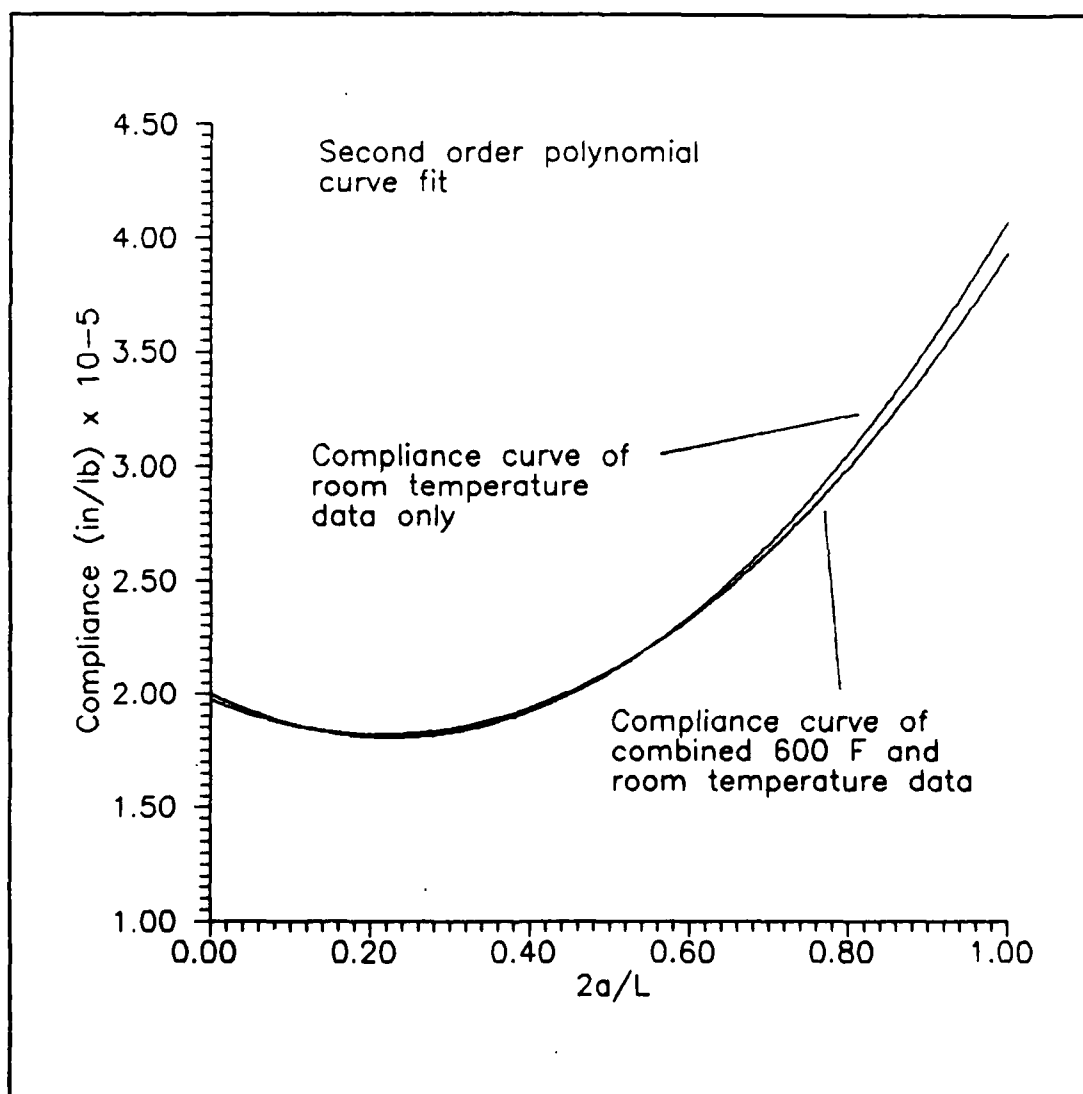
Fig. 27. Comparison of Room Temperature and Combined Room Temperature and 600 F Compliance Curves Second Order Polynomial Curve Fits Shown CGW 1723
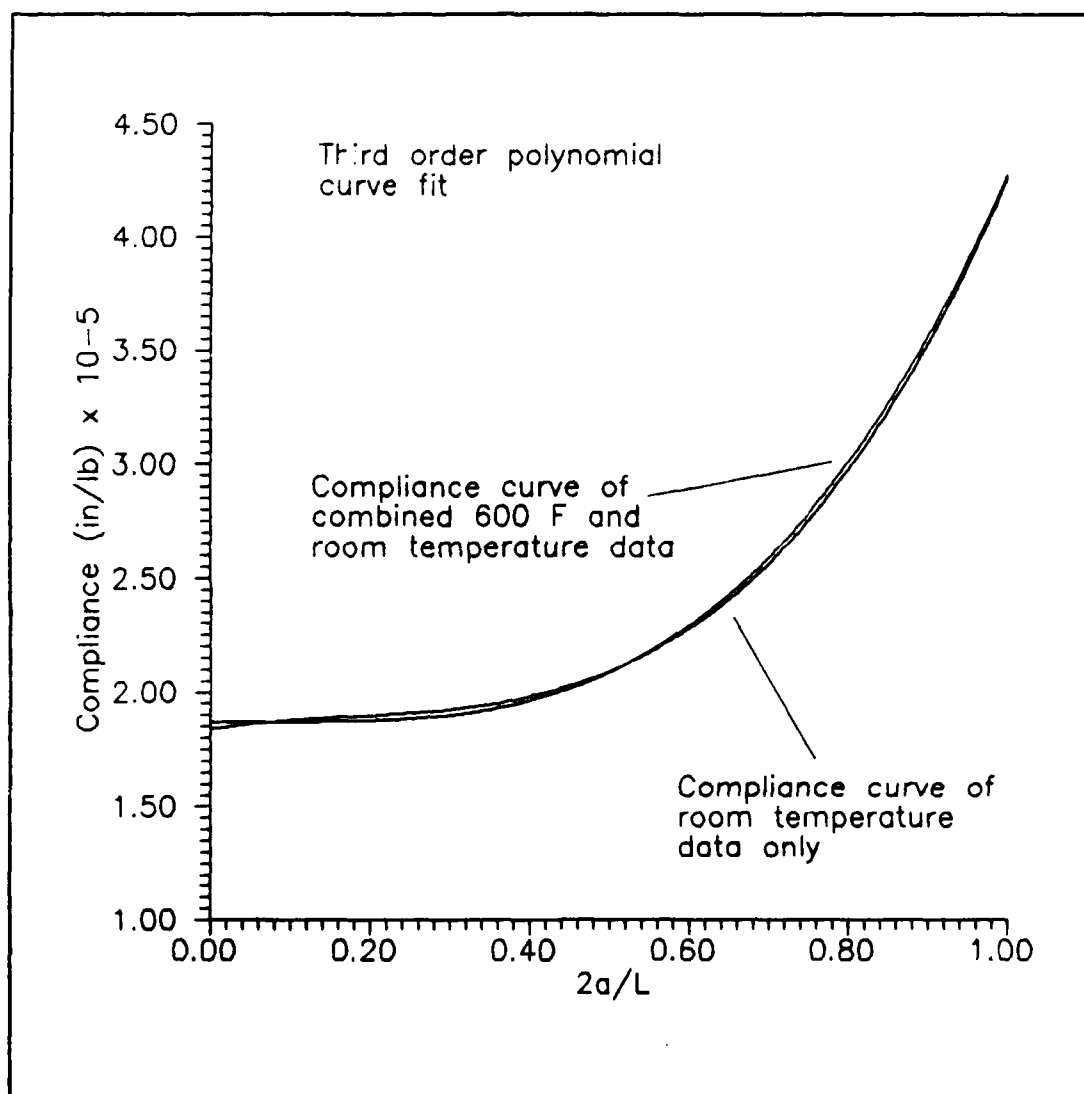
Fig. 28. Comparison of Room Temperature and
Combined Room Temperature and 600 F Compliance Curves
Third Order Polynomial Curve Fits Shown
CGW 1723

63
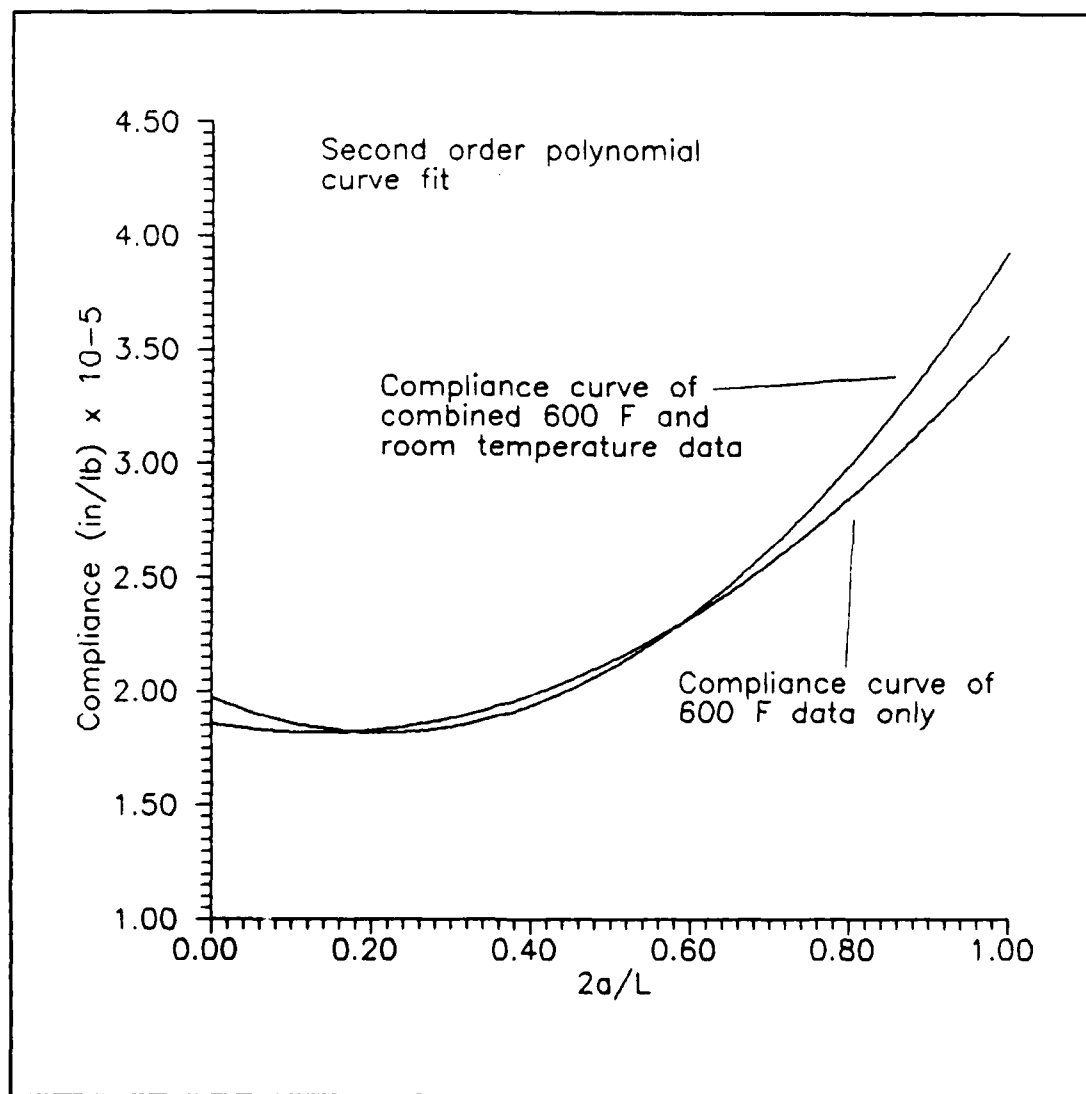
Fig. 29.   Comparison of 600 F and
Combined Room Temperature and 600 F Compliance Curves
Second Order Polynomial Curve Fits Shown
CGW 1723
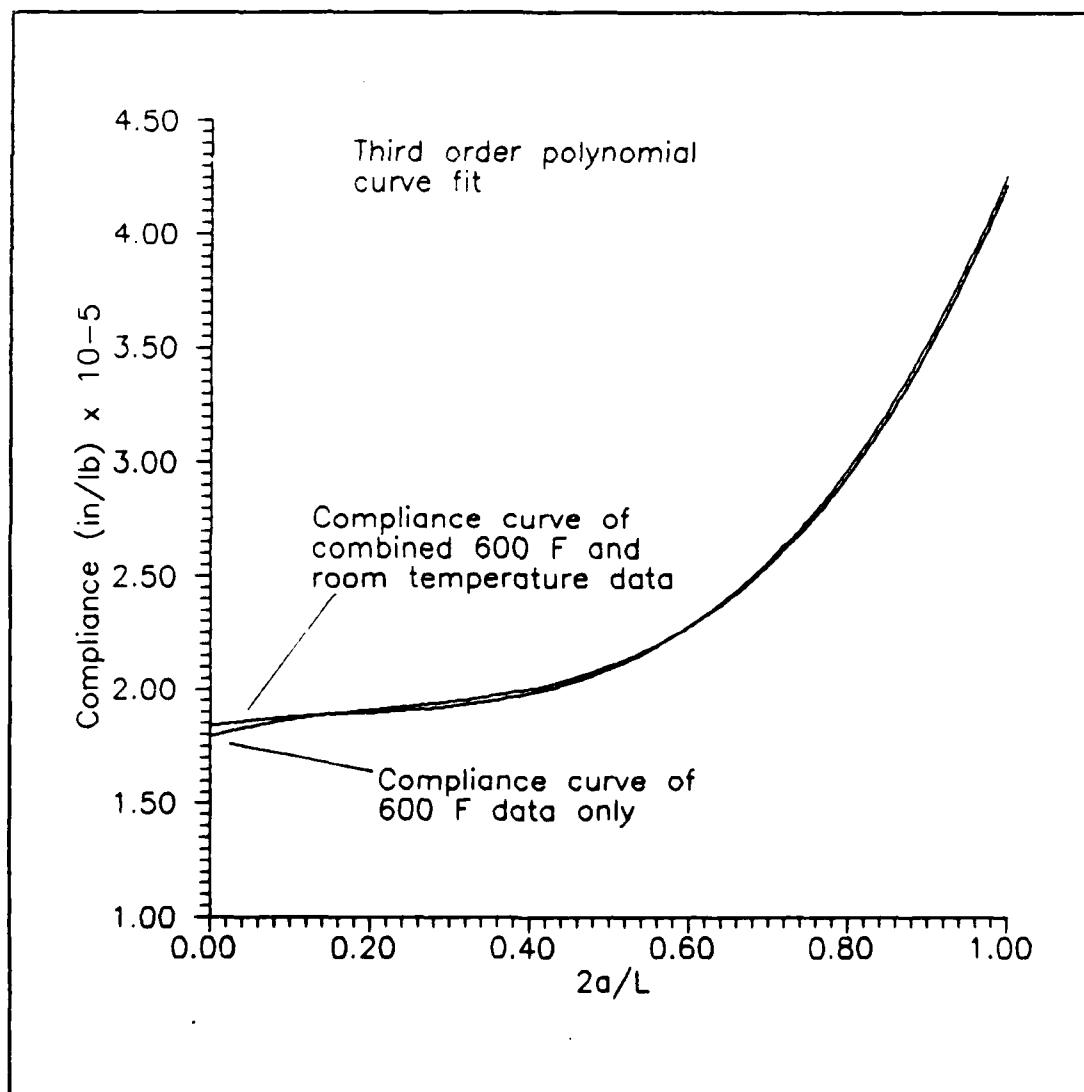
Fig. 30. Comparison of 600 F and
Combined Room Temperature and 600 F Compliance Curves
Third Order Polynomial Curve Fits Shown
CGW 1723

1000 F Compliance CGW 1723. The compliance of the
specimens at 1000 F was determined in the same way as in the
cases of room temperature and 600 F. The value of Young's
Modulus was calculated and found to have decreased slightly.
This value of 1.68E+07 was then used in Russell's equation to
generate a curve of expected compliance values that was
different than the one used at room temperature and 600 F.
Figure 31 shows the values of experimental compliance from
1000 F tests and the theoretical compliance from Russell's
equation along with its +/- 10% variation as a function of
non-dimensional crack length. It can be seen that the
majority of the data falls within this range.   Figures 32,
33, and 34 show the 1000 F compliance data plotted as a
function of non-dimensional crack length with Russell's
equation, 2nd, and 3rd order polynomial curve fits of the
data.   The equations for the 2nd and 3rd order polynomial
fits are

$$C = 2.95(2a/L)^2 - 0.49(2a/L) + 1.87 \tag{11}$$

$$C = 2.18(2a/L)^3 - 0.18(2a/L)^2 + 0.36(2a/L) + 1.88 \tag{12}$$

Russell's equation again appears to be a good representation
of the data.   The second and third order curve fits also
represent the data presented well.   However, no data was
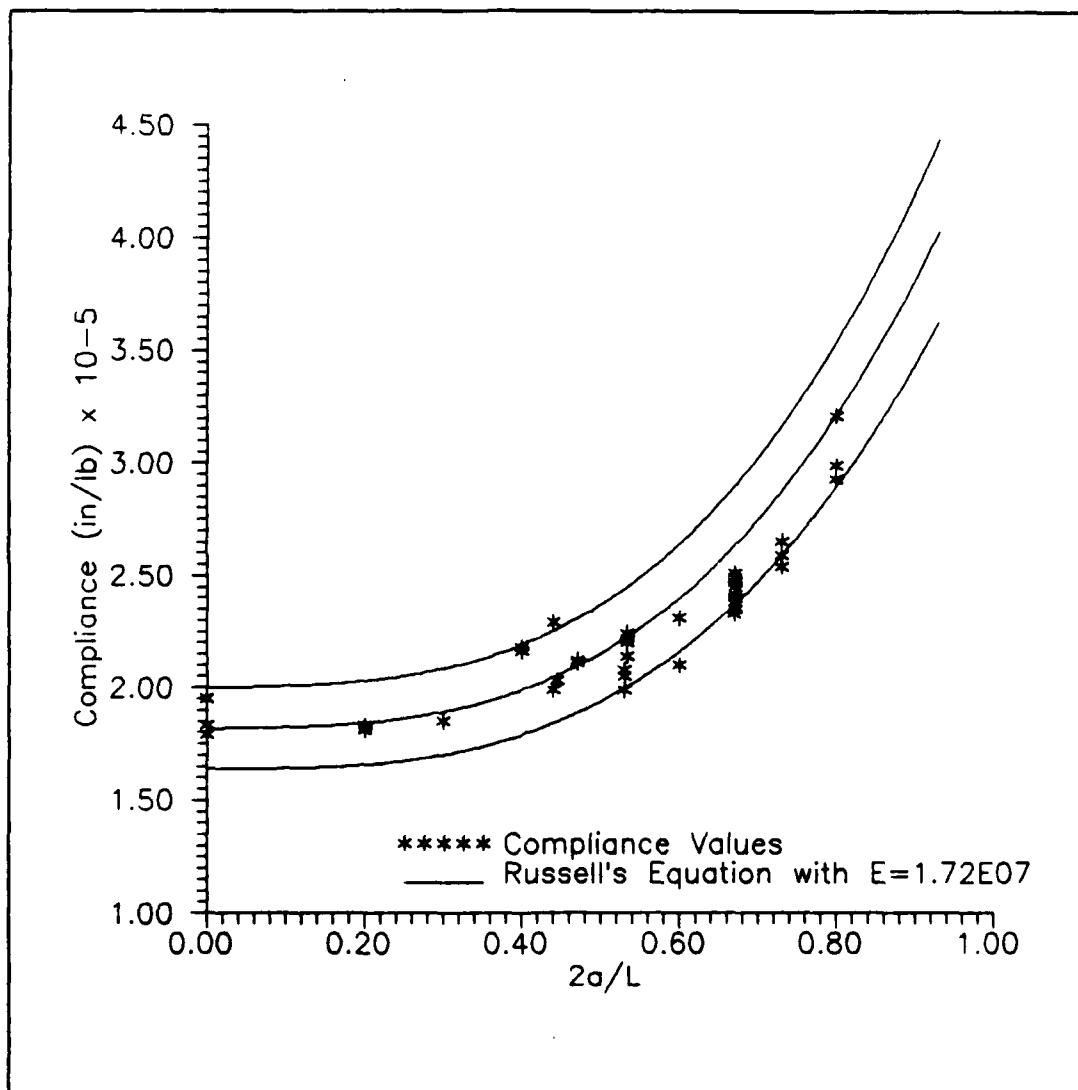collected at crack lengths of less than 2a/L < .36.   This was
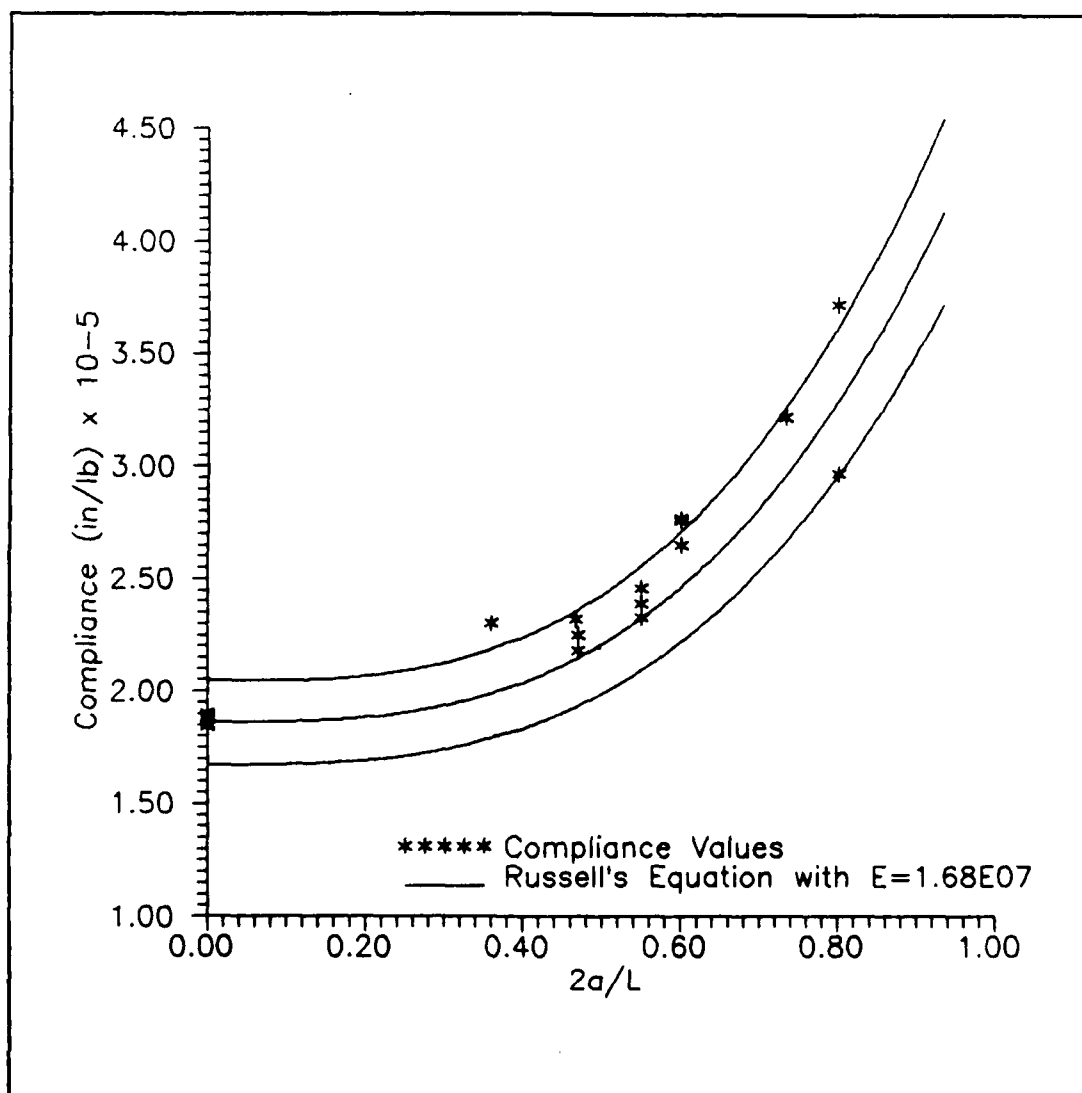
Fig. 31. 1000 F Compliance vs Non-dimensional
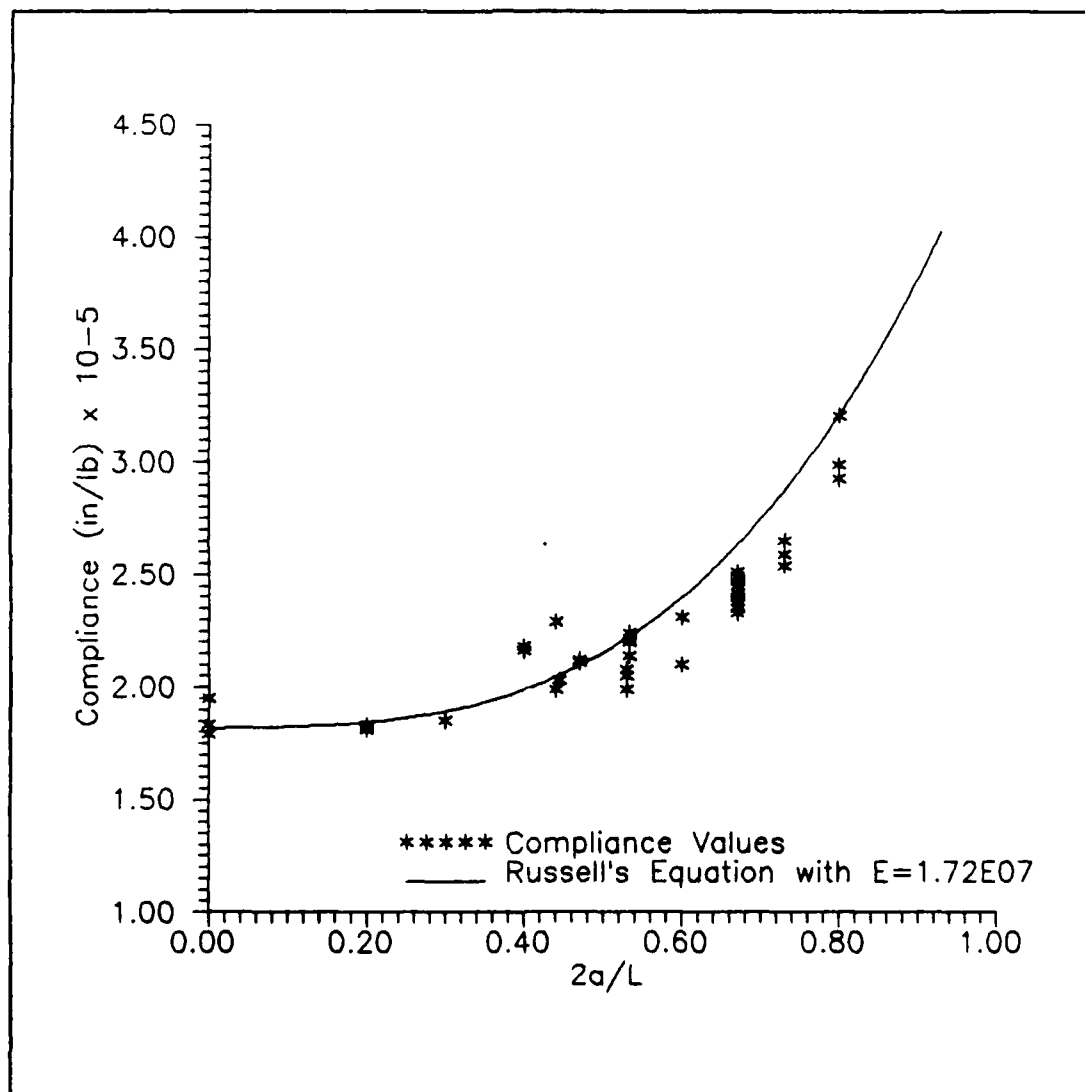Crack Length with +/- 10% Russell's Equation Shown
CGW 1723
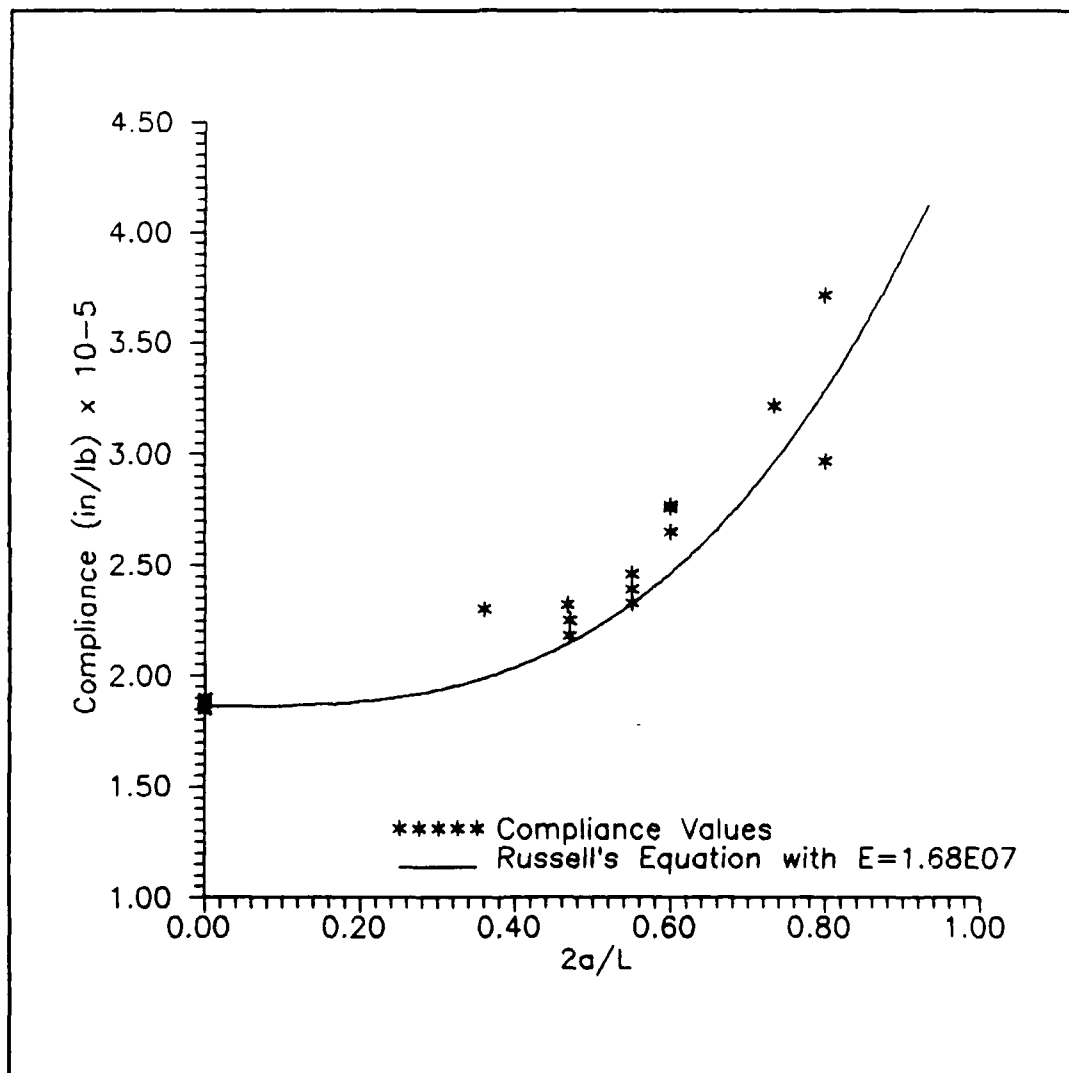
Fig. 32. 1000 F Compliance vs Non-dimensional
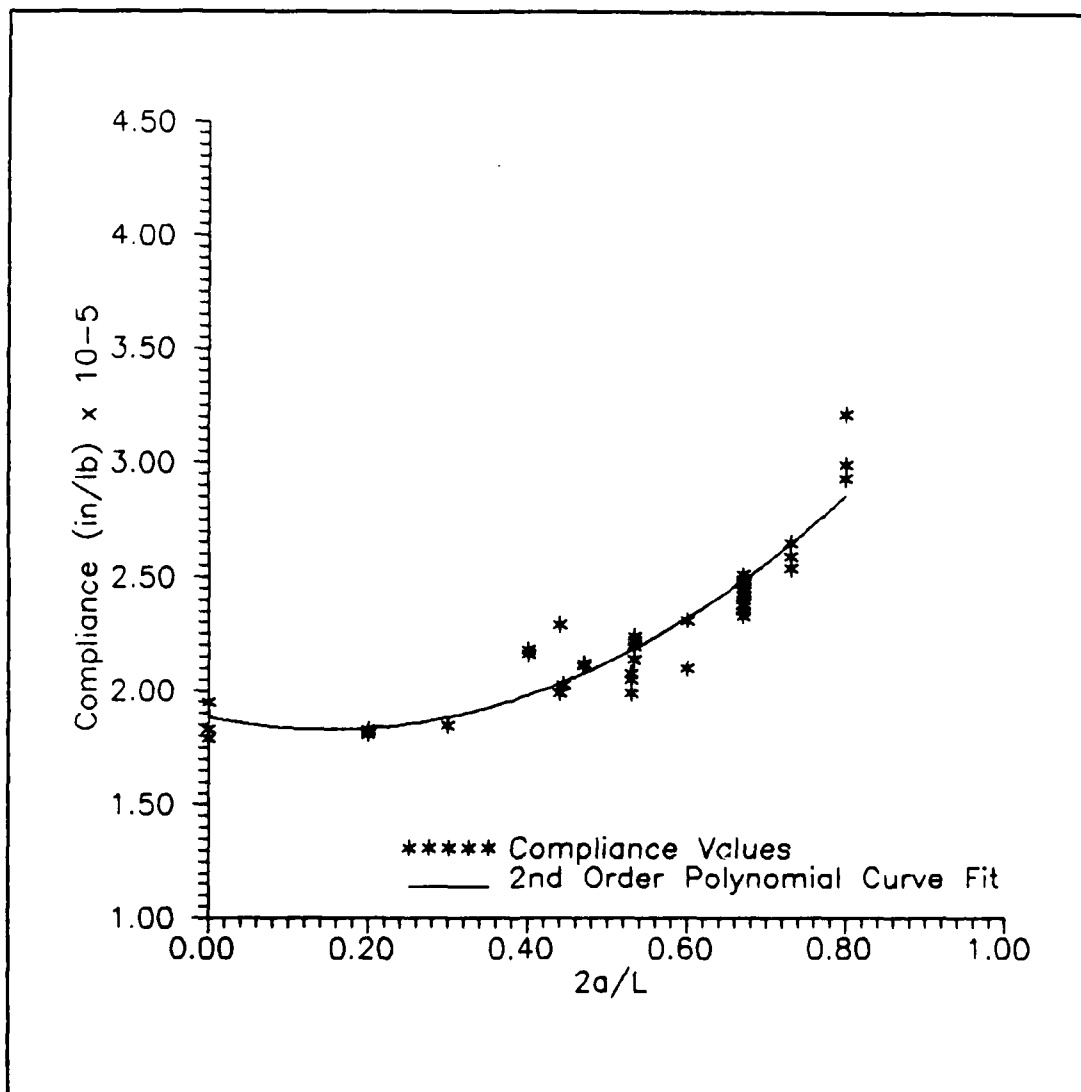Crack Length with Russell's Equation Shown
CGW 1723

68
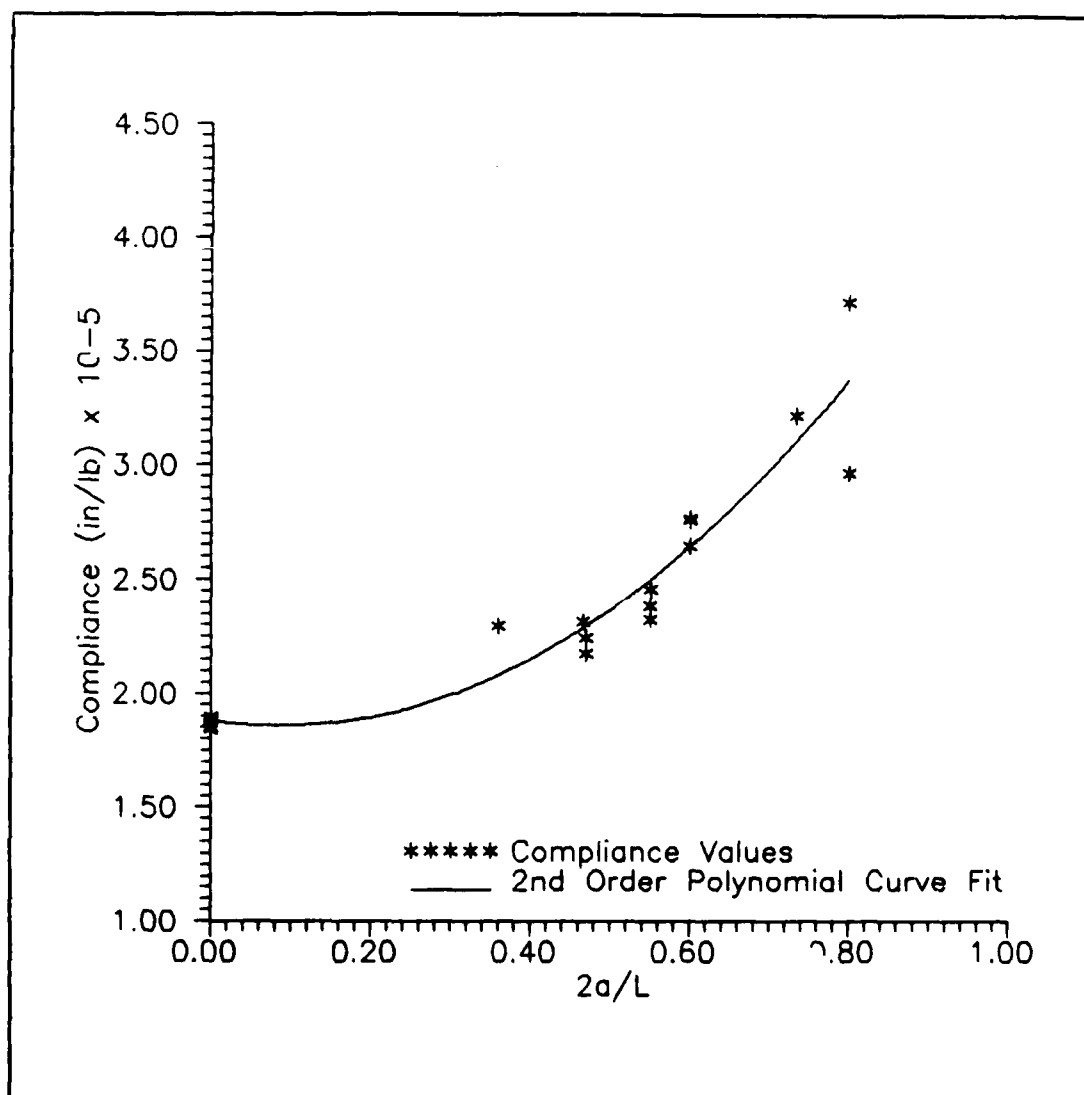
Fig. 33. 1000 F Compliance vs Non-dimensional
Crack Length with 2nd Order Polynomial Curve Fit Shown
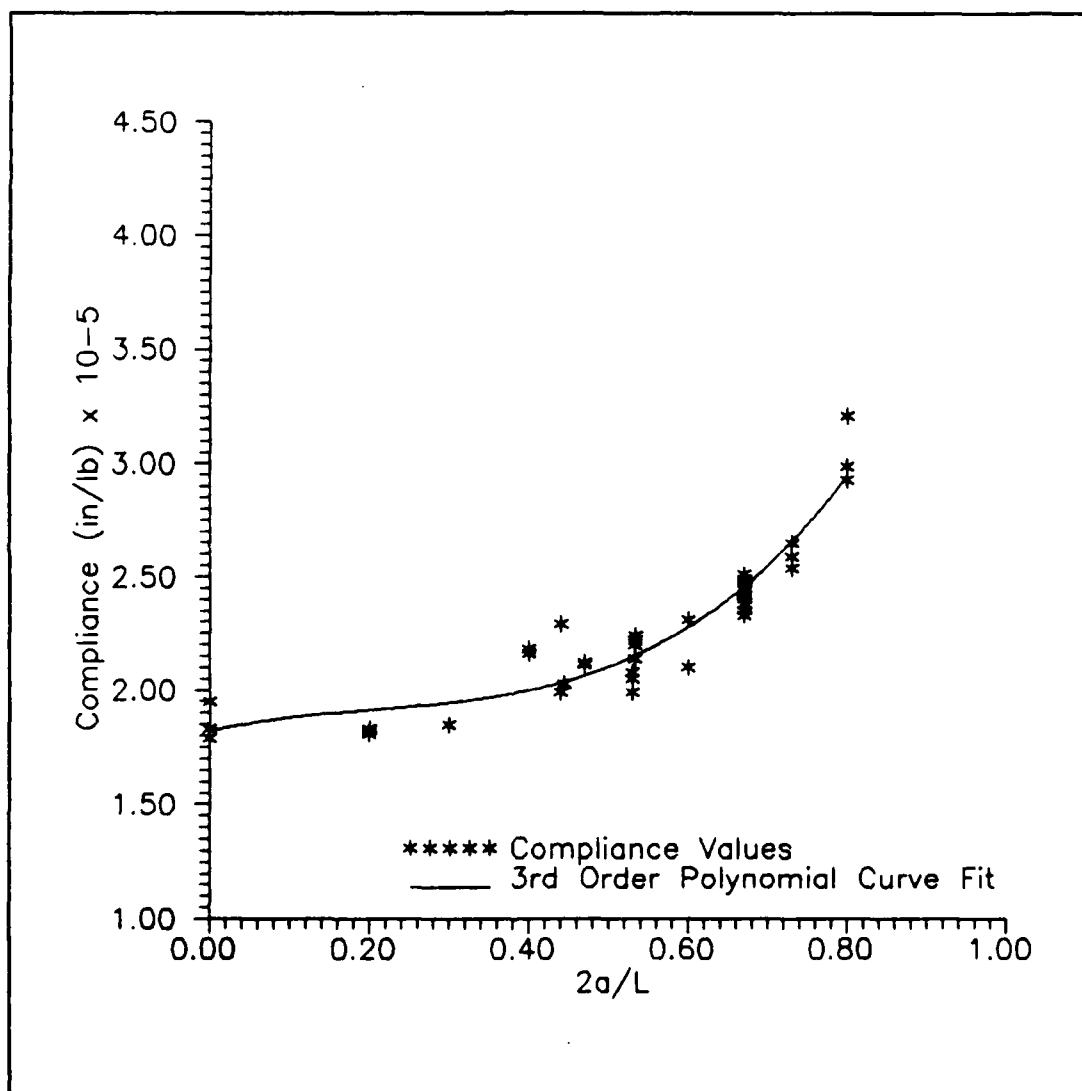CGW 1723

69

Fig. 34.   1000 F Compliance vs Non-dimensional
Crack Length with 3rd Order Polynomial Curve Fit Shown
CGW 1723

70

due to the fact that specimen 89C0403-10 failed in compression at 2a/L = .27 before the critical load was reached. The fibers on the top of the specimen, directly under the load application point, were crushed at 137 lb applied load. This did not happen at any other temperature. Due to the limited supply of material it was decided to only test at the longer crack lengths to prevent any further damaging of specimens. This lack of data in the shorter crack lengths resulted in the 2nd and 3rd order curve fits showing a greater slope in this region than can be expected to occur. Figures 35 and 36 show the change in the 2nd and 3rd order curve fits at 1000 F compared to the combined room temperature and 600 F curves. Russell's equation predicts a constant percentage difference in the two curves of the ratio of the values of Young's modulus (1.72/1.68); however, the second and third order polynomial fits show a change in this differential as the crack length increases that is not constant. This is expected since these curve fits incur bias based on the available data in a certain region. Overall, the Russell equation curve represents the data the best.

Post Thermal Cycling Compliance, CGW 1723. Two specimens were exposed to 25 thermal cycles of 130 F to 600 F and then cooled to room temperature for compliance and critical load tests. The fixture and procedures utilized in the cycling are described in Chapters 3 and 4. From the
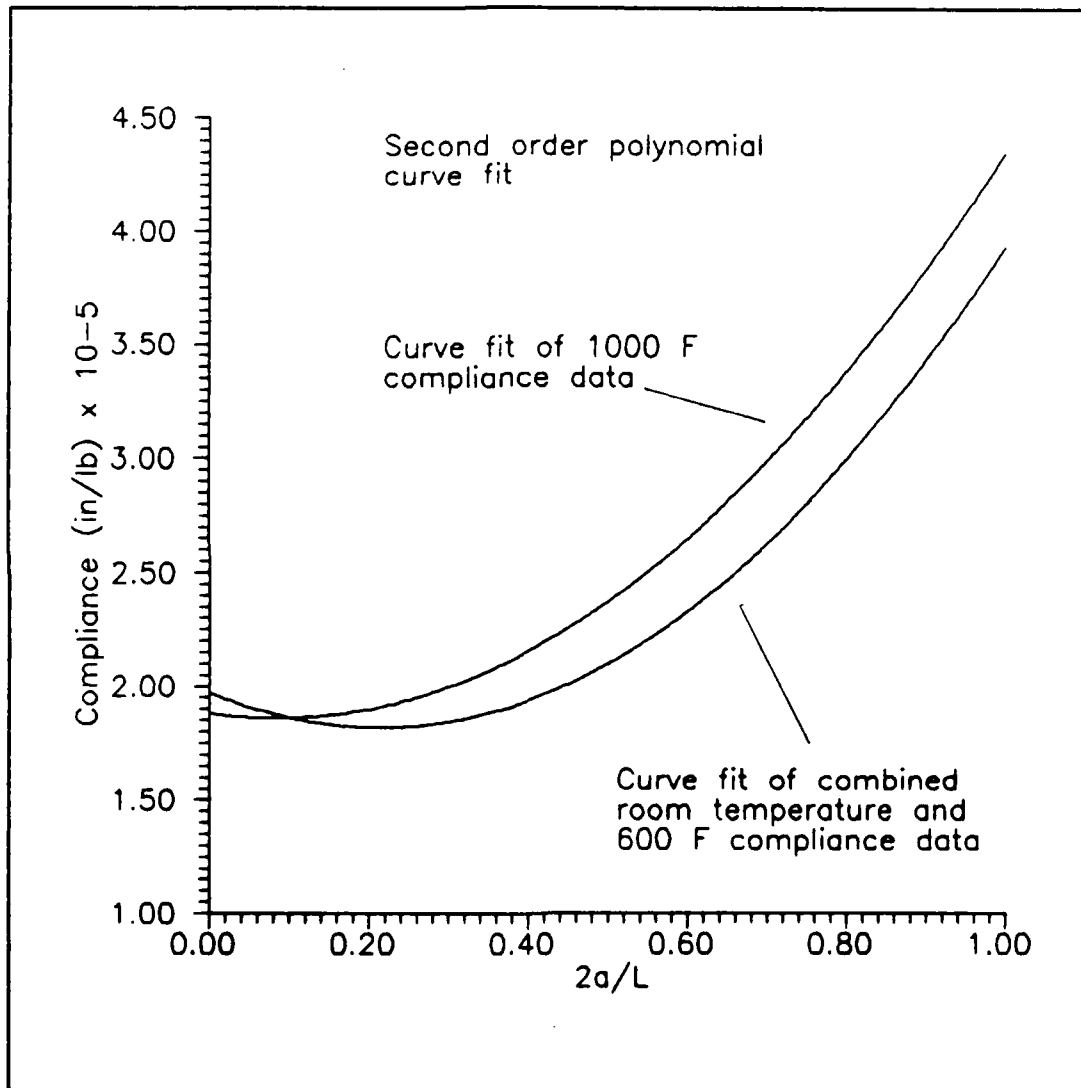
Fig. 35. Comparison of 1000 F and Combined Room Temperature
and 600 F Compliance Curves, 2nd Order Curve Fits Shown
CGW 1723

72
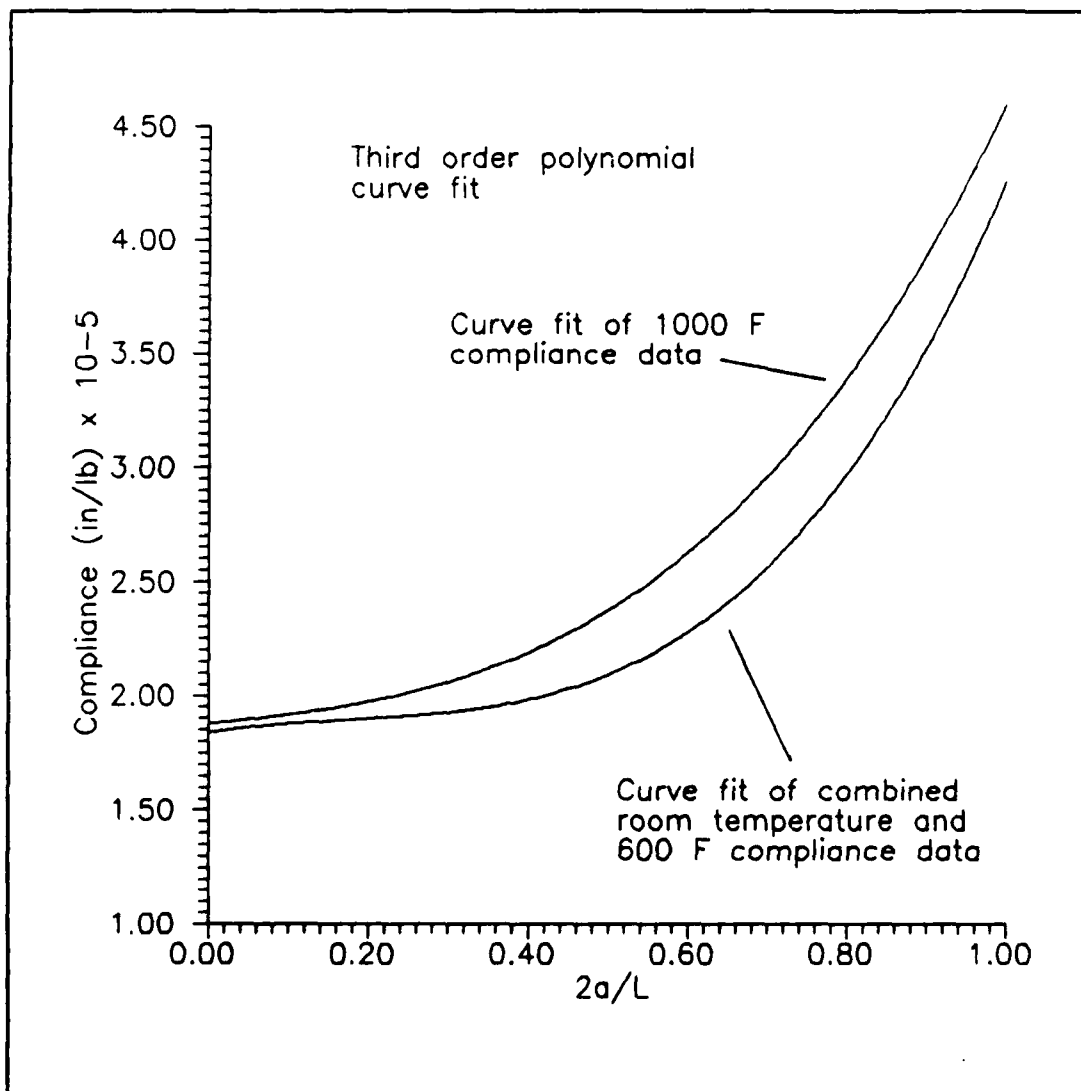
Fig. 36. Comparison of 1000 F and Combined Room Temperature
and 600 F Compliance Curves, 3rd Order Curve Fits Shown
CGW 1723

73

results of the room temperature and 600 F tests, and the fact that the measured Young's Modulus of the specimen after cycling did not change from value obtained for room temperature and 600 F specimens that were not exposed to thermal cycling, it was expected that the compliance of the specimens would be similar to the combined curve developed from the data taken at these temperatures. This was in fact the case. The post cycling compliance data falls very close to the combined curve developed and is within the range of experimental scatter that was observed in the room temperature and 600 F tests. See Figures 37, 38, and 39. It was therefore decided that the combined room temperature and 600 F compliance curve equations could be used in the calculation of the fracture toughness of the post-cycling specimens.

In order to insure that any changes in the fracture toughness of the cycling specimens was actually due to the cycling and not just from exposure to elevated temperatures for a prolonged period, one specimen was exposed to a steady 600 F for 125 minutes. This time is equal to the sum of the hold times in the cycling profile. After the exposure to this prolonged temperature, the specimen was cooled to room temperature and tested. The values of compliance for this specimen were also very close to the combined room temperature and 600 F curves. See Figures 40, 41, and 42.
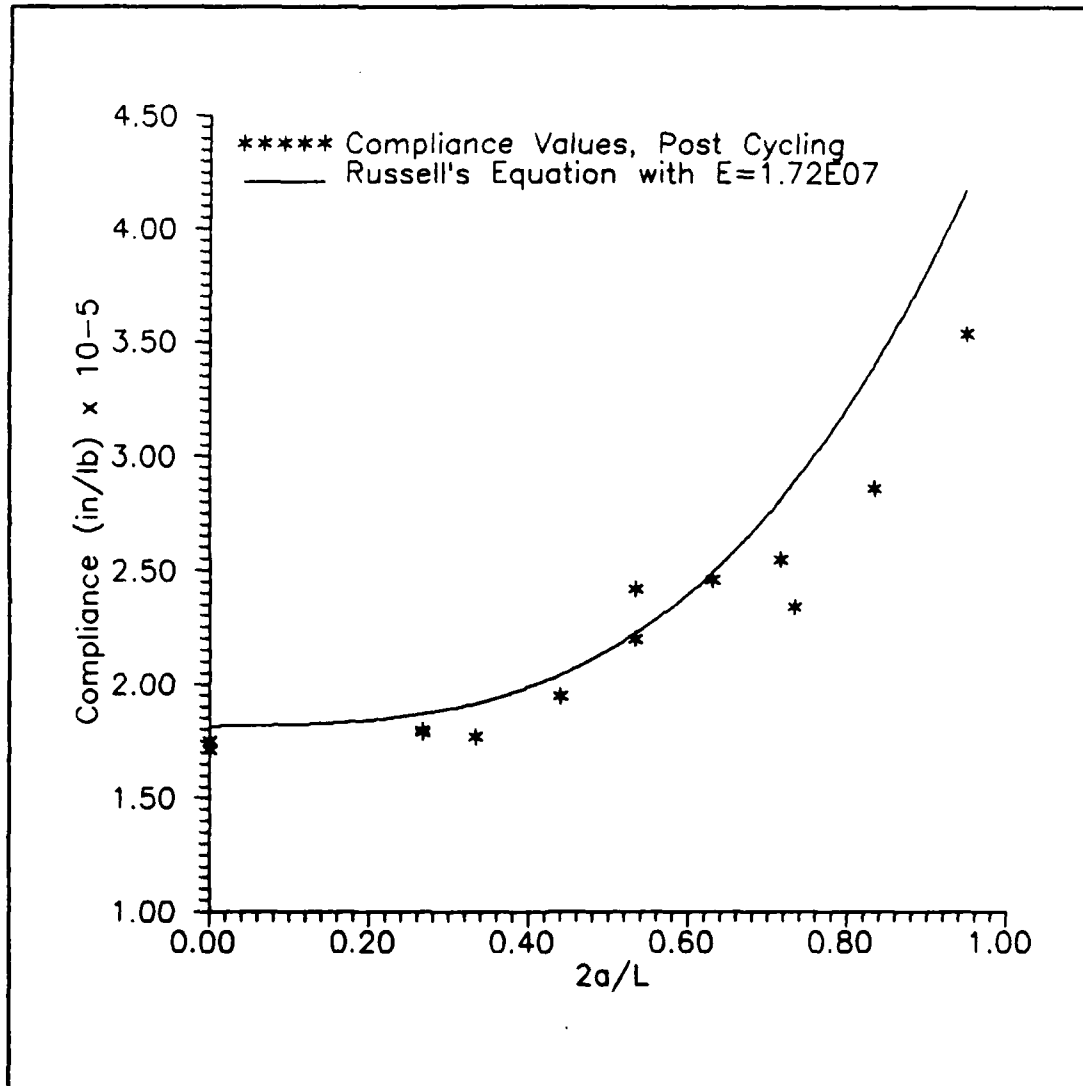
Fig. 37. Post Cycling Compliance vs Non-dimensional Crack Length with Russell's Equation Shown CGW 1723
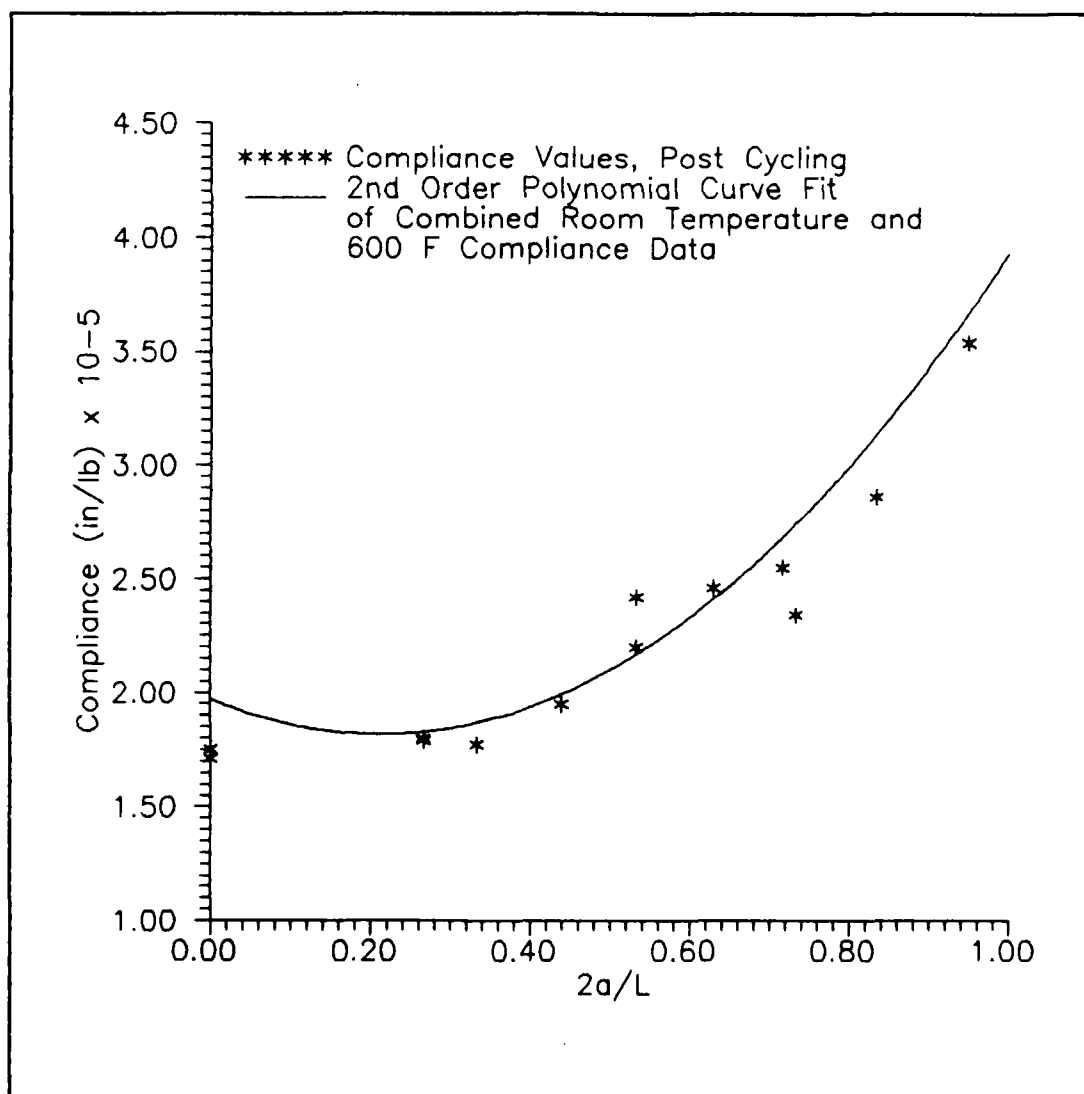
Fig. 38. Post Cycling Compliance vs Non-dimensional
Crack Length with 2nd Order Polynomial Curve Fit of
Combined Room Temperature and 600 F Data Shown
CGW 1723
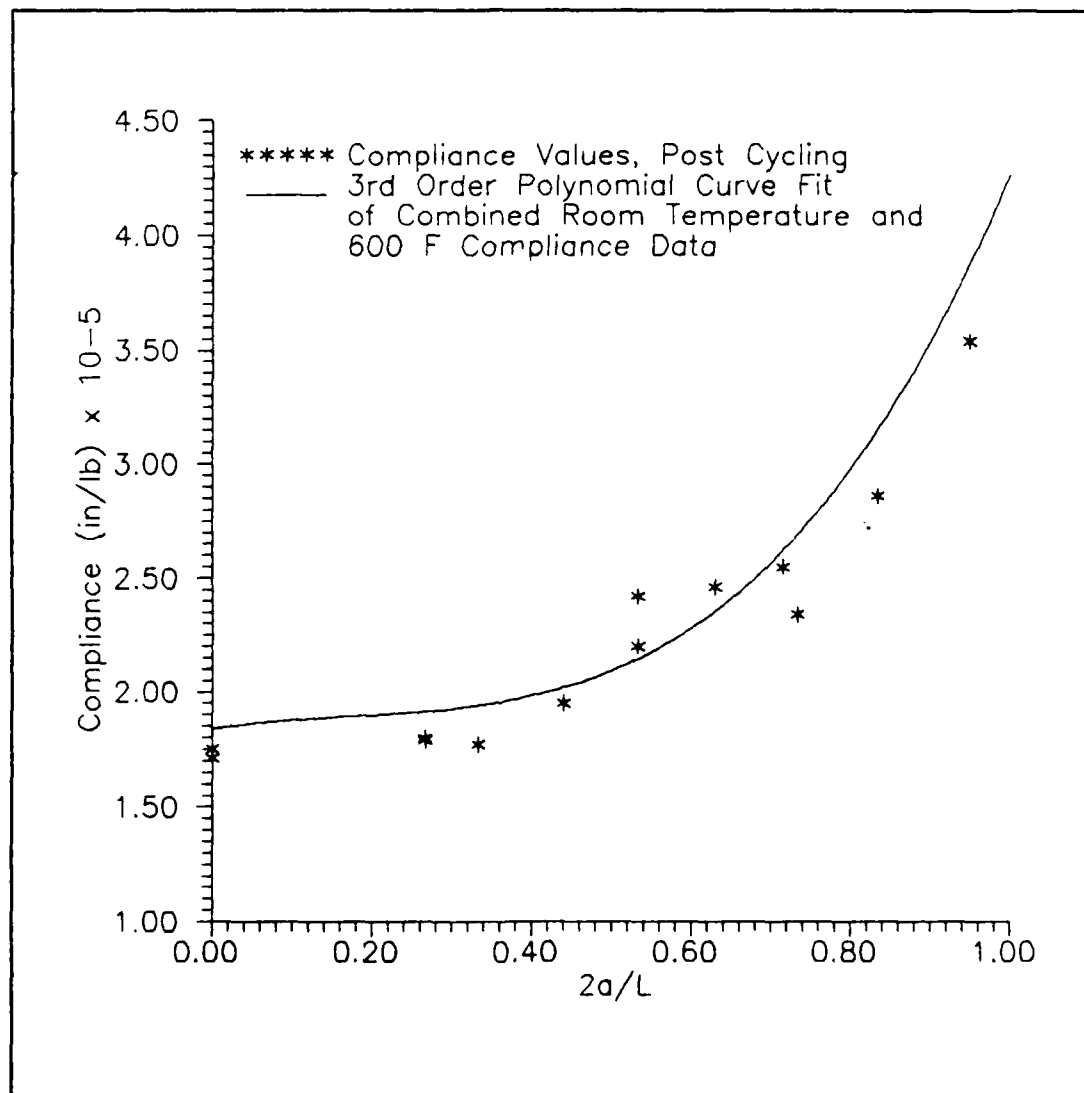
Fig. 39. Post Cycling Compliance vs Non-dimensional
Crack Length with 3rd Order Polynomial Curve Fit of
Combined Room Temperature and 600 F Data Shown
CGW 1723
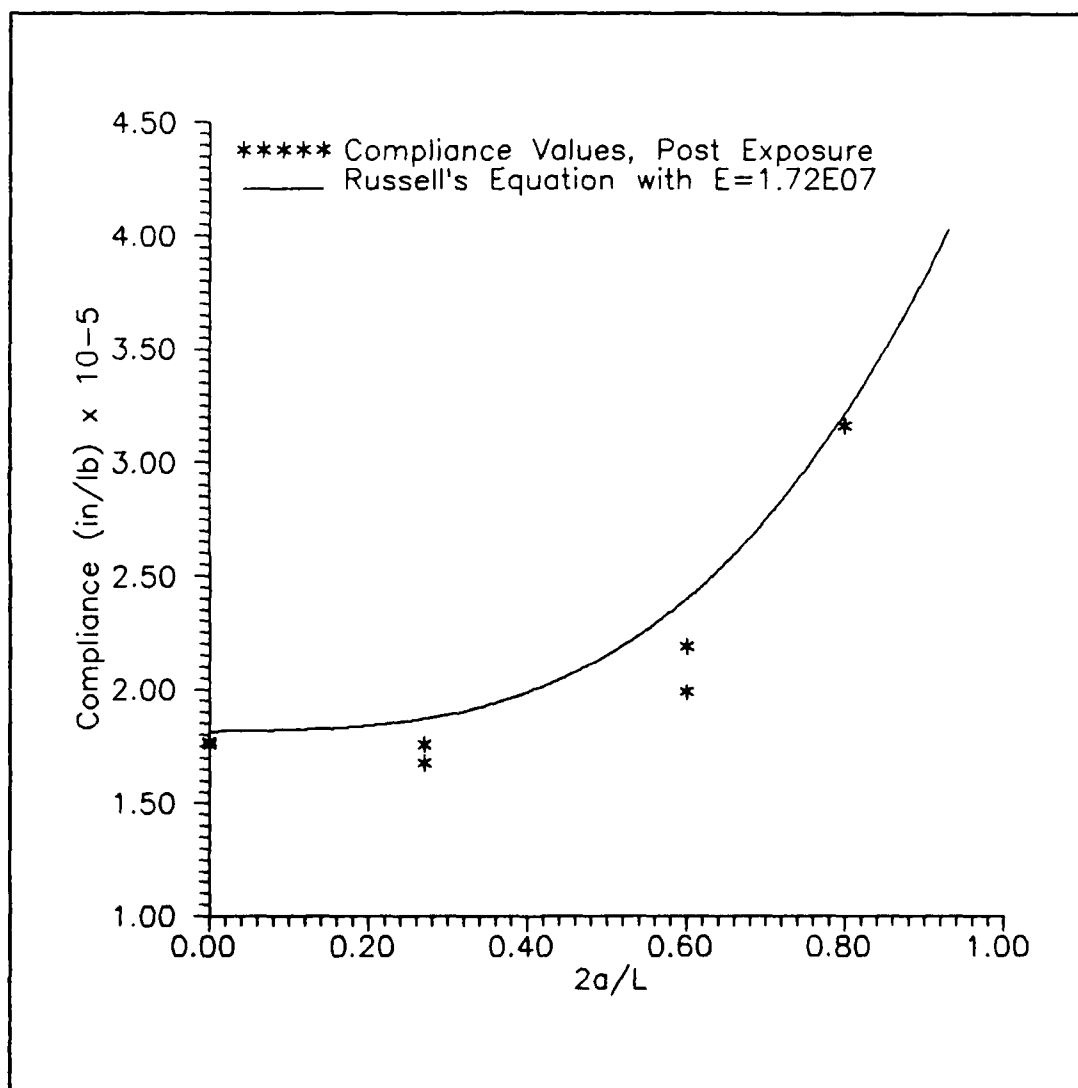
Fig. 40. Post Exposure Compliance vs Non-dimensional Crack Length with Russell's Equation Shown CGW 1723
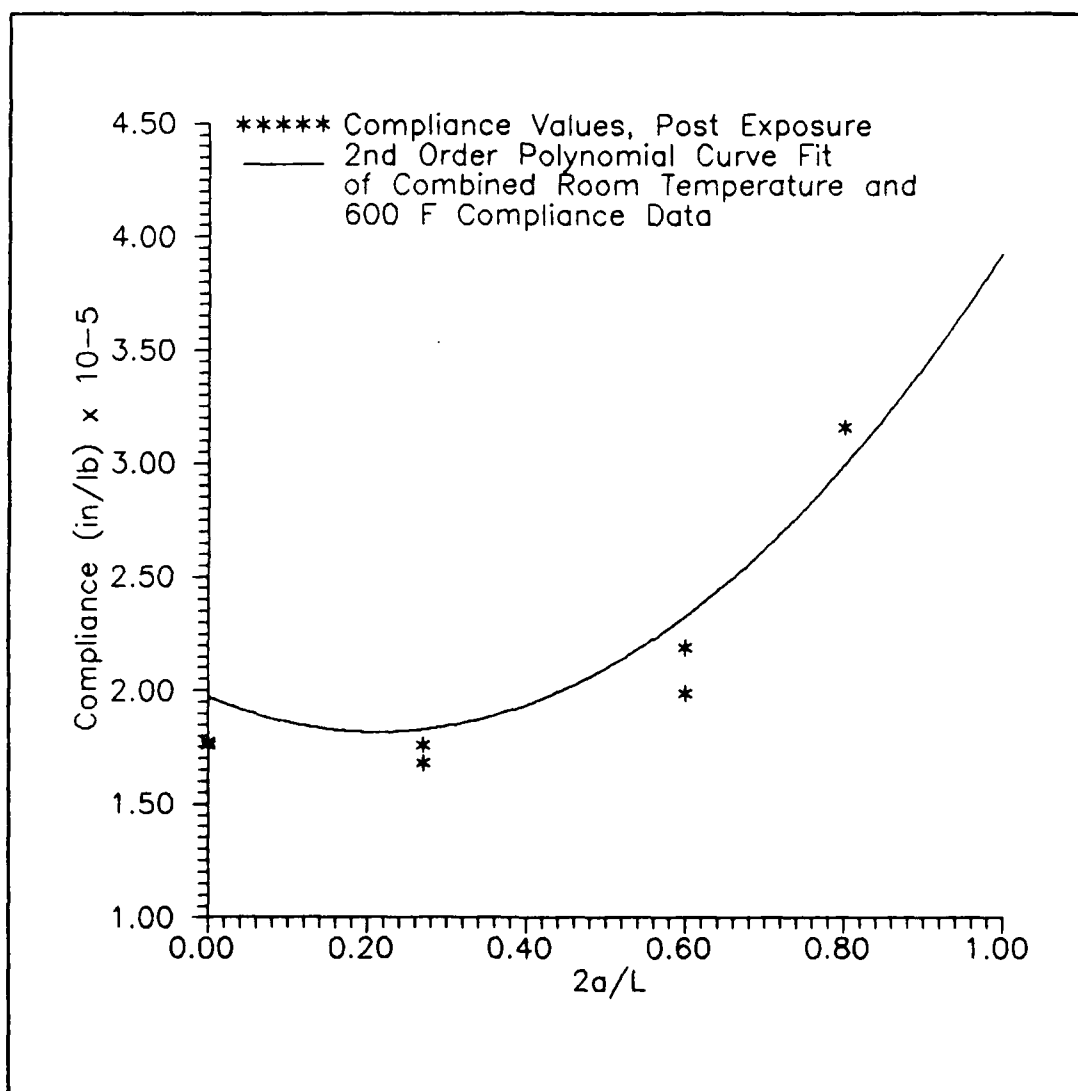
Fig. 41. Post Exposure Compliance vs Non-dimensional
Crack Length with 2nd Order Polynomial Curve Fit of
Combined Room Temperature and 600 F Data Shown
CGW 1723

79
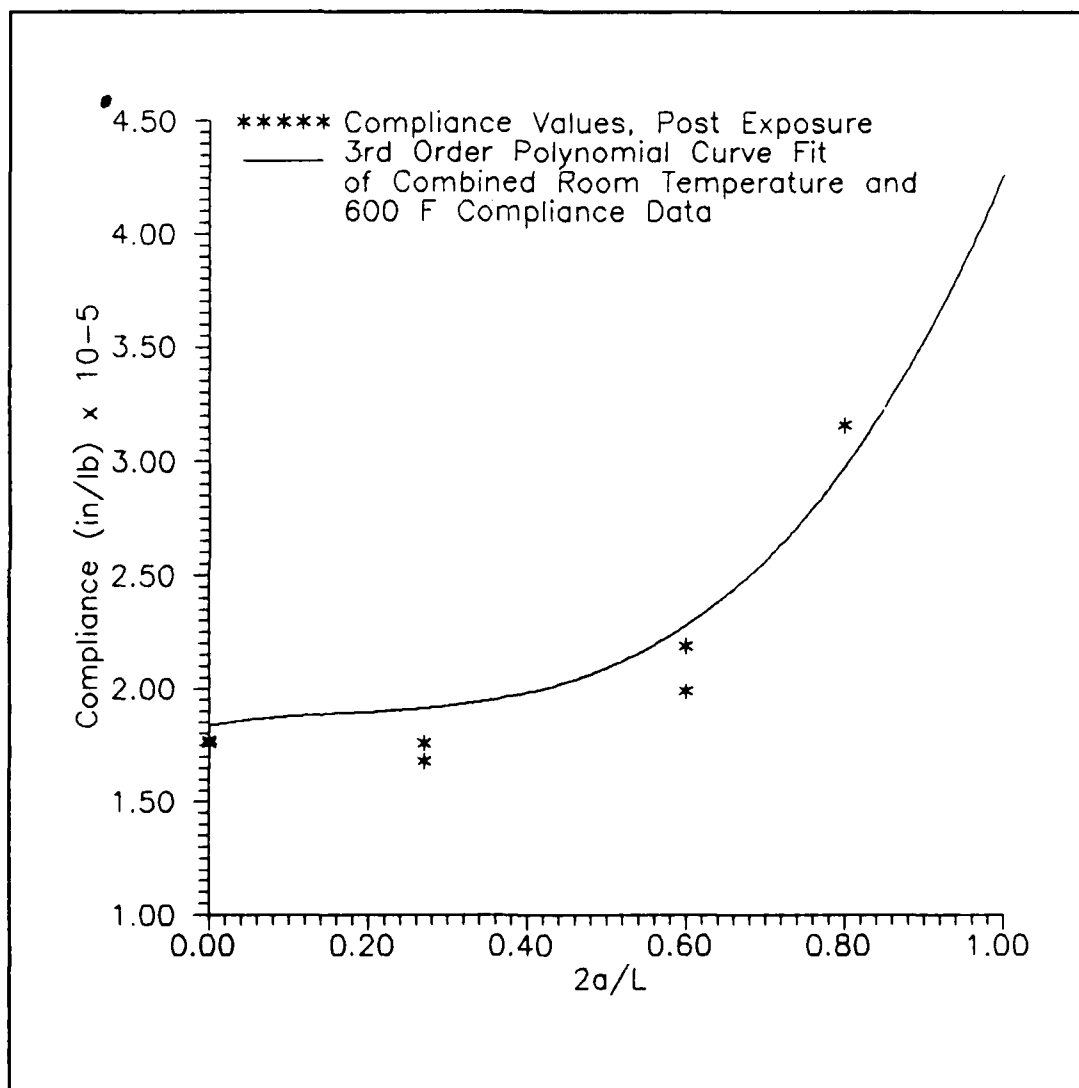
Fig. 42.   Post Exposure Compliance vs Non-dimensional
Crack Length with 3rd Order Polynomial Curve Fit of
Combined Room Temperature and 600 F Data Shown
CGW 1723

80

There was no significant change in the measured Young's modulus. It was decided to use this combined curve for the calculation of the fracture toughness of this specimen also.

Room Temperature Compliance, CGW 7740. The same procedures were used in these tests as were used with CGW 1723. The modulus was initially measured and found to be $1.20E07$ lbs/in^2. This is significantly lower than that found for the CGW 1723. This value was used in Russell's equation to generate a theoretical compliance vs crack length curve. Figure 43 shows the values of compliance obtained from tests and curves of +/- 10% Russell's equation. As can be seen, the data fell reasonably well within the range of +/- 10% of Russell's theoretical values. Figures 44, 45, and 46 show the experimental data plotted with Russell's equation, 2nd, and 3rd order polynomial curve fits. The equations for the 2nd and 3rd order curve fits are

$$C = 2.39(2a/L)^2 - 0.79(2a/L) + 2.39 \qquad (13)$$

$$C = 4.94(2a/L)^3 - 2.17(2a/L)^2 + 1.30(2a/L) + 2.36 \quad (14)$$

As can be seen from Figure 44, the curve of Russell's equation is a very good fit of the data. The same can be said for the 3rd order polynomial. See Figure 46. The 2nd order curve fits the data fairly well at the longer crack lengths, but does not accurately represent the data at the shorter crack lengths ($2a/L < .3$). See Figure 45. This is

81
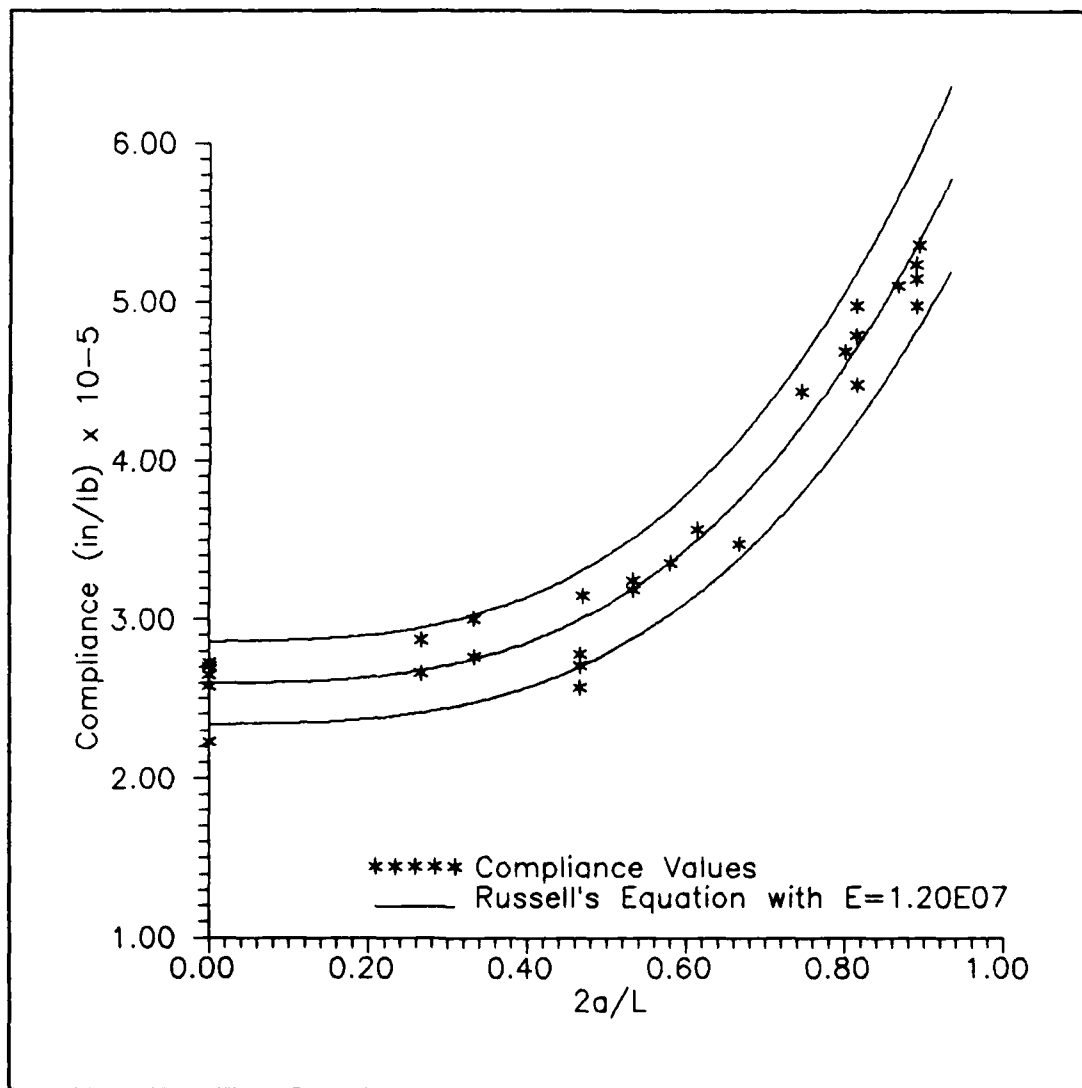
Fig. 43.   Room Temperature Compliance vs Non-dimensional
Crack Length with +/- 10% Russell's Equation Shown
CGW 7740

82
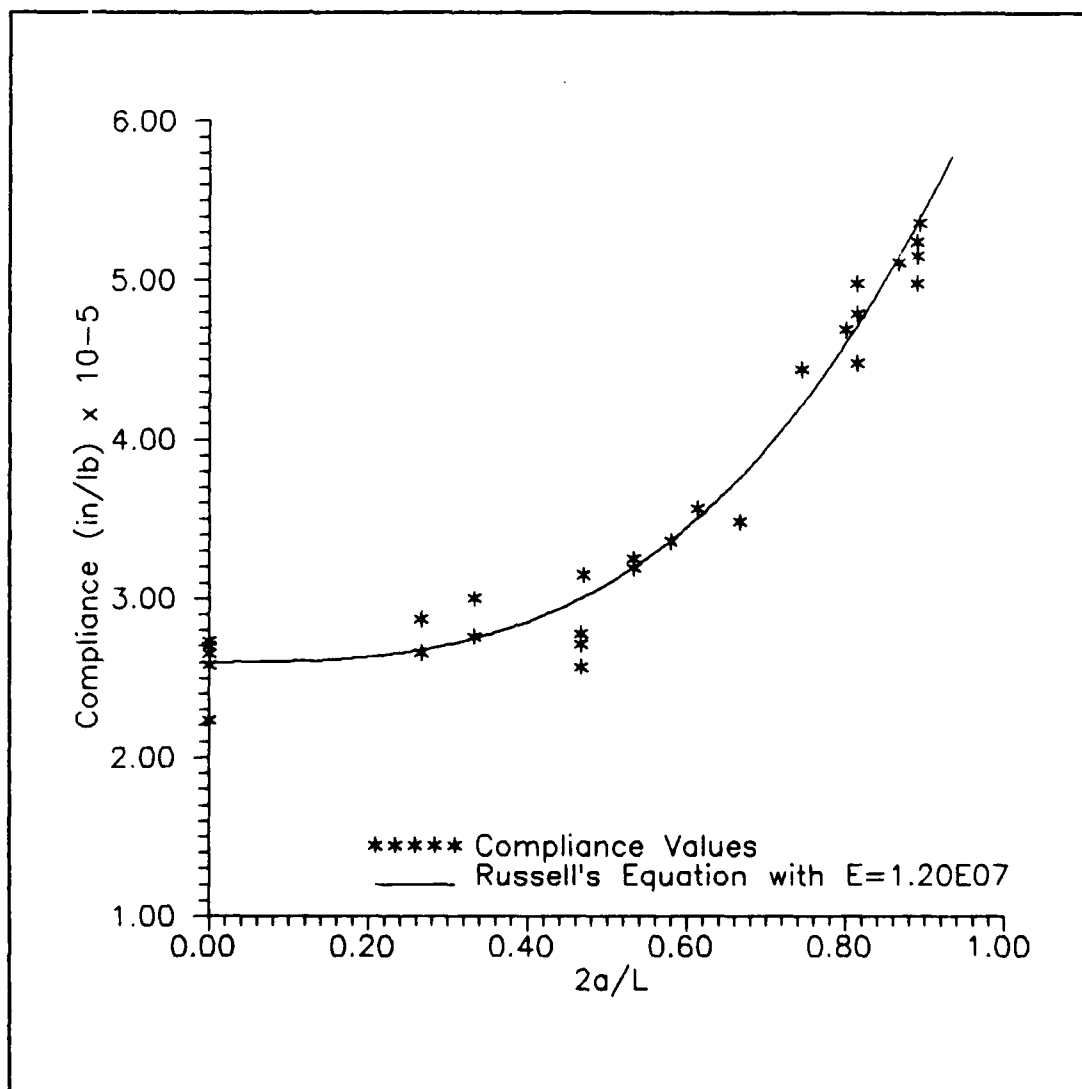
Fig. 44. Room Temperature Compliance vs Non-dimensional
Crack Length with Russell's Equation Shown
CGW 7740

83
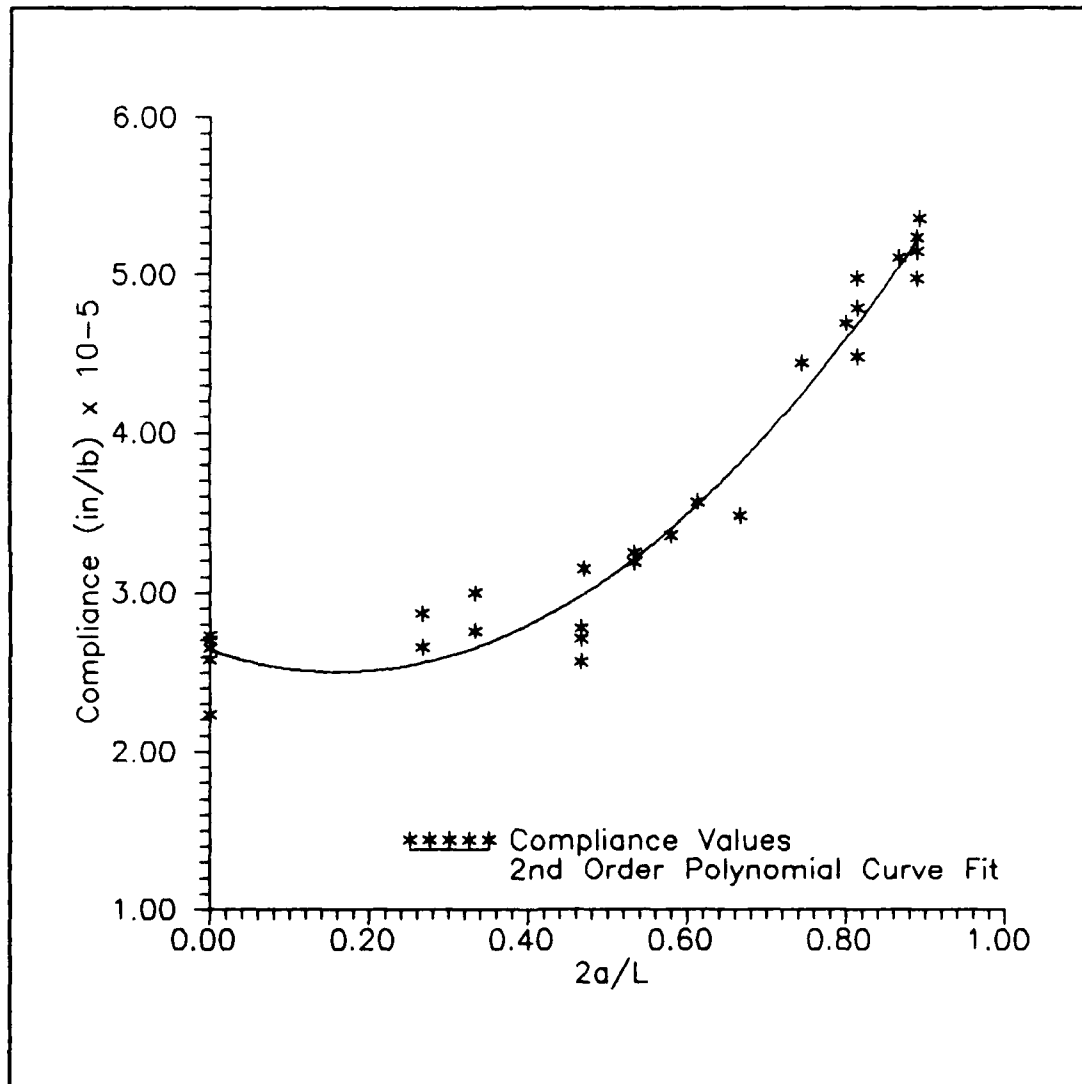
Fig. 45. Room Temperature Compliance vs Non-dimensional
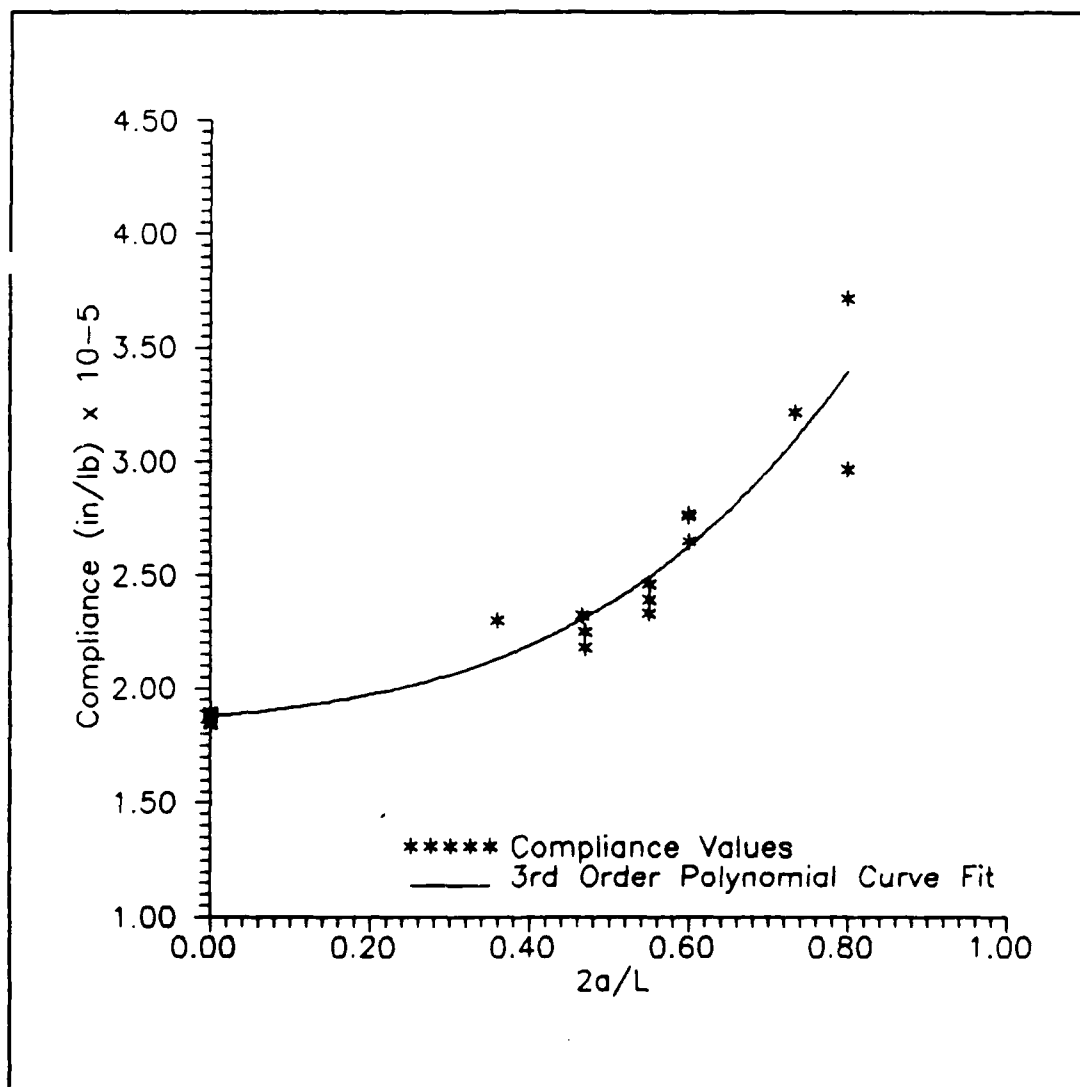Crack Length with 2nd Order Polynomial Curve Fit Shown
CGW 7740

84
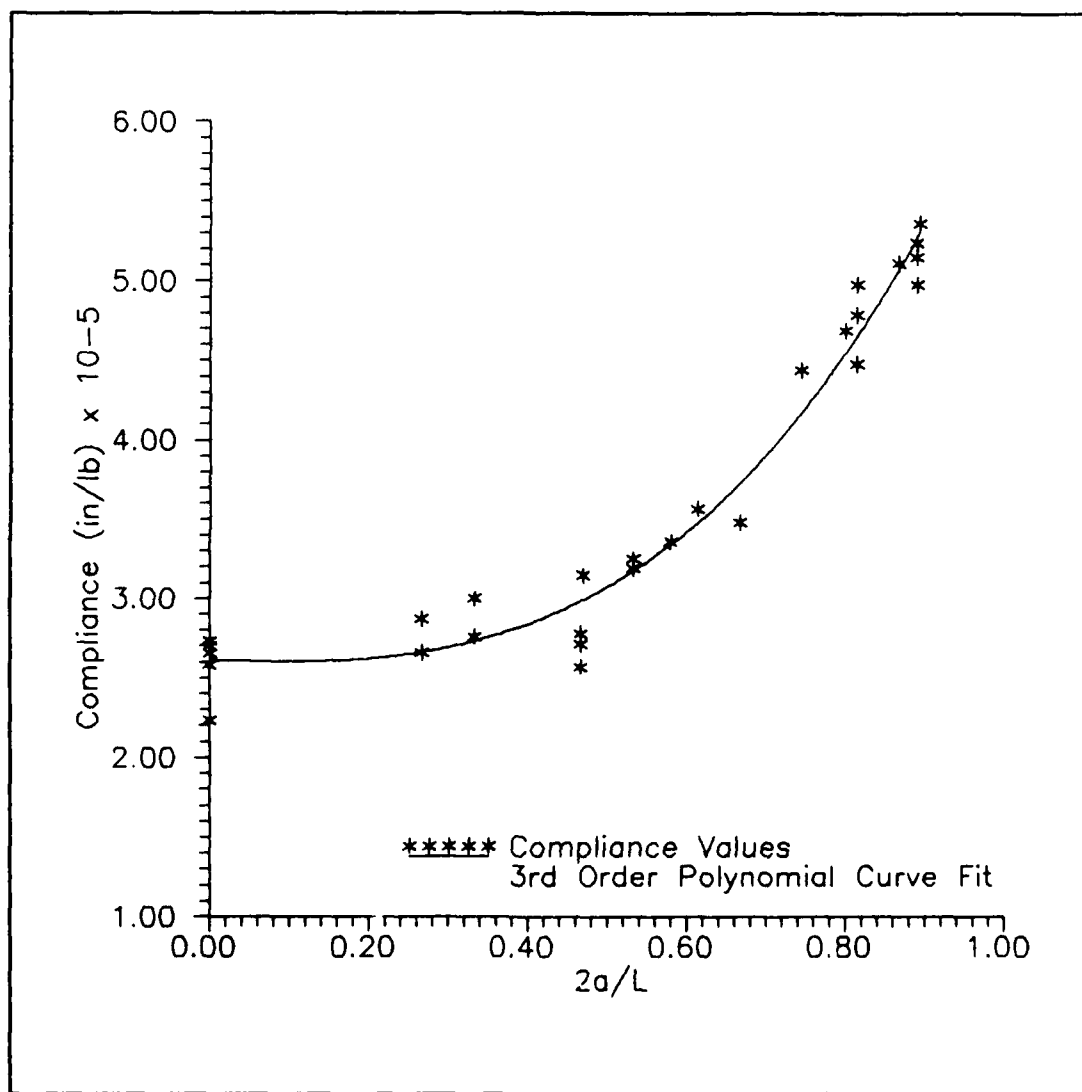
Fig. 46. Room Temperature Compliance vs Non-dimensional
Crack Length with 3rd Order Polynomial Curve Fit Shown
CGW 7740

the same type of problem that was seen in general with the 2nd order curve fits of the CGW 1723 compliance data. Although the third order curve represents the data well, Russell's equation was chosen as the best fit because it modeled the data well and the derivatives were expected to be better behaved than the 3rd order fit.

Critical Load Determination. The second piece of data required in the calculation of G_{IIc} was the critical load, or the load at which crack growth occurs. In this study, this load was taken to be the applied load at which the specimen compliance changed. The load vs displacement curve generated on the X-Y plotter was monitored during loading and when a definite and permanent change in the slope of the line occurred it was assumed that crack growth had initiated. On most specimens there was not a sudden change in the curve, which indicates that there was no large "pop-in" occurring. Instead, the norm was for the load-displacement curve, after the initial fixture settling, to be almost perfectly linear until the critical load was reached. The curve would then transition to a non-linear one, with the slope of the curve decreasing markedly indicating an increase in the compliance. Typical curves demonstrating this behavior are shown in Appendix B. Once the apparent critical load had been determined from the plotter output, the specimen was removed from the load fixture and examined under the travelling

microscope to visually confirm that crack growth had occurred. Ordinarily, crack extensions of the order of 0.05" - 0.08" occurred. If the crack growth could not be visually confirmed, or the change in the load-displacement curve was ambiguous as to the actual load at which the change in slope had occurred, the data point was not recorded. Critical load values were plotted vs crack length using log-log scales for the axis. In theory, the critical loads should fall on a line with slope of -1 when plotted with log-log scaling if G_{IIc} is to remain a constant for the material. Data for these plots was not normalized to account for differences in specimen geometry. This accounts for some of the apparent scatter in the data. The data was not normalized as was the compliance for two reasons. First, the compliance data was normalized in order to establish a general specimen relationship that could be used in the equation for G_{IIc}. No attempt was made to fit a precise curve through the critical load data, only general trends were of interest. The variations in specimen geometry were small enough that they had no significant impact on the overall trend of the data. Second, the equation for G_{IIc} takes into the account the actual width of the specimen and changes in the critical load due to differing widths will be taken care of here.

Critical load data vs crack length is plotted for CGW 1723 at room temperature, 600 F, and 1000 F in Figures 47, 48 and

87

49. These figures show that the slope of a line through these data points has a slope of approximately -1 as expected. Figure 50 is a comparison among the three temperatures. As can be seen from Figure 50, the critical loads for CGW 1723 decreased, in general, at all crack lengths as the temperature increased. Figures 51 and 52 are of the critical loads for the post thermal cycling and post thermal exposure specimens plotted with the critical loads for the 600 F specimens. The post cycling critical loads are generally lower than the 600 F loads. The critical loads from the post thermal exposure tests are indistinguishable from those of the 600 F tests. Critical load data for CGW 7740 at room temperature is shown in Figure 53.

Fracture Toughness. The primary objective of this part of this study was to calculate the Mode II fracture toughness of CMC end notched flexure specimens. The equation to calculate G_{IIc} is

$$G_{IIc} = \frac{P_{cr}^2}{2b} \frac{dC}{da} \tag{15}$$

where P_{cr} is the critical load, b is the thickness, and dC/da is the derivative of the compliance to crack length relationship at the tested crack length. Two methods for determining this derivative were used in this study. The first method was to take the derivative of Russell's equation with respect to crack length (a) and use this in equation 15.

88
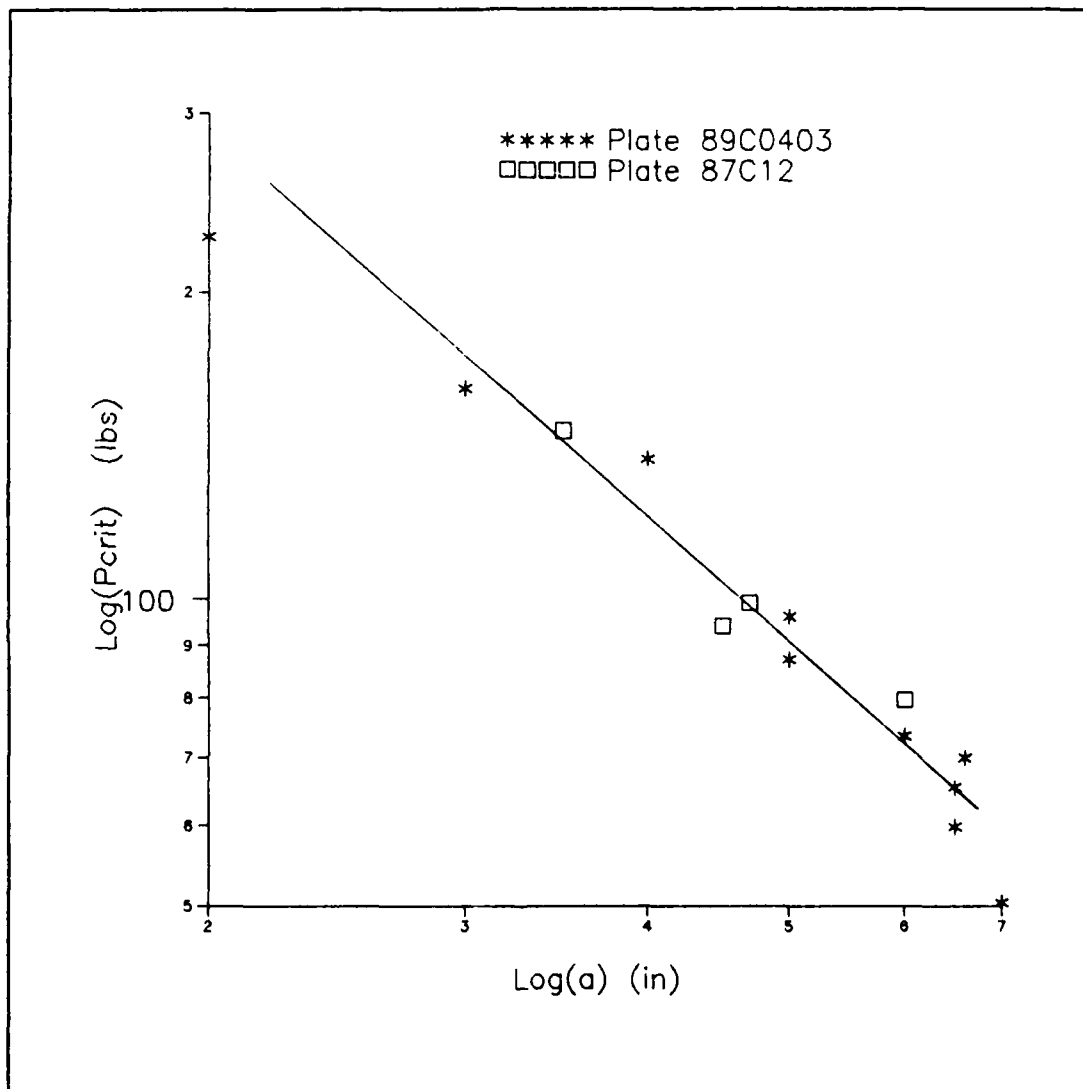
Fig. 47.   Critical Load vs Crack Length, Room Temperature
CGW 1723

89
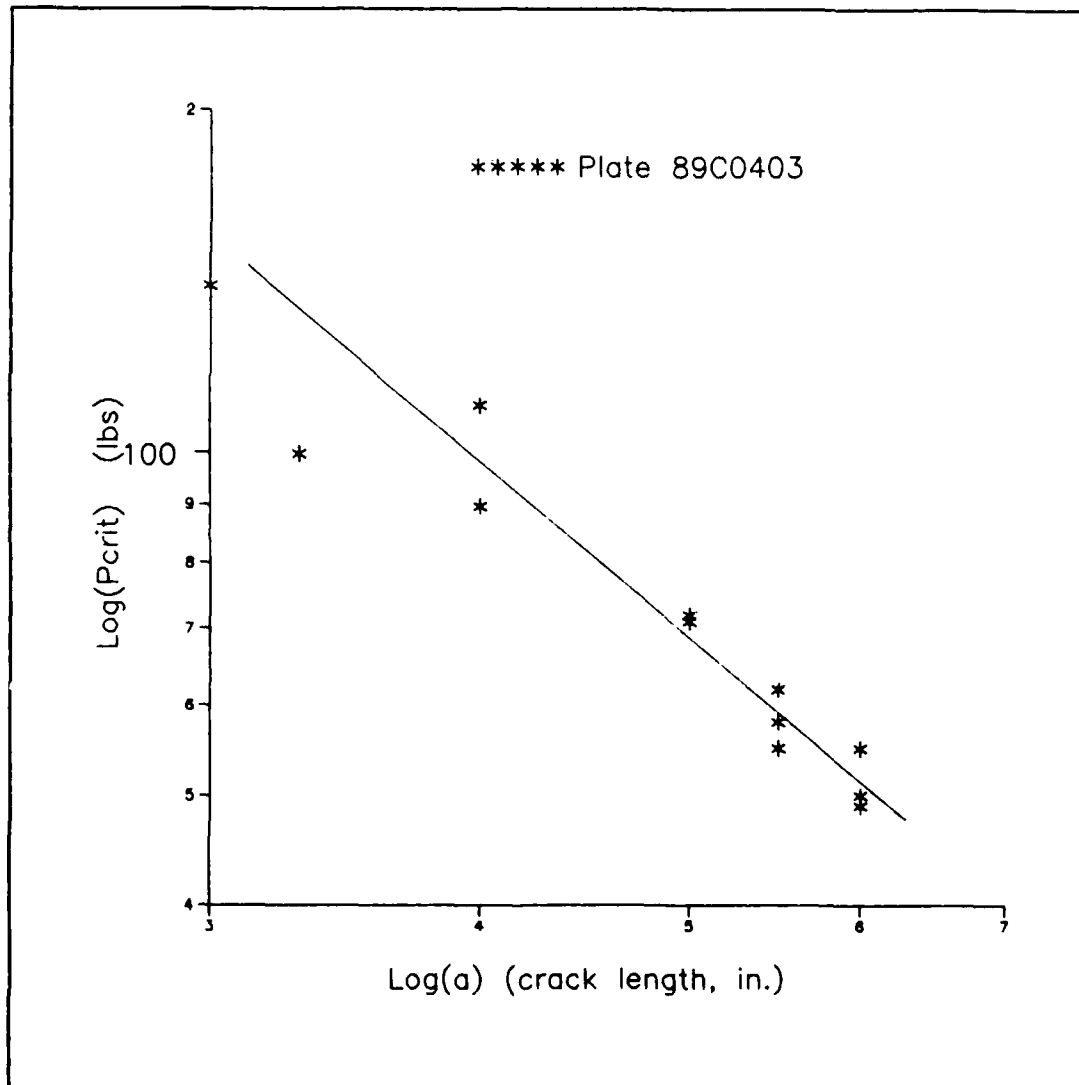
Fig. 48. Critical Load vs Crack Length, 600 F
CGW 1723
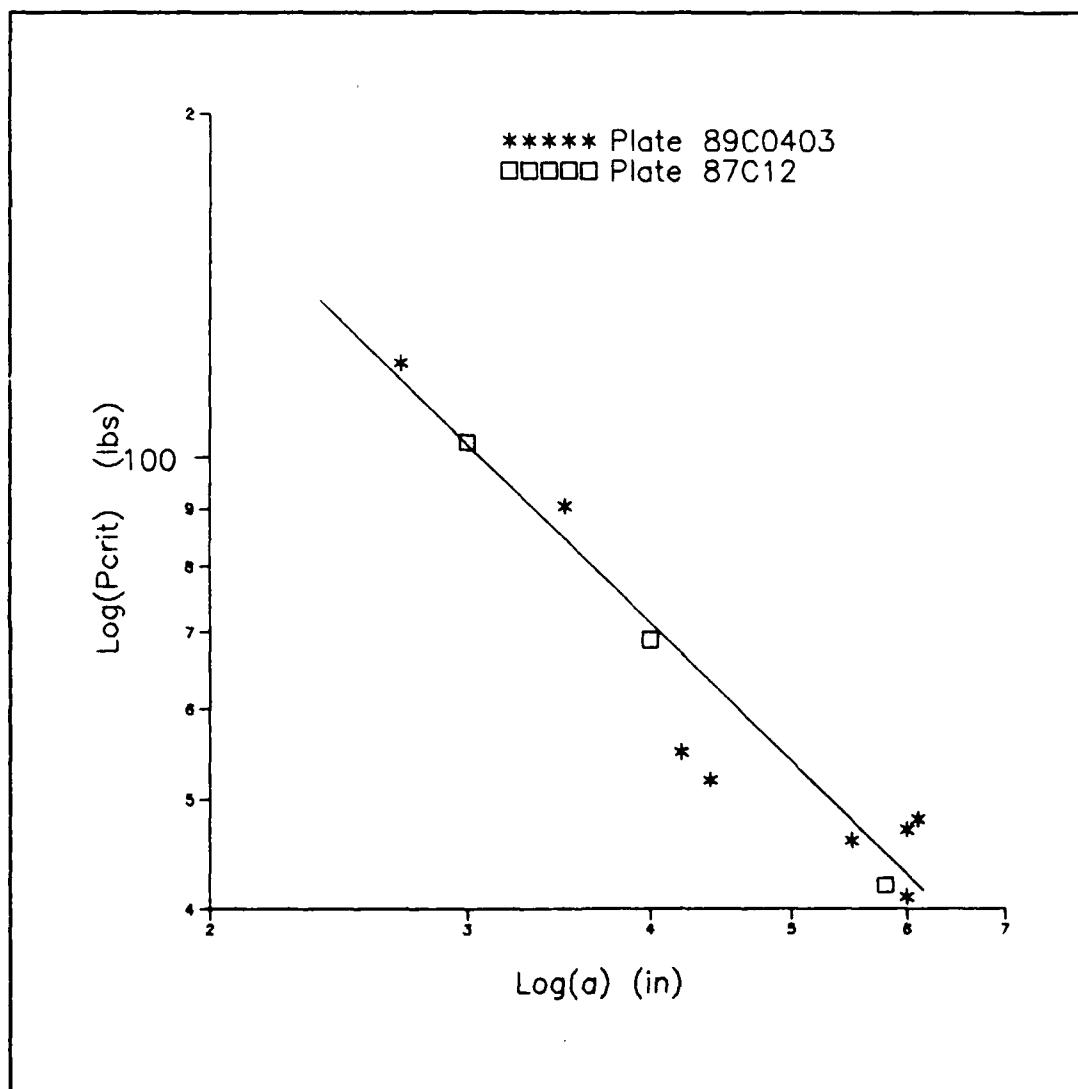
Fig. 49. Critical Load vs Crack Length, 1000 F
CGW 1723
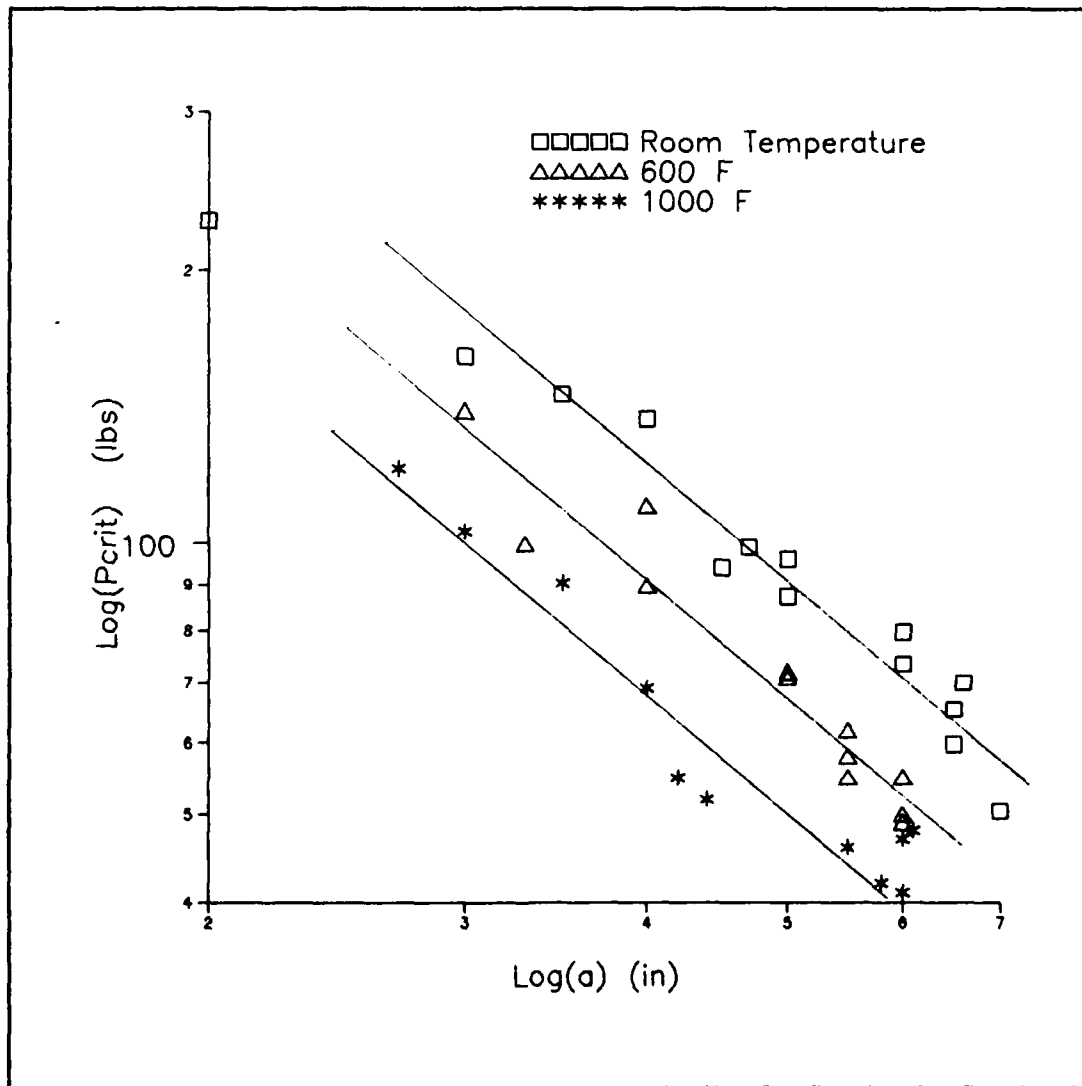
Fig. 50.   Comparison of Room Temperature, 600 F
and 1000 F Critical Load Values vs Crack Length
CGW 1723

92
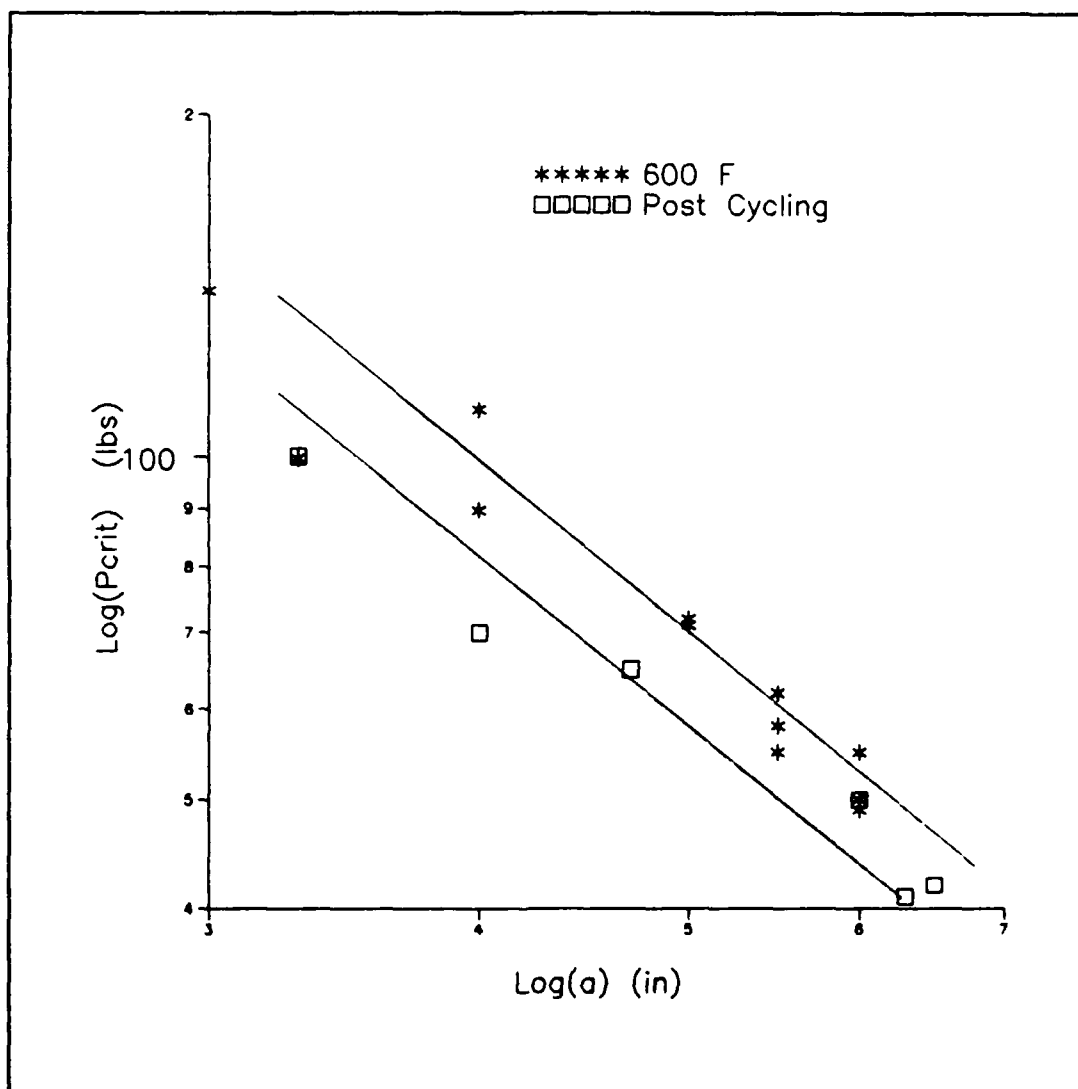
Fig. 51. Comparison of Post Thermal Cycling and 600 F
Critical Load Values vs Crack Length
CGW 1723
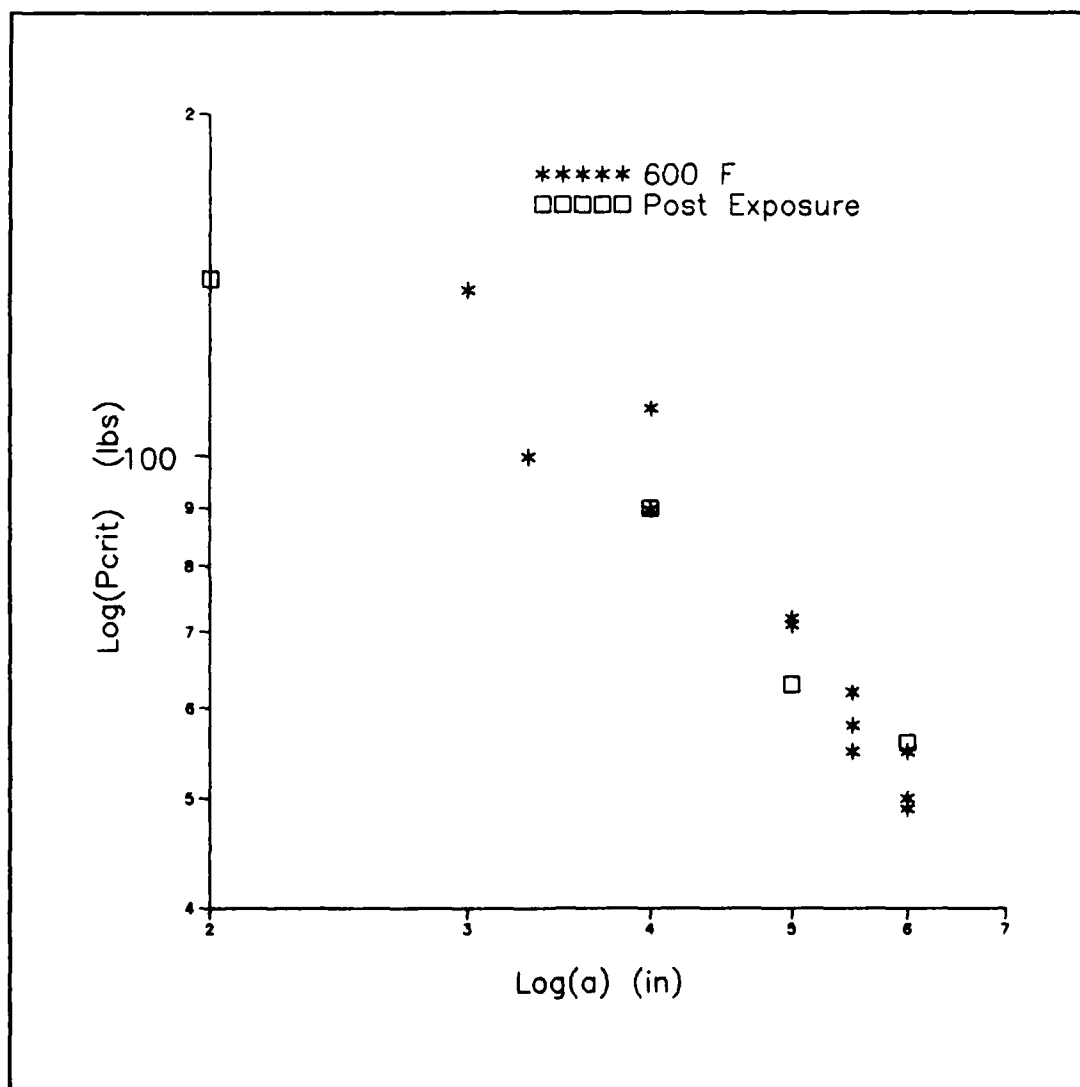
**Fig. 52. Comparison of Post Thermal Exposure and 600 F
Critical Load Values vs Crack Length
CGW 1723**
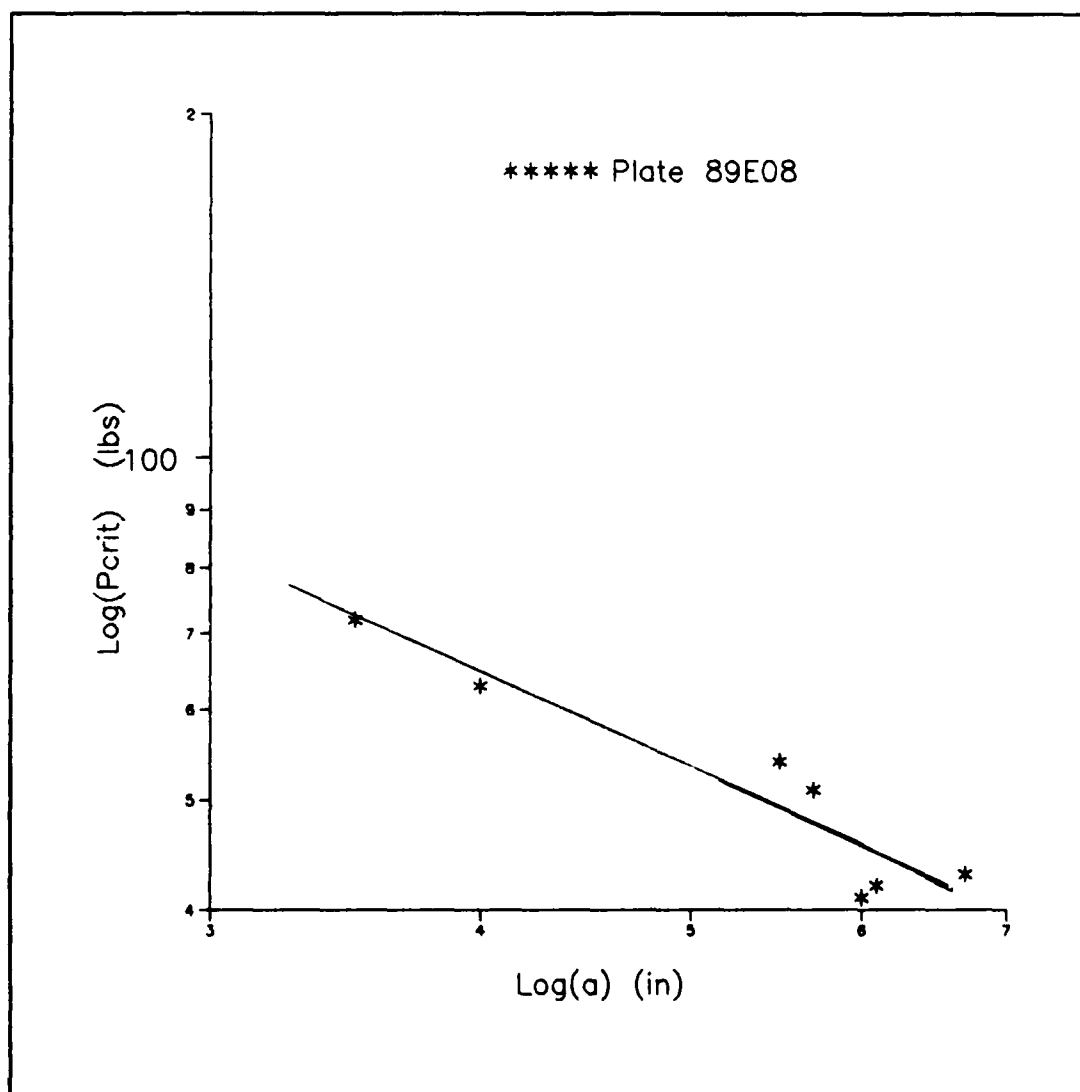
Fig. 53. Critical Load vs Crack Length, Room Temperature
CGW 7740

This yielded the following relationship:

$$G_{IIc} = \frac{9P_{cr}^2 a^2}{2Eb^2 h^3} \qquad (16)$$

The second method was to use the equation for the curve fit of the compliance data and take the derivative of it with respect to crack length. This resulted in equation 17 for the 2nd order curve fit and equation 18 for the third order curve fit:

$$G_{IIc} = \frac{P_{cr}^2}{2b} \left[2B \left(\frac{2}{L} \right)^2 a + C \left(\frac{2}{L} \right) \right] \qquad (17)$$

$$G_{IIc} = \frac{P_{cr}^2}{2b} \left[3A \left(\frac{2}{L} \right)^3 a^2 + 2B \left(\frac{2}{L} \right)^2 a + C \left(\frac{2}{L} \right) \right] \qquad (18)$$

where A is the coefficient of x^3 (if applicable), B is the coefficient of x^2, and C is the coefficient of x in the equations for the polynomial curve fits of compliance to non-dimensionalized crack length.

The values of G_{IIc} calculated are given by crack length and specimen in Appendix C for each temperature tested and for both materials. From the critical load data measured at room temperature and 600 F for CGW 1723 three values of G_{IIc} were calculated for each test. These values were based on the following equations for the compliance to crack length relationship: Russell's equation, Equation 4 with E = 1.72 lb/in^2; the 2nd order polynomial fit of the combined room temperature and 600 F compliance data, Equation 9; and the

96

3rd order polynomial fit of the combined room temperature and 600 F compliance data, Equation 10. Similarly, from the CGW 1723 1000 F critical loads three values of G_{IIc} were calculated for each test. These values were based on Russell's equation, Equation 4 with E = 1.68E07 lbs/in^2, and 2nd and 3rd order curve fits to the 1000 F compliance data, Equations 11 and 12. Values of G_{IIc} for the thermal cycling and thermal exposure specimens were calculated based on Russell's equation, Equation 4 with E = 1.72 lbs/in^2, and 2nd and 3rd order polynomial fits to the combined room temperature and 600 F compliance curves, Equations 9 and 10. At the two temperatures, room temperature and 1000F, where plate 87C12 was tested the fracture toughness of this plate was compared with plate 89C0403. At both temperatures, the fracture toughness values of plate 87C12 was within the experimental scatter of corresponding values from plate 89C0403. This shows that the two plates behaved as one. Therefore, data from both plates was combined to find the average fracture toughness at these temperatures. From room temperature critical loads of CGW 7740, fracture toughness was calculated based on Russell's equation, Equation 4 with E = 1.20 lbs/in^2, and 2nd and 3rd order curve fits of the room temperature compliance data for CGW 7740, Equations 13 and 14.

Figures 54 thru 71 show the fracture toughness

97

calculated for each temperature by each method for CGW 1723. Figures 72 thru 74 show the fracture toughness values for CGW 7740. Appendix C contains values for CGW 1723 specimens at room temperature and 600 F with calculations based on 2nd and 3rd order curve fits to their respective compliance data only. Appendix B also contains plots comparing the values obtained at the temperatures tested and post thermal cycling.

As can be seen from the figures, the values of G_{IIc} calculated from Russell's equation for the compliance to crack length relationship consistently show the smallest data scatter in comparison to the other methods. The third order polynomial curve fit produced the next best results, and in many cases showed almost the same spread of data as the calculations based on Russell's equation. This was especially the case at crack lengths greater than 2a/L = .4, where the 3rd order polynomial was better able to represent the actual compliance data. The second order polynomial curve fit showed too much scatter in data. Because of the consistency, i.e. minimum scatter in G_{IIc}, obtained from Russell's equation for the compliance to crack length relationship, it may be considered appropriate to state that this method is the most reliable.

Table 3 gives the average fracture toughness values for all temperatures tested using equation 15 and Russell's equation and 2nd and 3rd order curve fits of experimental
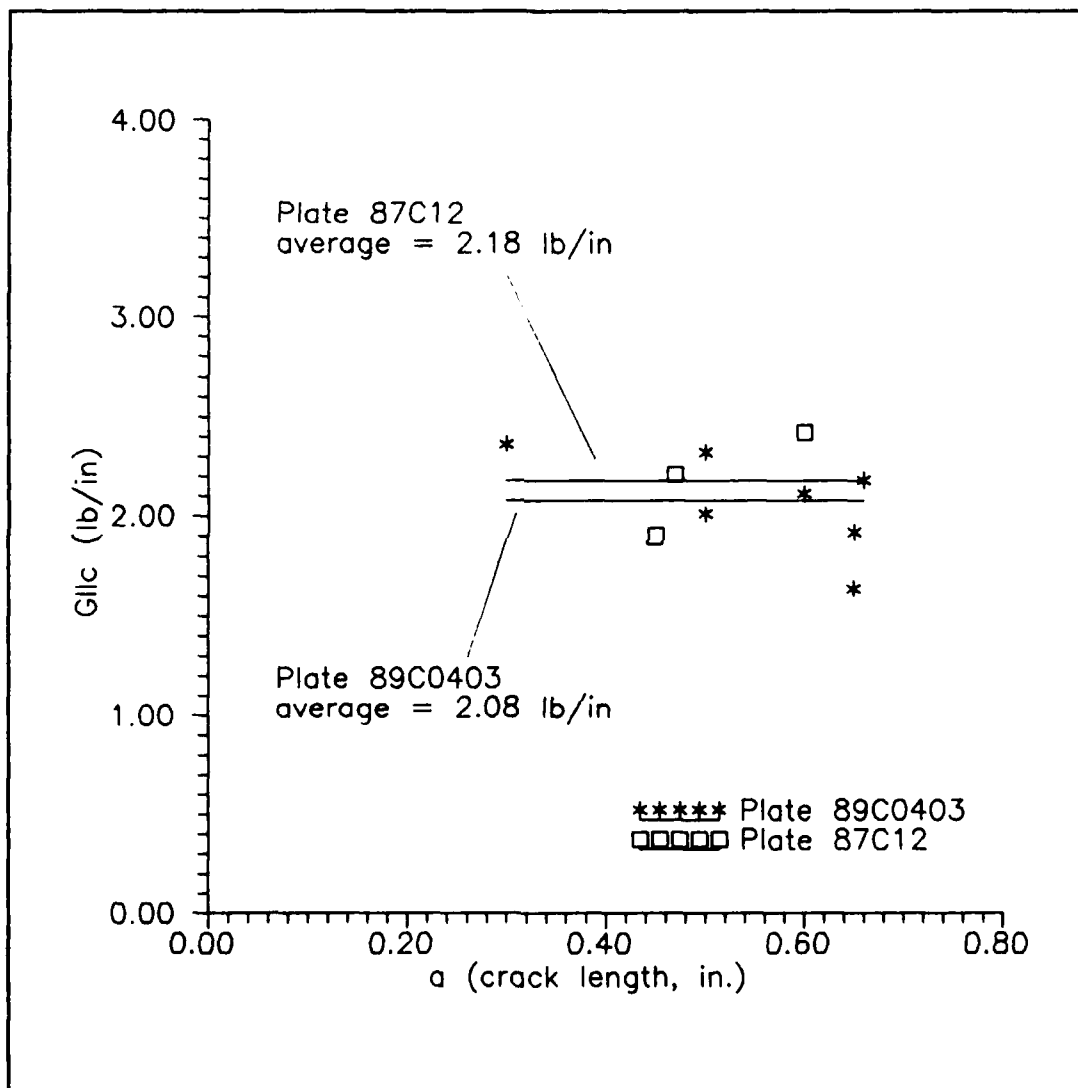
Fig. 54. Room Temperature Fracture Toughness of Plates 89C0403 and 87C12 Based on Russell's Equation for Compliance to Crack Length Relationship
CGW 1723

99
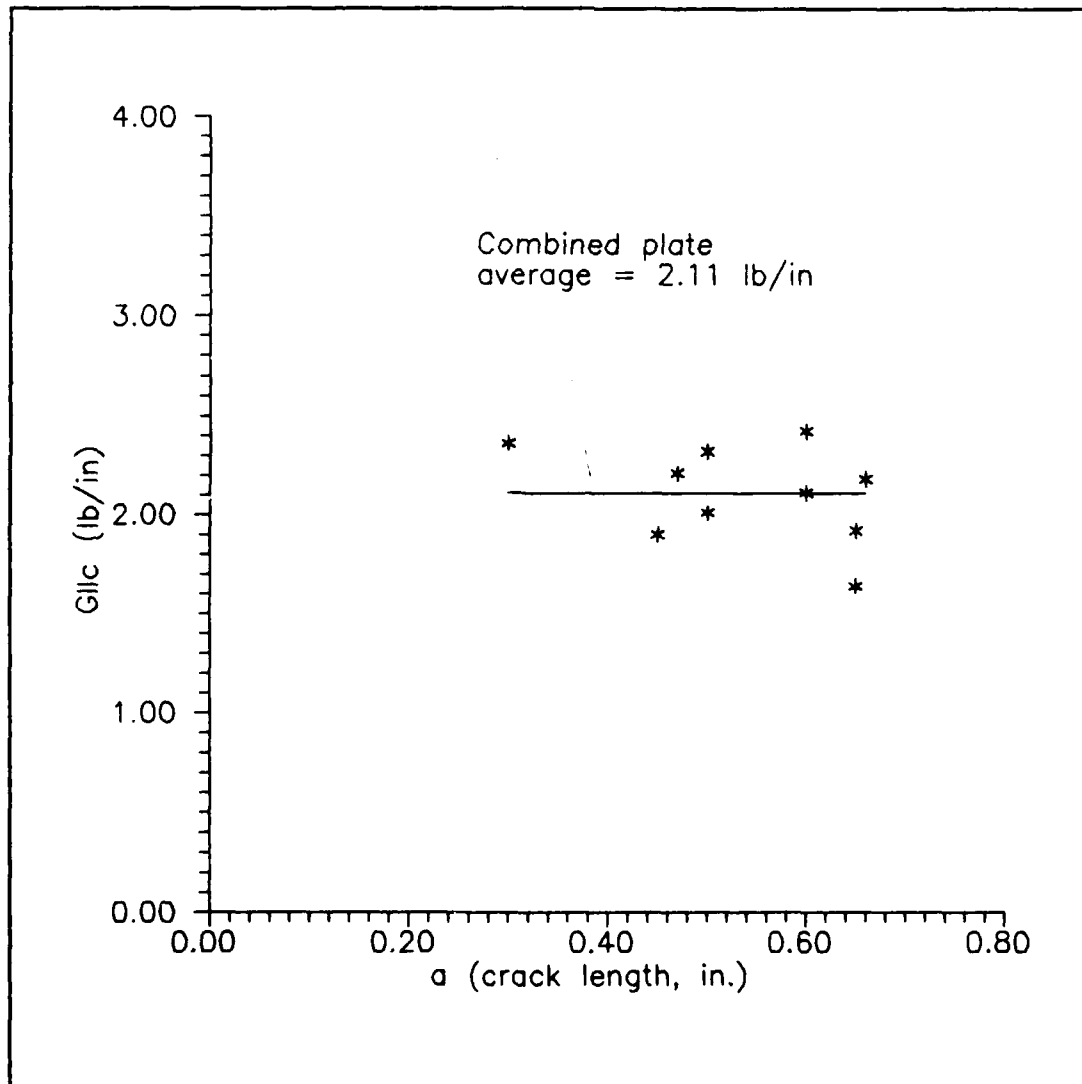
Fig. 55. Average Room Temperature Fracture Toughness of
Plates 89C0403 and 87C12 Based on Russell's Equation for
Compliance to Crack Length Relationship
CGW 1723

100
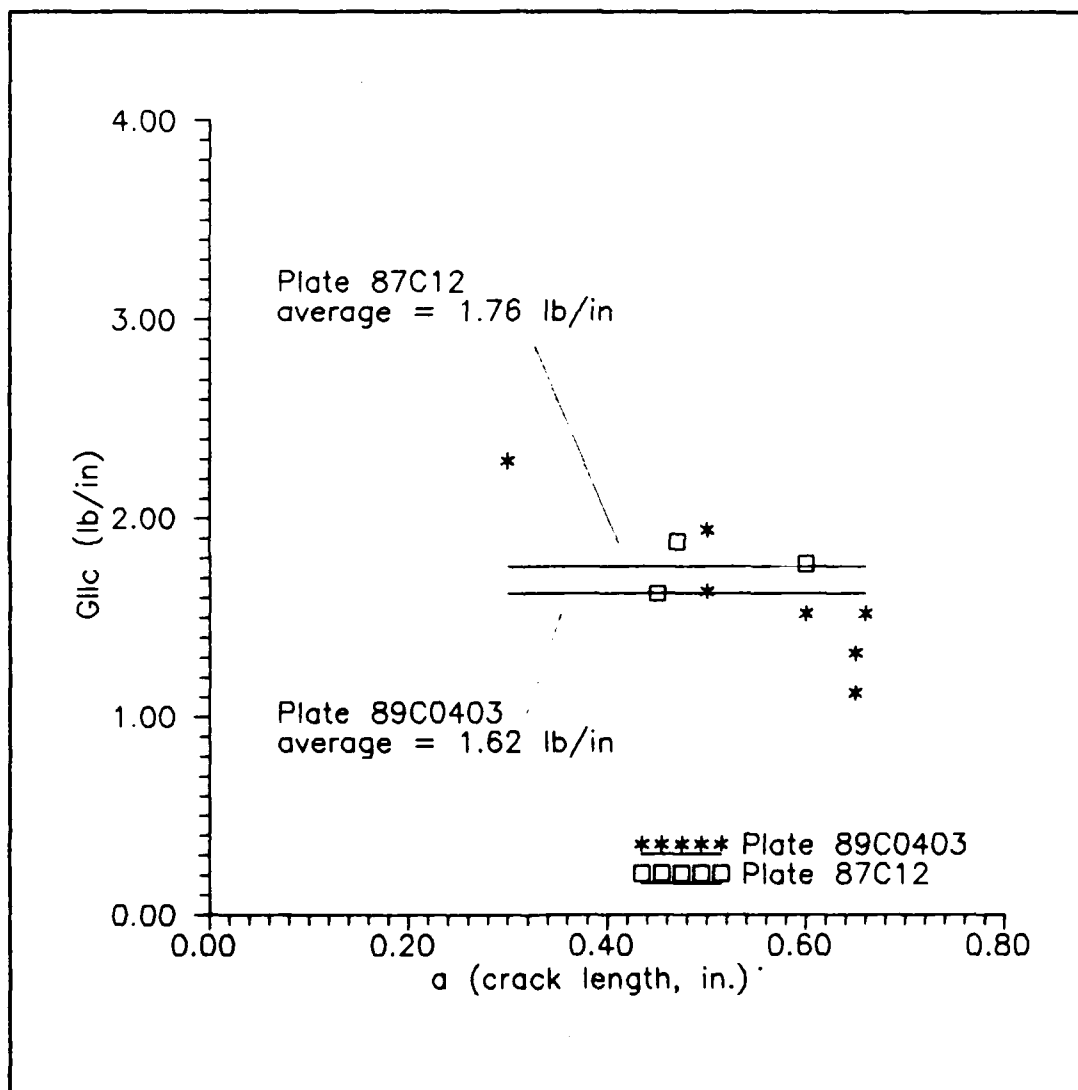
Fig. 56. Room Temperature Fracture Toughness of
Plates 89C0403 and 87C12 Based on 2nd Order Curve Fit
of Combined Room Temperature and 600 F Compliance Data
for Compliance to Crack Length Relationship
CGW 1723

101
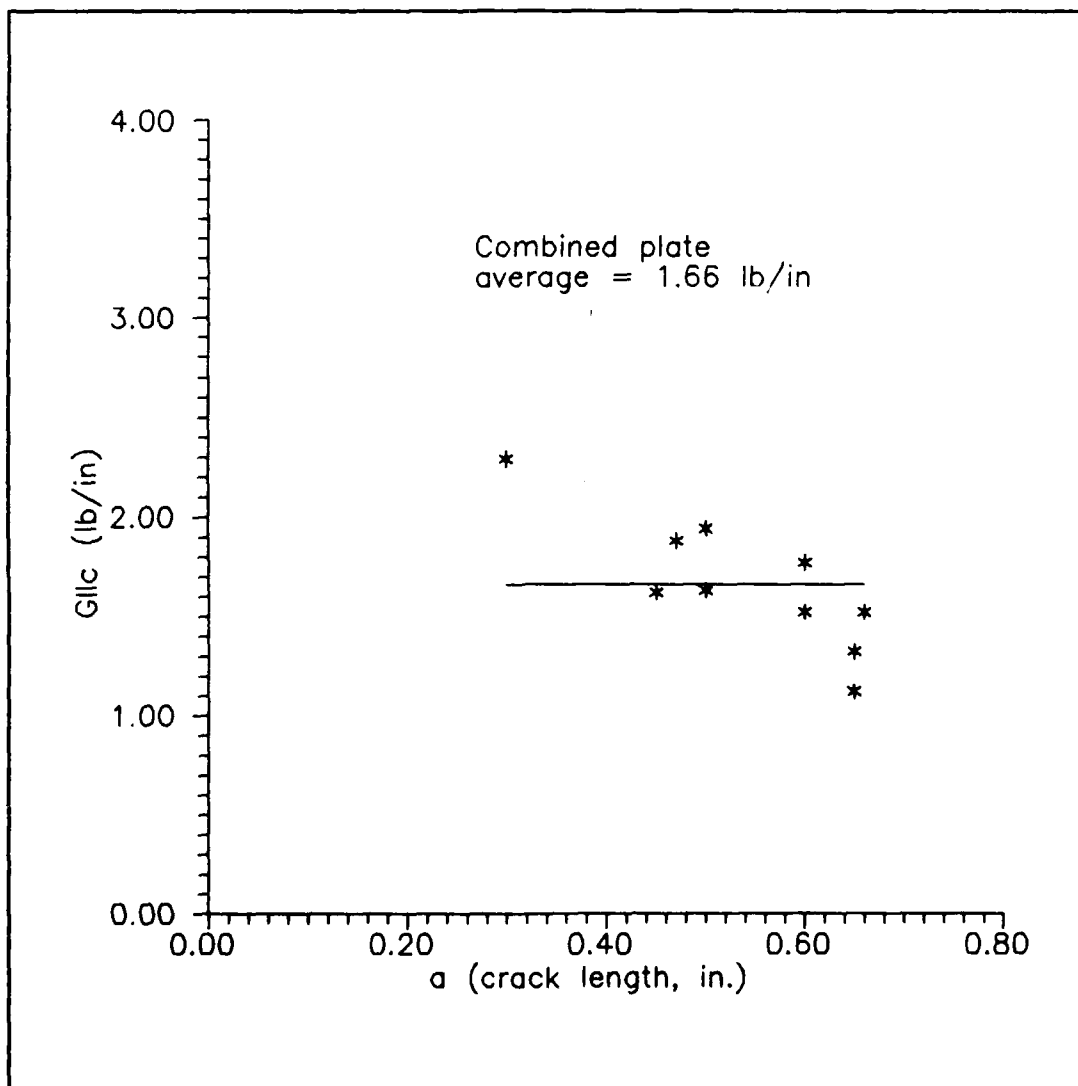
Fig. 57. Average Room Temperature Fracture Toughness of
Plates 89C0403 and 87C12 Based on 2nd Order Curve Fit
of Combined Room Temperature and 600 F Compliance Data
for Compliance to Crack Length Relationship
CGW 1723

102
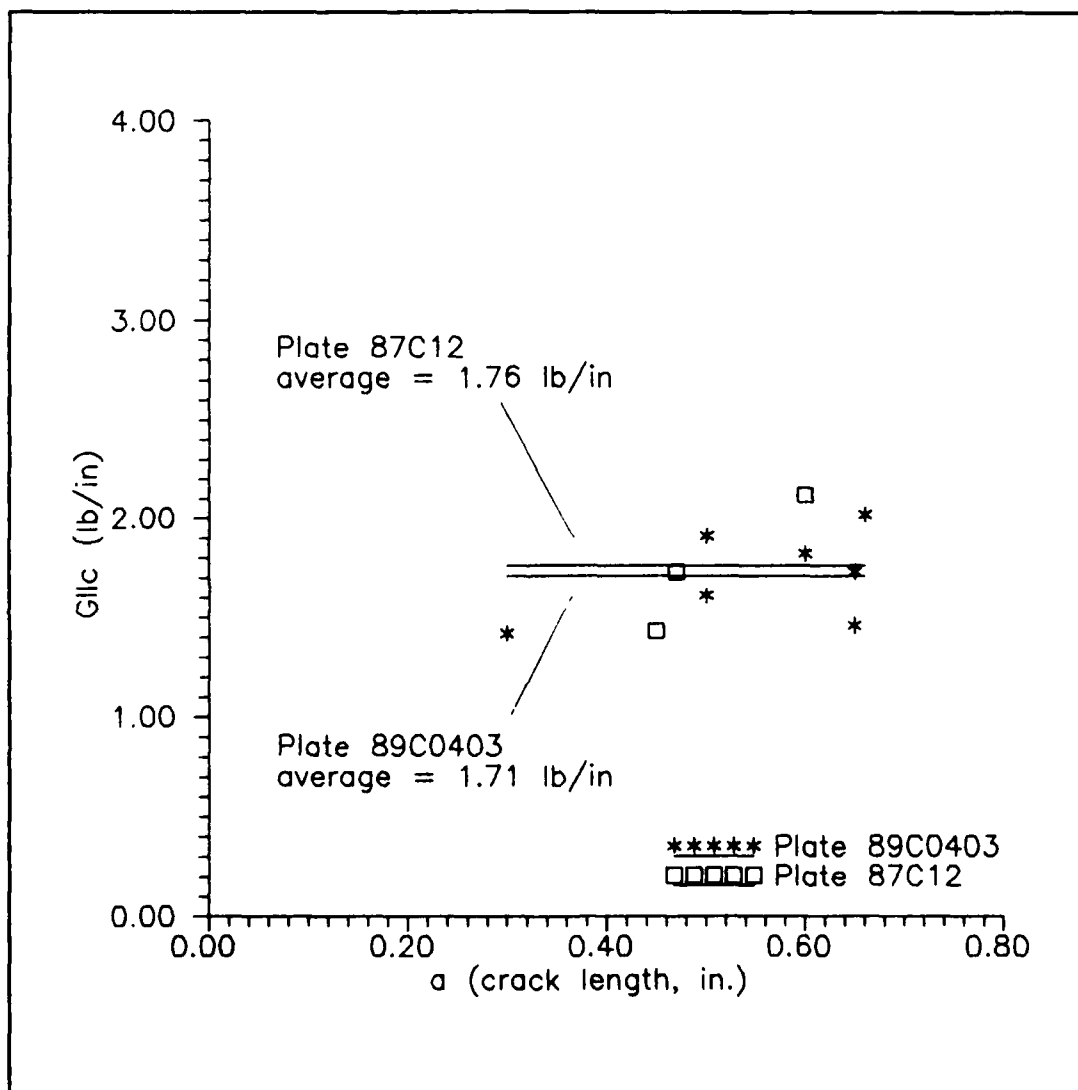
Fig. 58. Room Temperature Fracture Toughness of
Plates 89C0403 and 87C12 Based on 3rd Order Curve Fit
of Combined Room Temperature and 600 F Compliance Data
for Compliance to Crack Length Relationship
CGW 1723

103
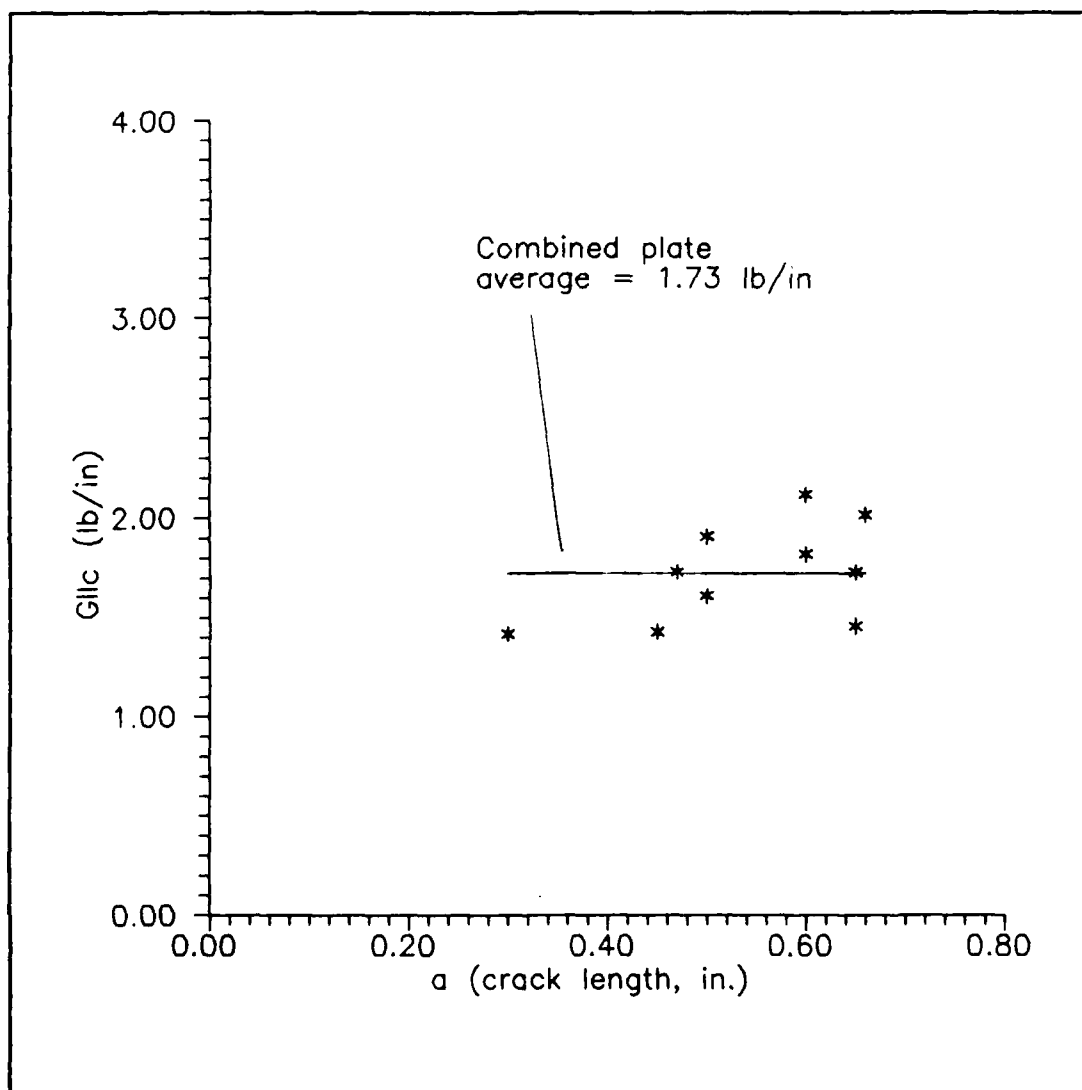
Fig. 59. Average Room Temperature Fracture Toughness of Plates 89C0403 and 87C12 Based on 3rd Order Curve Fit of Combined Room Temperature and 600 F Compliance Data for Compliance to Crack Length Relationship CGW 1723

104
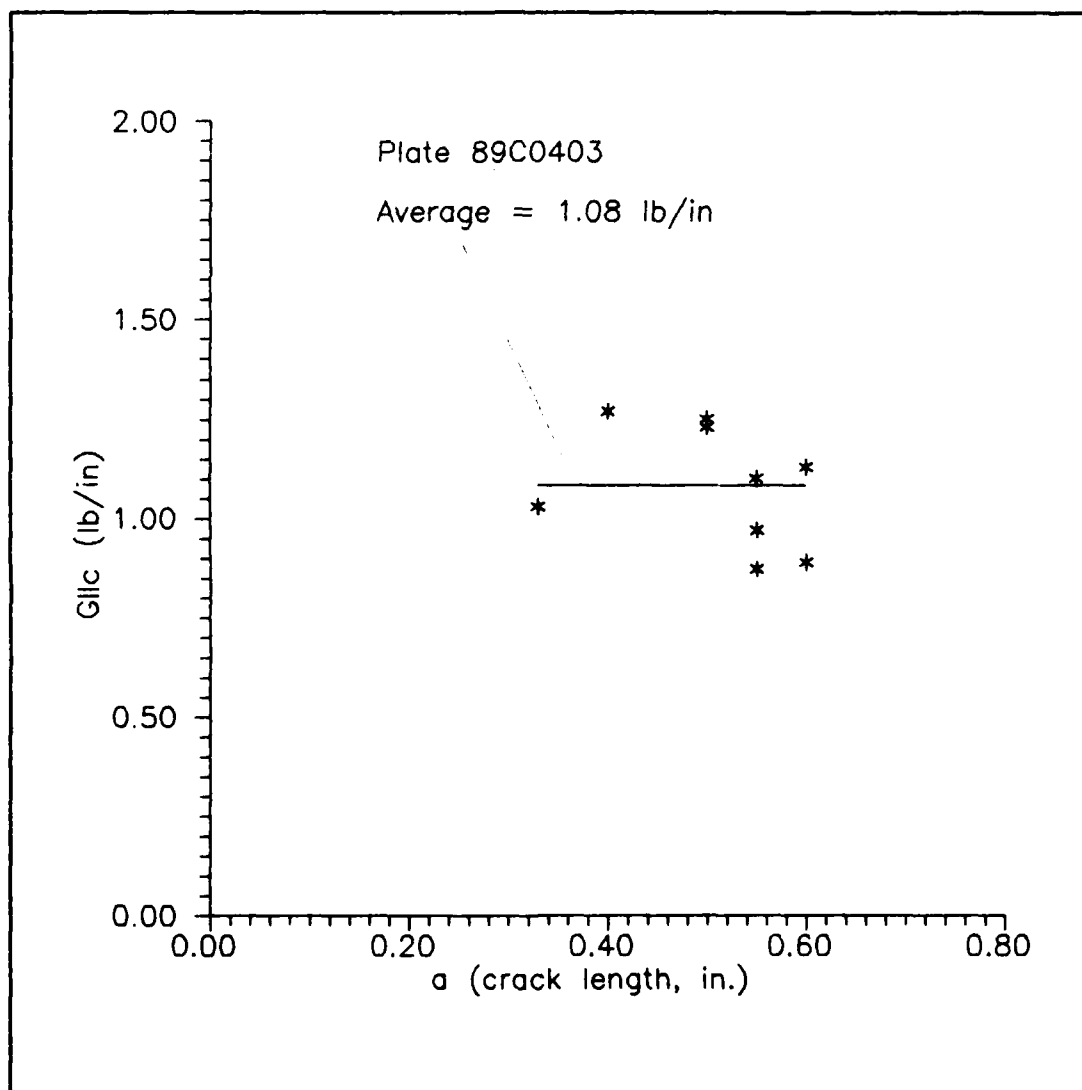
**Fig. 60. 600 F Fracture Toughness
Based on Russell's Equation for Compliance to Crack
Length Relationship
CGW 1723**

105
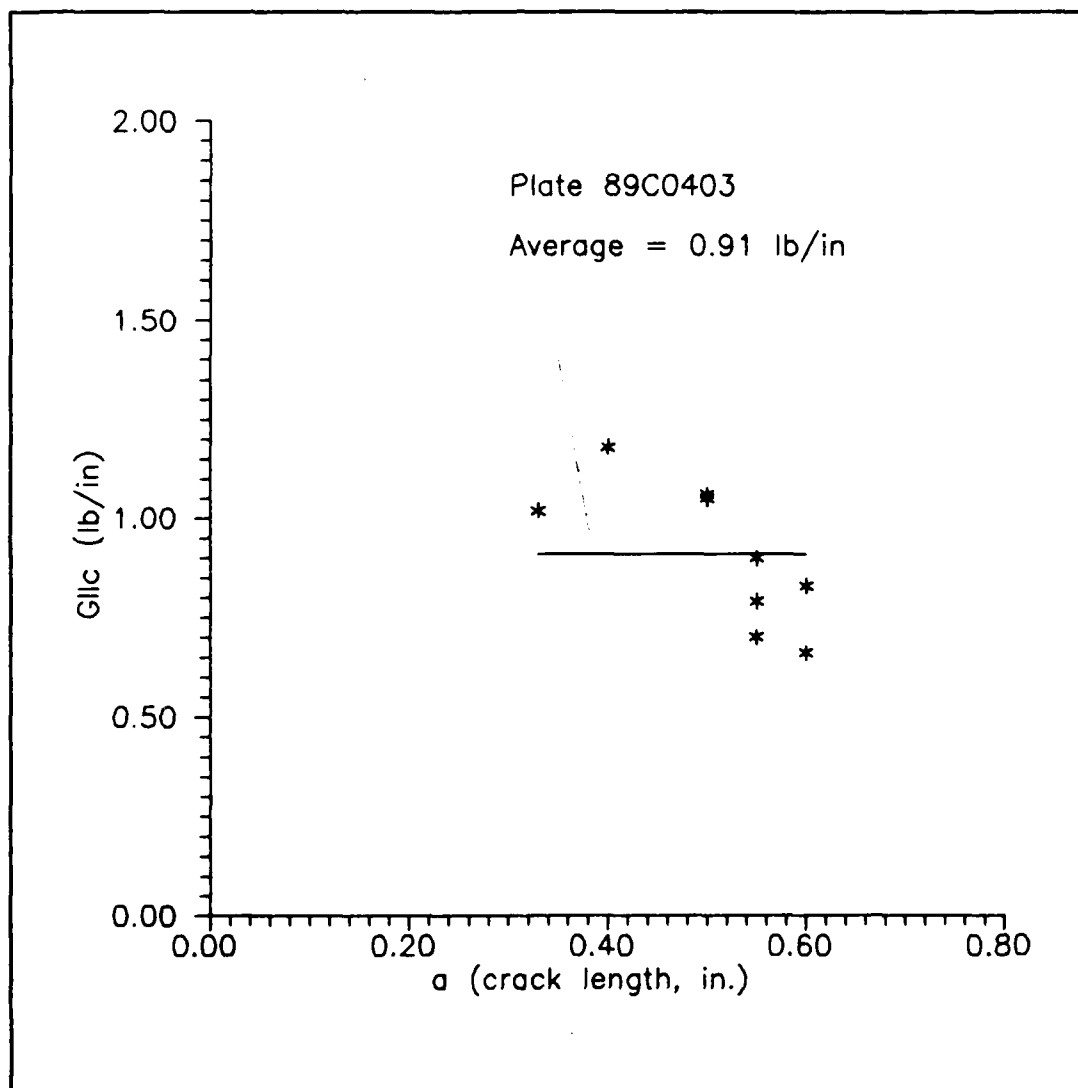
Fig. 61. 600 F Fracture Toughness Based on
2nd Order Curve Fit of Combined Room Temperature and 60) F
Compliance Data For Compliance to Crack Length Relation:hip
CGW 1723

106
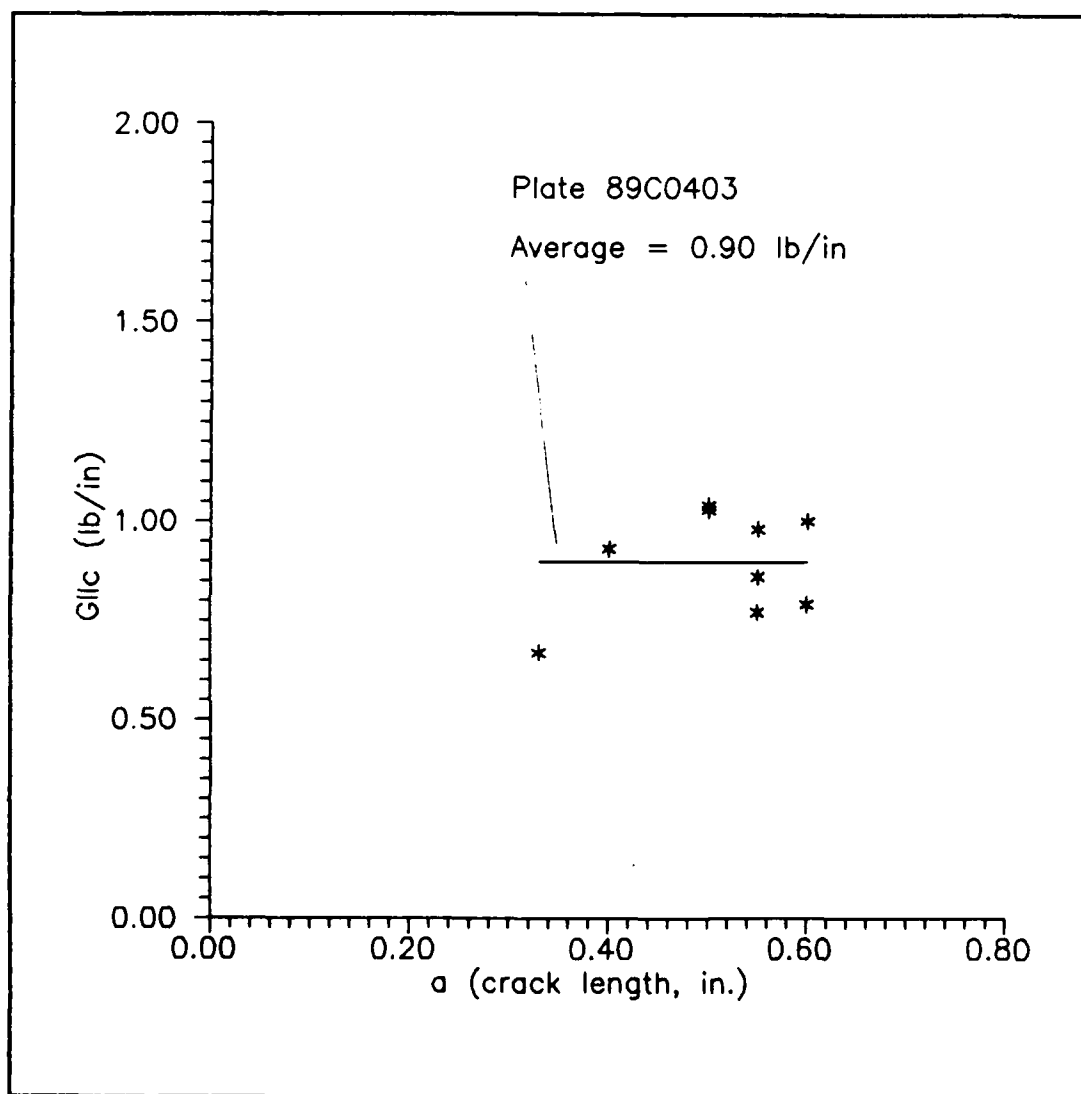
Fig. 62.   600 F Fracture Toughness Based on
3rd Order Curve Fit of Combined Room Temperature and 600 F
Compliance Data for Compliance to Crack Length Relationship
CGW 1723

107
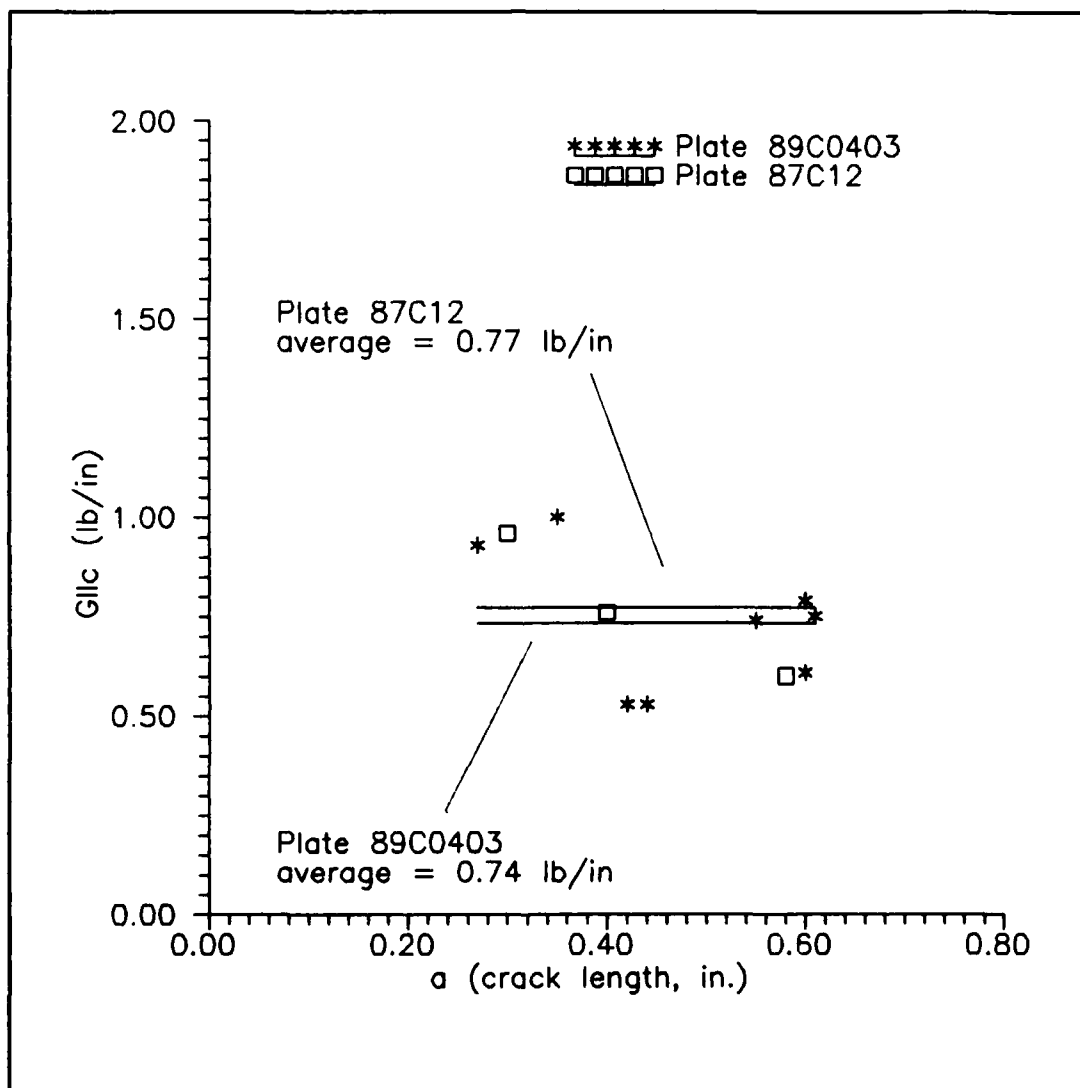
**Fig. 63. 1000 F Fracture Toughness of
Plates 89C0403 and 87C12 Based on Russell's Equation for
Compliance to Crack Length Relationship
CGW 1723**

108
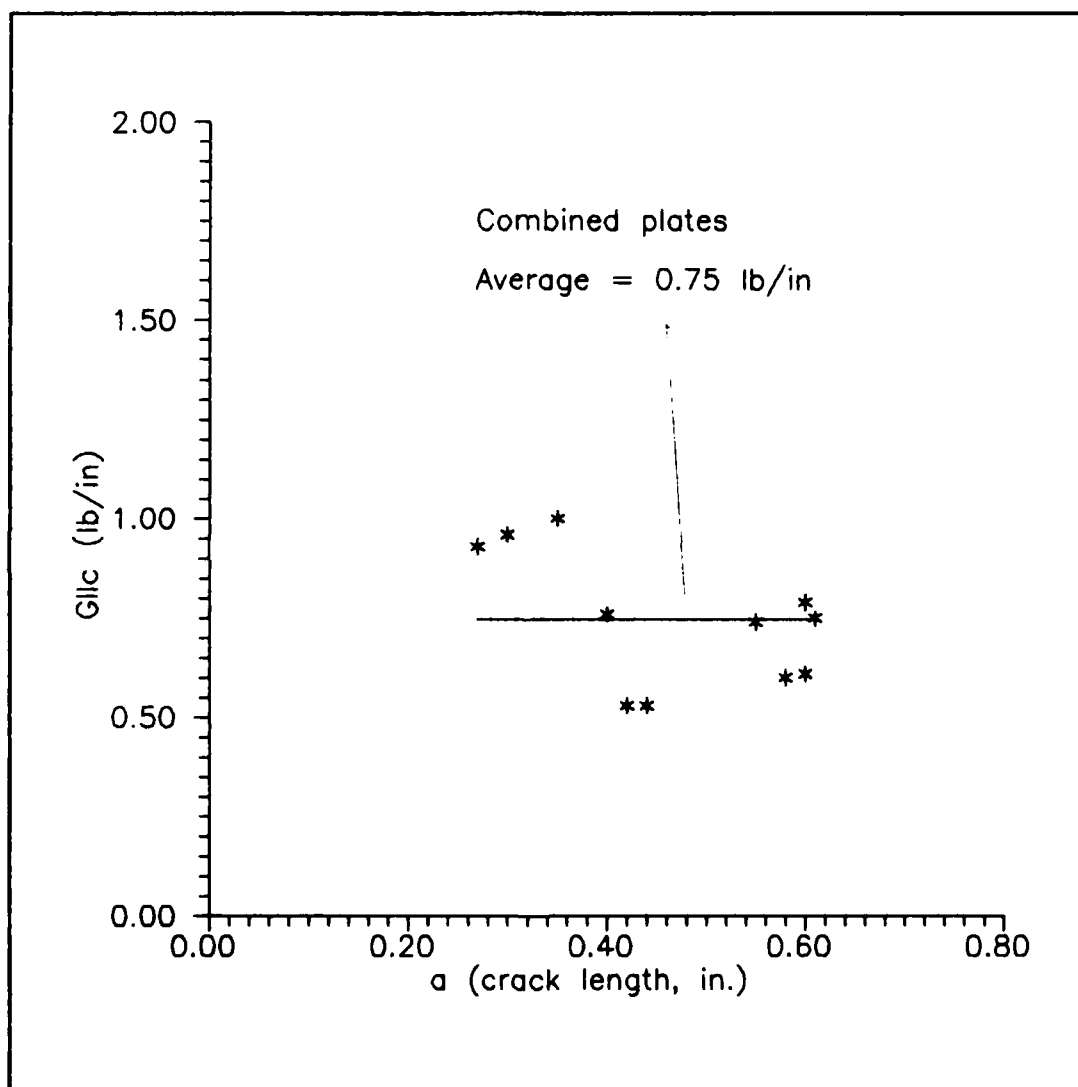
Fig. 64. Average 1000 F Fracture Toughness of Plates 89C0403 and 87C12 Based on Russell's Equation for Compliance to Crack Length Relationship CGW 1723

109
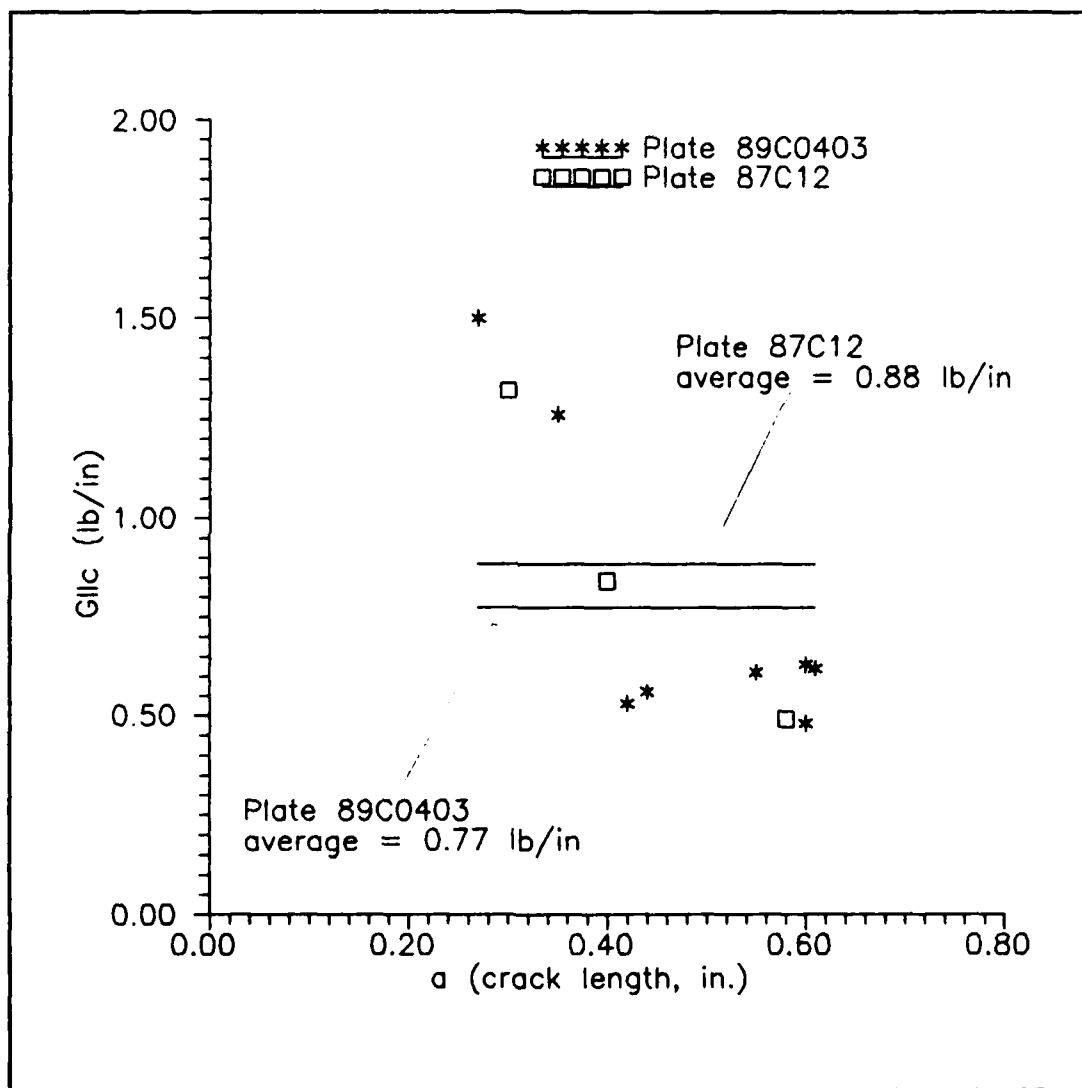
Fig. 65. 1000 F Fracture Toughness of Plates 89C0403 and 87C12 Based on 2nd Order Curve Fit of 1000 F Compliance Data for Compliance to Crack Length Relationship CGW 1723
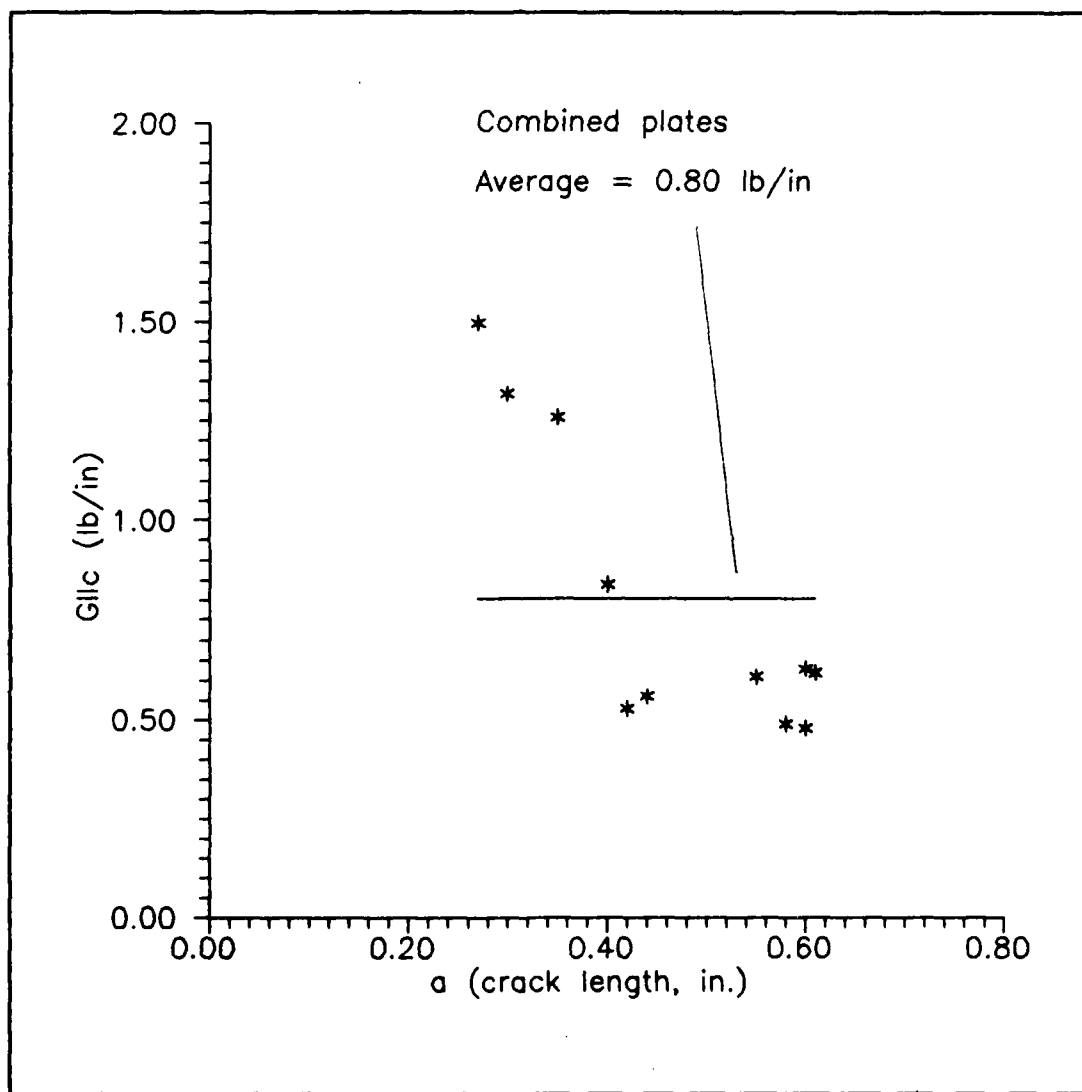
Fig. 66. Average 1000 F Fracture Toughness of Plates 89C0403 and 87C12 Based on 2nd Order Curve Fit of 1000 F Compliance Data for Compliance to Crack Length Relationship CGW 1723

111
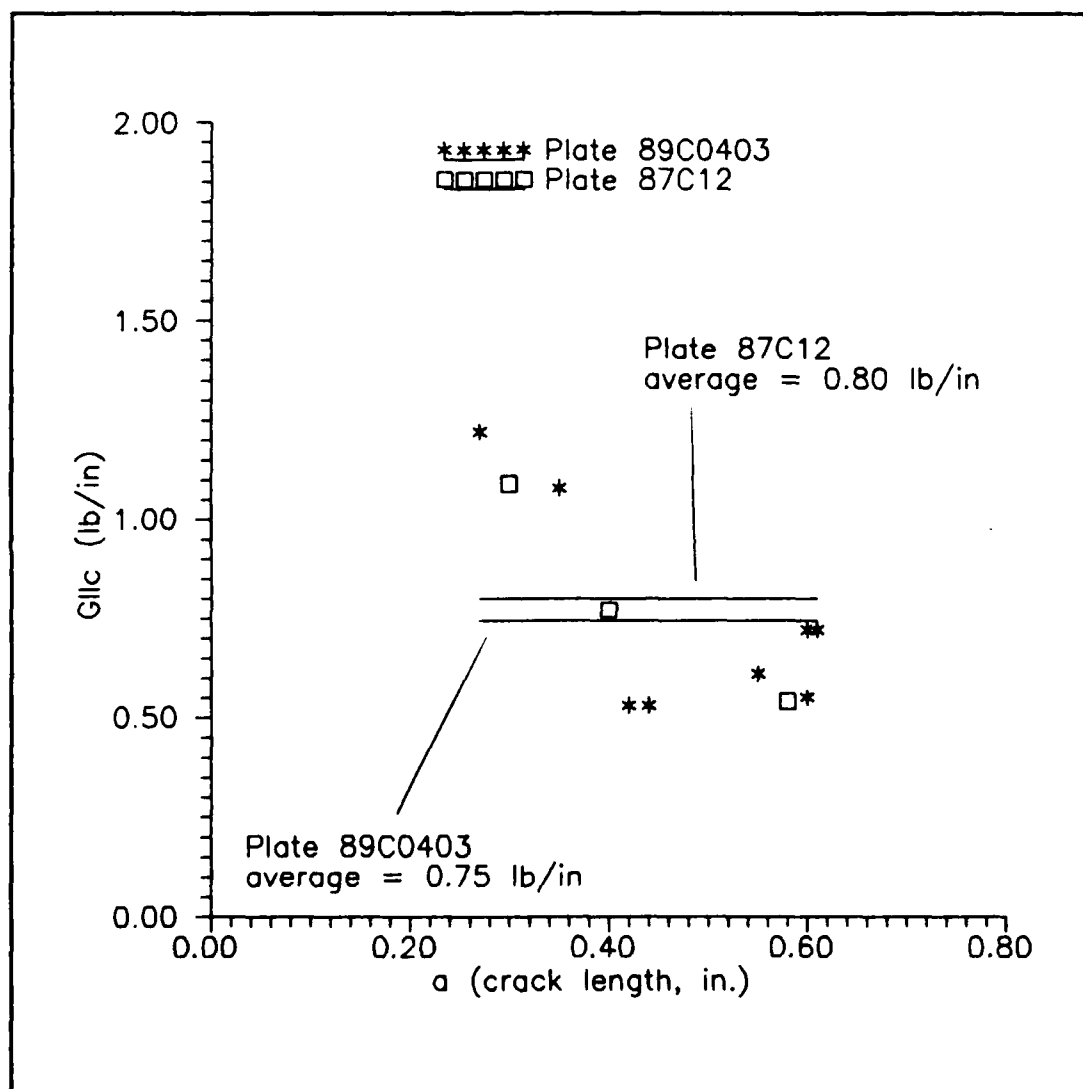
Fig. 67.   1000 F Fracture Toughness of Plates
89C0403 and 87C12 Based on 3rd Order Curve Fit of 1000 F
Compliance Data for Compliance to Crack Length Relationship
CGW 1723
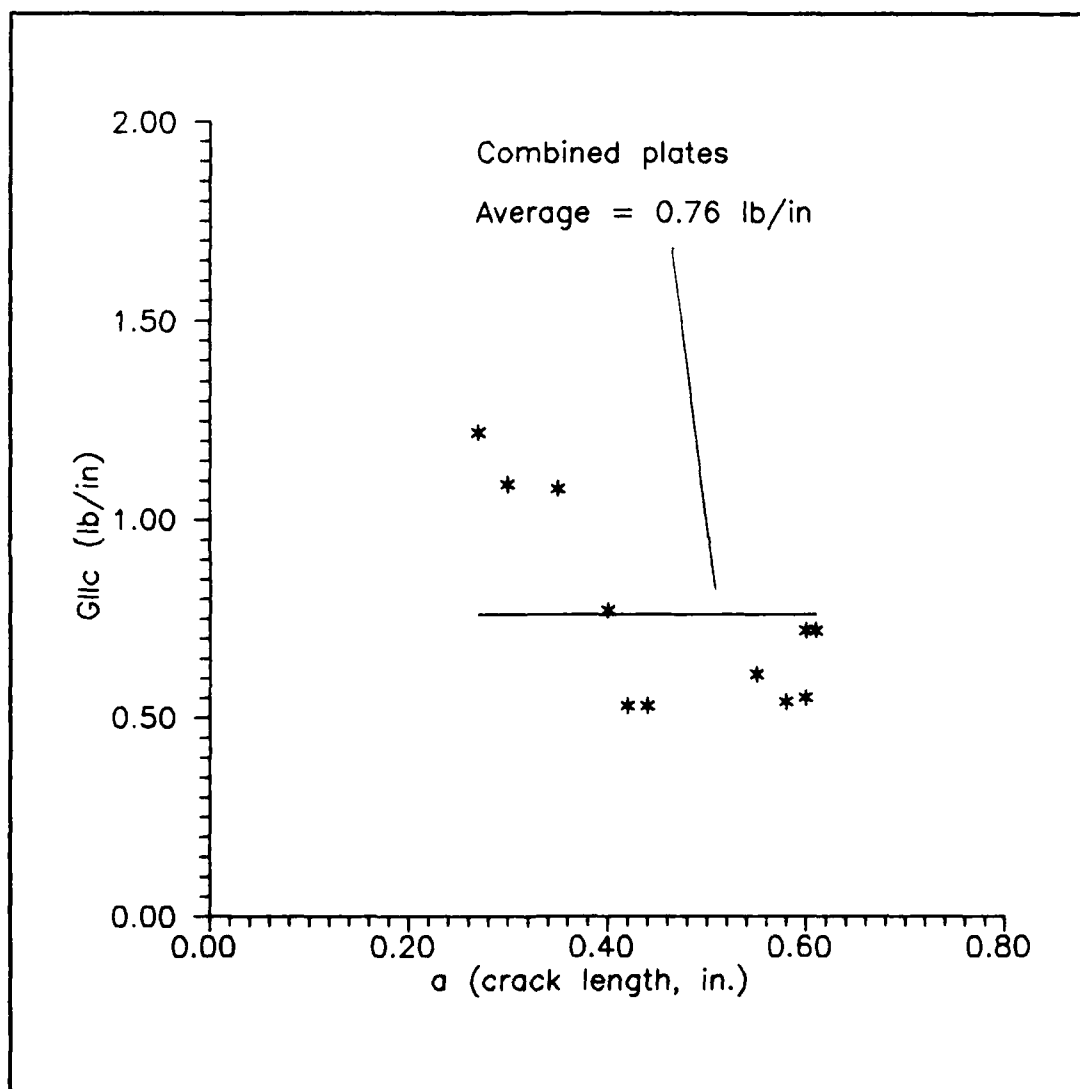
**Fig. 68.   Average 1000 F Fracture Toughness of Plates
89C0403 and 87C12 Based on 3rd Order Curve Fit of 1000 F
Compliance Data for Compliance to Crack Length Relationship
CGW 1723**

113
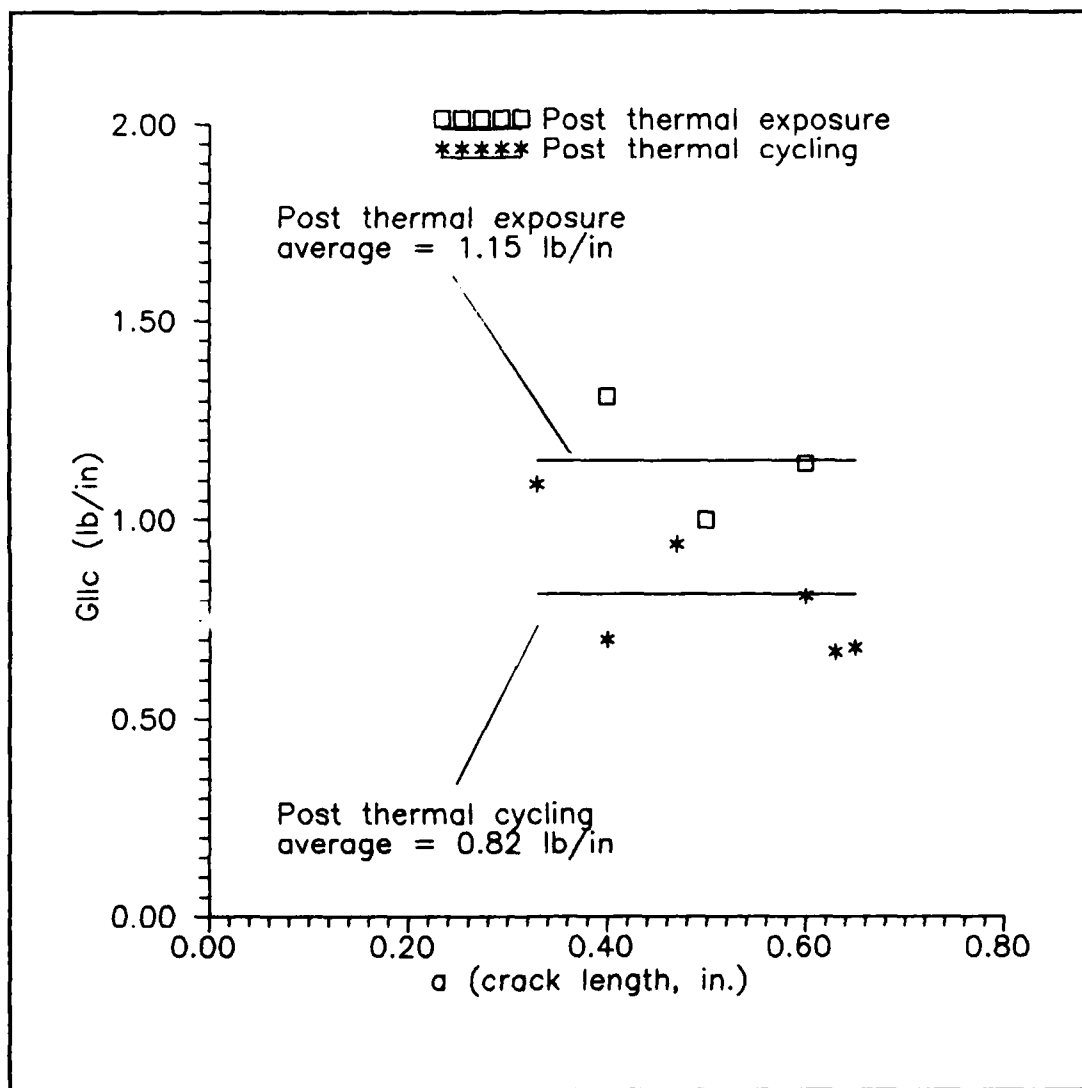
**Fig. 69. Post Thermal Cycling Fracture Toughness
Based on Russell's Equation for Compliance to Crack
Length Relationship
CGW 1723**

114
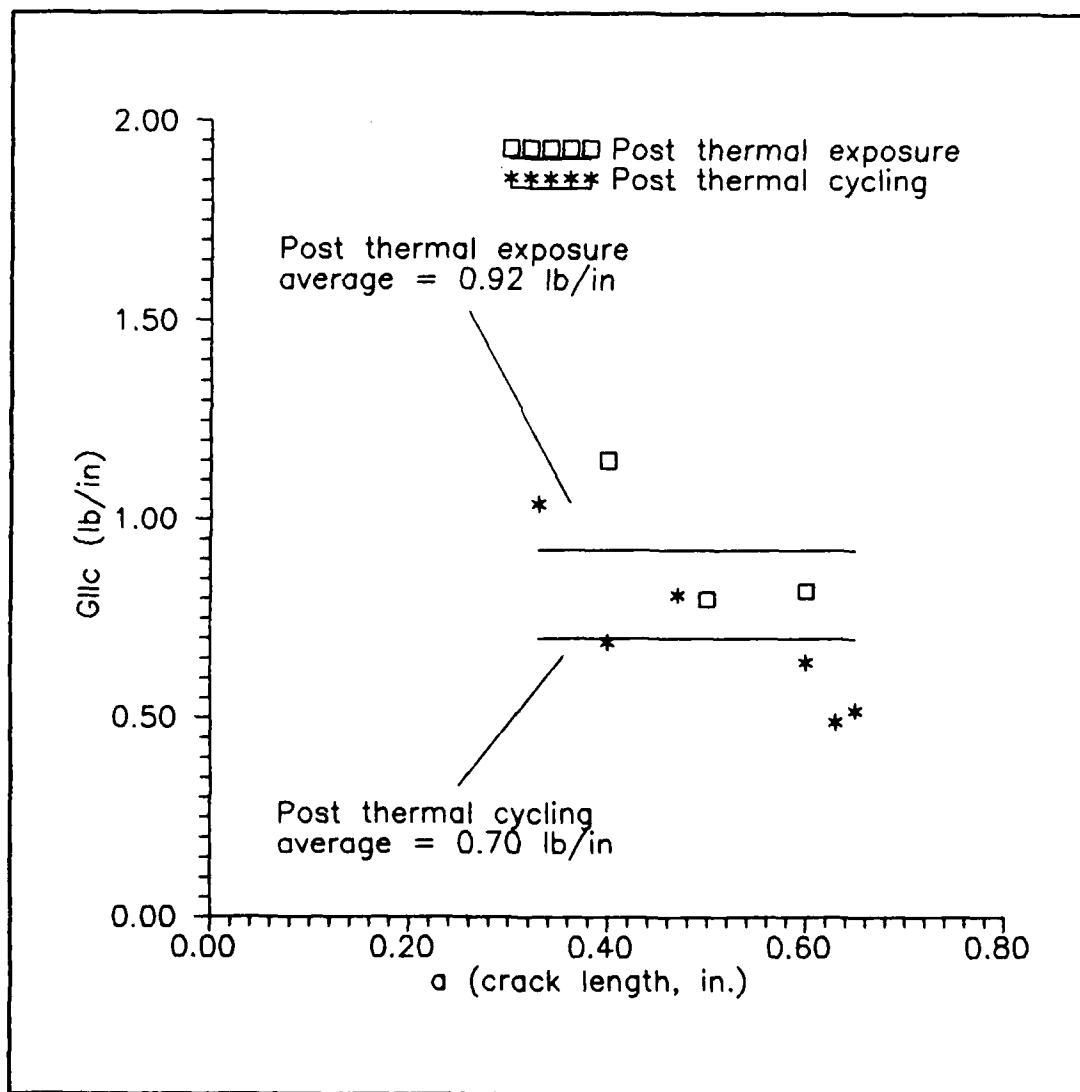
**Fig. 70. Post Thermal Cycling Fracture Toughness
Based on 2nd Order Curve Fit of Combined Room Temperature
and 600 F Compliance Data for Compliance to
Crack Length Relationship
CGW 1723**

115
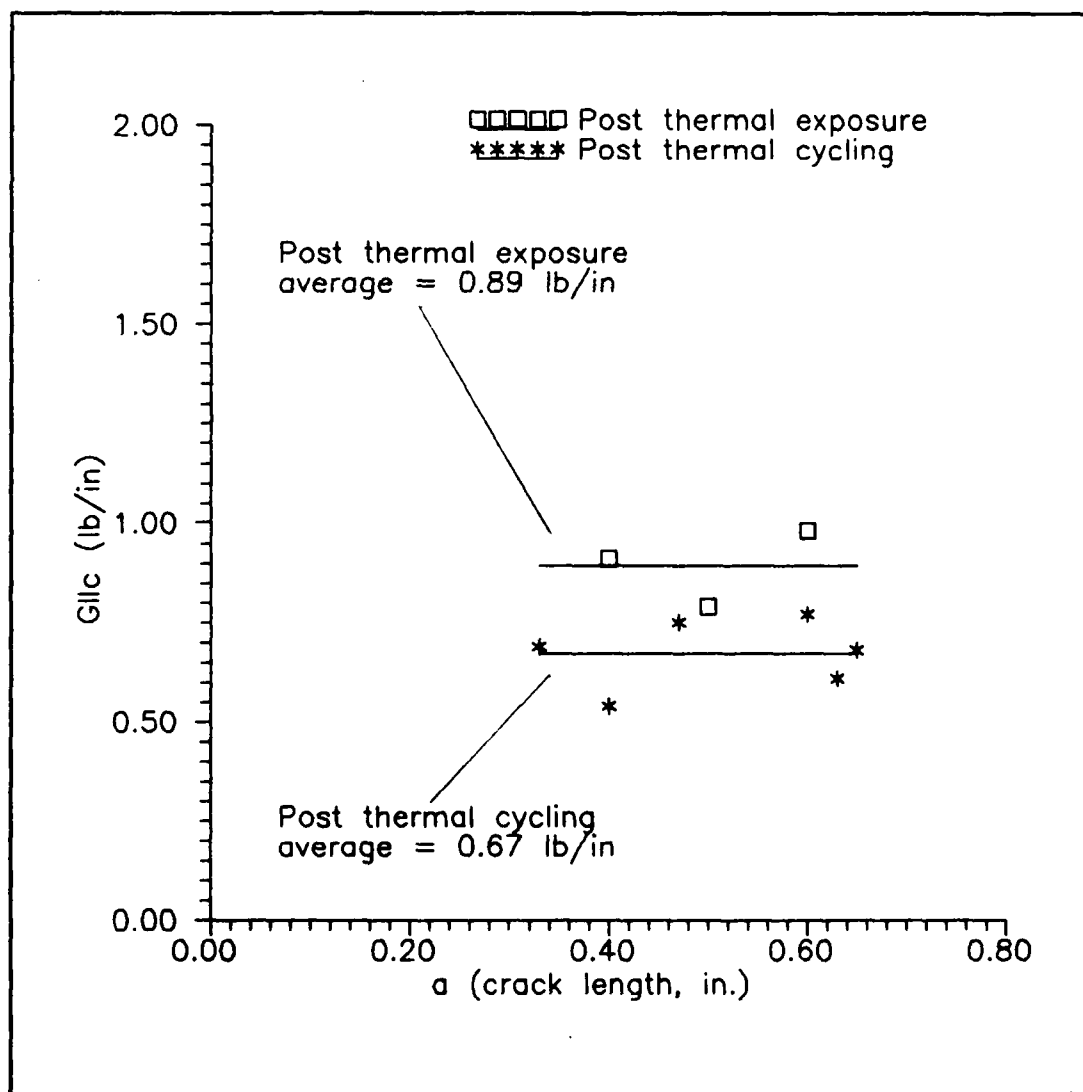
Fig. 71. Post Thermal Cycling Fracture Toughness Based on 3rd Order Curve Fit of Combined Room Temperature and 600 F Compliance Data for Compliance to Crack Length Relationship CGW 1723

116
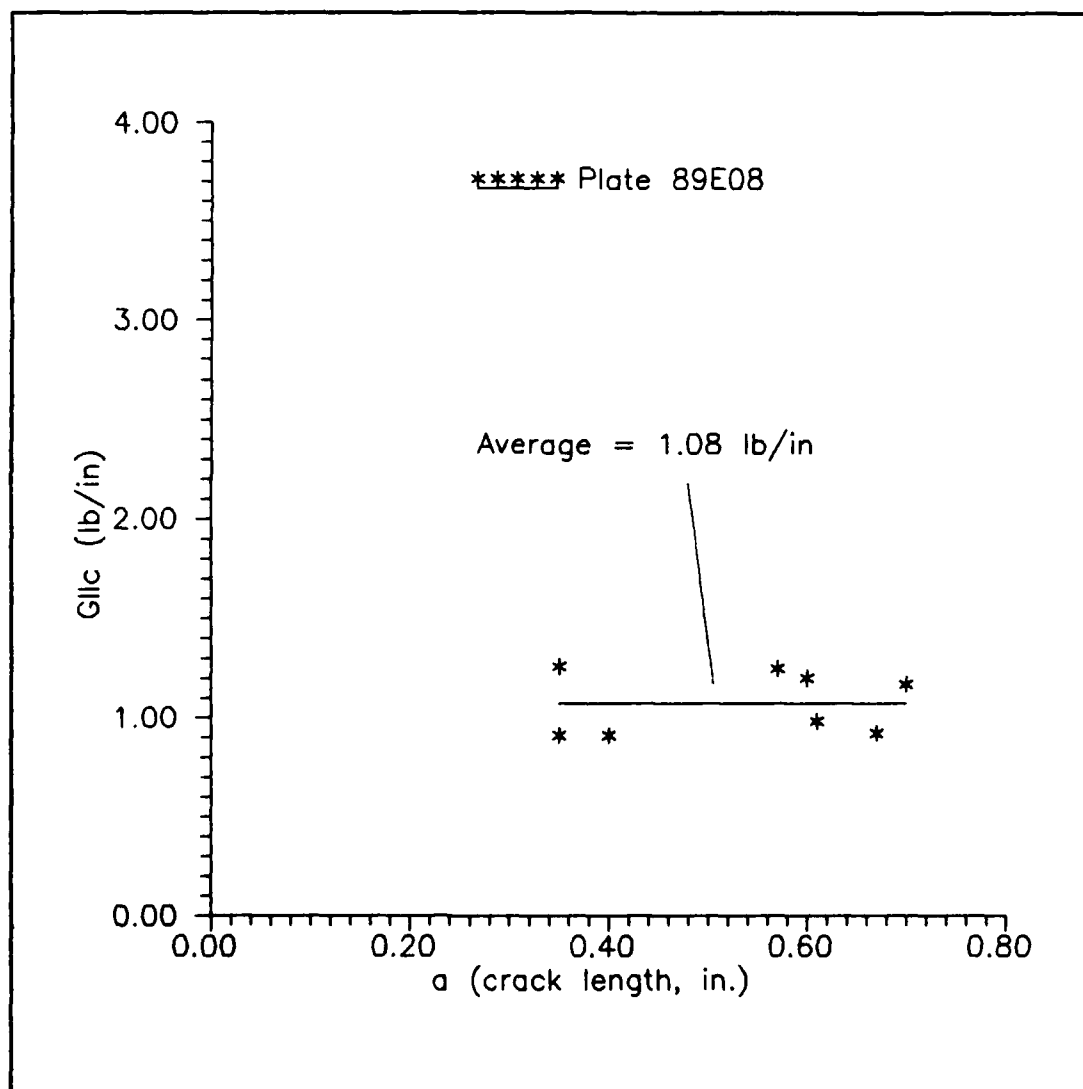
Fig. 72. Room Temperature Fracture Toughness Based on Russell's Equation for Compliance to Crack Length Relationship
CGW 7740

117
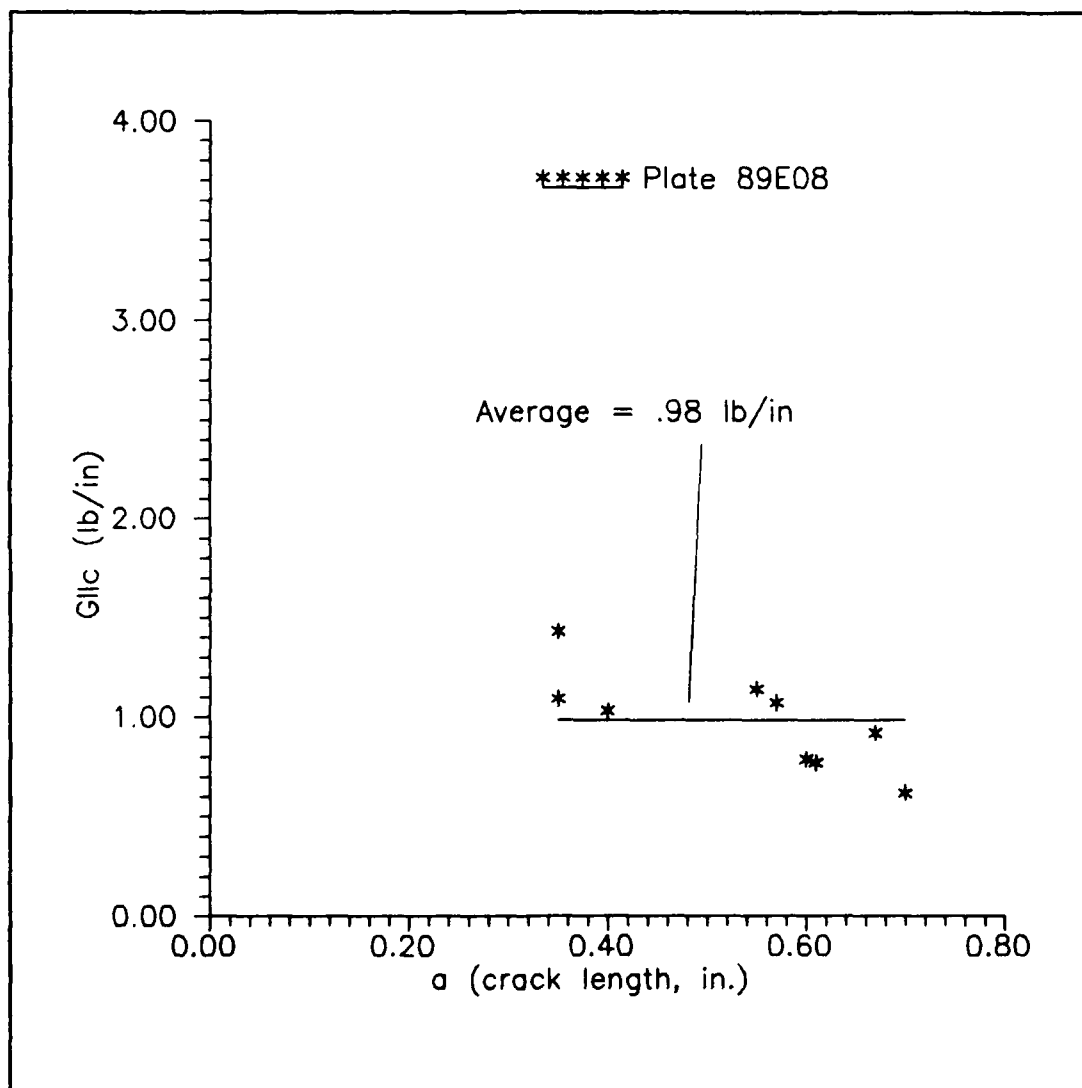
Fig. 73. Room Temperature Fracture Toughness Based on 2nd Order Curve Fit of Room Temperature Compliance Data for Compliance to Crack Length Relationship CGW 7740

118
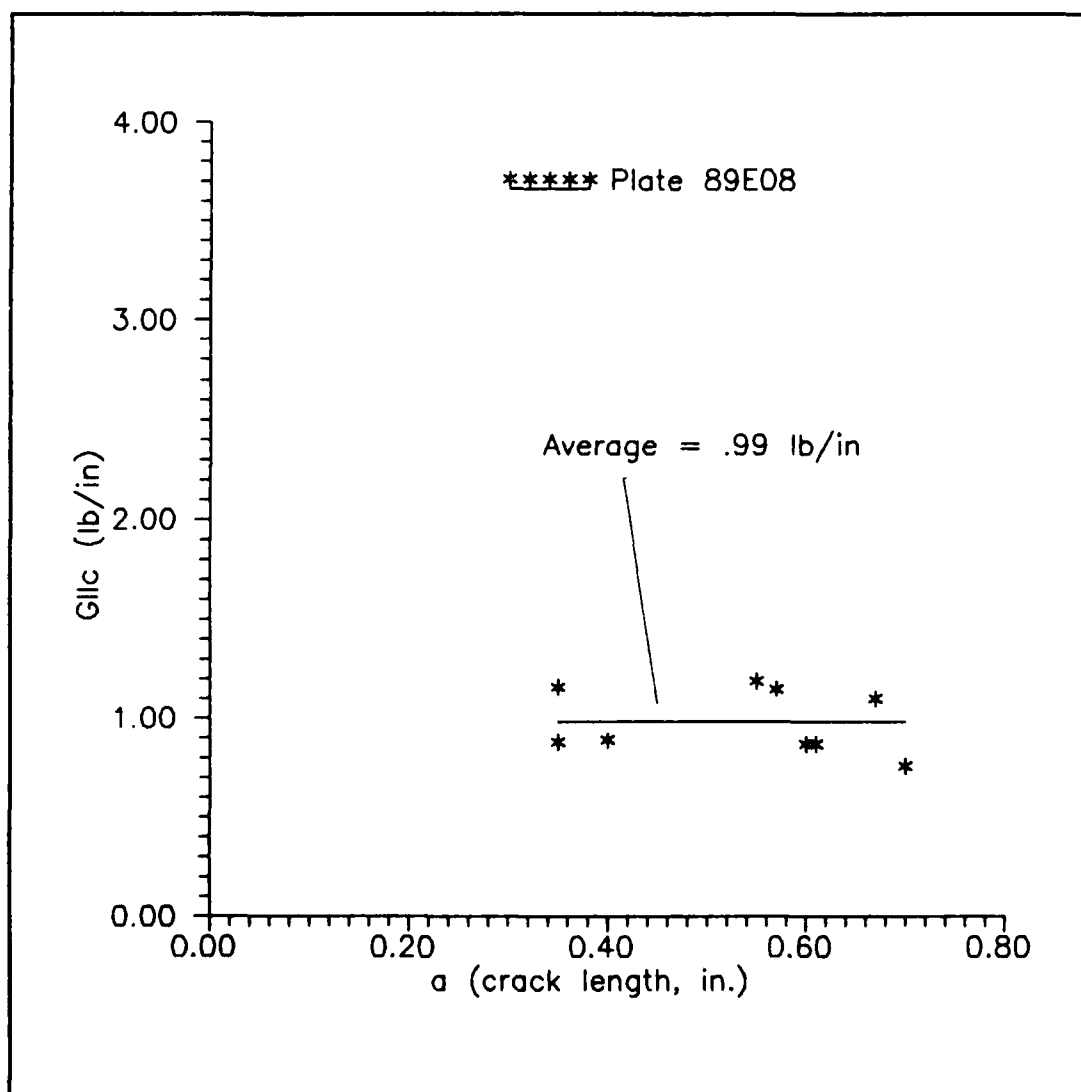
Fig. 74. Room Temperature Fracture Toughness
Based on 3rd Order Curve Fit of Room Temperature
Compliance Data for Compliance to Crack Length Relationship
CGW 7740

119

data for the compliance to crack length relationship.

Table 3. Average G_{IIc} Values

CGW code	Temperature	G_{IIc} (lb/in) Russell's Equation	G_{IIc} (lb/in) 2nd Order Curve Fit	G_{IIc} (lb/in) 3rd Order Curve Fit
1723	Room Temperature	2.11	1.66	1.73
1723	600 F	1.08	0.91	0.90
1723	1000 F	0.75	0.80	0.76
1723	Post thermal cycling	0.82	0.70	0.67
1723	Post thermal exposure	1.15	0.92	0.89
7740	Room Temperature	1.08	0.98	0.99

These values of G_{IIc} show a definite trend toward decreasing fracture toughness when CGW 1723 is exposed to the temperatures used in this study. In the 600 F temperature tests, the fracture toughness of the specimen drops to half of its room temperature value. The 1000 F tests show an additional decrease of 30% from the 600 F value. The G_{IIc} value of 2.11 lb/in from the present study is higher than that found by Mol of 1.698 lb/in in room temperature tests (16). This value is very close to that found at room temperature by Vozzola of 2.17 lb/in (18). The 600 F value

of 1.08 lb/in is less than that found by Mol at 600 F of 1.367 lb/in (16). The value of G_{IIc} found in this study at 1000 F of 0.75 lb/in showed a large difference from that found at 1000 F by Mol in the previous study of this material which was 5.334 lb/in (16). This large difference appears to be due to the different matrix characteristics observed in this study than were observed by Mol at this temperature. Mol observed a ductility occurring in the matrix in which it flowed over the fibers at 1000 F. This was not observed in this study and will be discussed later in the section on post mortem examination.

The thermal cycling and thermal exposure results show an interesting phenomena. The specimens exposed to thermal cycling from 130 - 600 F for 25 cycles showed a 23% lower fracture toughness than the specimens tests at a constant 600 F. This was expected. The thermal cycling would cause a change in the residual stresses at the fiber matrix interface which may damage the material, or may cause some local microdebonding. Limited studies have been done on the exact damage mechanism that occurs in composites subjected to thermal fatigue. What is of interest is the decrease in the fracture toughness of the specimen that was exposed to a constant 600 F for 125 minutes and then tested at room temperature. G_{IIc} for this specimen is within 8% of that for the specimens tested at 600 F. This shows that the extended

121

exposure to elevated temperature lowers the fracture toughness of this material, and thermal cycling has an additive effect.

Post Mortem Examination. Once the tests were completed, the tested specimens were examined under magnification in an attempt to understand the crack growth mechanism and relate it to the results discussed above. The specimens were viewed from three perspectives: overall characteristics; general characteristics of the fracture surface; and microstructure characteristics of the fracture surfaces. Micrographs were taken of typical specimen characteristics and are discussed here.

The exterior crack surface was examined first for overall understanding of the crack growth. Magnification ranged from 50X to 400X. The primary emphasis of this examination was on general crack propagation character and appearance. The specimens were also examined for matrix cracking in front of the crack tip. Figures 75 thru 78 show side views of the Mode II crack surface of room temperature, 600 F, 1000 F, and thermal cycled specimens. These figures show the typical growth of the crack under Mode II conditions. The crack surface of the room temperature specimen is smoother than any of the other specimens. The specimens that were exposed to elevated temperatures showed more jagged features. Also, all the elevated temperature

Fig. 75.   Crack Surface of Room Temperature Specimen
C890403-1 Magnified 400X
CGW 1723   .
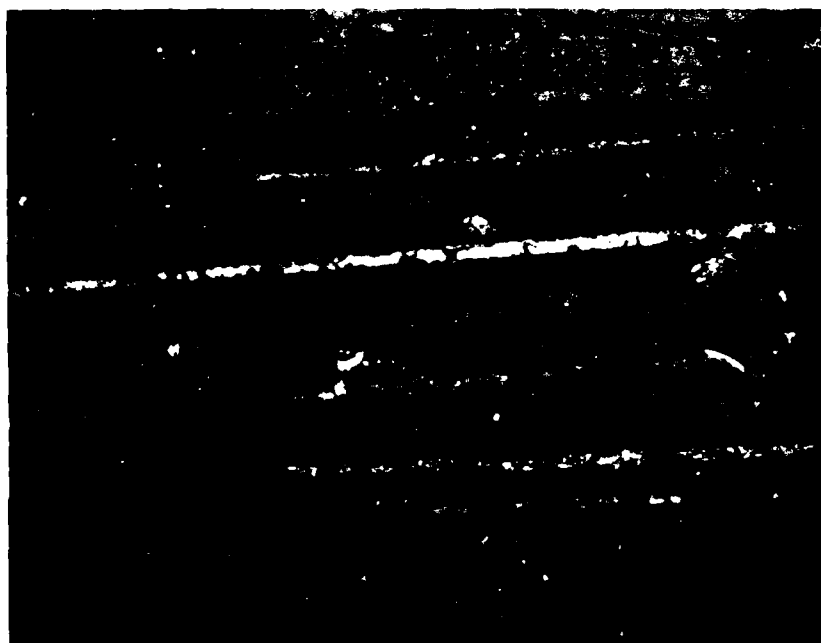
Fig. 76.   Crack Surface of 600 F Specimen C890403-11
Magnified 400X
CGW 1723

123
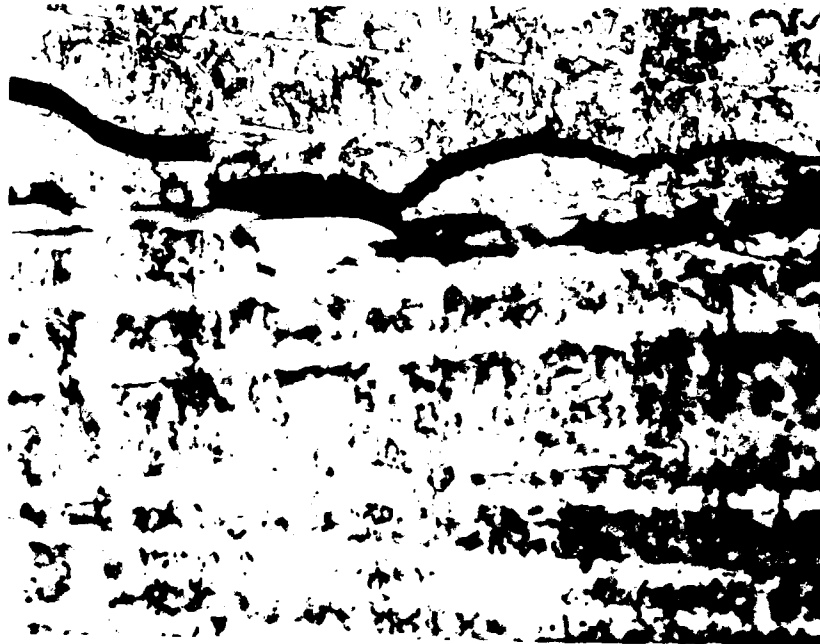
Fig. 77.   Crack Surface of 1000 F Specimen C890403-19
Magnified 400X
CGW 1723
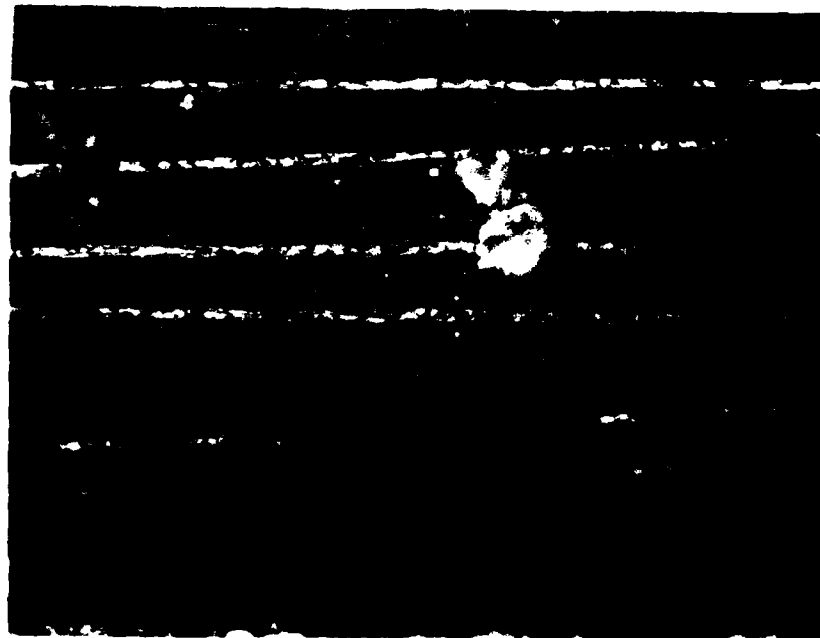
Fig. 78.   Crack Surface of Thermal Cycling Specimen
C890403-14 Magnified 400X
CGW 1723

124

specimens showed rounded pockets of matrix material broken out in what appears to be a brittle fracture. The 1000 F specimen showed instances of sharp edged islands of matrix in the gap of the crack. No evidence of matrix cracking ahead of the crack tip was observed in any of the specimens.

Once the overall crack growth behavior was examined, specimens were pulled apart with a Mode I type of force to allow the fracture surfaces to be seen. There were three primary areas of interest here. The first was to determine if the change in the fracture type, Mode I for the pre-crack and Mode II for the actual tests, could in fact be seen. The second area of interest was to evaluate the accuracy of the measurements of the pre-crack length if this change in fracture type could be seen. The third area looked at was the general nature of the fracture surface and any changes that could be observed between specimens tested at different temperatures.

In the majority of CGW 1723 specimens examined, the point at which the fracture mode changed could be readily determined. Actual pre-crack length from post-mortem examination was compared to measured length before testing. It was determined that the measured pre-crack length was accurate within +/- .03" of the length obtained from examination of the fracture surfaces. In both materials, the Mode I region is characterized by a comparatively smooth

125

surface with all the fibers aligned. The Mode II region, in the CGW 1723, appears much rougher, with some of the fibers being pulled-up out of the plane of the surface since they had been bent before breaking during Mode II crack growth. The fibers in the Mode II region did not stay as well aligned as in the Mode I region. Figures 79 and 80 show fracture surfaces that demonstrate this. The white pointers are placed at the location of the pencil mark that was used for pre-crack length determination before the tests. Looking from left to right in Figure 79, the change from the relatively smooth Mode I surface to the rougher Mode II surface occurs just slightly left of the pointer. Looking again from left to right in Figure 80, the fracture surface changes from Mode I to Mode II just slightly to the right of the first pointer, then changes back to Mode I, and finally back to Mode II at the second pointer. These areas represent the initial pre-crack, Mode II crack growth during testing, pre-cracking of the specimen for another test, and again Mode II crack growth during a test. For the CGW 7740 the change from Mode I to Mode II was impossible to identify on any of the specimens examined. This material showed no out of plane movement or change in alignment of the fibers. Figure 81 shows the fracture surface of a CGW 7740 specimen with the pointer at the measured pre-crack length. No noticeable change in the fracture surface takes place in this region.

126

Fig. 79.   Fracture Surface of Room Temperature Specimen
89C0403-3 Showing Change From Mode I to Mode II
Magnified 10X   CGW 1723
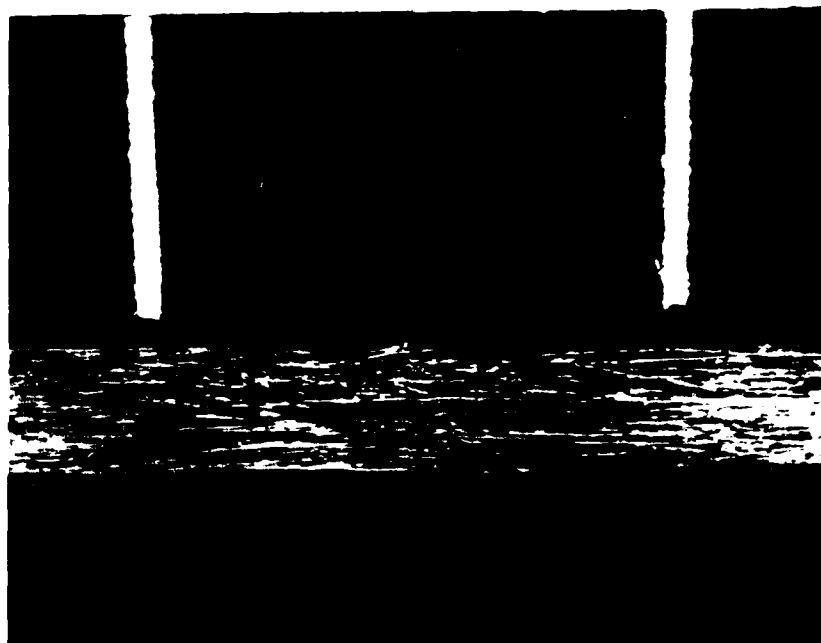
Fig. 80.   Fracture Surface of Thermal Cycled Specimen
89C0403-14 Showing Change From Mode I to Mode II
Magnified 10X   CGW 1723

127
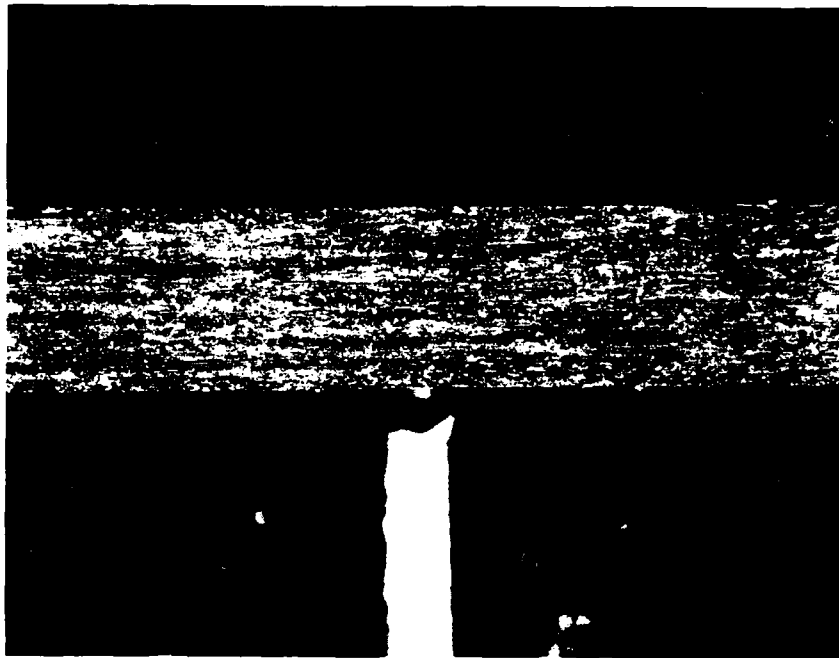
Fig. 81.   Fracture Surface of Room Temperature Specimen
89E08-6 Showing No Discernable Change From Mode I to Mode II
CGW 7740

The third area of interest was to see if the specimens
exposed to the different temperatures showed any change in
the fracture surface that indicated the corresponding change
in their measured fracture toughness values.   Figure 82 shows
three specimens, room temperature, 600 F, and 1000 F with the
room temperature specimen at the top, 600 F in the middle,
and 1000 F specimen at the bottom.   The elevated temperature
specimens exhibit an apparent increasing "whitening" on the
fracture surface with increasing temperature.   This was
originally thought to be due to a chemical change or
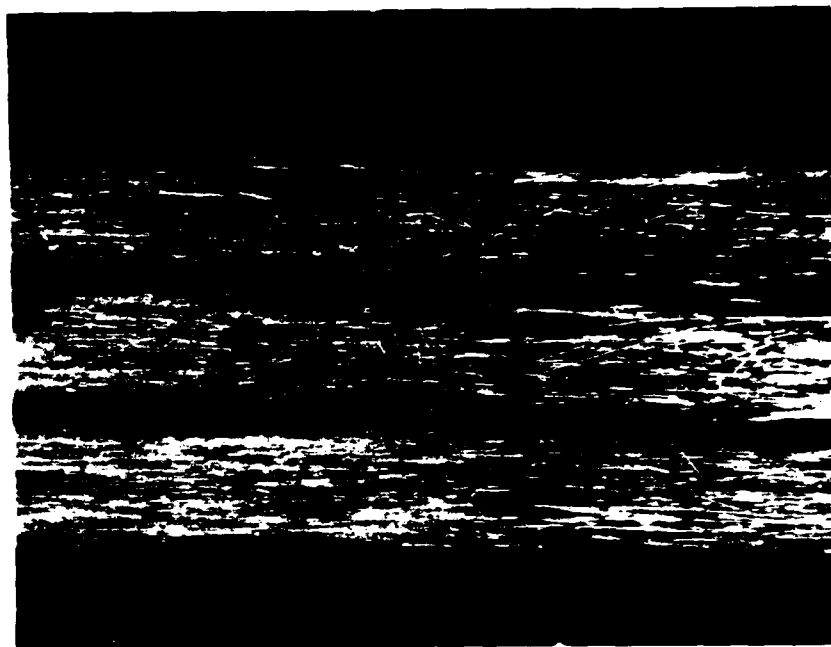
Fig. 82.   Comparison of Fracture Surfaces of Room
Temperature (Top), 600 F (Middle), and 1000 F (Bottom)
Specimens #'s 89C0403-3, 89C0403-7, 89C0403-13
CGW 1723

oxidation of the matrix.   Neither of these two hypotheses

proved to be the case.   In order to determine exactly what

was causing this effect, the specimens were examined with a

scanning electron microscope (SEM).

For sake of comparison, each specimen was photographed

at various locations and at differing magnifications.   Both

Mode I pre-crack and Mode II grown crack were looked at.

Micro- graphs were taken in both these regions at 100X and

500X.   This allowed both the general surface and the fiber-

interface characteristics to be examined.   Figures 83 thru 96

show these micrographs for the CGW 1723 room temperature, 600 F, 1000 F, and thermal cycling specimens. Figures 97 and 98 show the Mode I and Mode II fracture surfaces of the CGW 7740 at 100X and 200X respectively.

From the 100X photographs of the CGW 1723, the cause of the apparent "whitening" was determined. This effect was not caused by oxidation of the matrix or direct chemical change. The effect was caused by the increased reflection of light on the higher temperature specimens due to minute particles of the matrix on the surface. As can be seen from the micrographs, especially those taken at 100X, the fracture surfaces of the specimens tested at elevated temperatures have a large number of very small pieces of matrix material on them. This is almost like a glass powder and reflects the light from the microscope giving the "whitening" effect. These tiny glass pieces are created when the fibers break out of the matrix and the matrix fractures. This is a characteristic of a brittle fracture and the increased occurrence of the matrix fracturing into small pieces coincides with the decrease in fracture toughness found in the elevated temperature specimens. The thermal cycled specimen shows more of this action than the 600 F specimen and it is about the same amount as the 1000 F specimen. This also coincides with the values of G_{IIc} found for this specimen. Another difference in the specimens can be seen

130
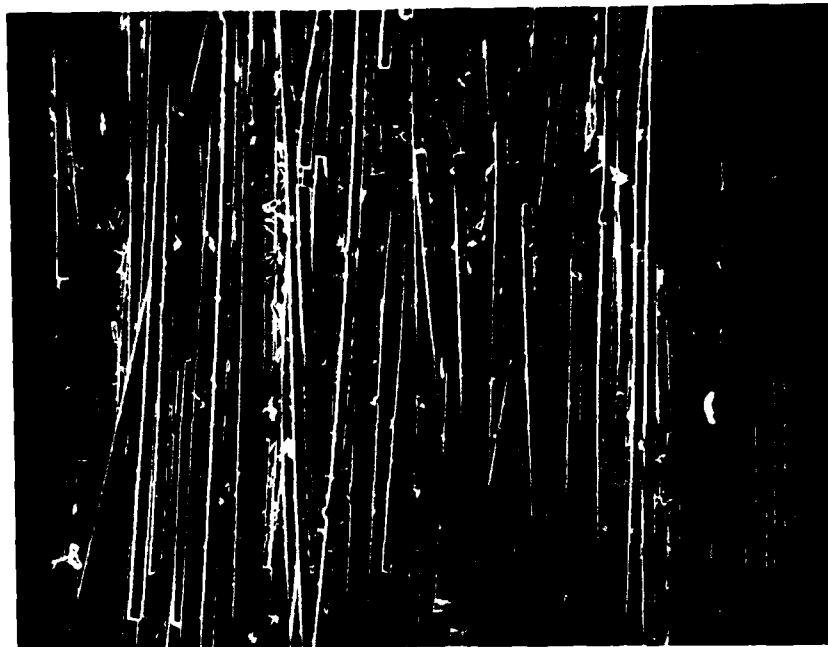
Fig. 83.   Mode I Fracture Surface of
Room Temperature Specimen 89C0403-3
CGW 1723   Magnified 100X

Fig. 84.   Mode I Fracture Surface of
Room Temperature Specimen 89C0403-3
CGW 1723   Magnified 500X

131

Fig. 85.   Mode II Fracture Surface of
Room Temperature Specimen 89C0403-3
CGW 1723   Magnified 100X

Fig. 86.   Mode II Fracture Surface of
Room Temperature Specimen 89C0403-3
CGW 1723   Magnified 500X

132
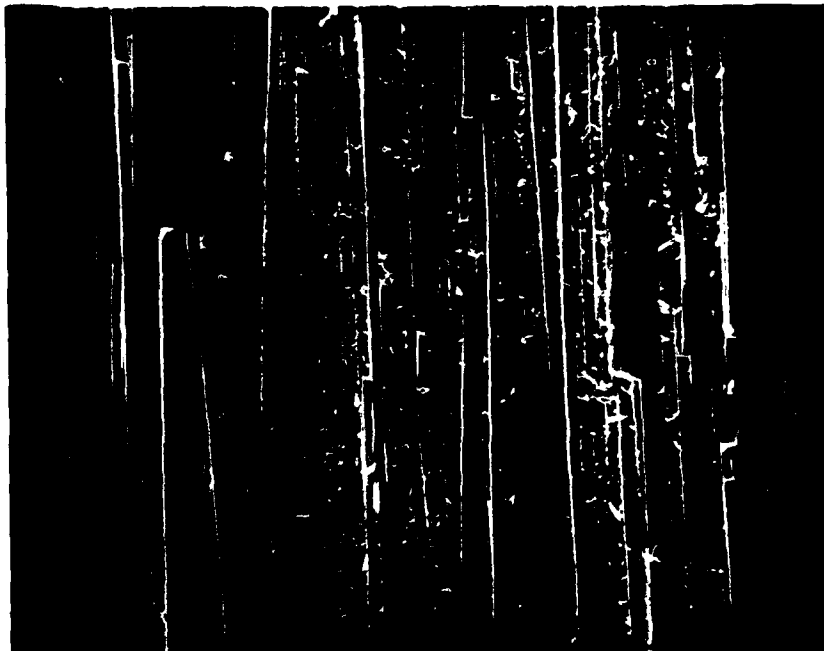
Fig. 87.   Mode I Fracture Surface of
600 F Specimen 89C0403-7
CGW 1723   Magnified 100X
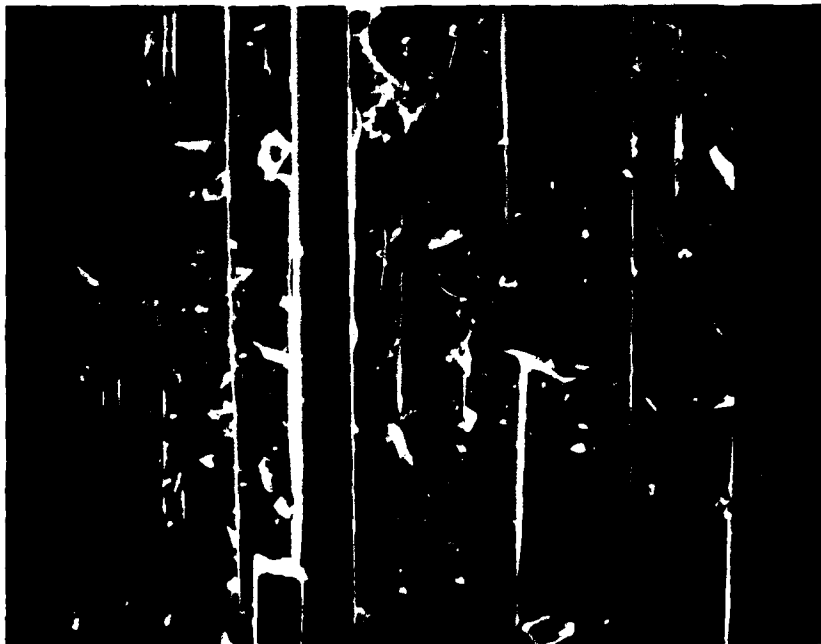
Fig. 88.   Mode I Fracture Surface of
600 F Specimen 89C0403-7
CGW 1723   Magnified 500X

133
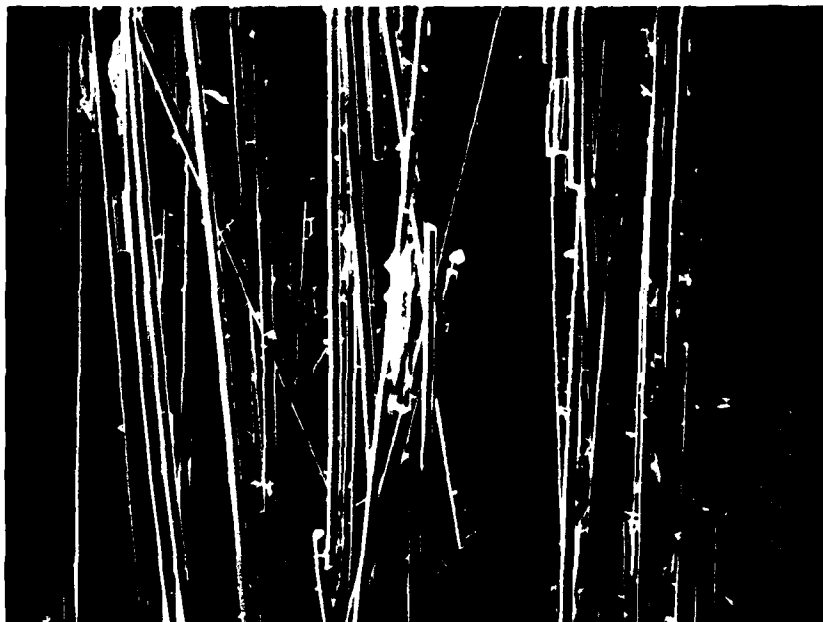
Fig. 89.   Mode II Fracture Surface of
600 F Specimen 89C0403-7
CGW 1723   Magnified 100X

Fig. 90.   Mode II Fracture Surface of
600 F Specimen 89C0403-7
CGW 1723   Magnified 500X
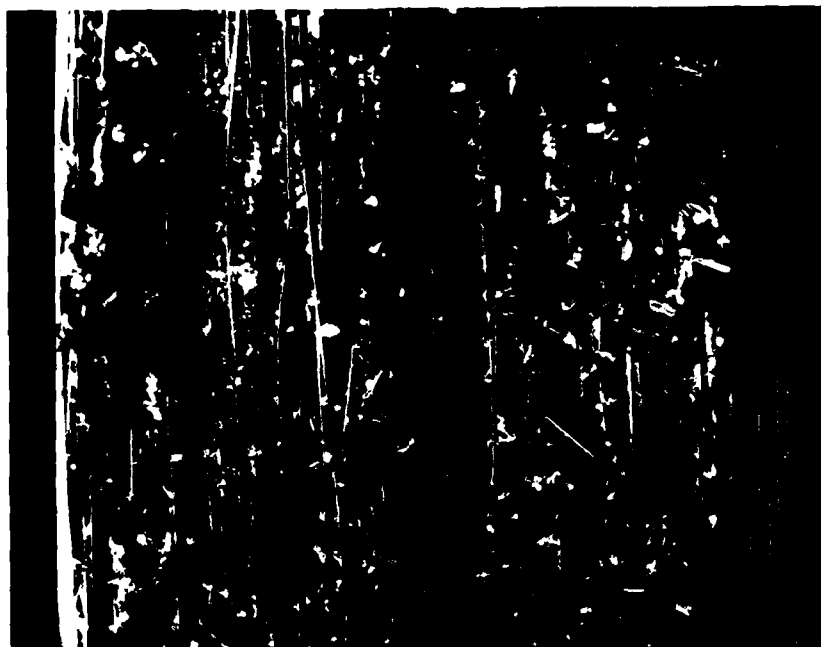
Fig. 91. Mode I Fracture Surface of
1000 F Specimen 89C0403-19
CGW 1723   Magnified 100X
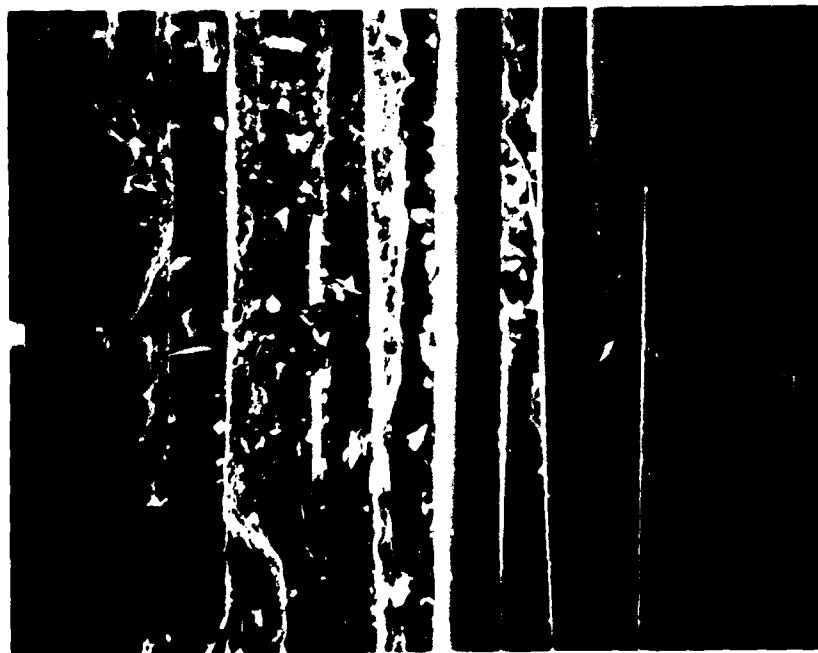
Fig. 92. Mode I Fracture Surface of
1000 F Specimen 89C0403-19
CGW 1723   Magnified 500X

135

Fig. 93.   Mode II Fracture Surface of
1000 F Specimen 89C0403-19
CGW 1723   Magnified 100X

Fig. 94.   Mode II Fracture Surface of
1000 F Specimen 89C0403-19
CGW 1723   Magnified 500X
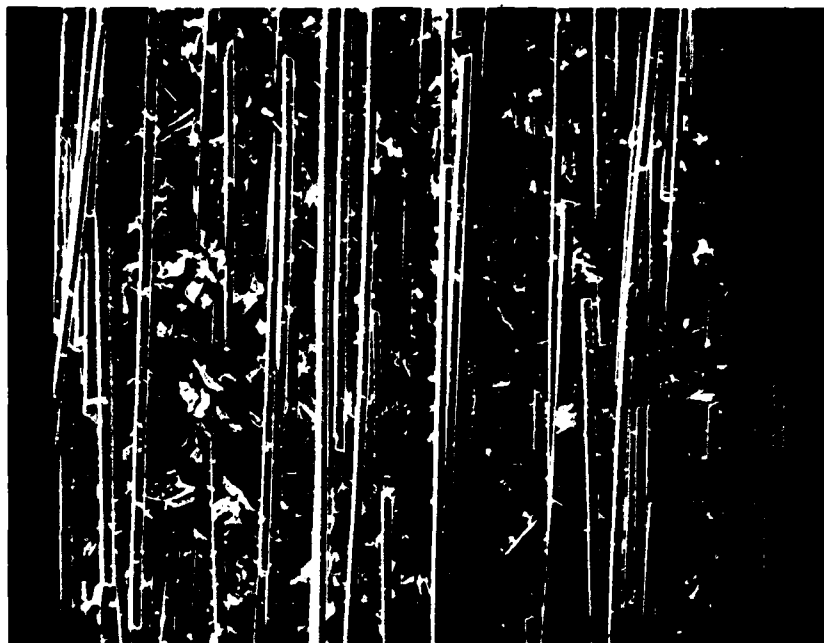
Fig. 95.   Mode I Fracture Surface of
Thermal Cycling Specimen 89C0403-14
CGW 1723   Magnified 100X
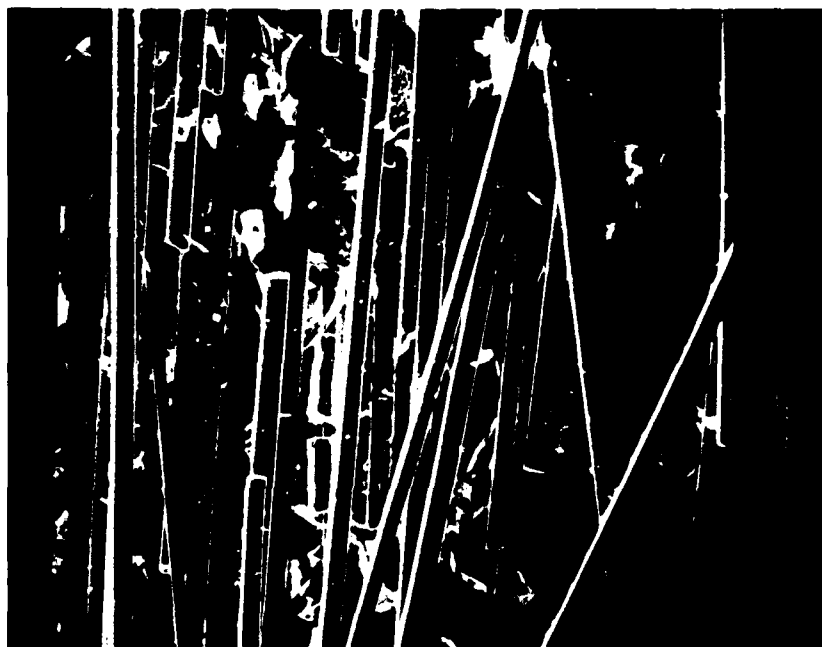
Fig. 96.   Mode II Fracture Surface of
Thermal Cycling Specimen 89C0403-14
CGW 1723   Magnified 200X

137
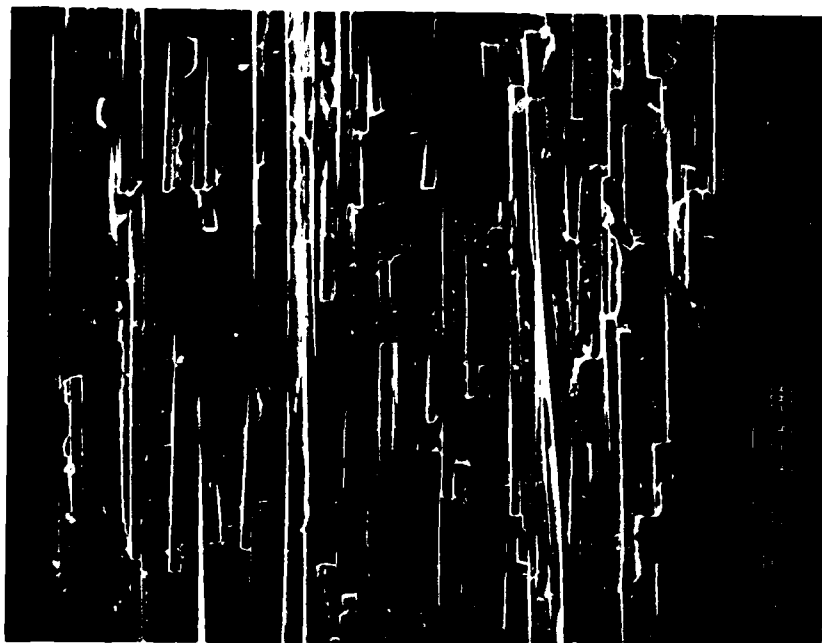
Fig. 97. Mode I Fracture Surface of
Room Temperature Specimen 89E08-4
CGW 7740   Magnified 100X
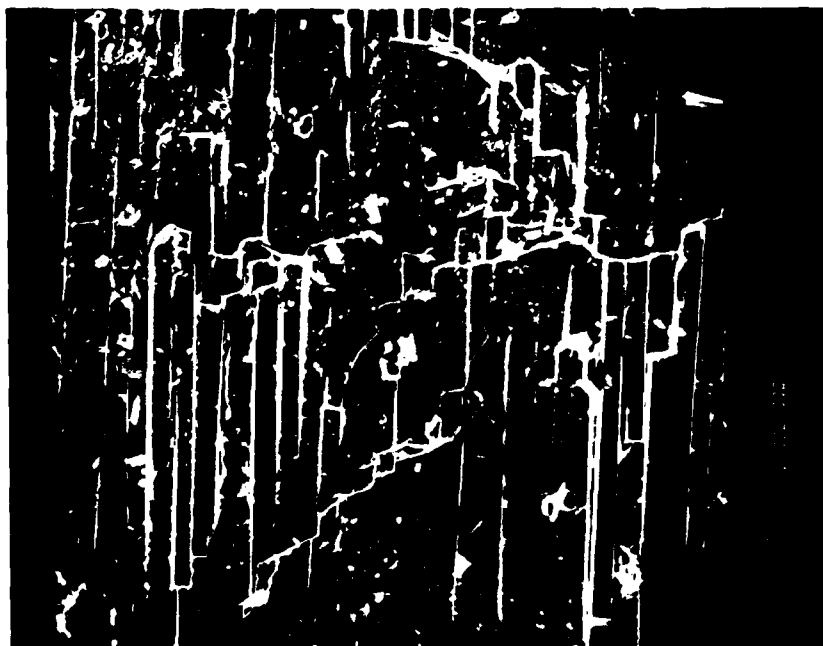
Fig. 98. Mode II Fracture Surface of
Room Temperature Specimen 89E08-4
CGW 7740   Magnified 200X

138

from the 100X micrographs. This is the amount of fiber pullout and out of plane fiber buckling that occurred in the Mode II region. The room temperature specimens show much more of these actions than either the 600 F or 1000 F specimens. The 600 F specimen shows some of this behavior, but the 1000 F specimen shows almost none. See Figures 85, 89, 93. Since fiber pullout is an important part of the toughening mechanism of fiber reinforcement of these materials, this lower amount of pullout is indicative of lower fracture toughness. The 200X micrograph of the thermal cycled specimen is misleading because of the greater magnification. A quality 100X photograph was not available, but personal observations of this region revealed a similar pattern to that of the 1000 F specimen. See Figure 96.

This lower fiber pullout at high temperatures can also be seen in the 500X micrographs. The room temperature surface reveals fibers that are completely pulled out of the matrix and are well above the surface. They protrude far enough that the matrix itself can be only barely seen in the background, see Figure 86. In the 600 F specimen, the fibers are pulled out in most cases but are only slightly above the surface. The matrix can be seen in the background. The matrix displays characteristics of a brittle material, the one piece has a crack in it and part of it is broken out. See Figure 90. This is the origin of the very small pieces

139

of matrix previously discussed. The 1000 F specimen shows almost no appreciable fiber pullout, the fibers are almost all still imbedded in the matrix and in the plane of the fracture surface. In the places where the matrix has broken, the edges are sharp and jagged. It can be seen that some of the fibers have fractured while still imbedded in the matrix grooves. See Figure 94. Once again, this is characteristic of low fracture toughness.

The micrographs of the CGW 7740, Figures 97 and 98, show a different type of fracture surface at room temperature than the CGW 1723 did at room temperature, and in some ways look more like the 1000 F specimen. See Figures 83-86, 91-94, 97-98. The Mode I and Mode II regions show almost no fiber pullout. In both regions, the fibers are still firmly imbedded in the matrix. The Mode II micrograph shows the matrix has shattered and the fibers have broken off while still imbedded. This again is indicative of low fracture toughness. It also appears that this plate was possibly overly matrix rich. These micrographs, combined with the unexpected fracture of 3 specimens perpendicular to the fibers led to the suspension of further tests of this material.

Mode I

Mode I fracture toughness, (G_{Ic}), and apparent Mode I fracture toughness, G_{Ic}^*, values of CGW 1723 were determined in three point bend tests at room temperature and 1000 F. These tests used material from plate 87C12, 89C0403, and 87C17. For the determination of G_{Ic} the crack was grown parallel to the fibers. In the determination of G_{Ic}^* the crack was grown perpendicular to the fibers. It was not the intent of this study to determine a definitive value of G_{Ic} or G_{Ic}^* for this material. Instead, it was the goal of this study to determine if the Mode I and Mode II fracture toughness values followed the same trend when tested at elevated temperatures. Whereas the limited scope of this area of testing is not sufficient for precise determination of G_{Ic} or G_{Ic}^*, the trend analysis is valid.

Srawley (4:475-476) has provided a wide range stress intensity solution

$$K_{Ic} = \frac{P_{cr}S}{BW^{3/2}} \quad X$$

$$\frac{3\left(\frac{a}{W}\right)^{1/2}\left[1.99 - \frac{a}{W}\left(1 - \frac{a}{W}\right)\left(2.15 - 3.93\frac{a}{W} + 2.7\left(\frac{a}{W}\right)^2\right)\right]}{2\left(1 + 2\frac{a}{W}\right)\left(1 - \frac{a}{W}\right)^{3/2}} \qquad (19)$$

This solution was chosen for two reasons. The only

141

information required for this solution other than specimen geometry is the critical load and it is valid for wider range of a/W ratios than previously proposed solutions (4:180) For the determination of K_{Ic} the critical load is used. From this, the value of G_{Ic} was calculated from the equation (1)

$$G_{Ic} = K_{Ic}^2 \sqrt{\frac{1}{2E_{11}E_{22}}} \left[\sqrt{\frac{E_{22}}{E_{11}}} + \frac{\frac{-2\upsilon}{E_{11}} + \frac{1}{G_{12}}}{\frac{2}{E_{11}}} \right] \qquad (20)$$

The value of G_{Ic}^* was calculated from Equation 20 with K_{Ic}^* and G_{Ic}^* substituted for K_{Ic} and G_{Ic} respectively.

The testing procedures described in Chapter 4 were used for the critical load determination. Table 4 shows the values of K_{Ic} and G_{Ic} calculated for each test by specimen and temperature.

Table 4 Mode I Fracture Toughness Calculations
CGW 1723

Temperature	Specimen #	P_{crit} (lb)	K_{Ic} ksi($in^{1/2}$)	G_{Ic} (lb/in)
Room Temp.	87C12-9	5.7	0.820	0.036
Room Temp.	87C12-11	4.2	<u>0.631</u>	<u>0.060</u>
Average			0.726	0.048
1000 F	87C12-5	2.8	0.407	0.015
1000 F	87C12-6	3.5	<u>0.495</u>	<u>0.022</u>
Average			0.451	0.018

142

The room temperature values of K_{Ic} values obtained here are much lower than those given by Atkins and Mai for similar ceramic composites, which are more of the order of what is usually quoted (2:798). This difference can be attributed to the fact that Atkins and Mai determined K_{Ic} with the crack growing perpendicular to the fibers, not parallel as in this study. That method allows for the fiber to deflect the crack and thereby increase the apparent toughness, a mechanism not present in crack growth parallel to the fibers. However, the values of K_{Ic} found in the present study fall near the value of bulk soda glass (2:798).

Table 5 shows the values of K_{Ic}^* and G_{Ic}^* calculated for each test by specimen and temperature. The values presented here are on the order of the values given by Atkins and Mai (2:798) for similar ceramic materials with initial crack growth perpendicular to the fibers.

The objective of this study was not to determine definitively the value of G_{Ic} for CGW 1723, but instead to determine its trend with temperature. There is a definite decrease in the both Mode I fracture toughness, G_{Ic}, and the Mode I apparent fracture toughness, G_{Ic}^*, of this material as was seen in the case of Mode II. And, this decrease is of the same order as in the case of G_{IIc} (in Mode II and both Mode I tests the fracture toughness at 1000 F was between 35 and 40 percent of its value at room temperature).

143

Table 5   Mode I Apparent Fracture Toughness Calculations
CGW 1723

Temperature	Specimen #	P_{crit} (lb)	K_{Ic}^{*} ksi($in^{1/2}$)	G_{Ic}^{*} (lb/in)
Room Temp.	87C12-12	28.3	3.638	1.196
Room Temp.	87C17-2	20.8	2.959	0.785
Average			3.299	0.991
1000 F	87C12-13	15.1	1.959	0.349
1000 F	87C17-1	15.7	2.192	0.437
Average			2.076	0.393

Figures 99 and 100 show the fracture surfaces of the a room
temperature and a 1000 F Mode I specimen with the crack grown
parallel to the fibers. As in the Mode II tests, the fibers
of the room temperature specimen have been pulled well away
from the matrix itself, where the 1000 F specimens fibers
remain in close proximity to the matrix. This is indicative
of a more rapid, brittle fracture in the 1000 F specimen, as
opposed to what looks like a slower pulling out of the fibers
in the room temperature specimen.

144

Fig. 99.   Mode I Fracture Surface of
Room Temperature Specimen 87C12-9
CGW 1723   Magnified 200X
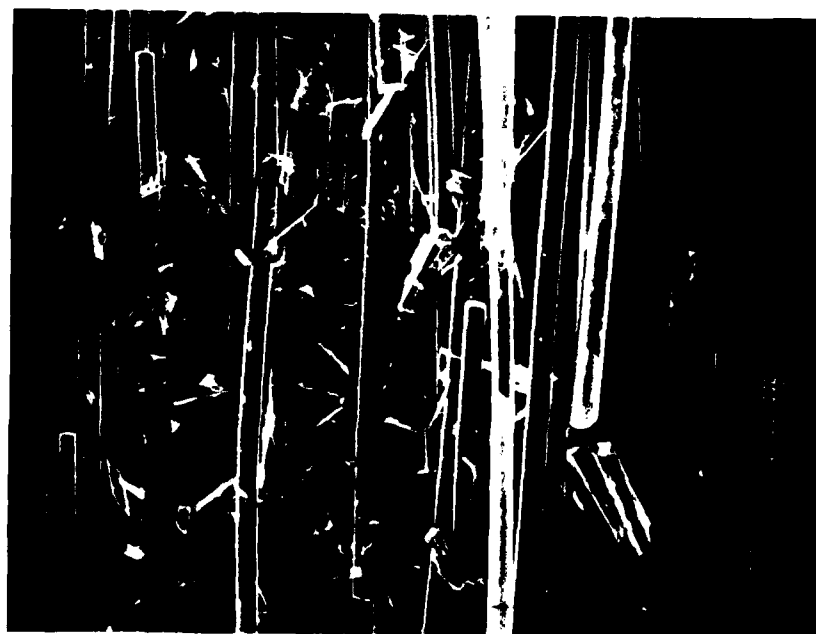
Fig. 100.   Mode I Fracture Surface of
1000 F Specimen 87C12-5
CGW 1723   Magnified 200X

145

VI. Conclusions and Recommendations

There were four primary objectives of this study: to
determine the Mode II fracture toughness of small CMC
specimens made from CGW 1723 material up to 1000 F; to study
the effects of thermal cycling on these materials; to
investigate the Mode I fracture toughness of these specimens;
and to determine the Mode II fracture toughness of CGW 7740
at room and elevated temperatures. The plate of CGW 7740
appeared to be overly brittle, and possibly defective. For
this reason only the room temperature Mode II tests were
conducted with this material. Several conclusion can be made
from this study along with recommendations for further
studies.

Conclusions

The following conclusion can be made as a result of the
findings of this study:

1) The Mode II fracture toughness of CGW 1723 decreased
by 50% at 600 F from that found at room temperature and
decreased an additional 30% at 1000 F compared to 600 F.

2) The Mode I fracture toughness and the Mode I apparent
fracture toughness showed the same trend from room
temperature to 1000 F as was found in the Mode II fracture

toughness.

3) Elevated temperatures cause a change in the matrix resulting in increased brittleness and changes in the fiber-matrix interface resulting in reduced fiber pullout. These mechanisms resulted in a decrease in G_{IIc}, G_{Ic}, and G_{Ic}^{*} with increased temperature.

4) Thermal cycling, at a moderate temperature range and with a small number of cycles, has a degrading effect on the fracture toughness and it was found to be greater than the effect of the increased temperature alone.

5) The theoretical compliance to crack length relation-ship, based on simple linear beam theory, obtained by Russell adequately models the actual data found. This relationship is thus suitable for use in the G_{IIc} calculations for these small ceramic specimens.

Recommendations

Several recommendations can be made based on experiences encountered during this study.

1) The thermal fatigue effects on this material should be further investigated. Additional cycles, different temperature profiles, and higher temperatures should be investigated.

2) Tests of specimens exposed to thermal cycling should be conducted at both the low and high temperature limits of

the cycle.

3) A computer controlled data acquisition system should be incorporated to measure the load and displacement of the specimen. This would permit a more accurate determination of the compliance and more importantly, the critical load.

4) The test fixture should be modified to allow the specimen to remain properly aligned on the test fixture and with the ram without the ram in actual contact. This is to prevent any thermal loading from occurring during the heating of the specimen.

5) The load cell should be changed to one with a maximum load of 250 lbs to get better resolution and require less magnification of the signal thus reducing the noise level.

Bibliography

1. Agarwal, Bhagwan D. and Lawrence J. Broutman. _Analysis and Performance of Fiber Composites_, New York: John Wiley & Sons, Inc., 1980.

2. Atkins, A. G. and Y. W. Mai. _Elastic and Plastic Fracture_. West Sussex: Ellis Horwood Limited, 1985.

3. Briggs, A. and R. W. Davidge. "Fabrication, Properties, and Applications of Borosilicate Glass Reinforced With Continuous Silicon Carbide Fibers," _Whisker- and Fiber-Toughened Ceramics (Proceeding of an International Conference), Oak Ridge, TN. 7-9 June 1988_. 153-164 ASM International, 1988.

4. Broek, David. _Elementary Engineering Fracture Mechanics_ (Fourth Revised Edition): The Hague: Martinus Nijhoff Pub. (1984)

5. Chawla, Krishan Kumar. _Composite Materials (Science and Engineering)_. New York: Springer-Verlag Inc., 1987.

6. Gakkaree, K. P. and K. C. Chyung. "SiC Whisker and Whisker/Fiber Reinforced Glass and Glass Ceramic Hybrid Composites," _Whisker- and Fiber-Toughened Ceramics (Proceeding of an International Conference), Oak Ridge, TN. 7-9 June 1988_. 97-104 ASM International, 1988.

7. Gere, James M. and Stephen P. Timoshenko. _Mechanics of Materials_ (Second Edition). Belmont CA: Wadsworth, Inc.: 1984.

8. Giare, G. S. "Fracture Toughness of Unidirectional Fiber Reinforced Composites in Mode II", _Engineering Fracture Mechanics_, vol. 20, No. 1:

9. Griffith, A. A. "The Theory of Rupture and Flow in Solids", _Phil. Trans. Roy. Soc. of London, A221_: (1921)

10. Griffith, A. A. "The Theory of Rupture," _Proc. 1st Int. Congress Appl. Mech., (1924)_: Biezeno and Burgers ed. Waltman. (1925)

11. Irwin, G. R. "Fracture Dynamics," <u>Fracturing of Metals</u>: ASM publ. (1948)

12. Jones, Robert M. <u>Mechanics of Composite Materials</u>. New York: Hemisphere Publishing Corp. (1975) (1984)

13. Lewis, D. III. "Strength and Toughness of Fiber Reinforced Ceramics and Related Interface Behavior," <u>Whisker- and Fiber-Toughened Ceramics (Proceeding of an International Conference), Oak Ridge, TN. 7-9 June 1988</u>. 265-273. ASM International, 1988.

14. Lowden, R. A. and others. "Characterization of Fiber-Matrix Interfaces in Ceramic Composites," <u>Whisker- and Fiber-Toughened Ceramics (Proceeding of an International Conference), Oak Ridge, TN. 7-9 June 1988</u>. 253-264. ASM International, 1988.

15. Mall, S and N. K. Kochhar. "Finite-Element Analysis of End-Notched Flexure Specimens." <u>Journal of Composites Technology & Research, Vol. 8, No. 2</u>, Summer of 1986: 54-75.

16. Mol, John H. <u>Fracture Toughness Testing of a Ceramic Matrix Composite at Elevated Temperatures</u>. MS Thesis, AFIT/GAE/AA/18D-26,School of Engineering, Air Force Institute of Technology (AU), Wright-Patterson AFB, OH. Dec.

17. Russell, A. J. "Factors Affecting the Interlaminar Fracture Energy of Graphite/Epoxy Laminate." <u>Progress in Science and Engineering of Composite, Proceedings of ICCMM-IV</u>, Tokyo, Japan, 1982, 279-286.

18. Vozzola, Robert P. <u>Fracture Toughness Testing of a Ceramic Matrix Composite</u>. MS Thesis, AFIT/GAE/AA/87D-24, School of Engineering, Air Force Institute of Technology (AU), Wright-Patterson AFB, OH. Dec.

19. Zavada, Larry. P., Ceramic Engineer, Metals and Ceramics Division. Personal interviews. AFWAL/MLLN, Wright-Patterson AFT, Oh. 9 Mar-1 Nov 1989.

20. Zawada, Larry P. and Robert C. Wetherhold. <u>Thermal Fatigue of Ceramic Fiber/Glass Matrix Composites</u>. Report for Future Publication, Prepared for AFWAL/MLLN, Wright-Patterson AFB, Oh. Oct 1989.

Appendix A: Specimen Dimensions

Table 6 gives the dimensions for all the specimens that were tested. CGW 1723 specimens 89C0403-15 and 89C0403-17 and CGW 7740 89E08-2 and 89E08-4 were not tested and are not listed. Specimens are by type of test performed, Mode II or Mode I, and by material within that group if applicable. All specimens had a effective length of 1.5" that was fixed by the roller spacing on the test fixture.

Table 6. Specimen Dimensions

Specimen #	Width (in)	Thickness (in)	Test Temperature
Mode II			
CGW1723			
89C0403-1	0.300	0.098	R.T.
89C0403-2	0.299	0.093	R.T.
89C0403-3	0.299	0.095	R.T.
89C0403-4	0.299	0.096	R.T.
89C0403-5	0.299	0.096	R.T.
89C0403-6	0.298	0.098	R.T.
89C0403-7	0.300	0.099	600 F
89C0403-8	0.300	0.101	600 F
89C0403-9	0.299	0.097	600 F
89C0403-10	0.298	0.098	600 F
89C0403-11	0.300	0.101	600 F
89C0403-12	0.300	0.101	1000 F
89C0403-13	0.303	0.098	1000 F
89C0403-14	0.301	0.103	Cycled
89C0403-16	0.299	0.099	Cycled
89C0403-18	0.299	0.107	1000 F
89C0403-19	0.293	0.096	1000 F
89C0403-20	0.292	0.102	Exposed
87c12-1	0.297	0.101	1000 F
87c12-2	0.300	0.100	1000 F
87c12-3	0.300	0.096	R.T.
87c12-4	0.300	0.098	R.T.
CGW 7740			
89E08-1	0.300	0.096	R.T.
89E08-3	0.300	0.098	R.T.
89E08-5	0.297	0.100	R.T.
89E08-6	0.298	0.100	R.T.
Mode I			
CGW 1723			
87C12-5	0.300	0.100	1000 F
87C12-6	0.300	0.100	1000 F
87C12-9	0.300	0.100	R.T.
87C12-11	0.300	0.100	R.T.
87C12-12	0.299	0.110	R.T.
87c17-2	0.291	0.113	R.T.
87C12-13	0.299	0.114	1000 F
87C17-1	0.292	0.113	1000 F

153

Appendix B: Compliance and Critical Load Curves

Figures 101 thru 104 are of typical X-Y plotter output
during a Mode II test. These were used for determining the
compliance and the critical load of the specimen. The date,
specimen, temperature, and crack length are given in the
upper left corner. The scales the X-Y plotter used are given
by run number at the bottom right. These scales were used in
conjunction with the load cell and LVDT input to output
calibration factors determine the actual applied load and
displacement at the midspan of the specimen. The calibration
factor for all tests for the LVDT was 6.59E-06 in/mv. For
the Mode II tests and the Mode I tests with the crack growth
perpendicular to the fibers, the load cell calibration factor
was 0.622978 lb/mv. For the Mode I tests with the crack
growth parallel to the fibers, the calibration factor for the
load cell was 0.078125 lb/mv. The amount of preload on the
specimen at the beginning of the test is the starting value
on the Y axis. The displacement value was always set to zero
at this point. The circles on the lines with corresponding X
and Y coordinates are the points from which the compliance
values were calculated as described in Chapter 4. When a
discernible change in the compliance curve (where the curve
changes from linear to non-linear) was identified it

154

corresponded to P_{crit}. In Figure 101 this occurs on the right
hand curve at Y = 112 mv, which is 69.7 lb. Critical load
was not reached on the left curve, only compliance data was
taken from that curve. In Figure 102, a typical curve for
1000 F, P_{crit} can be seen to occur at Y = 85 mv which equals
52.3 lb. Similar plots for room temperature and 600 F are
shown in Figures 103 and 104.

Figure 105 shows a typical critical load plot for a
Mode I test with the crack growing parallel to the fibers.
The LVDT was not used in these tests, only the maximum load
was measured. The initial Y axis value corresponds to the
preload put on the specimen. As can be seen from the figure,
the maximum load in this test was 36 mv, which equals
2.81 lb.

Figure 106 shows a typical critical load plot for a Mode I
test with the crack growth perpendicular to the fibers. The
specimen compliance changes at 24 mv which corresponds to a
P_{crit} of 15.1 lb.

29 Sep 89
89C0403-14
Post Cycling
130°F -600°F
X25
a=.4"

800,95

$P_{crit}= 112 mv$
$= 69.7 lb$

800,104

200,40

400,62

20

0   0

Scales X   Y
R1   .2 V/IN   .01 V/IN
R2   .2 V/IN   .02 V/IN
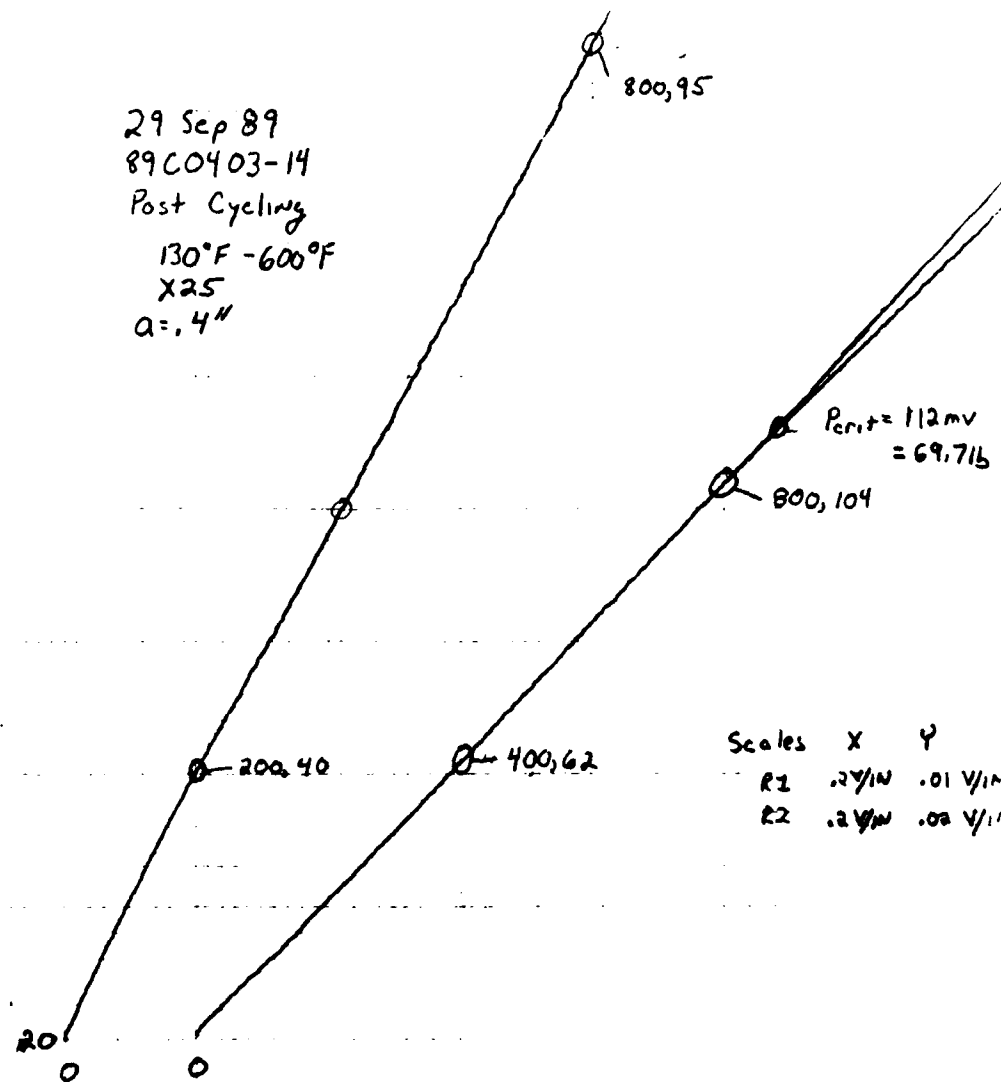
Fig. 101. Mode II Compliance and Critical Load Curves for
Specimen 89C0403-14, Post Thermal Cycling Test
CGW 1723

156
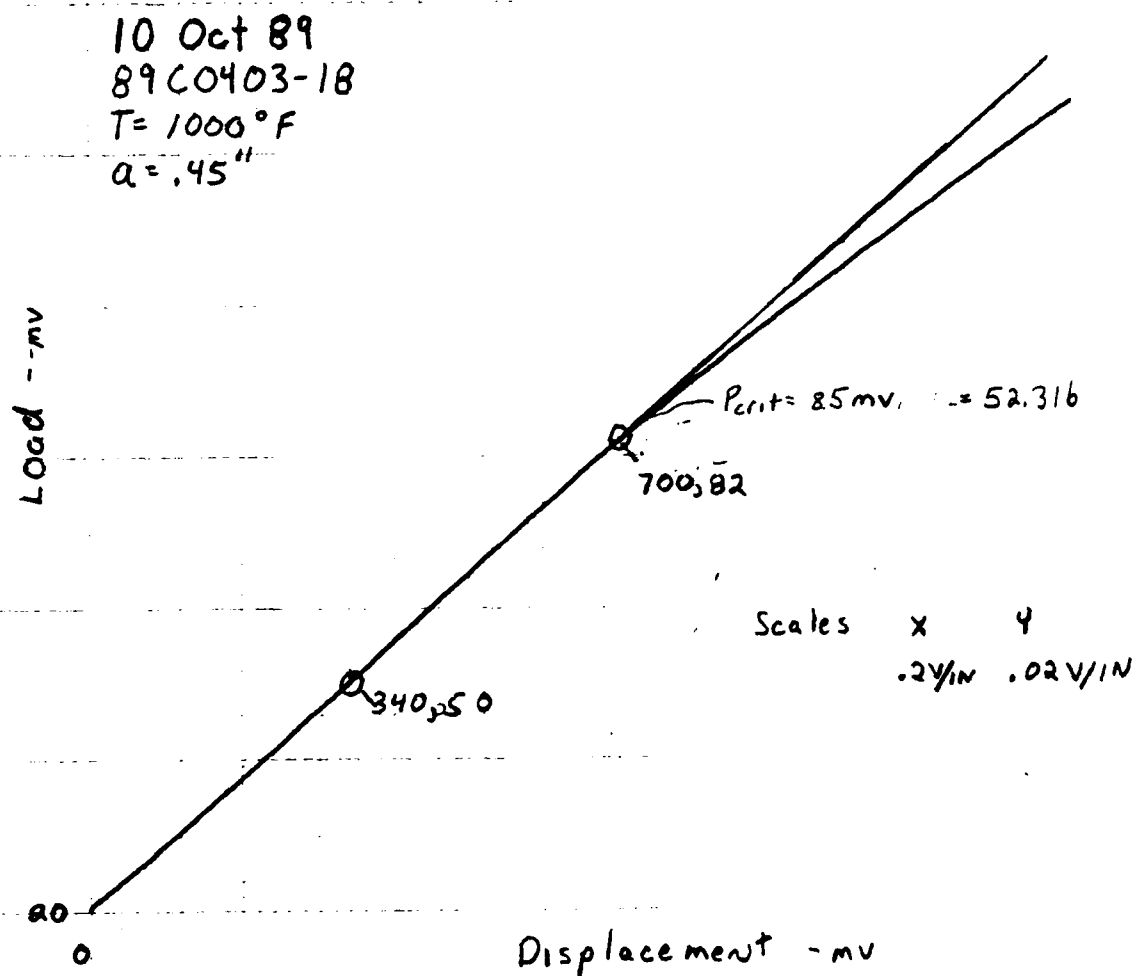
Fig. 102. Mode II Compliance and Critical Load Curves for
Specimen 89C0403-18, 1000 F Test
CGW 1723

157
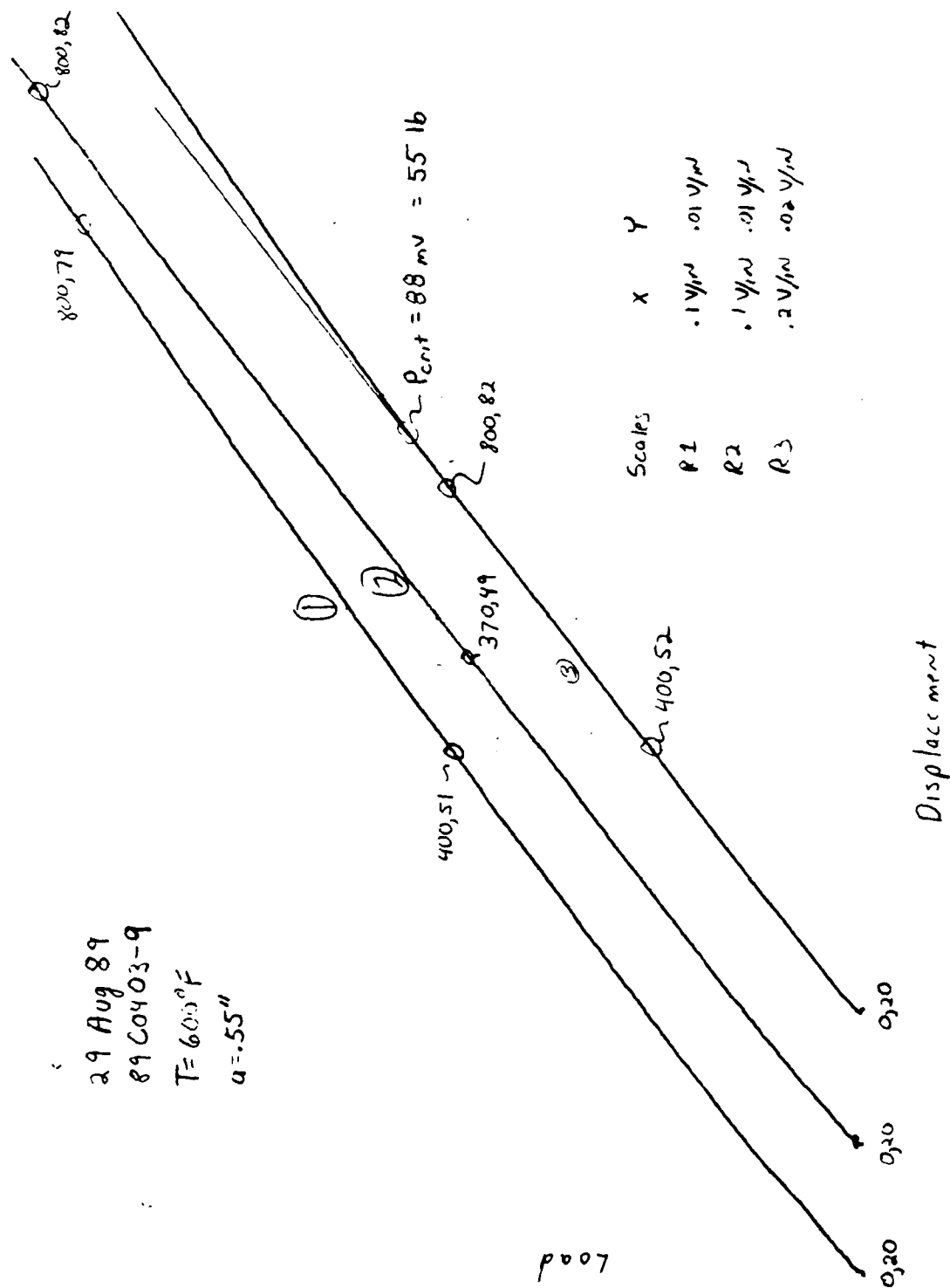
Fig. 103.   Mode II Compliance and Critical Load Curves for
Specimen 89C0403-9, 600 F Test
CGW 1723

158
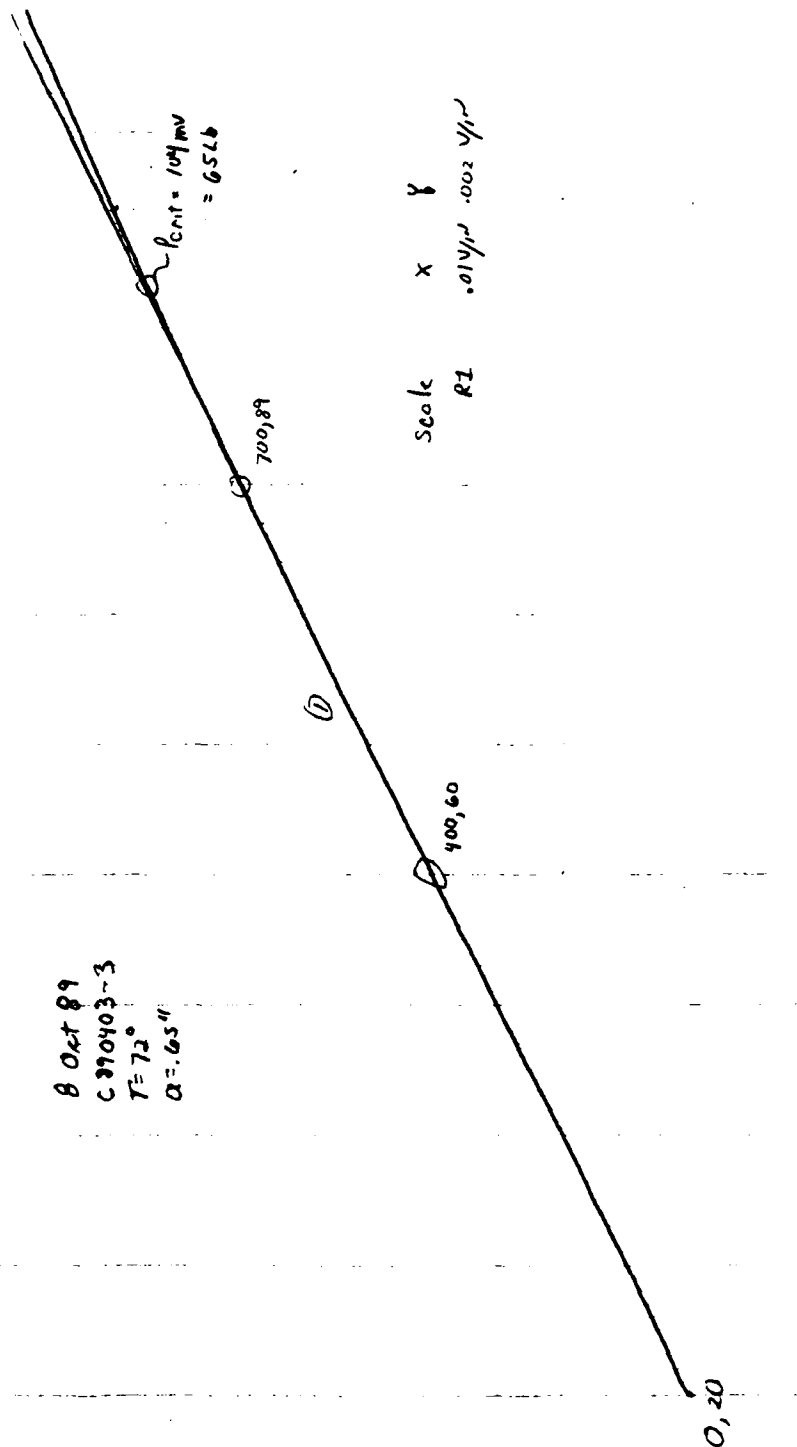
Fig. 104. Mode II Compliance and Critical Load Curves for
Specimen 89C0403-3, Room Temperature Test
CGW 1723

159

25 Oct 89
87C12-6
T= 1000°F
a=.121"

Mode I

192 mv
1 mv for ½ moon
        Piece
193 mv
-150
43mv = 3.5 Lb

LOAD

Scale
y = .01V/.N

x = NOT Used

150mv
= 0 LB
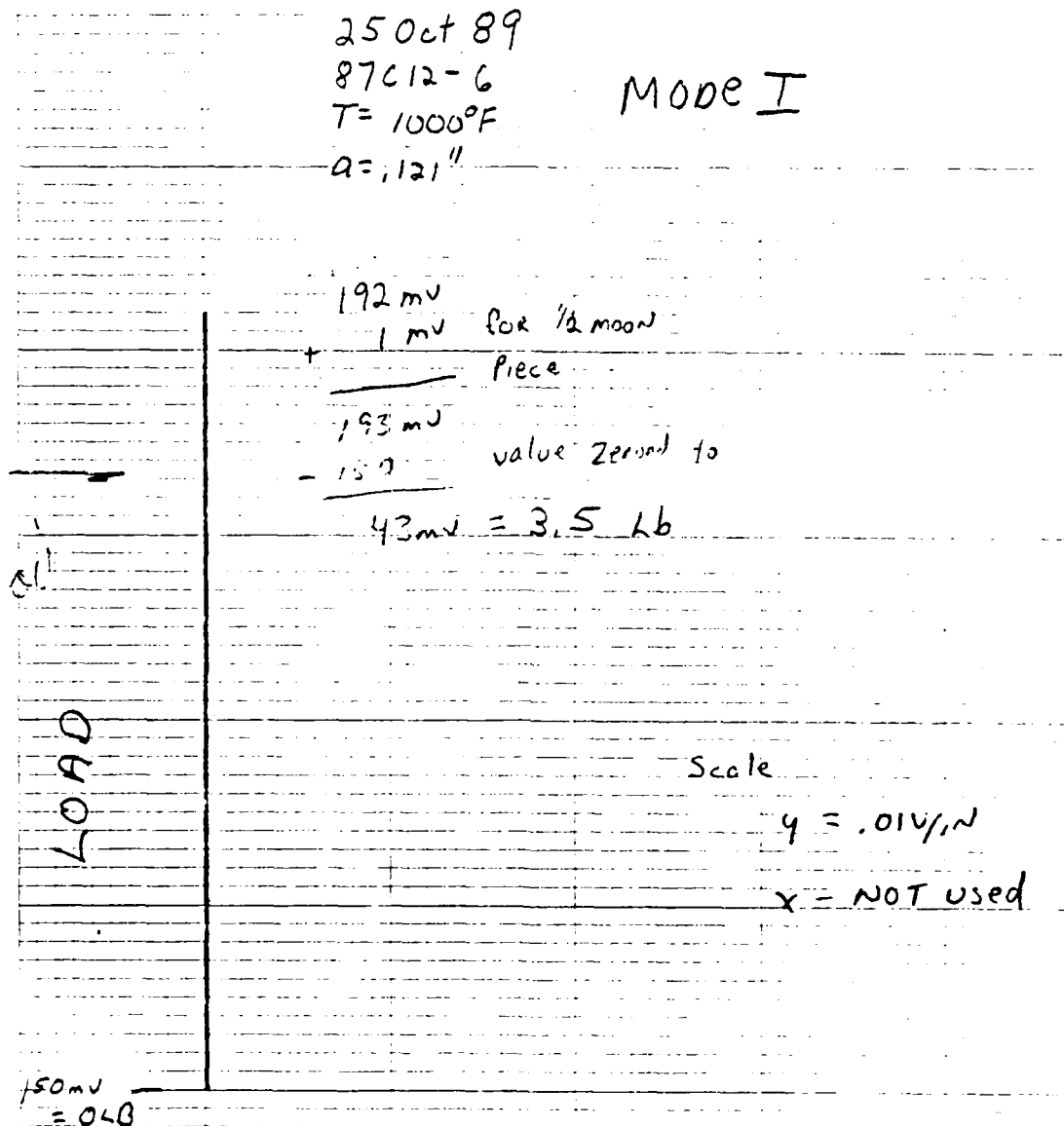
Fig. 105. Mode I Critical Load Curve for
Specimen 87C12-6, 1000 F Test, Crack Growth
Parallel to Fibers
CGW 1723

160
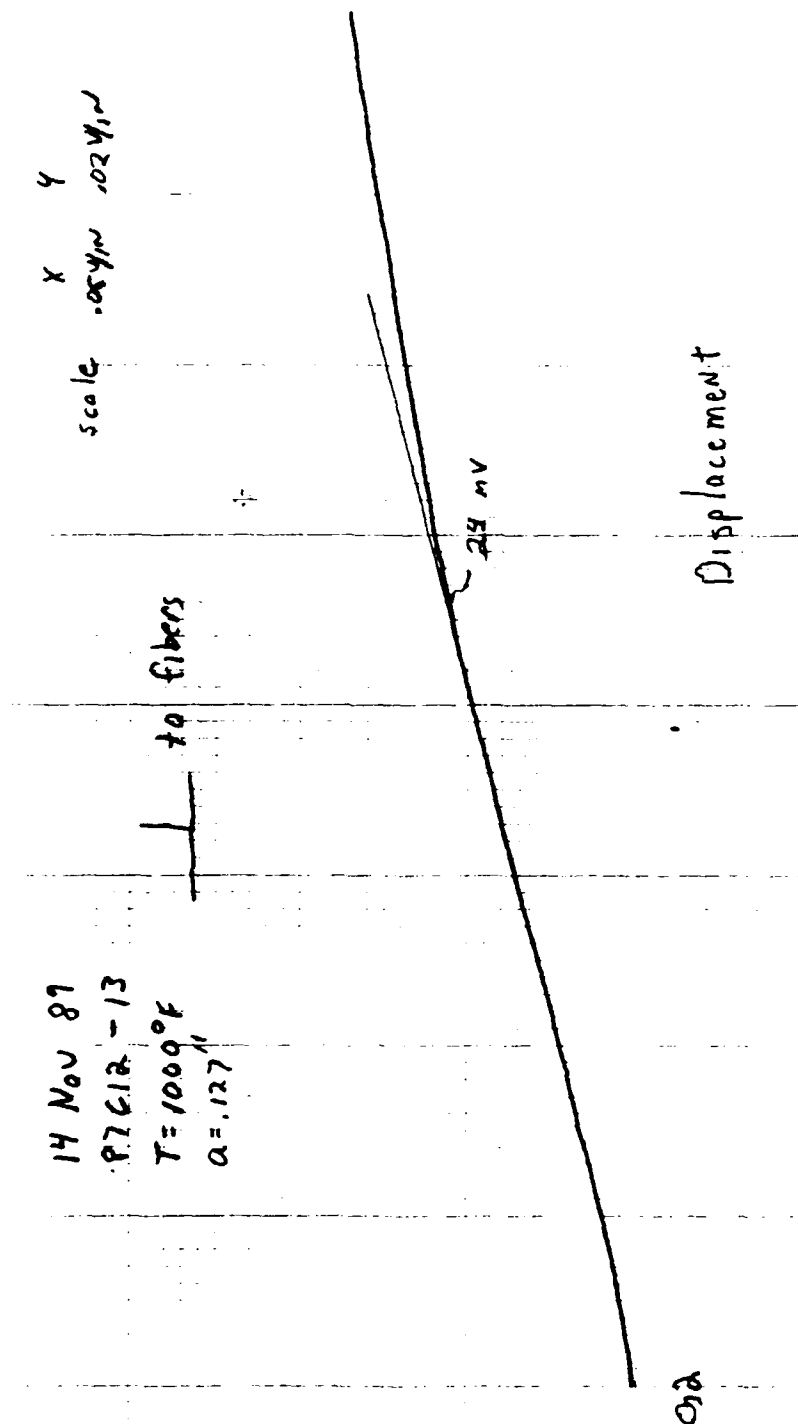
Fig. 106. Mode I Critical Load Curve for
Specimen 87C12-13, 1000 F Test, Crack Growth
Perpendicular to Fibers
CGW 1723

161

Appendix C: Fracture Toughness Values

Mode II

CGW 1723

Tables 7 thru 11 show the experimental fracture toughness values found in this study. Table 7 gives these values for room temperature tests based on the following equations for the compliance to crack length relationship: Equation 4, Russell's equation; Equation 5, the 2nd order curve fit to room temperature compliance data; Equation 6, the 3rd order curve fit to room temperature compliance data; Equation 9, the 2nd order curve fit to combined room temperature and 600 F compliance data; and Equation 10, the 3rd order curve fit to combined room temperature and 600 F compliance data.

Table 8 gives these values for 600 F tests based on the following equations for the compliance to crack length relationship: Equation 4, Russell's equation; Equation 7, the 2nd order curve fit to 600 F compliance data; Equation 8, the 3rd order curve fit to 600 F compliance data; Equation 9, the 2nd order curve fit to combined room temperature and 600 F compliance data; and Equation 10, the 3rd order curve fit to combined room temperature and 600 F compliance data. Table 9 gives the values for the 1000 F tests based on the

162

following equations for the compliance to crack length relationship: Equation 4, Russell's equation; Equation 11, the 2nd order curve fit to 1000 F compliance data; and Equation 12, the 3rd order curve fit to 1000 F compliance data.

Table 10 gives the values for the thermal cycling and thermal exposure specimens based on the following equation for the compliance to crack length relationship: Equation 4, Russell's equation; Equation 9, the 2nd order curve fit to the combined room temperature and 600 F compliance data; and Equation 10, the 3rd order curve fit to the combined room temperature and 600 F compliance data.

Figures 107 thru 110 show the fracture toughness values found for room temperature and 600 F based on 2nd and 3rd order curve fits to room temperature and 600 F compliance data only. Figure 111 shows the values of G_{IIc} for room temperature, 600 F, and 1000 F on the same plot for comparison and trend evaluation. Figure 112 shows the values for G_{IIc} for 600 F, post thermal cycling, and post thermal exposure for comparison purposes.

Table 7. Room Temperature Fracture Toughness Values
CGW 1723

specimen #	a (in)	P_{crit} (lb)	Eq.4 G_{IIc} (lb/in)	Eq.5 G_{IIc} (lb/in)	Eq.6 G_{IIc} (lb/in)	Eq.9 G_{IIc} (lb/in)	Eq.10 G_{IIc} (lb/in)
89C0403-5	0.30	160	2.36	2.43	1.62	2.29	1.42
89C0403-1	0.50	96	2.32	2.07	1.98	1.94	1.91
89C0403-4	0.50	87	2.01	1.74	1.67	1.63	1.61
89C0403-3	0.60	74	2.11	1.62	1.83	1.52	1.82
89C0403-4	0.65	60	1.64	1.20	1.46	1.32	1.73
89C0403-3	0.65	65	1.92	1.42	1.73	1.12	1.46
89C0403-6	0.66	70	<u>2.18</u>	<u>1.62</u>	<u>2.01</u>	<u>1.52</u>	<u>2.02</u>
	Average		2.08	1.73	1.76	1.62	1.71
87C12-3	0.45	94	1.90	1.73	1.51	1.62	1.43
87C12-4	0.47	99	2.21	2.01	1.82	1.88	1.73
87C12-3	0.60	80	<u>2.42</u>	<u>1.89</u>	<u>2.13</u>	<u>1.77</u>	<u>2.12</u>
	Average		2.18	1.87	1.82	1.76	1.76
	Combined Average		2.11	1.77	1.77	1.66	1.73

164

Table 8.   600 F Fracture Toughness Values
CGW 1723

Specimen #	a (in)	P_{crit} (lb)	Eq.4 G_{IIc} (lb/in)	Eq.7 G_{IIc} (lb/in)	Eq.8 G_{IIc} (lb/in)	Eq.9 G_{IIc} (lb/in)	Eq.10 G_{IIc} (lb/in)
89C0403-11	0.33	99	1.03	0.92	0.63	1.02	0.67
89C0403-7	0.40	89	1.27	1.01	0.87	1.18	0.93
89C0403-7	0.50	71	1.25	0.85	0.98	1.05	1.03
89C0403-8	0.50	72	1.23	0.86	0.99	1.06	1.04
89C0403-11	0.55	58	0.97	0.63	0.82	0.79	0.86
89C0403-11	0.55	62	1.10	0.72	0.94	0.90	0.98
89C0403-8	0.55	55	0.87	0.56	0.74	0.71	0.77
89C0403-9	0.60	55	1.13	0.65	0.96	0.83	1.00
89C0403-7	0.60	50	0.91	0.53	0.78	0.67	0.81
Average			1.08	0.75	0.86	0.91	0.90

Table 9. 1000 F Fracture Toughness Values
CGW 1723

specimen #	a (in)	P_{crit} (lb)	Eq.4 G_{IIc} (lb/in)	Eq.11 G_{IIc} (lb/in)	Eq.12 G_{IIc} (lb/in)
89C0403-18	0.27	121	0.93	1.50	1.22
89C0403-13	0.35	90	1.00	1.26	1.08
89C0403-13	0.42	55	0.53	0.58	0.53
89C0403-18	0.44	52	0.53	0.55	0.53
89C0403-19	0.55	46	0.74	0.58	0.61
89C0403-13	0.60	46	0.79	0.63	0.72
89C0403-13	0.60	41	0.61	0.48	0.55
89C0403-18	0.61	48	<u>0.75</u>	<u>0.62</u>	<u>0.72</u>
Average			0.72	0.77	0.80
87C12-1	0.30	103	0.96	1.30	1.09
87C12-2	0.40	69	0.76	0.84	0.77
87C12-1	0.58	42	<u>0.60</u>	<u>0.48</u>	<u>0.54</u>
Average			0.72	0.88	0.75
Combined Average			0.72	0.80	0.76

**Table 10.   Post Thermal Cycling and Exposure
Fracture Toughness Values
CGW 1723**

<u>Post cycling</u>

specimen #	a (in)	P_{crit} (lb)	Eq.4 G_{IIc} (in/lb)	Eq.9 G_{IIc} (in/lb)	Eq.10 G_{IIc} (in/lb)
89C0403-16	0.33	100	1.09	1.04	0.69
89C0403-14	0.40	70	0.70	0.69	0.54
89C1203-16	0.47	65	0.94	0.81	0.75
89C0403-14	0.60	50	0.81	0.64	0.77
89C0403-16	0.63	41	0.67	0.49	0.61
89C0403-14	0.65	42	<u>0.68</u>	<u>0.52</u>	<u>0.68</u>
Average			0.82	0.70	0.67

<u>Post exposure</u>

specimen #	a (in)	P_{crit} (lb)	Eq.4 G_{IIc} (lb/in)	Eq.9 G_{IIc} (lb/in)	Eq.10 G_{IIc} (lb/in)
89C0403-20	0.40	90	1.31	1.16	0.91
89C0403-20	0.50	63	1.00	0.80	0.79
89C0403-20	0.60	56	<u>1.14</u>	<u>0.82</u>	<u>0.98</u>
Average			1.15	0.92	0.89
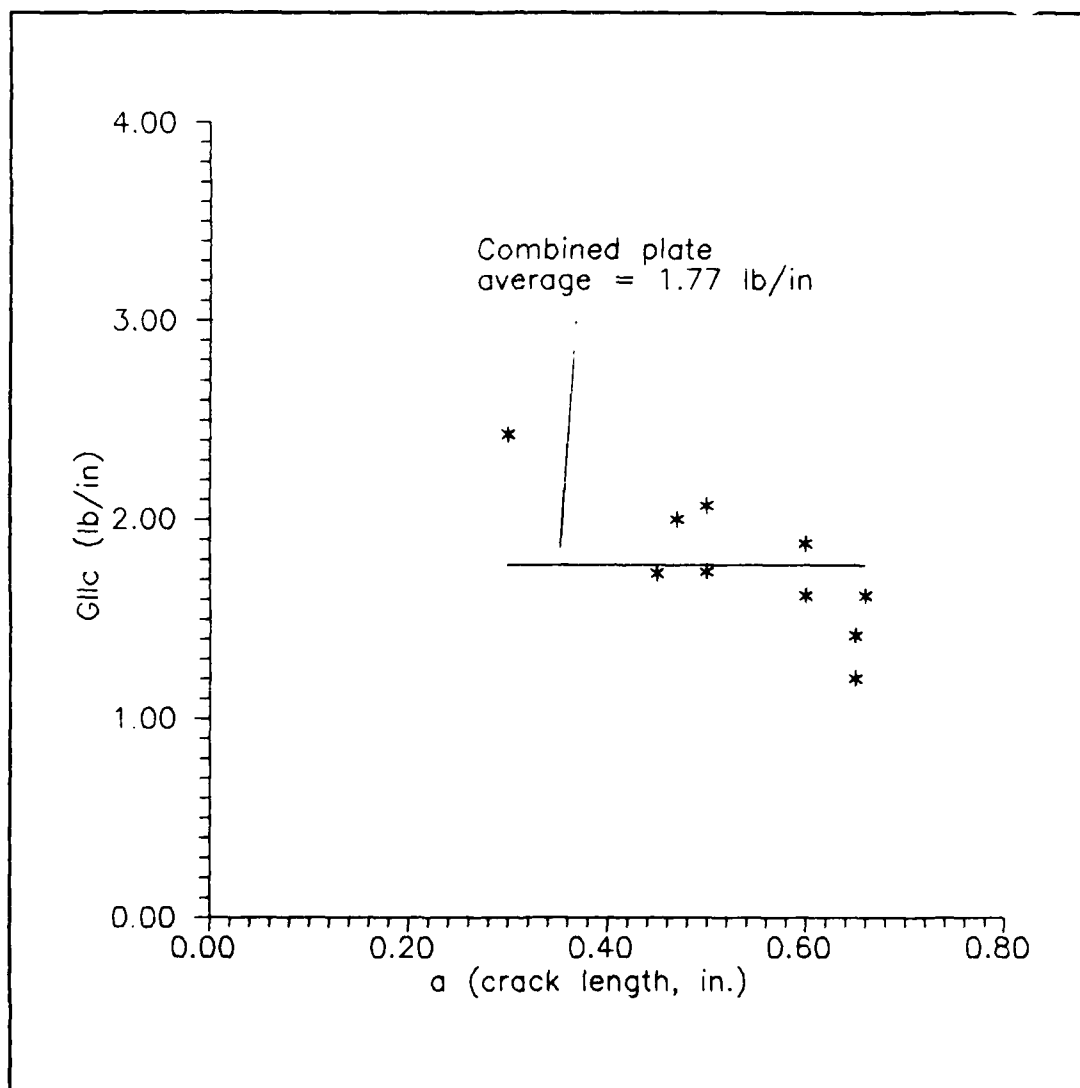
Fig. 107. Average Room Temperature Fracture Toughness of
Plates 89C0403 and 87C12 Based on 2nd Order Curve Fit
of Room Temperature Compliance Data
for Compliance to Crack Length Relationship
CGW 1723

168
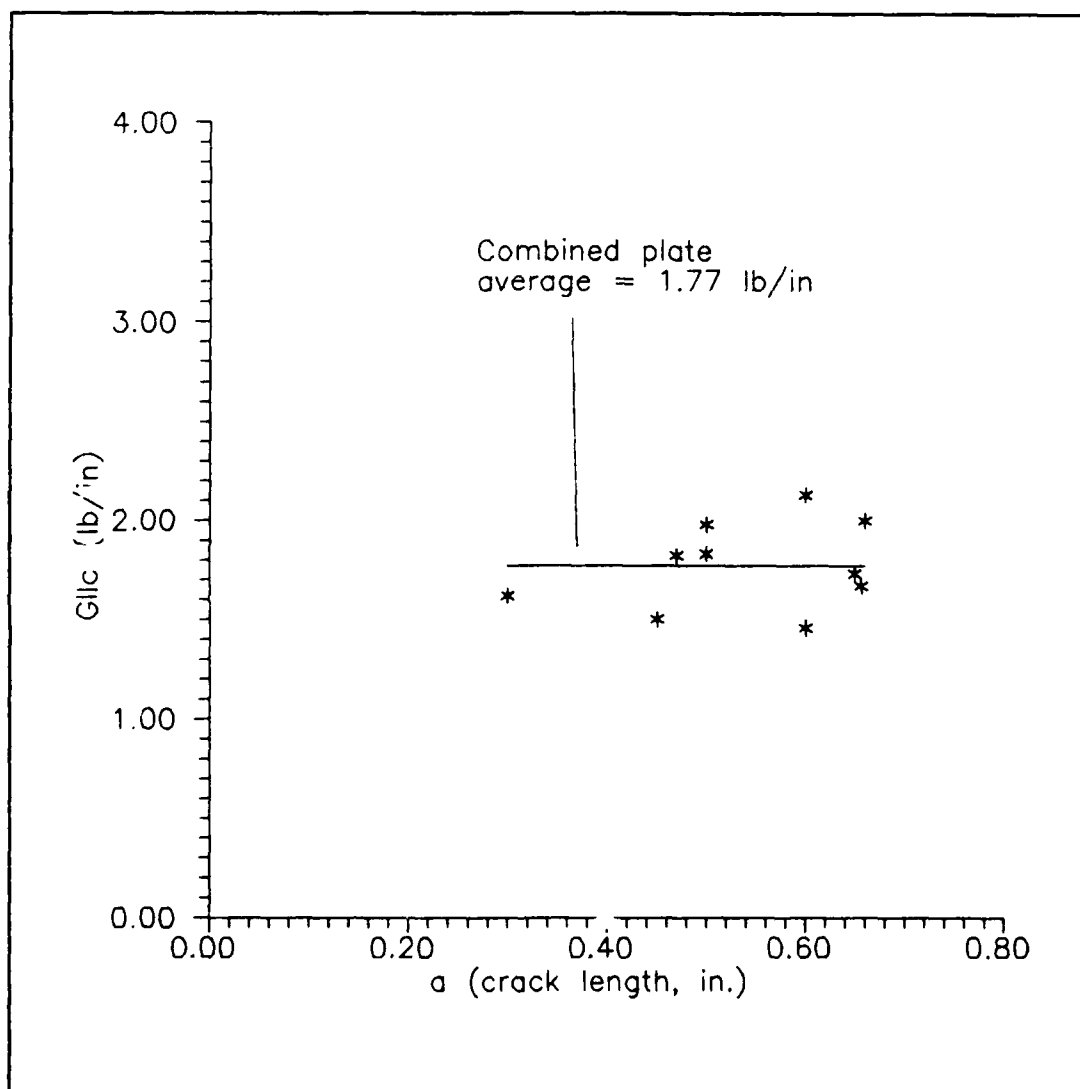
Fig. 108. Average Room Temperature Fracture Toughness of
Plates 89C0403 and 87C12 Based on 3rd Order Curve Fit
of Room Temperature Compliance Data
for Compliance to Crack Length Relationship
CGW 1723

169
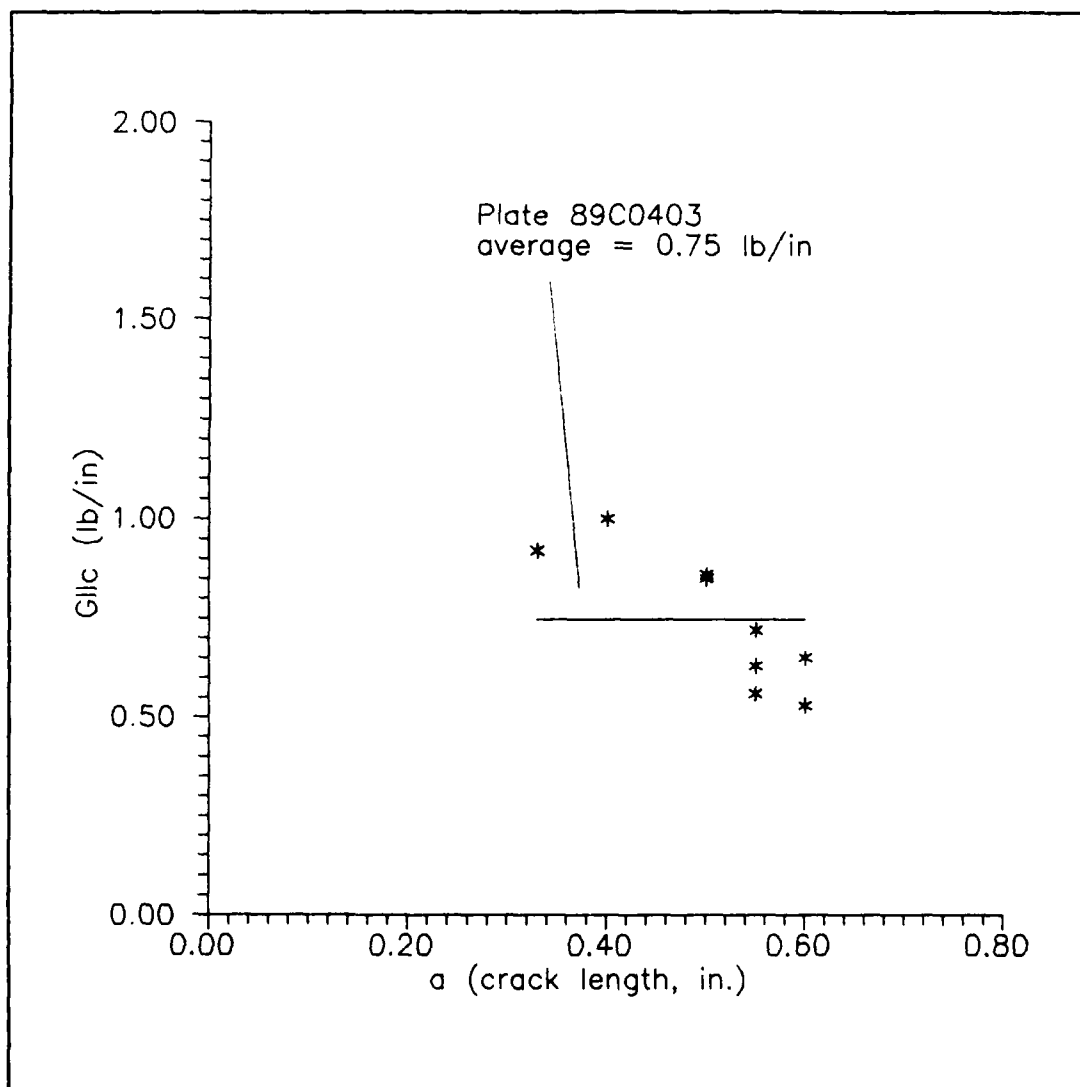
Fig. 109. 600 F Fracture Toughness
Based on 2nd Order Curve Fit of 600 F
Compliance to Crack Length Relationship
CGW 1723

170
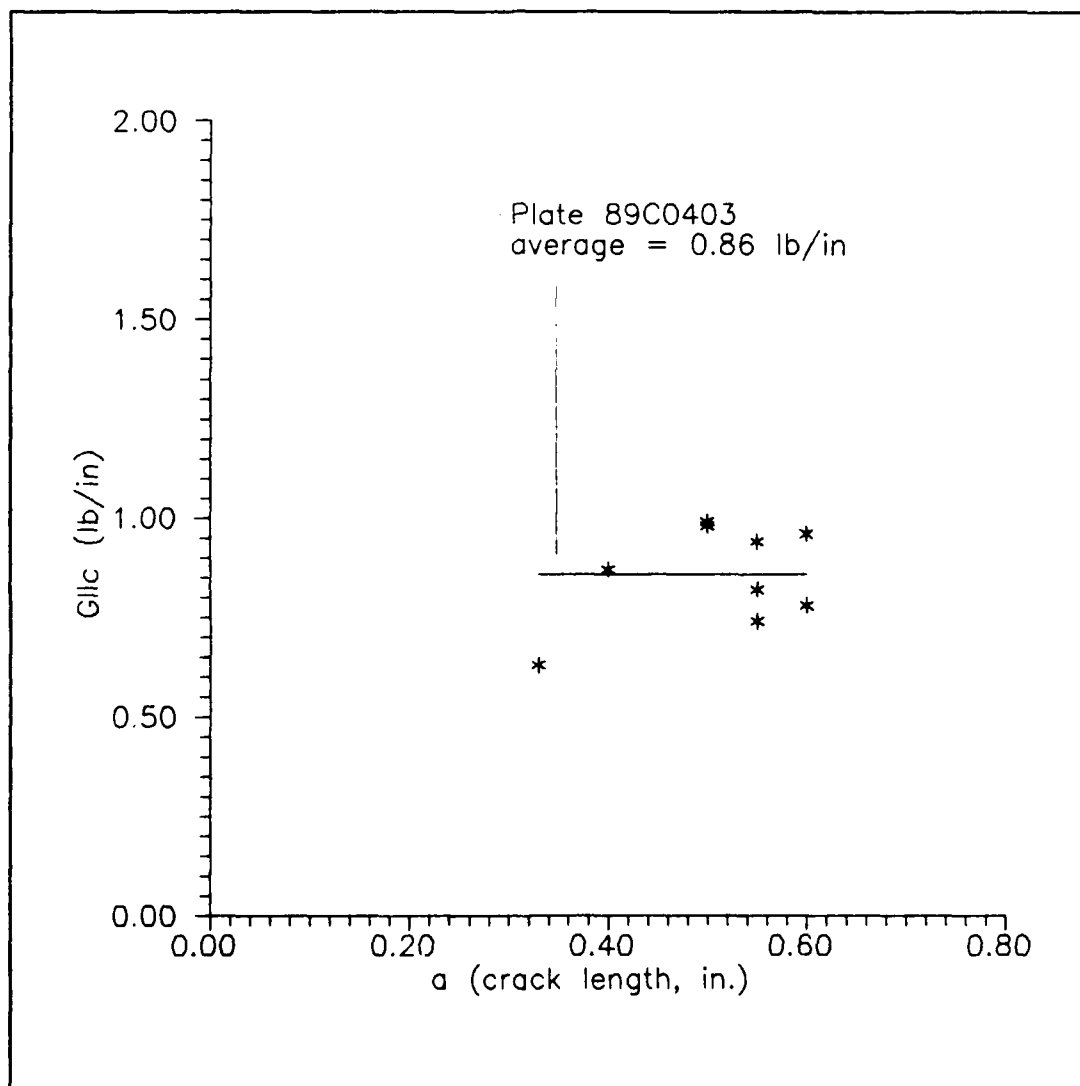
Fig. 110.   600 F Fracture Toughness
Based on 3rd Order Curve Fit of 600 F
Compliance to Crack Length Relationship
CGW 1723

171
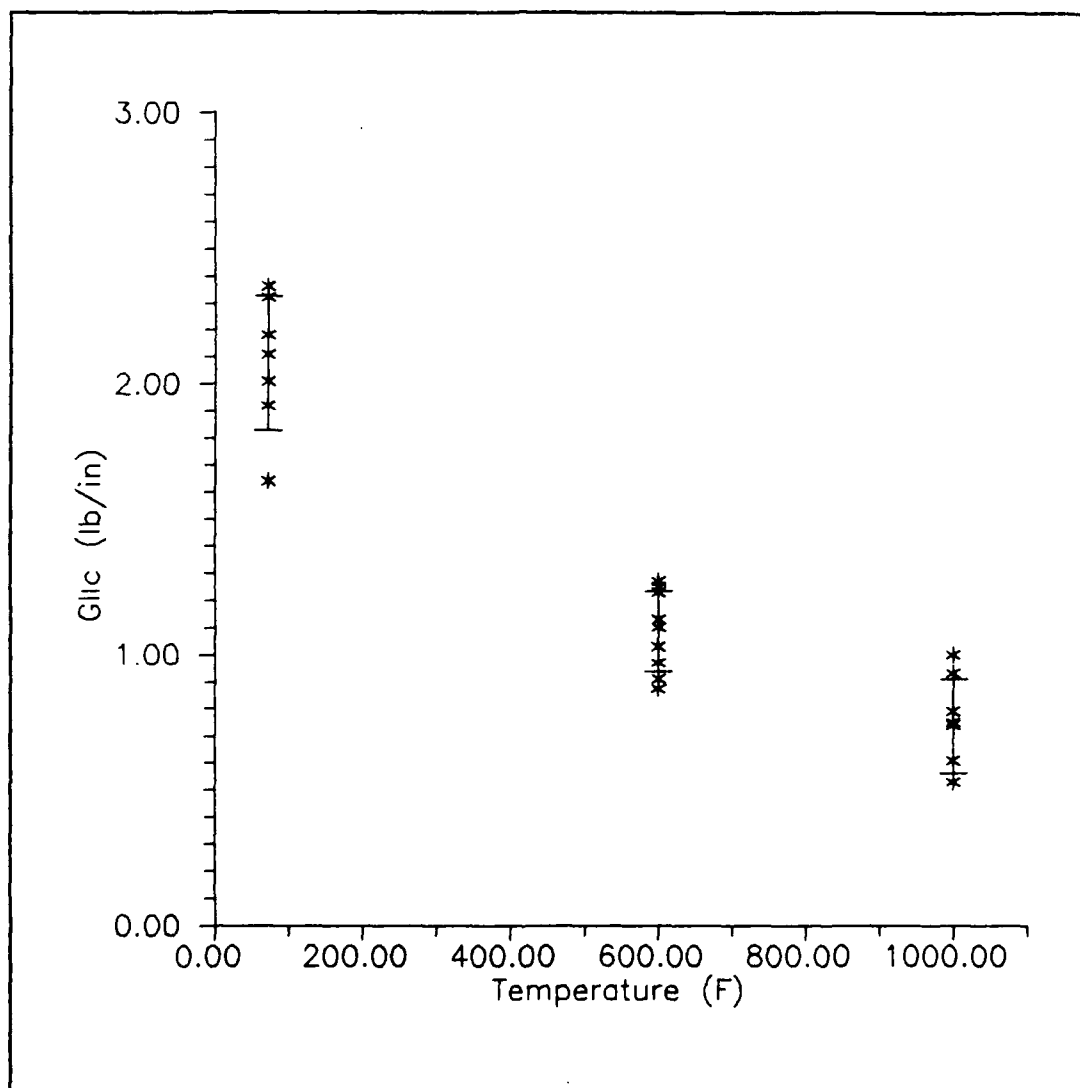
Fig. 111. Comparison of Fracture Toughness at
Room Temperature, 600 F, and 1000 F.
Standard Deviation of The Sample Shown
CGW 1723

172
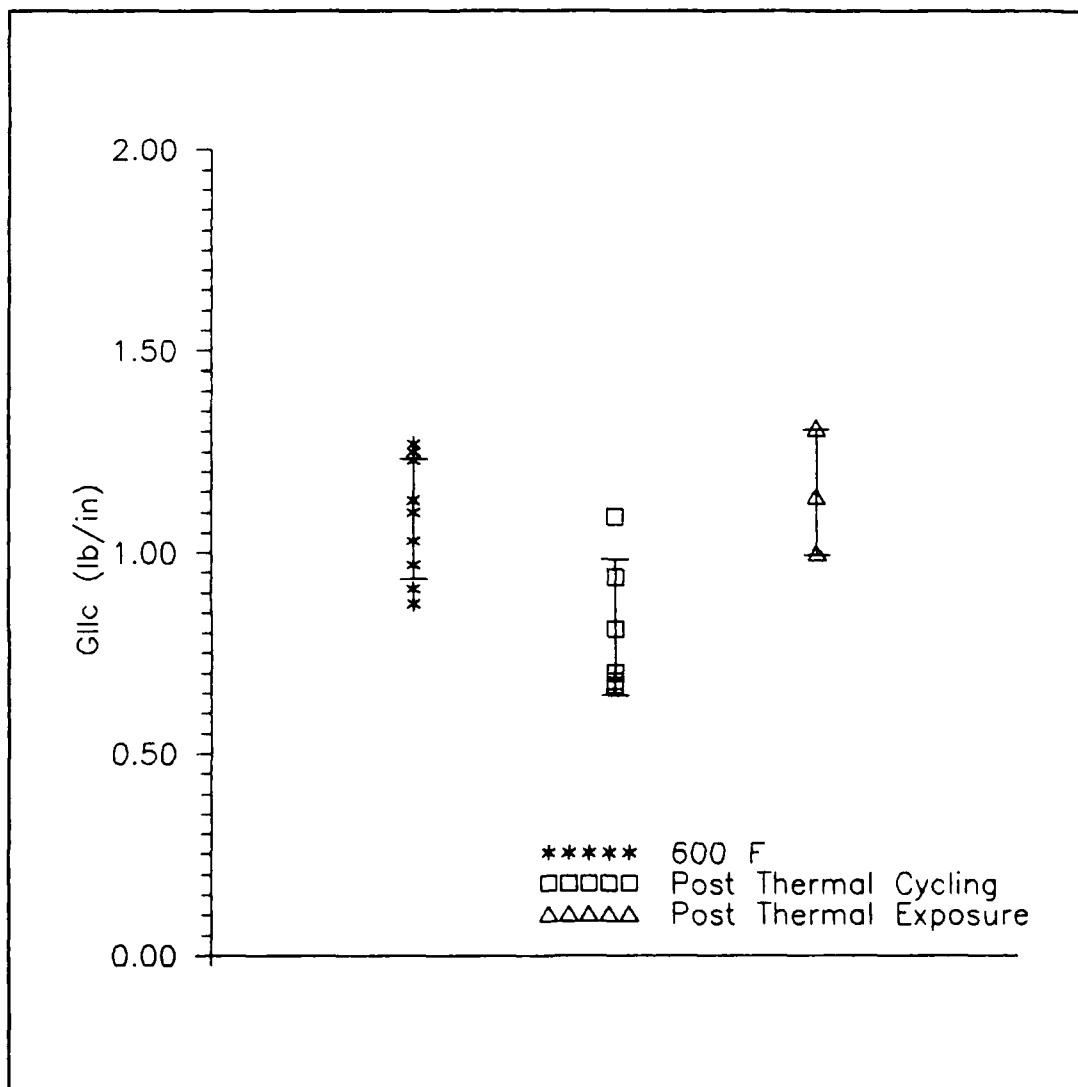
Fig. 112. Comparison of Fracture Toughness at
600 F, Post Thermal Cycling, and Post Thermal Exposure
Standard Deviation of The Sample Shown
CGW 1723

173

CGW 7740

Table 11 gives these values for room temperature tests based on the following equations for the compliance to crack length relationship: Equation 4, Russell's equation; Equation 13, the 2nd order curve fit to room temperature compliance data; and Equation 14, the 3rd order curve fit to room temperature compliance data.

Table 11. Room Temperature Fracture Toughness Values
CGW 7740

specimen #	a (in)	P_{crit} (lb)	Eq.4 G_{IIc} (lb/in)	Eq.9 G_{IIc} (lb/in)	Eq.10 G_{IIc} (lb/in)
89E08-6	0.35	72	0.91	1.09	0.89
89E08-1	0.40	64	0.91	1.03	0.89
89E08-6	0.55	55	1.25	1.14	1.19
89E08-1	0.57	51	1.20	1.07	1.15
89E08-3	0.60	41	0.97	0.79	0.87
89E08-6	0.61	42	0.92	0.77	0.87
89E08-6	0.67	43	<u>1.18</u>	<u>0.92</u>	<u>1.10</u>
Average			1.08	0.98	0.99

Appendix D. Heating Lamp Specifications

Figures 113 thru 115 show detailed drawing and specifications for the heat lamps used in the thermal cycling portion of this study. These lamps were designed by Mr. George Hartman of the University of Dayton Research Institute.
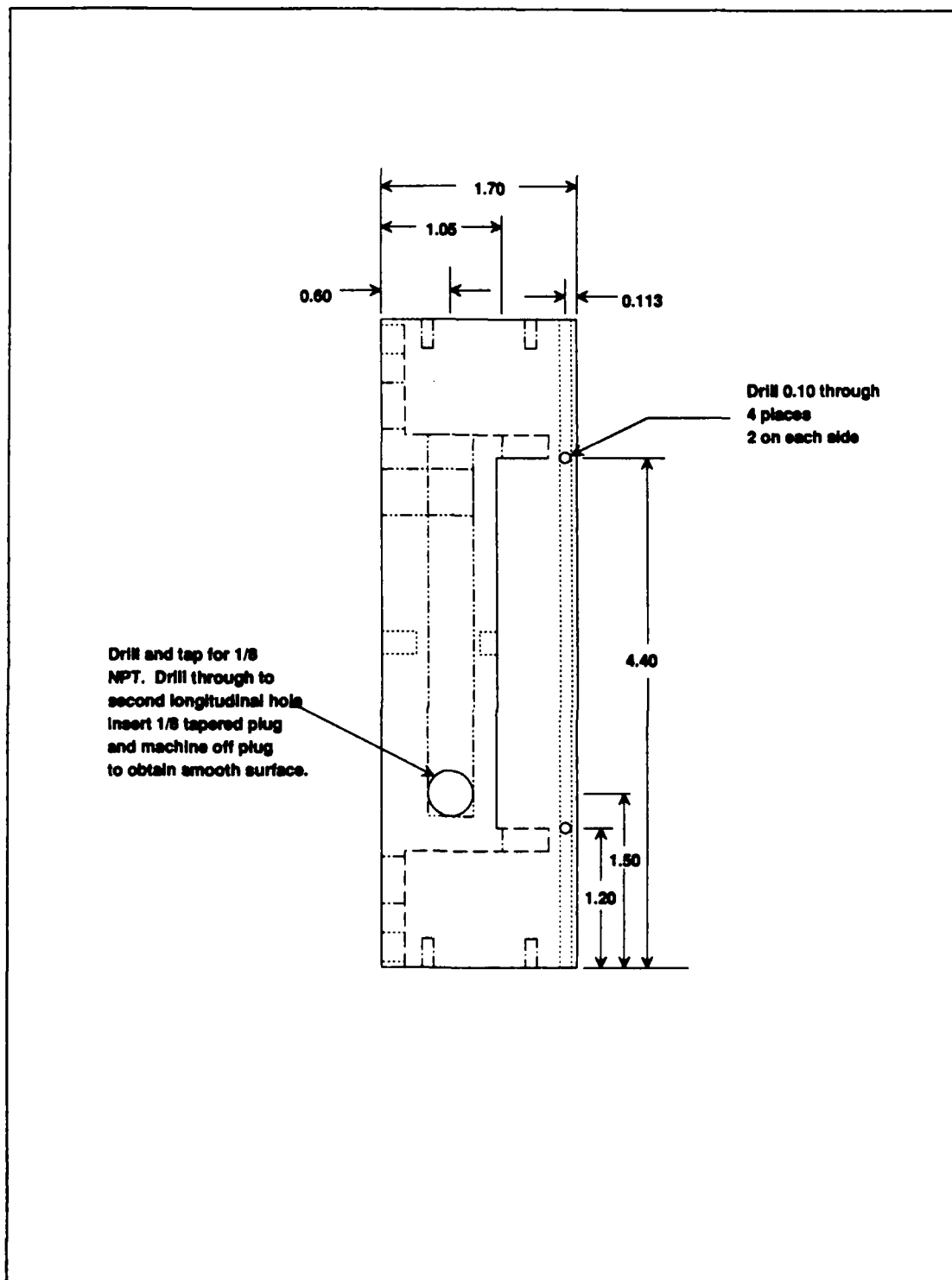
Fig. 113. Thermal Cycling Lamps, View 1

176
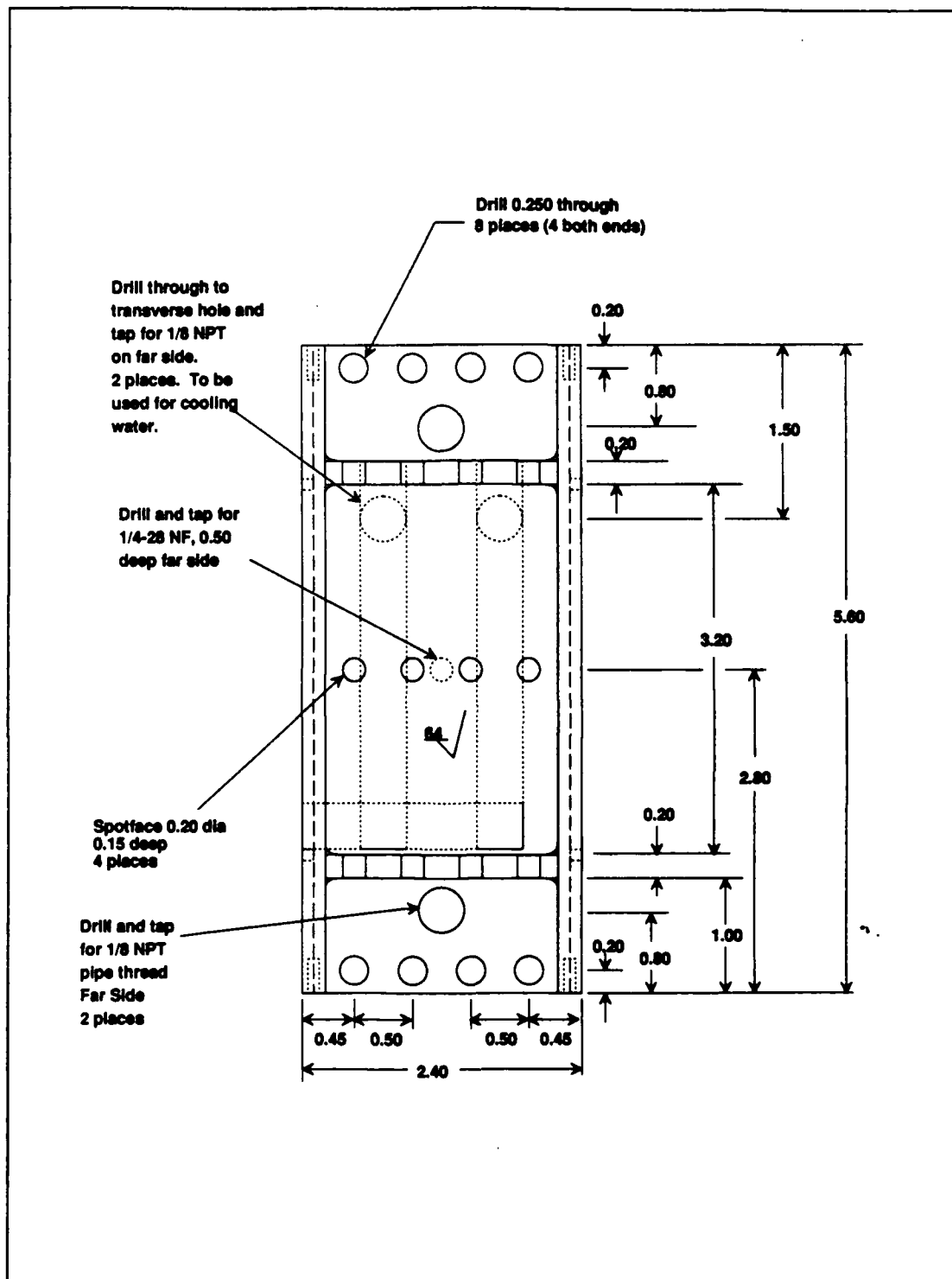
Fig. 114.   Thermal Cycling Lamps, View 2

177

Drill and tap for
#4-40 0.30 deep
4 places
each end

Drill and tap for
1/8 NPT. Insert
1/8 NPT tapered plug
and pressure check
using supplied fittings.
Machine off plugs
to obtain smooth
surface.
2 places.

1.05
0.85
0.55
0.20
0.05
0.125 0.175
0.10
0.25
1.70
0.05
1.15
1.00
0.60
0.40
0.70
0.20
2.40
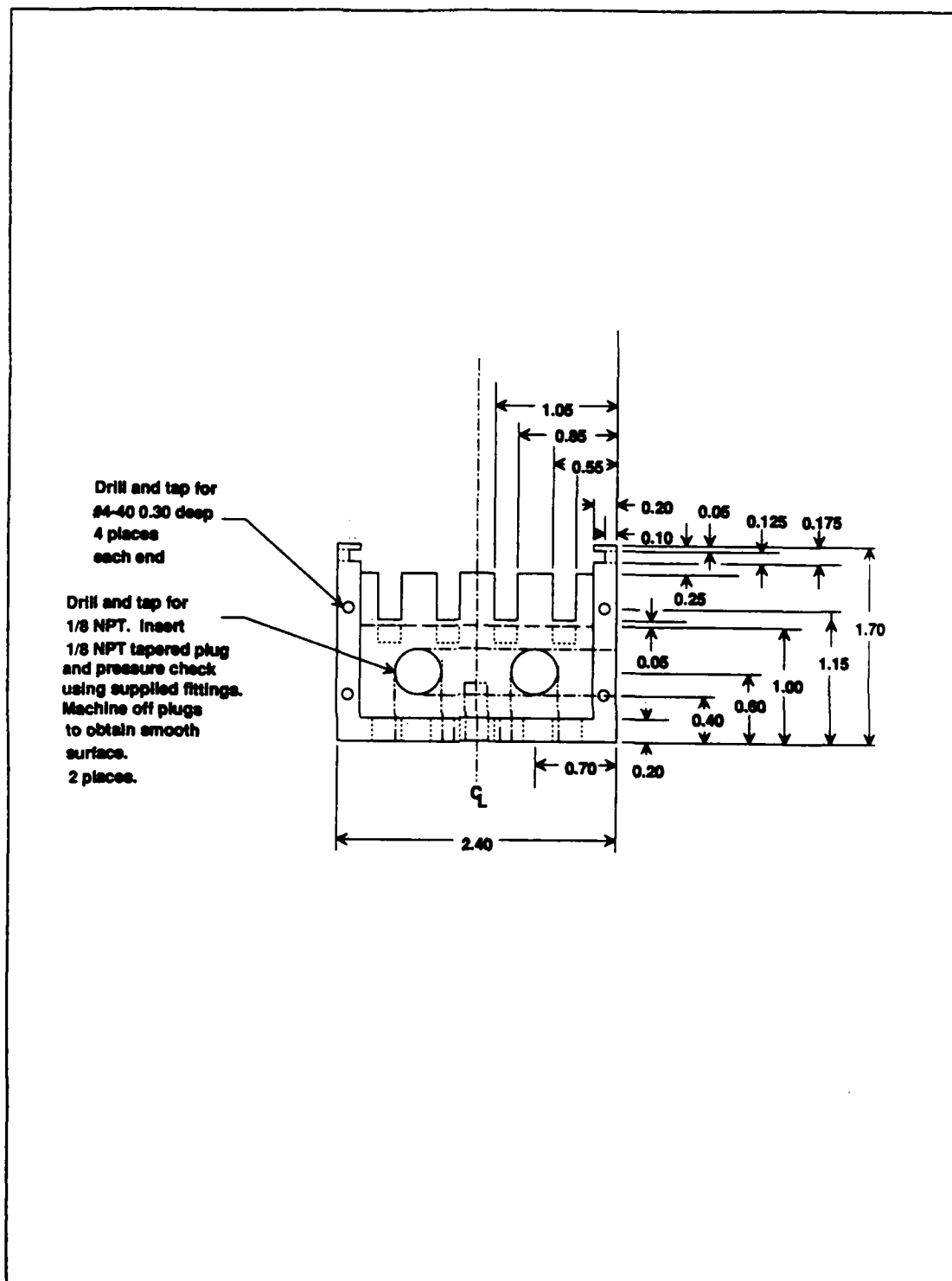
Thermal Cycling Lamps, View 3

178

<u>Vita</u>

Captain Michael A. Hoobler, ███████████████.
██

███████ He graduated from Mojave High School in Mojave,
California in 1975. He received an appointment to the United
States Air Force Academy and entered in the summer of 1975.
He graduated in 1979 with a Bachelor of Science in
Aeronautical Engineering degree and a commission as a 2nd
Lieutenant in the USAF. After 1 year of Undergraduate Pilot
Training at Reese AFB, Texas he was selected to remain at
Reese AFB where he upgraded to instructor pilot in the T-38
Talon. In February 1983 he was assigned to Williams AFB,
Arizona where he again flew as an instructor pilot in the
T-38. In July 1985 he was assigned to the 93 BMW at K.I.
Sawyer AFB, Michigan where he was an aircraft commander and
later an instructor pilot in the KC-135. In November 1987 he
was selected to attend the Air Force Institute of Technology
(AFIT) and entered with class GAE-89D. In January 1989 he
was selected to attend the United States Air Force Test Pilot
School at Edward AFB, California upon his graduation from
AFIT.

REPORT DOCUMENTATION PAGE

1a. REPORT SECURITY CLASSIFICATION	1b. RESTRICTIVE MARKINGS
UNCLASSIFIED	

2a. SECURITY CLASSIFICATION AUTHORITY	3. DISTRIBUTION/AVAILABILITY OF REPORT
	Approved for public release;
2b. DECLASSIFICATION/DOWNGRADING SCHEDULE	distribution unlimited

4. PERFORMING ORGANIZATION REPORT NUMBER(S)	5. MONITORING ORGANIZATION REPORT NUMBER(S)
AFIT7GAE/ENY/89D-14	

6a. NAME OF PERFORMING ORGANIZATION	6b. OFFICE SYMBOL (If applicable)	7a. NAME OF MONITORING ORGANIZATION
School of Engineering	AFIT/ENY	

6c. ADDRESS (City, State, and ZIP Code)	7b. ADDRESS (City, State, and ZIP Code)
Air Force Institute of Technology Wright Patterson AFB, OH 45433-5000	

8a. NAME OF FUNDING/SPONSORING ORGANIZATION	8b. OFFICE SYMBOL (If applicable)	9. PROCUREMENT INSTRUMENT IDENTIFICATION NUMBER
AFWAL	AFWAL/MLLN	

8c. ADDRESS (City, State, and ZIP Code)	10. SOURCE OF FUNDING NUMBERS			
	PROGRAM ELEMENT NO.	PROJECT NO.	TASK NO	WORK UNIT ACCESSION NO.
Air Force Wright Aeronautical Lab. Wright Patterson AFB, OH 45433-5000				

11. TITLE (Include Security Classification)
Effects of Elevated Temperatures and Thermal Cycling on the Fracture Toughness of Ceramic Composite Materials

12. PERSONAL AUTHOR(S)
Michael A. Hoobler, B.S., Captain, USAF

13a. TYPE OF REPORT	13b. TIME COVERED	14. DATE OF REPORT (Year, Month, Day)	15. PAGE COUNT
MS Thesis	FROM _____ TO _____	1989 December	197

16. SUPPLEMENTARY NOTATION

17. COSATI CODES			18. SUBJECT TERMS (Continue on reverse if necessary and identify by block number)
FIELD	GROUP	SUB-GROUP	Fracture Toughness of Fiber Reinforced Ceramic Composite
11	04		Materials, Mode II

19. ABSTRACT (Continue on reverse if necessary and identify by block number)

Thesis Advisor: Dr. S. Mall
                  Professor
                  Department of Aeronautics and Astronautics

Continued on Reverse

20. DISTRIBUTION/AVAILABILITY OF ABSTRACT	21. ABSTRACT SECURITY CLASSIFICATION
☒ UNCLASSIFIED/UNLIMITED ☐ SAME AS RPT. ☐ DTIC USERS	UNCLASSIFIED

22a. NAME OF RESPONSIBLE INDIVIDUAL	22b TELEPHONE (Include Area Code)	22c. OFFICE SYMBOL
Shankar Mall, Professor	513-255-2998	AFIT/ENY

DD Form 1473, JUN 86   *Previous editions are obsolete.*   SECURITY CLASSIFICATION OF THIS PAGE

UNCLASSIFIED   Abstract

        The need to determine the effects of elevated
temperature and thermal cycling on the mode II fracture
toughness of fiber reinforced ceramic composites was
identified. The two materials chosen for this purpose were
CGW 1723 and CGW 7740. In addition to mode II fracture
toughness, preliminary mode I fracture toughness values were
determined in order to evaluate similarities or dissimi-
larities in fracture toughness trends with increasing
temperature. A pre-cracking fixture was designed and built
to allow for precise pre-cracking of the specimens. A test
stand for subjecting specimens to thermal cycling was
designed and constructed. CGW 1723 Mode II specimens were
tested at room temperature, 600 F, 1000 F, after being cycled
from 130 F to 600 F for 25 cycles, and after exposure to 600
F for 125 minutes. CGW 7740 mode II specimens were tested at
room temperature. Compliance data was plotted as a function
of non-dimensional crack length. 2nd and 3rd order
polynomial curves were fitted to the data. These curve fits
were compared to a theoretical compliance to crack length
relationship. Critical loads were determined from the load-
displacement curves by identifying the load at which the
specimens compliance changed. Mode II critical strain energy
release rate was then calculated. The three methods of
determining the compliance to crack length relationship were
compared to find the one that produced the narrowest band of
fracture toughness values. The theoretical solution was
found to be the best method and fracture toughness values
were computed from this method. The fracture toughness
value, G_{IIc}, at 600 F decreased by 50% in comparison to its
value at room temperature and the G_{IIc} value at 1000 F
decreased by another 30%. The specimens subjected to thermal
cycling showed a decrease in fracture toughness from that of
the 600 F specimens. The specimen exposed to a constant
600 F for 125 minutes had almost the same fracture toughness
value as that of the 600 F specimen. CGW 1723 mode I
specimens were tested at room temperature and 1000 F. They
displayed the same trend of decreasing fracture toughness,
G_{Ic}, at elevated temperatures as did the mode II specimens.
Post mortem examination for both modes revealed an
embrittlement of the matrix that increased with increasing
temperatures. Fiber pullout was decreased in the elevated
temperature tests, showing a degradation in the fiber matrix
interface. These mechanisms were the primary cause for the
decrease in G_{IIc} and G_{Ic} with increasing temperature.